**Title**

Inorganic Carbon and Nitrogen Exchange Mechanisms of Cnidarian-Algal Photosymbioses



**Author**

Thies, Angus Blacklaw

**Publication Date**

2024

Peer reviewed|Thesis/dissertation

UNIVERSITY OF CALIFORNIA SAN DIEGO

# Inorganic Carbon and Nitrogen Exchange Mechanisms of Cnidarian-Algal Photosymbioses

A Dissertation submitted in partial satisfaction of the requirements
for the degree Doctor of Philosophy

in

Marine Biology

by

Angus Blacklaw Thies

Committee in charge:

Professor Martin Tresguerres, Chair
Professor Ronald S. Burton
Professor Julian I. Schroeder
Professor Jennifer E. Smith

2024

The Dissertation of Angus Blacklaw Thies is approved, and it is acceptable in quality and form for publication on microfilm and electronically.

University of California San Diego

2024

# DEDICATION

I dedicate this work to all the mentors, friends, and family who supported me on my journey over the past five years of graduate school. Only through your love, patience, and kindness was this accomplishment possible. Thank you.

# EPIGRAPH

"Thus, then, for a vegetable cell no more ideal existence can be imagined than that within the body of an animal cell of sufficient active vitality to manure it with abundance of carbonic anhydride and nitrogenous waste, yet of sufficient transparency to allow the free entrance of the necessary light. And conversely, for an animal cell there can be no more ideal existence than to contain a sufficient number of vegetable cells, constantly removing its waste products, supplying it with oxygen and starch, and being digestible after death."
-Patrick Geddes, 1882, *On the Nature and Functions of the "Yellow Cells" of Radiolarians and Cœlenterates*

"It don't gotta be fun to be fun."
-Carl Tobin
…it was pretty fun though

"When in doubt, run it out."
-Some wise, foolish soul

TABLE OF CONTENTS

LIST OF FIGURES

**Chapter 2**



**Chapter 3**

**Chapter 4**



**Chapter 5**

LIST OF TABLES

**Chapter 2**

LIST OF ABBREVIATIONS

| | |
|---|---|
| ayRhp1 | *Acropora yongei* rhesus protein |
| ACC | Amorphous calcium carbonate |
| CA | Carbonic anhydrase |
| CCM | Carbon concentrating mechanism |
| ConcA | ConcanamycinA |
| DCMU | 3-(3,4-dichlorophenyl)-1,1-dimethylurea |
| DIC | Dissolved inorganic carbon ($CO_2 + HCO_3^- + CO_3^{2-}$) |
| DMSO | Dimethyl sulfoxide |
| ECF | Extracellular calcifying fluid |
| EZ | Ethoxzolamide |
| FSW | 0.2μm filtered seawater |
| IHC | Immunohistochemistry |
| IACM | Immunohistochemical confocal microscopy |
| LEC | Light enhanced calcification |
| NCM | Nitrogen concentrating mechanism |
| NKA | $Na^+/K^+$-ATPase |
| PAM | Pulse amplitude modulated fluorometry |
| $P_N$ | Net photosynthesis |
| PSII | Photosystem II |
| $R_D$ | Dark respiration |
| Rh | Rhesus protein |
| sAC | Soluble adenyl cyclase |

| | |
|---|---|
| Tamm | Total ammonia ($NH_3 + NH_4^+$) |
| μE | Micro-Einstein, μmol quanta photons $m^{-2}$ $s^{-1}$ |
| VHA, $VHA_B$ | V-type $H^+$-ATPase, B subunit |

ACKNOWLEDGEMENTS

I owe thanks to an innumerable list of individuals who have directly helped produce the work in this dissertation, enriched my life as a graduate student, helped foster my love for science, or contributed to several of these roles.

I must start by acknowledging the mentorship of Dr. Martin Tresguerres, my good friend and Chair of my doctoral committee. We first met in 2016 when I was a young(er) student in his undergraduate Marine Biochemistry course. Martin is a passionate educator who cares deeply for his students and the experience of being in his class ignited my interest in cellular biology and physiology. Recognizing my curiosity, he graciously afforded me the opportunity to volunteer in his lab later that fall. To use a cliché, the rest is history…I fell head over heels for physiological research, completed an independent study in 2017, stayed for a contiguous MS degree in 2018, and returned to the lab to complete my PhD in 2019. None of those decisions were in small part owed to Martin's mentorship and leadership style. When I'm asked by perspective graduate students what working for Martin is like, or why I chose to stay in the Tresguerres Lab instead of completing a PhD in Baltimore, I always give the same reply: I've never met a PI who advocates harder for their students, genuinely cares for their well-being, or works harder to actualize students' career aspirations, no matter how they shift over time. I will always be thankful for the patience, mentorship, and honesty he has afforded me over the past 8 years. I would additionally like to thank my committee members, Drs. Ronald S. Burton, Julian I. Schroeder, and Jennifer E. Smith, for their contributions to shaping this dissertation.

My tenure in the Tresguerres Lab was enriched by overlapping with numerous volunteers, graduate students, and postdocs who helped shape my career aspirations, refine my scientific skillset, and mature into a well-rounded man. Beginning with my original graduate mentor, Dr.

Megan Barron, thank you for taking the time to share your knowledge, guide me through a research lab, and help me find a passion for coral biology. To Drs. Garfield Kwan, Daniel Yee, Lauren Linsmayer, and Jinae Roa, thank you for making the Tresguerres Lab a welcoming home away from home, teaching me endless skills, and providing sound council over beers at TG. To Mikayla Ortega, thank you for being a supportive teammate during my MS and helping me find my footing. To Drs. Cristina Salmerón, Till Harter, Alex Clifford, and Claudia Galindo Martinez, thank you for proving endless experimental guidance, encouraging me to try new research approaches, and being genuine friends during my PhD. To Samantha Nöel, thank you for showing me the joys of mentorship and helping me to remember how much I love doing science each day; your friendship and laughter made my MS possible. To Charles Trautner, Elisa Prohroff, Victoria Vasquez, Bryan Delgado, and Qianqian Tao, thank you for being wonderful volunteers and MS students who kept me laughing in lab and helped me complete the final chapters of my dissertation. To Ryan Myers, thank you for helping keep our little world spinning around and being a good friend. To Maitri Paul, thank you for your endless cheer, despite reminding me constantly that I'm now somehow the "old" PhD student. Finally, to Joani Viliunas, thank you for showing me how awesome Bobtail Squid are and making the summer of '22 an absolute blast.

I would also like to thank the many mentors that helped me cultivate my passion for science. To Sandra Trentowsky, my middle school science teacher, the impact you had on my life as my first scientific mentor will always be special to me. Your humor, kindness, and passion made science approachable and inspired me to study the natural world; thank you. To Dr. Karina Baum, my AP Biology teacher, thank you for pushing me to follow my passions and explore beyond what was required. You were instrumental in helping me find my path to UC San Diego and Scripps Institution of Oceanography. To Dr. Ana Širović, my first mentor at SIO, thank you for giving me

my first taste of academic research, taking a chance by hiring me to process data, and pushing me to find my niche in marine biology.

I would also like to single out several staff members at SIO who go above and beyond to keep Hubbs Hall and aquarium operations running. To Dejan Ristic, the Czar of Hubbs Hall, your ceaseless efforts to keep our sinking building afloat, make sure labs remain operational, and keep science progressing from behind the scenes does not go unnoticed. Thank you for your kindness, determination to see all problems solved fairly, and friendship. To Phil Zerofski and Christine Steinke, if Dejan represents the powers on high, you must be the powers on Earth. On numerous occasions you have both collected species for my dissertation work and even saved many of my research animals from the perils of Hubbs Hall's ageing guts. The volume of your responsibilities is staggering yet you never fail. You have my deepest thanks. Additionally, thank you to the many individuals who work behind the administrative curtain: Gilbert Bretado, Maureen McGreevy, Denise Darling, Shelley Weisel, Josh Reeves, and Josh Schmidt. Thank you for helping graduate students navigate the murky waters of UCSD policy and keeping us swimming in the right direction.

I would like to acknowledge two major events that took place during 2019-2024: the UAW strike of '22 and Covid-19. The UAW strike was an eye-opening experience that taught me much about how I envision my life as a scientist and a member of society. Thank you to my union, UAW Local 2865, for fighting for the future of UC graduate students. Now that I'm defending, it's easy to gloss over Covid-19 as a mere bump in the road of grad school however, it was anything but insignificant. Hubbs Hall and the Tresguerres Lab completely closed for several months, graduate funding was uncertain, and leaving your home provoked anxiety and fear. My ability to complete dissertation research, chance to perform field work, and opportunity to attend conferences and

travel to collaborating labs were all nixed. Covid-19 did however afford me an invaluable opportunity to take time to venture into the wilderness with friends, rediscover the passions I have outside of science, and let me take a breath to refocus my career aspirations and goals for my life. I believe I would be a very different man if grad school had all "gone to plan;" I'm thankful it didn't.

I wish to express my deepest gratitude, thanks, and love to my family. To my parents, Carrie and Rocky, thank you for raising me to think critically, be curious, and feel strongly. Your generosity has never gone unnoticed and I'm deeply thankful that you helped me attend college on the other side of the country so that I could pursue my dreams of studying Marine Biology. Thank you both for wanting to be a part of my life and being present from across the country. I love you both dearly. To Austin, my brother, words cannot describe what your friendship means to me. Thank you for sharing your laughter, accomplishments, struggles, and time with me. I'm so thankful that we still prioritize spending time with one another at this point in our busy lives. I love you deeply.

To the colorful circus of individuals who claim me as a friend, thank you for the support, patience, and continuous love you've shown me for five years. I dare not list you all here for fear of missing one of the many names I feel obliged to mention. Suffice it to say, to my climbing/cooking/laughing/drinking/smoking/traveling/Dungeons&Dragons-playing family, I love each one of you dearly and I will treasure your friendship forever, no matter where time takes us. Thank you all for the contributions you each have made in making me a better man and friend.

Finally, and certainly not least, I would like to thank Allyssa Strohm, my partner and future (medical) doctor for supporting me over the last three years. Your ability to love completely, face each day with a smile, dive in headfirst to the unknown, and do it all while making fun of me has

both enriched my life and inspired me to be a better friend and partner. Thank you for sharing your life with me. I love you…and please remember to call me Dr. Thies for *at least* one week.

Chapter 2, in full, is a reprint of the material as it appears in Thies AB, Quijada-Rodriguez AR, Zhouyao H, Weihrauch D, Tresguerres M. 2022 A Rhesus channel in the coral symbiosome membrane suggests a novel mechanism to regulate $NH_3$ and $CO_2$ delivery to algal symbionts. Sci. Adv. 8. (doi:10.1126/sciadv.abm0303). The dissertation author was the primary investigator and author of this paper. The material is used by permission of the American Association for the Advancement of Science (AAAS).

Chapter 3 is currently being prepared for submission for publication of the material. Thies AB, Wangpraseurt D, Tresguerres M (*in prep*). V-type $H^+$-ATPase and Carbonic Anhydrase Support Symbiont Photosynthesis in *Cassiopea* Amoebocytes. The dissertation author was the primary investigator and author of this material.

Chapter 4 is currently being prepared for submission for publication of the material. Thies AB and Tresguerres M (*in prep*). Effects of light on the expression, localization, and function of V-type $H^+$-ATPase in *Stylophora pistillata*. The dissertation author was the primary investigator and author of this material.

Chapter 5, in part, is a reprint of the material as it appears in Tresguerres M, Clifford AM, Harter TS, Roa JN, Thies AB, Yee DJ, and Brauner CJ. 2020. Evolutionary links between intra- and extracellular acid-base regulation in fish and other aquatic animals. Journal of Experimental Zoology Part A: Ecological and Integrative Physiology 1, 17 (10.1002/jez.2367). The dissertation author was a co-author of this paper. The material is used by permission of John Wiley & Sons, Inc.

Chapter 5, in part, is a reprint of the material as it appears in Barott KL, Venn AA, Thies AB, Tambutté S, Tresguerres M. 2020. Regulation of coral calcification by the acid-base sensing enzyme soluble adenylyl cyclase. Biochemical and Biophysical Research Communications 525, 3 (10.1016/j.bbrc.2020.02.115). The dissertation author was a co-author of this paper. The material is used by permission of Elsevier.

Chapter 5, in part, is a reprint of the material as it appears in Chang WW, Thies AB, Tresguerres M, Hu MY. 2023. Soluble adenylyl cyclase coordinates intracellular pH homeostasis and biomineralization in calcifying cells of a marine animal. American Journal of Physiology-Cell Physiology 324, 3 (10.1152/ajpcell.00524.2022). The dissertation author was a co-author of this paper. The material is used by permission of The American Physiological Society.

Chapter 5, in part, is a reprint of the material as it appears in Harter TS, Smith EA, Salmerón C, Thies AB, Delgado B, Wilson RW, Tresguerres M. 2024. Soluble adenylyl cyclase is an acid-base sensor in rainbow trout red blood cells that regulates intracellular pH and haemoglobin- $O_2$ binding. Acta Physiologica. The dissertation author was a co-author of this paper. The material is used by permission of Acta Physiologica (10.1111/apha.14205).

Chapter 5, in part, is a reprint of the material as it appears in Barott KL, Thies AB, Tresguerres M. 2022. V-type $H^+$-ATPase in the symbiosome membrane is a conserved mechanism for host control of photosynthesis in anthozoan photosymbioses. Royal Society Open Science 9, 1 (10.1098/rsos.211449). The dissertation author was a co-author of this paper. The material is used by permission of The Royal Society.

Chapter 5, in part, contains material currently being prepared for submission for publication. Allard C, Thies AB, Leatz E, Tresguerres M, Bellono N. (in prep) VHA Does Not

Drive a CCM in the Kleptoplastic Sacoglossan *Elysia crispata*. The dissertation author was a co-author of this paper.

Chapter 5, in part, is a reprint of the material as it appears in McFall-Ngai M, Viliunas J, Hargadon A, Koehler S, Chen G, Ladinsky M, Kuwabara J, Thies AB, Tresguerres M, Ruby E. (in prep) The acidic microenvironment produced by a V-type ATPase promotes specificity during symbiont recruitment in the squid-vibrio association. The dissertation author was a co-author of this paper.

VITA

## Education

2024 Doctor of Philosophy in Marine Biology, Scripps Institution of Oceanography, University of California San Diego

2018 Master of Science in Marine Biology, Scripps Institution of Oceanography, University of California San Diego

2017 Bachelor of Science in Marine Biology, Scripps Institution of Oceanography, University of California San Diego

## Awards & Fellowships

2021 Achievement Rewards for College Scientists (ARCS) Fellowship

2021 Best Student Research Presentation, 4th International Cassiopea Workshop

2019 National Science Foundation Graduate Research Fellowship

2019 Scripps Institution of Oceanography Fellowship

## Publications

Harter TS, Smith EA, Salmerón C, **Thies AB**, Wilson RW, Tresguerres M. 2024 Soluble adenylyl cyclase is an acid-base sensor in rainbow trout red blood cells that regulates intracellular pH and haemoglobin-oxygen binding. Acta Physiologica. (10.1111/apha.14205)

Chang WW, **Thies AB**, Tresguerres M, Hu MY. 2023 Soluble adenylyl cyclase coordinates intracellular pH homeostasis and biomineralization in calcifying cells of a marine animal. Am. J. Physiol. Physiol. 324, C777–C786. (doi:10.1152/ajpcell.00524.2022)

Camacho-Jiménez L, Peregrino-Uriarte AB, Leyva-Carrillo L, Gómez-Jiménez S, **Thies AB**, Tresguerres M, Yepiz-Plascencia G. 2023 Effects of severe hypoxia and glyceraldehyde-3-phosphate dehydrogenase (GAPDH) knock-down on its gene expression, activity, subcellular localization, and apoptosis in gills of the shrimp *Penaeus vannamei*. Mar. Freshw. Behav. Physiol. 56, 91–110. (doi:10.1080/10236244.2023.2216346)

**Thies AB**, Quijada-Rodriguez AR, Zhouyao H, Weihrauch D, Tresguerres M. 2022 A Rhesus channel in the coral symbiosome membrane suggests a novel mechanism to regulate $NH_3$ and $CO_2$ delivery to algal symbionts. *Sci. Adv.* 8. (doi:10.1126/sciadv.abm0303)

Barott KL, **Thies AB**, Tresguerres M. 2022 V-type $H^+$-ATPase in the symbiosome membrane is a conserved mechanism for host control of photosynthesis in anthozoan photosymbioses. R. Soc. Open Sci. 9. (doi:10.1098/rsos.211449)

Barott KL, Venn AA, **Thies AB**, Tambutté S, Tresguerres M. 2020 Regulation of coral calcification by the acid-base sensing enzyme soluble adenylyl cyclase. Biochem. Biophys. Res. Commun. 525, 576–580. (doi:10.1016/j.bbrc.2020.02.115)

Tresguerres M, Clifford AM, Harter TS, Roa JN, **Thies AB**, Yee DP, Brauner CJ. 2020 Evolutionary links between intra- and extracellular acid-base regulation in fish and other aquatic animals. J. Exp. Zool. Part A Ecol. Integr. Physiol., 1–17. (doi:10.1002/jez.2367)

Barron ME, **Thies AB**, Espinoza JA, Barott KL, Hamdoun A, Tresguerres M. 2018 A vesicular $Na^+/Ca^{2+}$ exchanger in coral calcifying cells. *PLoS One* **13**, e0205367. (doi:10.1371/journal.pone.0205367)

**Conference Presentations**

2022 **Thies AB**, Tresguerres M, Sabatini S, Linsmayer L, Hamilton T, Kline D. Common and species-specific effects of ocean acidification on coral photosynthesis and oxidative damage: broad implications for reef organisms. Oral presentation to the American Physiological Society Intersociety Meeting, San Diego, California, USA.

2021 **Thies AB** and Tresguerres M. Conserved carbon and nitrogen delivery mechanisms in Cnidarian photosymbioses? Oral presentation at the 4th International Cassiopea Workshop.

2018 **Thies AB**, Barron M, Tresguerres M. Potential Role of a Rh Channel in Delivery of Ammonium from Coral Host Cells to Their Endosymbiotic Algae. Oral presentation to the American Physiological Society Intersociety Meeting, New Orleans, Louisiana, USA.

2017 Barron M, **Thies AB**, Hamdoun A, Espinoza J, Tresguerres M. Sodium calcium exchanger (NCX) in coral: a potential role in calcification. Oral presentation to the Society of Experimental Biology Annual Meeting, Gothenburg, Sweden.

2017 Tresguerres M, Ortega M, **Thies AB**, Barron M, Kline D. Coral cell physiology: discovering novel mechanisms in the laboratory and testing their relevance in the field. Oral presentation to the Society of Experimental Biology Annual Meeting, Gothenburg, Sweden.

ABSTRACT OF THE DISSERTATION

Inorganic Carbon and Nitrogen Exchange Mechanisms of Cnidarian-Algal Photosymbioses

by

Angus Blacklaw Thies

Doctor of Philosophy in Marine Biology

University of California San Diego, 2024

Professor Martin Tresguerres, Chair

Photosymbioses between cnidarian hosts and Symbiodiniaceae algae enable the success of coral reef ecosystems. Algae remain photosynthetically active in symbiosis capturing light energy to fix $CO_2$, evolve $O_2$, and produce photosynthates which are transferred to hosts as substrate for growth and metabolism. Host cells phagocytose free-living algae and sequester them in arrested phagosomes, termed "symbiosomes," enabling control over symbionts' metabolisms promoting the production of photosynthates while regulating symbiont population growth. The underlying

cellular mechanisms are mostly unknown and only a V-type $H^+$-ATPase (VHA)-dependent carbon-concentrating mechanism (CCM) is documented in corals. My thesis sought to identify whether the CCM is widespread in cnidarian photosymbioses, establish the CCM's importance under various environmental conditions, and identify nitrogen transport mechanisms. Chapter 2 describes the cloning of a candidate coral $NH_3/NH_4^+$ (total ammonia, Tamm) channel (ayRhp1) from *Acropora yongei*. Heterologous expression in *Xenopus* oocytes and flux assays determined ayRhp1 is a dual $NH_3/CO_2$ gas channel. Immunofluoresence Airyscan confocal microscopy (IACM) revealed ayRhp1 is present in the symbiosome membrane where, together with VHA, it concentrates Tamm in the symbiont's microenvironment. Furthermore, ayRhp1 is preferentially present in the symbiosome membrane during the day; presumably to provide algae with Tamm to ensure photosynthate production during photosynthesis. Chapter 3 tested whether *Cassiopea* jellyfish, which host their symbiotic algae in motile cells called amebocytes, employ a CCM like that from coral host cells. Western blotting and IACM revealed that *Cassiopea* amebocytes express both VHA and carbonic anhydrase (CA) and that both proteins localized to the symbiosome membrane. Respirometry using VHA and CA inhibitors revealed significant reductions in $O_2$ evolution rate, a proxy for photosynthetic activity, suggesting that host VHA and CA are functionally coupled in the CCM. Chapter 4 explored the prevalence of the CCM in the coral *Stylophora pistillata* after acclimation to various environmental light conditions. While VHA protein abundance correlated with increased irradiance, IACM found limited symbiosomal VHA and respirometry experiments did not detect functional evidence for CCMs. Instead, VHA was prominently observed in calcifying cells, where it may contribute to pH regulation for biomineralization. Together, my thesis advances our mechanistic understanding of nutrient exchange in cnidarian photosymbioses.

# Chapter 1

# General Introduction

**Nutrient Exchange in Coral Photosymbiosis**

Tropical coral reef ecosystems are hotspots of biodiversity that house varied assemblages of fishes, invertebrates, and microbial life. Reef-building corals (phylum Cnidaria, order Scleractinia) are the keystone species in this ecosystem and are responsible for producing reef structures through the deposition of $CaCO_3$ skeletons underneath their tissues. Coral biomineralization gives rise to a diversity of skeletal structures which increase the reef's structural complexity and provide shelter for reef fauna. In addition, corals provide multiple benefits to human populations: reef structures absorb and dissipate wave energy mitigating coastal erosion (reviewed in Knowlton et al. 2010), reefs supply ~10% of human-consumed fish feeding millions worldwide (Smith 1978), and reef-associated sponges, cnidarians, seaweeds, mollusks, and microbes produce natural products of biomedical interest (reviewed in Carté 1996).

The success of coral reef ecosystems in oligotrophic oceans is owed to a metabolic photosymbiosis between coral animals and endosymbiotic dinoflagellate algae (family Symbiodiniaceae). The algae remain photosynthetically active in symbiosis capturing light energy to fix $CO_2$, evolve $O_2$, and produce photosynthates (i.e. sugars, lipids, amino acids). Any photosynthates produced in excess of the algae's needs are released to the coral host (reviewed in Davy et al. 2012) as fuel for growth and metabolism that in some cases can satisfy over 100% of the daily organic carbon demands of the animal (Verde and R. McCloskey 1998; Allemand et al. 2011; Tanaka et al. 2018). In turn, host respiration generates ample $CO_2$ that fuels symbiont photosynthesis and allows abundant release of photosynthates during the day. Protein catabolism by the coral host additionally generates a pool of nitrogenous waste that provides symbionts the majority of their nitrogen budget (Rahav et al. 1989; Tanaka et al. 2018). Algae need nitrogen to sustain a high turnover of photosystem proteins and pigments that are continuously being damaged

by ultraviolet radiation and electron transfer; therefore, nitrogen delivery to symbionts is essential for efficient photosynthesis and photosynthate supply to the coral host (Grover et al. 2002; Kopp et al. 2013; Beraud et al. 2013). Notably, corals preferentially deliver nitrogen to their symbionts during daytime when repair of photoproteins is necessitated (Grover et al. 2002; Kopp et al. 2013). This strategy helps maintain symbionts in a nitrogen-limited state and potentially regulates algal growth rates to match that of slower-dividing coral cells (Falkowski et al. 1993; Yellowlees et al. 2008). As shifts away from regulated nitrogen delivery can result in symbiont overgrowth, host cell death, and termination of the symbiosis (dysbiosis) (Rädecker et al. 2021), host-regulated nutrient cycling is an essential hallmark underpinning photosymbiosis. Nitrogen limitation of coral symbionts has been known/considered since at least 1983 (D'Elia et al. 1983; Cook and D'Elia 1987); however the molecular mechanisms enabling host control over nitrogenous metabolite exchange are unclear.

Coral hosts are believed to control the metabolism of their symbionts to promote the production and release of photosynthates while regulating their growth. This control is possible because of the architectural arrangement whereby coral gastrodermal cells phagocytose free-living algae and sequester them in arrested phagosomes, termed "symbiosomes" (reviewed in Davy et al. 2012). This arrangement entails a coral-derived intracellular membrane that isolates the symbionts both from the host cell's cytosol and the external environment and mediates all nutrient transfer into- and out of the symbiosome. The host may additionally manipulate the alga's microenvironment to promote nutrient cycling and the production and release of photosynthates. For example, some symbiosomes can be highly acidic (pH ~4) because of active $H^+$ pumping by host V-type $H^+$-ATPases (VHAs) located in the symbiosome membrane (Barott et al. 2015). The acidic nature of the symbiosome drives $CO_2$ accumulation as part of a carbon concentrating

mechanism (CCM) that helps overcome the low affinity of algal Rubisco for $CO_2$, thereby promoting algal photosynthesis (Barott et al. 2015). This $H^+$ gradient has been proposed to additionally energize the movement of other essential nutrients and metabolites into or out of the symbiosome including nitrogen, phosphorus, and sugars, and to slow down algal division (Barott et al. 2015; Tang 2015). However, no additional molecular players or regulatory mechanisms have been identified. The first goal of my doctoral research was to identify the mechanisms that mediate and regulate nitrogen transfer to symbionts; this work is presented in Chapter 2 of this dissertation.

**Nutrient Exchange in Other Cnidarians**

While the vast majority of marine photosymbiosis research has focused on coral and anemone models, photosymbiosis with Symbiodiniaceae algae has evolved multiple times within phylum Cnidaria; extant examples are present in classes Hexocoralia (corals and anemones), Octocorallia (octocorals), Scyphozoa (jellyfish), and Hydrozoa (hydroids) (Clavijo et al. 2018). Interestingly, all these hosts retain algal symbionts in symbiosomes (Davy et al. 2012; Tang 2015). This shared architectural feature has unfortunately encouraged researchers to widely apply findings from corals to all other cnidarian taxa. For example, the original VHA-dependent CCM identified in *Acropora yongei* and *Stylophora pistillata* corals grown in laboratory aquaria (Barott et al. 2015) is frequently assumed to apply to all cnidarian hosts without regard to environmental conditions (Suggett et al. 2017; Ros et al. 2021; Jacobovitz et al. 2023). However, this assumption overlooks potential evolutionary, physiological and environmental variation inherent to the various hosts.

This problem is epitomized by the Upside-Down Jellyfish, *Cassiopea ssp.* (class Scyphozoa). Like corals, *Cassiopea ssp*. hosts Symbiodiniaceae algae in symbiosomes; however, *Cassiopea ssp*. exhibit numerous differences from corals: they are highly mobile, do not produce

a skeleton, and their layer of mesoglea that connects ectodermal and endodermal tissues is greatly expanded forming the bell. These characteristics can have important implications on the physiology of the symbiosis. Furthermore, instead of hosting symbiotic algae in gastrodermal cells, *Cassiopea* host theirs in amoebocytes, which are highly mobile cells that participate in immune functions akin to vertebrate macrophages (discussed in Chapter 3). In addition, each amebocyte can host six or more symbionts (Lyndby et al. 2020; Toullec et al. 2024a, b) while coral gastrodermal cells typically host one, and two or three on rare occasions (Venn et al. 2009; Barott et al. 2015).

*Cassiopea ssp*. are a rapidly emerging model to study nervous system development, sleep and circadian rhythms, tissue regeneration, chemosensing, and photosymbiosis (Ohdera et al. 2018; Medina et al. 2021). However, it is not known whether their amebocytes utilize the same VHA-driven CCM described for coral gastrodermal cells (Barott et al 2015) or if they have evolved different mechanisms. These factors inspired my investigation of CCMs in *Cassiopea xamachana* amoebocytes, which is presented in Chapter 3 of this dissertation.

**Influence of Light on the VHA-Dependent CCM**

Solar irradiance attenuates exponentially with depth but coral hosts can be found across pronounced depth gradients: *S. pistillata* corals for example grow in light environments ranging from >1500 μE at ≥ 5m to <50 μE of photosynthetically active radiation (PAR) at 65m (Mass et al. 2007). Algal symbionts are sensitive to this gradient and remain photosynthetically active in low light environments by employing a suite of light-absorbing photopigments enabling high photosynthetic efficiency (reviewed in Roth 2014, Anthony and Hoegh-Guldberg 2003a, b; Mass et al. 2007). Notably, corals used to elucidate the VHA-driven CCM were tested at 150 μE and displayed robust photosynthetic oxygen evolution (Barott et al. 2015). In contrast, symbionts in

high light environments decrease their photosynthetic pigment content and photosynthetic efficiency. The reduction in pigments is understood to limit light absorption in excessively high light environments that would otherwise lead to photo- and oxidative damage (reviewed in Roth 2014). Despite their lower pigment content and photosynthetic efficiency, symbionts exhibit higher rates of gross photosynthesis and photosynthate production in high light conditions due to overall greater solar input. As a result, symbionts in high light environments are predicted to require two to four fold more $CO_2$/DIC to sustain photosynthesis than their low-light adapted counterparts (Mass et al. 2007). Given our current understanding that the coral CCM saturates Rubisco with $CO_2$, we asked whether corals regulate VHA-driven CCM expression across light gradients to match DIC delivery rates with algal DIC demands. While one might intuit that corals employ more CCMs at high light conditions based on increased algal DIC demand, work on CCMs in other marine models paint a complicated picture. VHA-driven CCMs in giant clams (phylum Mollusca) contribute equally to symbiont photosynthesis in light environments ranging from 235-2000 μE PAR (Armstrong et al. 2018). In contrast, VHA-driven CCMs in free-living diatoms make the largest contribution to photosynthesis in light-limiting environments (<500 μE PAR) (Yee et al. 2023). We addressed this question by raising *S. pistillata* corals under three ambient light conditions and exploring the contributions of coral CCMs to symbiont photosynthesis. Assessing VHA's contribution to coral CCMs is complicated as VHA is present in multiple cell types and localizes to a myriad of intracellular compartments including golgi, endoplasmic reticulum, and vesicles (Jefferies et al. 2008); therefore, transcriptomic and Western blotting analysis of bulk coral tissues cannot adequately predict VHA's function. Instead, we utilized a combination of Western blotting on samples enriched for coral host cells, immunolocalization confocal and

Airyscan microscopy, and functional respirometry experiments to assess VHA's contribution to CCMs across light environments; this data is presented in Chapter 4 of this dissertation.

**Additional Topics of Study**

Active research in the Tresguerres Comparative Marine Physiology Lab focuses on topics related to acid/base regulation in cnidarians, mollusks, echinoderms, chondrichthyans, and teleosts. In addition to my thesis research on cnidarians, I contributed to seven studies as a co-author which focused on acid/base related topics. These studies (1) review pH microenvironments in corals, explore the role of the molecular pH sensor soluble adenyl cyclase (sAC) in (2) coral and (3) sea urchin calcification, (4) identify sAC's role in pHi regulation and hemoglobin-$O_2$ binding in trout red blood cells, (5) demonstrate VHA's involvement in promoting anemone photosynthesis, (6) examine the role of VHA in sacoglossan sea slug kleptoplasty, and (7) establish VHA's contribution to promoting symbiont selectivity in the bobtail squid. Study abstracts and data I contributed are presented in Chapter 5.

**References**


Allemand D, Tambutté É, Zoccola D, Tambutté S (2011) Coral Calcification, Cells to Reefs. In: Dubinsky Z, Stambler N (eds) Coral Reefs: An Ecosystem in Transition. Springer Netherlands, Dordrecht, pp 119–150

Armstrong EJ, Roa JN, Stillman JH, Tresguerres M (2018) Symbiont photosynthesis in giant clams is promoted by V-type H + -ATPase from host cells. Journal of Experimental Biology. https://doi.org/10.1242/jeb.177220

Barott KL, Venn AA, Perez SO, et al (2015) Coral host cells acidify symbiotic algal microenvironment to promote photosynthesis. Proceedings of the National Academy of Sciences of the United States of America 112:607–612. https://doi.org/10.1073/pnas.1413483112

Beraud E, Gevaert F, Rottier C, Ferrier-Pages C (2013) The response of the scleractinian coral Turbinaria reniformis to thermal stress depends on the nitrogen status of the coral holobiont. Journal of Experimental Biology 216:2665–2674. https://doi.org/10.1242/jeb.085183

Carté BK (1996) Potential of Marine Biomedical Natural Products research and medical applications. Oxford Journals 46:271–286

Clavijo JM, Donath A, Serôdio J, Christa G (2018) Polymorphic adaptations in metazoans to establish and maintain photosymbioses. Biological Reviews 93:2006–2020. https://doi.org/10.1111/brv.12430

Cook CB, D'Elia CF (1987) Are Natural Populations of Zooxanthellae Ever Nutrient-Limited? Symbiosis 4:199–211

Davy SK, Allemand D, Weis VM (2012) Cell biology of cnidarian-dinoflagellate symbiosis. Microbiology and Molecular Biology Reviews 76:229–261. https://doi.org/10.1128/MMBR.05014-11

D'Elia C, Domotor S, Webb K (1983) Nutrient uptake kinetics of freshly isolated zooxanthellae*. Marine Biology 167:157–167

Falkowski PG, Dubinsky Z, Muscatine L, McCloskey L (1993) Population control in symbiotic corals - Ammonium ions and organic materials maintain the density of zooxanthellae. BioScience 43:606–611. https://doi.org/10.2307/1312147

Grover R, Maguer J-F, Reynaud-vaganay S, Ferrier-Pagès C (2002) Uptake of ammonium by the scleractinian coral Stylophora pistillata: Effect of feeding, light, and ammonium concentrations. Limnology and Oceanography 47:782–790. https://doi.org/10.4319/lo.2002.47.3.0782

Jacobovitz MR, Hambleton EA, Guse A (2023) Unlocking the Complex Cell Biology of Coral–Dinoflagellate Symbiosis: A Model Systems Approach. Annual Review of Genetics 57:1–24. https://doi.org/10.1146/annurev-genet-072320-125436

Jefferies KC, Cipriano DJ, Forgac M (2008) Function, structure and regulation of the vacuolar (H+)-ATPases. Archives of Biochemistry and Biophysics 476:33–42. https://doi.org/10.1016/j.abb.2008.03.025

Knowlton N, Brainard RE, Fisher R, et al (2010) Coral Reef Biodiversity. In: Life in the World's Oceans: Diversity, Distribution, and Abundance. Wiley-Blackwell, pp 65–78

Kopp C, Pernice M, Domart-Coulon I, et al (2013) Highly Dynamic Cellular-Level Response of Symbiotic Coral to a Sudden Increase in Environmental Nitrogen. mBio 4:1–9. https://doi.org/10.1128/mBio.00052-13

Lyndby NH, Rädecker N, Bessette S, et al (2020) Amoebocytes facilitate efficient carbon and nitrogen assimilation in the Cassiopea-Symbiodiniaceae symbiosis: Nutrient transport in Cassiopea. Proceedings of the Royal Society B: Biological Sciences 287:. https://doi.org/10.1098/rspb.2020.2393rspb20202393

Mass T, Einbinder S, Brokovich E, et al (2007) Photoacclimation of Stylophora pistillata to light extremes: metabolism and calcification. Mar Ecol Prog Ser 334:93–102. https://doi.org/10.3354/meps334093

Medina M, Sharp V, Ohdera A, et al (2021) The upside-down Jellyfish Cassiopea xamachana as an emerging model system to study Cnidarian-Algal symbiosis. Handbook of Marine Model Organisms in Experimental Biology: Established and Emerging 149–171. https://doi.org/10.1201/9781003217503-9

Ohdera AH, Abrams MJ, Ames CL, et al (2018) Upside-down but headed in the right direction: Review of the highly versatile Cassiopea xamachana system. Frontiers in Ecology and Evolution 6:1–15. https://doi.org/10.3389/fevo.2018.00035

Rädecker N, Pogoreutz C, Gegner HM, et al (2021) Heat stress destabilizes symbiotic nutrient cycling in corals. Proceeding of the National Academy of Sciences of the United Stated of America 118:e2022653118. https://doi.org/10.1073/pnas.2022653118

Rahav O, Dubinsky Z, Achituv Y, Falkowski PG (1989) Ammonium metabolism in the zooxanthellate coral, *Stylophora pistillata*. Proc R Soc B 337:325–337

Ros M, Suggett DJ, Edmondson J, et al (2021) Symbiont shuffling across environmental gradients aligns with changes in carbon uptake and translocation in the reef-building coral Pocillopora acuta. Coral Reefs 40:595–607. https://doi.org/10.1007/s00338-021-02066-1

Roth MS (2014) The engine of the reef: photobiology of the coral-algal symbiosis. Front Microbiol 5:. https://doi.org/10.3389/fmicb.2014.00422

Smith SV (1978) Coral-reef area and the contributions of reefs to processes and resources of the world ' s oceans Production of methane and carbon dioxoue from methane thiol and dimethyl sulphide by anaerobic lake sediments. Nature 273:225–226

Suggett DJ, Warner ME, Leggat W (2017) Symbiotic Dinoflagellate Functional Diversity Mediates Coral Survival under Ecological Crisis. Trends in Ecology & Evolution 32:735–745. https://doi.org/10.1016/j.tree.2017.07.013

Tanaka Y, Suzuki A, Sakai K (2018) The stoichiometry of coral-dinoflagellate symbiosis: carbon and nitrogen cycles are balanced in the recycling and double translocation system. ISME Journal 12:860–868. https://doi.org/10.1038/s41396-017-0019-3

Tang BL (2015) Thoughts on a very acidic symbiosome. Frontiers in Microbiology 6:4–7. https://doi.org/10.3389/fmicb.2015.00816

Toullec G, Lyndby NH, Banc-Prandi G, et al (2024a) Symbiotic nutrient exchange enhances the long-term survival of cassiosomes, the autonomous stinging-cell structures of *Cassiopea*. mSphere 9:e00322-23. https://doi.org/10.1128/msphere.00322-23

Toullec G, Rädecker N, Pogoreutz C, et al (2024b) Host starvation and in hospite degradation of algal symbionts shape the heat stress response of the Cassiopea-Symbiodiniaceae symbiosis. Microbiome 12:42. https://doi.org/10.1186/s40168-023-01738-0

Venn AA, Tambutté E, Lotto S, et al (2009) Imaging intracellular pH in a reef coral and symbiotic anemone. Proceedings of the National Academy of Sciences of the United States of America 106:16574–9. https://doi.org/10.1073/pnas.0902894106

Verde E, R. McCloskey L (1998) Production, respiration, and photophysiology of the mangrove jellyfish Cassiopea xamachana symbiotic with zooxanthellae: effect of jellyfish size and season. Marine Ecology Progress Series 168:147–162

Yee DP, Samo TJ, Abbriano RM, et al (2023) The V-type ATPase enhances photosynthesis in marine phytoplankton and further links phagocytosis to symbiogenesis. Current Biology 33:2541-2547.e5. https://doi.org/10.1016/j.cub.2023.05.020

Yellowlees D, Rees TAV, Leggat W (2008) Metabolic interactions between algal symbionts and invertebrate hosts. Plant, Cell & Environment 31:679–694. https://doi.org/10.1111/j.1365-3040.2008.01802.x

Chapter 2

# A Rhesus channel in the coral symbiosome membrane suggests a novel mechanism to regulate $NH_3$ and $CO_2$ delivery to algal symbionts

CELL BIOLOGY

# A Rhesus channel in the coral symbiosome membrane suggests a novel mechanism to regulate $NH_3$ and $CO_2$ delivery to algal symbionts

**Angus B. Thies[1]*, Alex R. Quijada-Rodriguez[2], Haonan Zhouyao[2], Dirk Weihrauch[2], Martin Tresguerres[1]***



**Reef-building corals maintain an intracellular photosymbiotic association with dinoflagellate algae. As the algae are hosted inside the symbiosome, all metabolic exchanges must take place across the symbiosome membrane. Using functional studies in *Xenopus* oocytes, immunolocalization, and confocal Airyscan microscopy, we established that *Acropora yongei* Rh (ayRhp1) facilitates transmembrane $NH_3$ and $CO_2$ diffusion and that it is present in the symbiosome membrane. Furthermore, ayRhp1 abundance in the symbiosome membrane was highest around midday and lowest around midnight. We conclude that ayRhp1 mediates a symbiosomal $NH_4^+$-trapping mechanism that promotes nitrogen delivery to algae during the day—necessary to sustain photosynthesis—and restricts nitrogen delivery at night—to keep algae under nitrogen limitation. The role of ayRhp1-facilitated $CO_2$ diffusion is less clear, but it may have implications for metabolic dysregulation between symbiotic partners and bleaching. This previously unknown mechanism expands our understanding of symbioses at the immediate animal-microbe interface, the symbiosome.**

## INTRODUCTION

Photosymbiotic associations between invertebrates and microalgae are widespread in aquatic environments. Perhaps the most well known of these partnerships is that of reef-building corals (phylum: Cnidaria) and dinoflagellate symbiotic algae (family: Symbiodiniaceae), which is key to the evolutionary success of coral reef ecosystems (*1*). In an otherwise oligotrophic environment, the cnidarian host satisfies the majority of its energetic needs using photosynthates derived from its symbiotic algae (*2*). The host cells are believed to exercise considerable control over the metabolism of their symbionts, which favors both the production and release of algal photosynthates. This control is possible because of an architectural arrangement whereby coral gastrodermal cells host the algal symbionts intracellularly within an arrested phagosome known as the symbiosome [reviewed in (*3*)]. Because the symbiosome isolates the alga from the cytosol of the host cell, the symbiosome membrane necessarily mediates all metabolic exchanges between the symbiotic partners. In addition, the symbiosome membrane may serve as an interface for the coral to manipulate the alga's microenvironment. For example, the coral symbiosome is markedly acidic (pH ~4) because of active $H^+$ pumping by V-type $H^+$-ATPases (VHAs) located in the symbiosome membrane (*4*). The acidic nature of the symbiosome drives $CO_2$ accumulation as part of a carbon concentrating mechanism (CCM) that helps overcome the low affinity of algal Rubisco for $CO_2$, thereby promoting algal photosynthesis (*4*). This $H^+$ gradient has been proposed to additionally energize the movement of other essential nutrients and metabolites into or out of the symbiosome including nitrogen, phosphorus, and sugars (*3*, *4*). However, no additional molecular players or regulatory mechanisms have been definitely identified to date.

The vast majority of the symbiotic algae's nitrogen demand is supplied by protein catabolism by their animal host, which produces waste as ammonia gas ($NH_3$) and ammonium ion ($NH_4^+$), which exist in a pH-dependent equilibrium [collectively referred to as "total ammonia" (Tamm)] (*2*, *5*). Rather than excreting its nitrogenous waste into the environment like most other aquatic animals (*6*), the coral symbiosis recycles a substantial portion of Tamm via the glutamine synthase/glutamate dehydrogenase/glutamine oxoglutarate aminotransferase pathways (GS/GDH/GOGAT) (*5*, *7*, *8*). In addition, corals are able to take up $NH_4^+$ from seawater and transport it to their algal symbionts (*9*), and isolated algal symbionts take up and use $NH_4^+$ (*10*). Moreover, coral host cells are known to regulate Tamm delivery to their symbionts, and as a result, the algae accumulate significantly more nitrogen in the light than in the dark (*9*, *11*). The diel regulation of Tamm delivery by corals allows for host control over the carbon and nitrogen metabolisms of symbionts (*12*) and, by extension, the growth rate and biomass of the symbiont population to prevent symbiont overgrowth that would disrupt the symbiosis (*13*). Transcriptomic analyses on whole coral colonies have identified candidate transporters proposed to mediate Tamm delivery to symbionts (*14*), but a lack of localization studies precludes a definite assessment of their involvement in symbiosis. Overall, the mechanisms that mediate and regulate nitrogen transport to symbionts across the symbiosome membrane remain unknown.

$NH_3$ and $NH_4^+$ exist in pH-dependent equilibrium with pKa ~9.25, and thus >96% of Tamm is found as $NH_4^+$ both in seawater (pH ~8) and in coral host cells (pH ~7.4) (*15*). However, the much lower pH in the symbiosome space has three critical and interlinked implications: first, a virtually nil $NH_3$ partial pressure ($pNH_3$) in the symbiosome space that should drive $NH_3$ gas diffusion from the host cytoplasm; second, the immediate "trapping" of $NH_3$ as $NH_4^+$ in the symbiosome space, which can be taken up by the alga, thus maintaining the inwardly directed $NH_3$ diffusion gradient; and lastly, an unfavorable electrochemical gradient for $NH_4^+$ transport into the symbiosome.

However, despite being a gas, $NH_3$ has limited permeability through lipidic membranes because of its strong dipole moment that makes

[1]Marine Biology research Division, Scripps Institution of Oceanography, University of California, San Diego, La Jolla, CA 92093, USA. [2]Department of Biological Sciences, University of Manitoba, Winnipeg, MB, Canada.
*Corresponding author. Email: athies@ucsd.edu (A.B.T.); mtresguerres@ucsd.edu (M.T.)

it a polar molecule [reviewed in (*16*)]. In some plant-bacteria symbioses, $NH_3$ transport across the symbiosome membrane is facilitated by nodulin-intrinsic proteins (*17*, *18*); however, this protein family is exclusive to plants. In addition, $NH_3$ diffusion across biological membranes can be significantly enhanced by Rhesus (Rh) channels, a family of evolutionary conserved proteins present in eubacterial, invertebrate, and vertebrate lineages (*19*–*21*). On the basis of the observed up-regulation of an Rh-like mRNA transcript upon establishment of symbiosis in anemones (*22*–*24*), Rh channels have been suggested to play important roles in cnidarian-algae symbioses. However, the Rh-like mRNA was expressed in many soft coral cell subtypes (*25*), and therefore, the coded protein probably plays multiple physiological roles. In addition, Rh channels are typically present in the cell outer plasma membrane [reviewed in (*16*, *26*)], and few studies have localized Rh-like proteins to intracellular compartments or organelles (*27*, *28*). Last, the various Rh protein isoforms have different substrate specificity: some may transport both $NH_3$ and $NH_4^+$ (*16*), some act as dual $NH_3$ and $CO_2$ gas channels (*19*, *29*, *30*), and others do not facilitate Tamm/$CO_2$ transport across membranes at all and have structural functions instead (*31*, *32*). However, detailed functional studies about transport properties by "primitive" Rh proteins from invertebrate animals (termed "Rhp") are very scarce. As a result, assessing the physiological role of the coral Rh-like coded protein and its potential involvement in delivering Tamm to algal endosymbionts requires elucidating its actual function as well as its cellular and subcellular localizations. Furthermore, if coral Rh facilitated $CO_2$ diffusion and was present on the symbiosome membrane, it would provide a pathway for $CO_2$ backflow from the symbiosome into the coral gastrodermal cells and affect interactions between nitrogen transport and the CCM.

Given that $NH_3$ diffusion through biological membranes is limited, we hypothesized that corals use Rh-like proteins to deliver $NH_3$ to their algae across the symbiosome membrane, which would subsequently get trapped as $NH_4^+$ in the acidic symbiosome. To investigate this possibility, we cloned an Rh-like gene from the coral *Acropora yongei* (*ayRhp1*) and determined its phylogenetic relationship to other Tamm-transporting proteins. Then, we heterologously expressed ayRhp1 protein in *Xenopus* oocytes and measured Tamm transport under a range of pHs to determine whether it transports $NH_3$, $NH_4^+$, or both. In additional oocyte experiments, we determined whether ayRhp1 facilitates $CO_2$ diffusion. Using custom-made antibodies and immunocytochemistry, we established the localization of ayRhp1 protein in the various cell subtypes throughout the coral colony, and, using confocal Airyscan microscopy, we investigated whether ayRhp1 was specifically located in the symbiosome membrane. Last, we quantified the subcellular localization of ayRhp1 within algae-containing coral gastrodermal cells throughout a diel cycle to explore a potential mechanism whereby coral host cells could regulate Tamm delivery to their algal symbionts.

## RESULTS AND DISCUSSION

### *Rhp1* genes are widespread in corals

The cloned *ayRhp1* cDNA open reading frame contains 1440 base pairs encoding a protein with a predicted molecular weight of 51.8 kDa. BLAST searches in genomic and transcriptomic databases revealed predicted ayRhp1 homologs in multiple coral species from both the robust and complex clades, which diverged from each other 300 million to 400 million years ago (*33*). These coral Rh proteins clustered together with *Rhp1* genes from invertebrate animals (fig. S1).

The protein features of ayRhp1 are similar to those of well-studied Rh channels from mammals (fig. S2). It has 12 transmembrane helices and an N-linked glycosylation site (N61), which differentiate all animal Rh50 channels capable of Tamm transport (Rhag-cg, Rhp1-2) (*16*) from the Rh30 proteins involved in structural functions (*27*). Crystallography and simulation studies have identified several key amino acid residues that are required for $NH_3$ transport across mammalian RhCG (*20*, *21*): a phenylalanine gate (F130 and F235) and a cytosolic shunt (L193, T325, L328, I334, N341, and N342), which recruit $NH_4^+$ at the external and internal vestibules, respectively, twin histidines that deprotonate $NH_4^+$ to $NH_3$ (H185 and H344), two highly conserved aspartic acid residues that help shuttle the $H^+$ back to the original compartment (D177 and D336), and a hydrophobic transmembrane channel that selectively conducts $NH_3$ but not $NH_4^+$ (*32*, *34*). An alignment of ayRhp1 with RhCG reveals that the phenylalanine gate (F147 and F251), the twin histidines (H202 and H364), and analogous aspartate residues (D195 and D356) are all conserved in ayRhp1, while the cytosolic shunt and hydrophobic channel-lining residues are highly conserved (~83 and ~70%, respectively). In addition, ayRhp1 contains the nine residues that form the putative cytoplasmic $CO_2$ binding pocket of mammalian RhCG [which facilitates $CO_2$ transport (*19*)]: L91, F94, D234, A237, M238, M299, V300, Q303, and N304. Six of these residues are also conserved in the Rh protein from the bacterium *Nitrosomonas europaea*, where the $CO_2$ binding pocket was definitely identified using x-ray crystallography (*35*). In summary, the overall high conservation of these key structures suggests that ayRhp1 can facilitate both $NH_3$ and $CO_2$ transport; this was experimentally tested through functional studies.

### ayRhp1 facilitates $NH_3$ and $CO_2$ diffusion

ayRhp1 was functionally characterized by measuring Tamm uptake rates in *Xenopus* oocytes injected with ayRhp1 cRNA. To avoid potential artifacts resulting from using radiolabeled [$^{14}$C]-methylammonium as a Tamm analog (*16*), we used a hypochlorite-salicylate-nitroprusside–based colorimetric assay to directly measure Tamm accumulation in oocytes and estimate Tamm uptake rate. The bath solutions contained 1 mM Tamm at pH 6.5, 7.5, or 8.5, resulting in 10-fold pKa-dependent [$NH_3$] increases for every pH unit (1.8, 17.4, and 150.5 μM, respectively). ayRhp1-expressing oocytes had consistently higher Tamm uptake rates than those of controls in all conditions tested ($P < 0.001$; fig. S3). In addition, Tamm uptake rate in ayRhp1 oocytes significantly increased from 10.2 ± 1.4 pmol Tamm min$^{-1}$ at pH 6.5, to 36.9 ± 2.8 pmol Tamm min$^{-1}$ at pH 7.5, and to 49.6 pmol Tamm min$^{-1}$ at pH 8.5 (Fig. 1A), an apparent $J_{max}$ and $K_m$ of 51.93 ± 1.45 pmol Tamm min$^{-1}$ and 7.14 ± 0.91 μmol Tamm liter$^{-1}$, respectively (Fig. 1B). These results indicate that ayRhp1 transports $NH_3$ following the partial pressure difference. In addition, Tamm uptake rate of oocytes incubated in a solution with 10 mM Tamm at pH 7.5 was 50.3 ± 10.0 pmol Tamm min$^{-1}$ (i.e., indistinguishable from the rate in the 1 mM Tamm pH 8.5 solution) (Fig. 1B). These two solutions have similar [$NH_3$] (174.0 versus 150.5 μM), but the former has >10-fold greater [$NH_4^+$] than the latter (9826.0 μM versus 849.5 μM). Together, these results established that ayRhp1 can facilitate $NH_3$ diffusion following pH-dependent partial pressure gradients and that Tamm transport is not directly dependent on the [$NH_4^+$] difference.

Next, we preloaded control and ayRhp1 cRNA-injected oocytes with 5% $CO_2$ and measured $CO_2$ release into normocapnic media

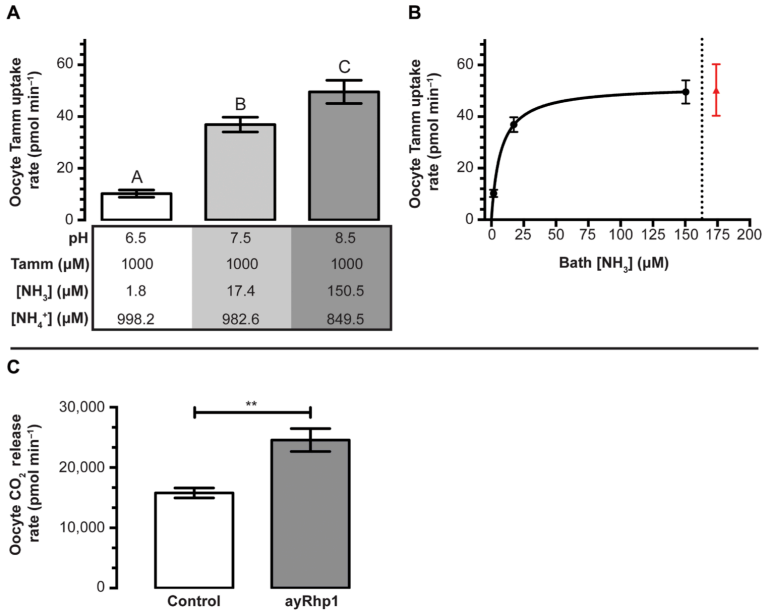


**Fig. 1. Functional characterization of total ammonia (Tamm) and $CO_2$ transport by *Acropora yongei* Rhesus protein (ayRhp1).** (**A**) Effect of [$NH_3$] on Tamm uptake rate in *Xenopus* oocytes expressing ayRhp1. Control Tamm uptake rates have been subtracted. Data show means ± SEM of six to eight oocytes; the letters denote significant differences [one-way analysis of variance (ANOVA) followed by Tukey's multiple comparisons test; pH 6.5 versus pH 7.5, $P < 0.0001$; pH 7.5 versus pH 8.5, $P = 0.0222$; pH 6.5 versus pH 8.5, $P < 0.0001$]. (**B**) Michaelis-Menten Tamm uptake kinetics calculated from the data shown in (A) (black dots to the left of the dotted line). Apparent $J_{max} = 51.93 \pm 1.45$ pmol Tamm $min^{-1}$ and $K_m = 7.14 \pm 0.91$ μmol Tamm $liter^{-1}$. The red triangle indicates Tamm uptake rate obtained in a solution with 10 mM Tamm at pH 7.5 (175 μM $NH_3$ and 9.825 mM $NH_4^+$) (i.e., similar [$NH_3$] to the previous data point, but ~10-fold higher [$NH_4^+$]). (**C**) Functional characterization of $CO_2$ transport by ayRhp1. *Xenopus* oocytes expressing ayRhp1 (ayRhp1) display a higher rate of $CO_2$ release than control oocytes after equal $CO_2$ preloading. Data show means ± SEM of $n = 8$, 25 oocytes per $n$; ** denotes significant differences (Welch's $t$ test; $P = 0.0019$).

using a custom-built $CO_2$ analyzer (*36*). These experiments revealed that ayRhp1-expressing oocytes released $CO_2$ at a rate ~50% faster than control oocytes ($P = 0.0019$; Fig. 1C). As wild-type *Xenopus* oocytes lack notable $HCO_3^-$ efflux (*37*), this demonstrates that ayRhp1 can facilitate the diffusion of $CO_2$ in addition to $NH_3$.

### ayRhp1 protein is present in multiple coral cell types

Immunofluorescence microscopy using custom-made–specific antibodies revealed high ayRhp1 protein expression throughout *A. yongei* coral tissue sections (Fig. 2A). In the epidermis, ayRhp1 was present in the apical membrane of columnar cells along the seawater-coral interface (Figs. $2B_1$ and 3A). Although corals recycle most of their nitrogen waste through their algal symbionts, they also excrete some Tamm to the environment (*2*, *7*). Thus, we hypothesize that ayRhp1 in epidermal cells aids in nitrogenous waste excretion as previously described in gills and skin from fish and aquatic invertebrates (*38*, *39*). Moreover, Tamm excretion may be facilitated by stirring of the boundary layer by ciliary beating, akin to mussels and polychaetes (*38*, *40*).

In the calicodermis, ayRhp1 was expressed in both calcifying cells that deliver dissolved inorganic carbon (DIC), $Ca^{2+}$, and matrix proteins for skeletal formation and in desmocytes that anchor living coral tissue to the skeleton. The ayRhp1 signal in desmocytes was very intense, especially at the apical membrane adjacent to the skeleton (Figs. $2C_1$ and 3B and fig. $S4A_1$). Previous studies have provided morphological descriptions of coral desmocytes (*41*, *42*); however, to our knowledge, this is the first description of any protein specifically expressed in this cell type. As an $NH_3$ channel, ayRhp1 may contribute to coral calcification by enhancing $NH_3$ diffusion to buffer the pH of the extracellular calcifying medium (ECM) and maintain conditions favorable for calcification. Metabolic $NH_3$ has been proposed to promote biological calcification of avian egg shells (*43*), land snail shells (*44*), and coral skeletons (*45*) by buffering $H^+$ produced during $CaCO_3$ precipitation as $NH_4^+$. As a $CO_2$ channel, ayRhp1 could help deliver DIC to the ECM following the outwardly directed $pCO_2$ gradient favoring $CO_2$ diffusion from calicodermis cells into the ECM, which is an important source of DIC for calcification in multiple coral species (*46*, *47*). In the gastroderm, ayRhp1 was highly expressed in alga-hosting coral cells surrounding the symbiotic algae (Fig. $2D_1$), in a pattern that resembled that of VHA in the symbiosome membrane (*4*). This was explored in further detail.

### ayRhp1 is present in the symbiosome membrane

Confocal Airyscan microscopy and coimmunostaining of ayRhp1 and $Na^+/K^+$-ATPase (NKA) allowed us to definitively establish ayRhp1's subcellular localization within the tightly packaged host cells in coral

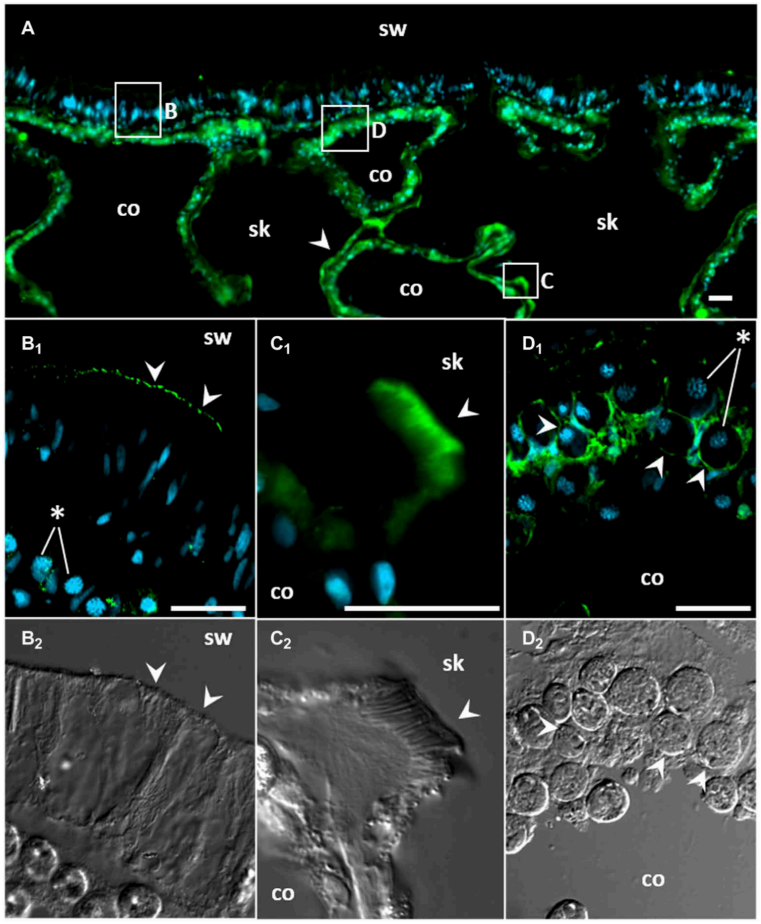


**Fig. 2. Immunolocalization of *Acropora yongei* Rhesus protein (ayRhp1).** (**A**) Overview of *A. yongei* tissues; the boxes indicate regions of interest shown at higher magnification below, and the white arrowhead indicates ayRhp1-labeled calcifying cells. (**$B_1$**) Apical membrane of columnar cells in the oral epidermis. (**$C_1$**) Desmocyte with intense signal in its apical region. (**$D_1$**) Alga-containing gastrodermal cells. (**$B_2$**, **$C_2$**, and **$D_2$**) Corresponding bright-field differential interference contrast images; the white arrowheads mark corresponding locations in (B), (C), and (D). Coral and algal nuclei are shown in blue, and ayRhp1 immunofluorescence is shown in green. Several algal nuclei are marked with asterisks in ($B_1$) and ($D_1$) for clarity. This coral was sampled at midday. sw, seawater; co, coelenteron; sk, skeleton. Scale bars, 20 μm.

tissues. Consistent with its universal presence in the plasma membrane (*48*), NKA outlined the perimeter of all alga-containing host cells (Fig. 4, A and B). The ayRhp1 signal was also present around the algae; but in most cells, it was internal to that of NKA and also present in the thin region between the host cell nucleus and the alga (Fig. 4 $A_1$). Since these cells are tightly packed, this region is occupied by the symbiosome membrane (*4*, *49*). This was most readily evident in the region adjacent to the coral nucleus where a region of cytosol separates the external NKA and internal ayRhp1 signals, further indicating their respective presence in the plasma and symbiosome membranes (Figs. 4$A_2$ and 3). The symbiosomal localization of ayRhp1 was further confirmed in host cells containing two algae (fig. S5C), which are rather scarce but contain a larger cytoplasmic region that allows for better visualization of subcellular compartments. In addition, a minority of cells lacked ayRhp1 in the region between the host nucleus and the algae (Fig. 4B), which instead colocalized with or appeared slightly internal to NKA around the nuclear periphery, indicating ayRhp1's presence in the host plasma membrane, cytosolic vesicles, or both. We attempted to quantify the two ayRhp1 subcellular localization patterns using tissue sections; however, the high density of tightly packed gastrodermal cells coupled with their intense NKA signal confounded imaging and prevented an unbiased approach. To circumvent these limitations, we immunostained isolated coral cells, an approach we previously used to confirm

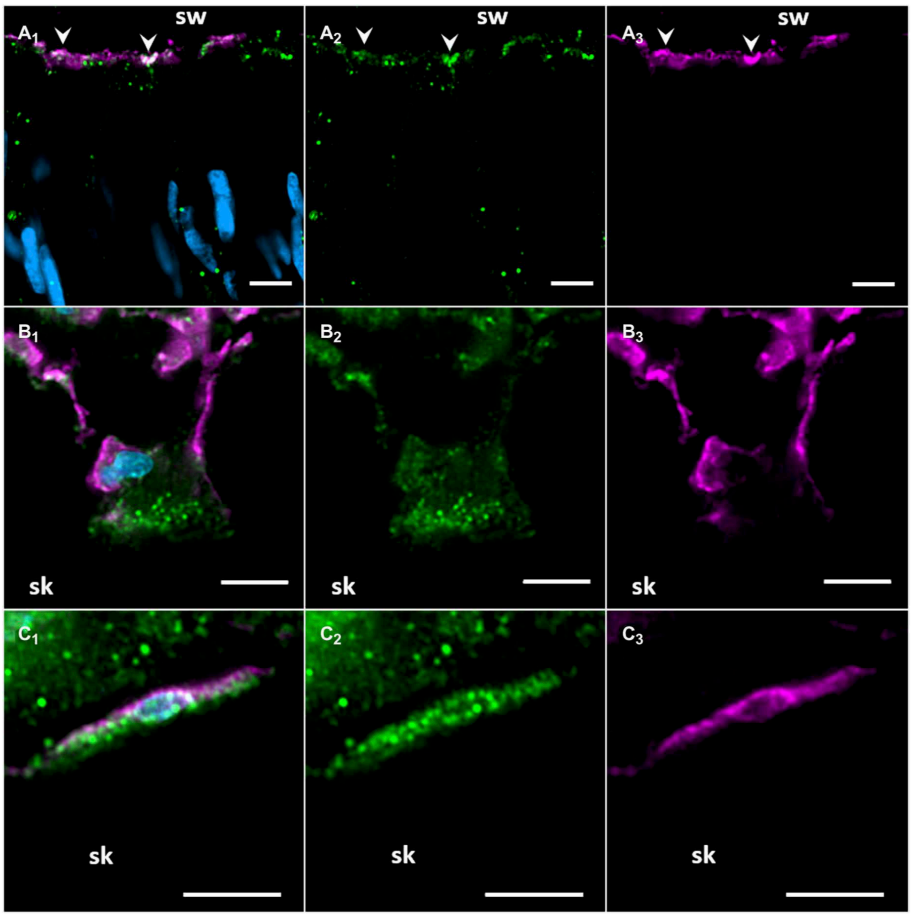


**Fig. 3. Confocal Airyscan immunolocalization of *Acropora yongei* Rhesus protein (ayRhp1) in the oral epidermis, desmocytes, and calcifying cells.** (**$A_{1–3}$**) ayRhp1 on the apical membrane of columnar cells in the oral epidermis. (**$B_{1–3}$**) Desmocyte with intense ayRhp1 signal in its apical region. (**$C_{1–3}$**) Calcifying cells displaying ayRhp1 signal on membranes and in the cytosol. Corresponding areas between panels are marked with arrowheads. [($A_1$) to ($C_1$)], [($A_2$) to ($C_2$)], and [($A_3$) to ($C_3$)] show ayRhp1, $Na^+/K^+$-ATPase (NKA), and 4′,6-diamidino-2-phenylindole (DAPI) signals, ayRhp1 signal alone, or NKA signal alone, respectively. Nuclei (DAPI) are shown in blue, ayRhp1 in green, and the NKA in purple. Scale bars, 5 μm.

the presence of VHA in the symbiosome membrane (*4*). Similar to tissue sections, a majority of isolated cells displayed ayRhp1 signal in the thin region between the host cell nucleus and the alga, indicative of ayRhp1 symbiosomal localization (fig. S5, B, C, and E to I). We also observed a minority of cells with ayRhp1 signal around the host cell nucleus (fig. S5, D and J to N), indicative of ayRhp1's presence in the cytoplasm or plasma membrane of the host cell. Free algal cells released during the isolation procedure, identified by the lack of an adjacent host nucleus, did not have ayRhp1 signal (fig. S5A).

### Diel trafficking of ayRhp1

On the basis of established patterns of nitrogen delivery to coral algal symbionts (*9*, *11*), we hypothesized that the ayRhp1 subcellular localization would change in a diel fashion. We therefore quantified ayRhp1 subcellular localization patterns using epifluorescence microscopy on isolated alga-containing coral cells over a diel cycle. This allowed us to achieve sufficient replication (50 cells from 18 coral branches, 3 coral branches at each of six time points, for a total of 900 cells observed in blind fashion). Once an algal-containing coral host cell was identified, the observer rapidly and continuously shifted the focal plane and alternated between fluorescence and bright-field DIC while looking through the microscope eyepiece. This technique allowed the observer to determine whether the ayRhp1 signal was present in between the host cell nucleus and the alga (classified as "symbiosomal localization"; Fig. 4A and fig. S5, B, C, and E to I), or around the periphery of the host cell's nucleus ("nonsymbiosomal

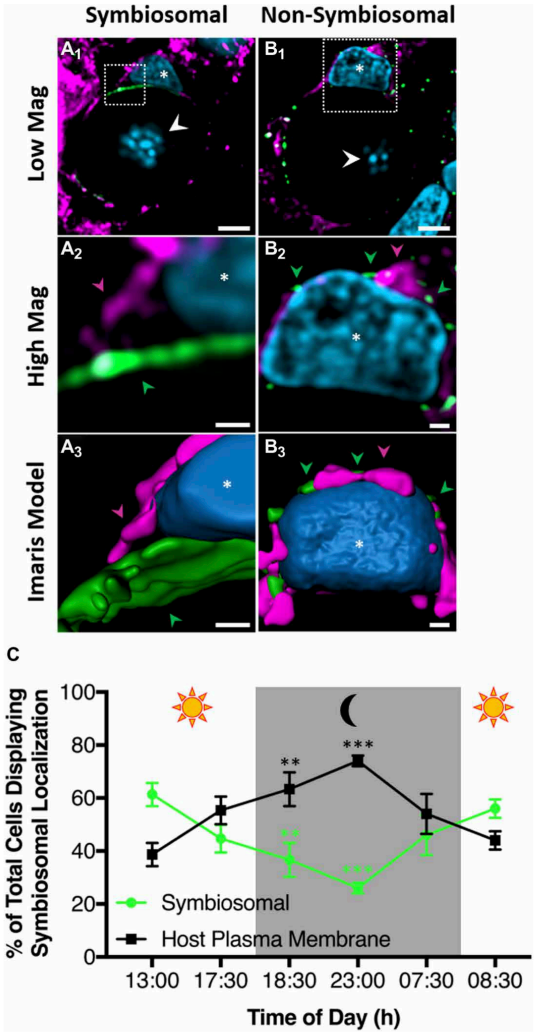


**Fig. 4. Confocal Airyscan immunolocalization of *Acropora yongei* Rhesus protein (ayRhp1) in alga-containing coral cells.** (**$A_1$**) Cells displaying ayRhp1 in the symbiosome membrane of tissue sections. (**$B_1$**) Cells displaying nonsymbiosomal ayRhp1 of tissue sections. (**$A_2$** and **$B_2$**) Higher magnification of the region denoted by the white boxes in ($A_1$) and ($B_1$). (**$A_3$** and **$B_3$**) Three-dimensional renderings of ($A_2$) and ($B_2$). Corresponding areas between ($A_2$) and ($B_2$) and ($A_3$) and ($B_3$) are marked. Nuclei are shown in blue, ayRhp1 in green, and the NKA in purple. Notice the separation ($A_{1–3}$) or colocalization ($B_{1–3}$) of ayRhp1 and NKA corresponding to symbiosomal or nonsymbiosomal ayRhp1 localizations, respectively. Host nuclei are denoted with an asterisk, and algal nuclei with arrowheads. Scale bars, 5 μm ($A_1$ and $B_1$), 0.5 μm ($A_2$ and $B_2$), and 0.5 μm ($A_3$ and $B_3$). (**C**) Percentage of total alga-containing *A. yongei* host cells with symbiosomal ayRhp1 over a diel cycle. Data show means ± SEM. $n = 3$ per time point, 50 cells per $n$, 900 cells total. The asterisks indicate significant differences with the 1300-hour time point (two-way repeated-measures ANOVA followed by Dunnett's posttest; $^{**}P < 0.01$; $^{***}P < 0.0001$).

localization"; Fig. 4B and fig. S5, D and J to N). The percentage of cells displaying ayRhp1 symbiosomal localization was significantly higher during the day, with a maximum of 61.3 ± 4.4% cells displaying this pattern at 1300 hours in contrast to only 26.0 ± 2.0% of cells at 2300 hours ($P < 0.001$) (Fig. 4C). These results indicate that ayRhp1 is preferentially present in the symbiosome membrane during the day. To our knowledge, this is the first report of diel changes in proteomic makeup of the cnidarian symbiosome membrane and furthers the notion that this interface that separates symbiotic partners can be dynamically modified by the host cell to control the physiology of the alga.

### A putative host-controlled nitrogen concentrating mechanism

The pKa for Tamm combined with the pH difference between the host cell's cytosol and the symbiosome dictates >2000 higher $pNH_3$ in the former. Although this establishes a steep partial pressure gradient favoring $NH_3$ diffusion into the symbiosome, diffusion across lipidic membranes is generally limited [reviewed in (*16*)]. The presence of ayRhp1 in the symbiosome membrane is poised to overcome this limitation, thus enhancing $NH_3$ delivery to the algal symbionts in an analogous manner to nodulin-intrinsic proteins in plant-*Rhizobium* symbioses (*17*, *18*). Once inside the highly acidic symbiosome, $NH_3$ will be immediately converted into $NH_4^+$, which cannot move across the plasma membrane, or through ayRhp1. This mechanism is known as "$NH_4^+$ acid trapping" and is well documented in diverse excretory epithelia from humans (*20*), teleost fishes (*39*), cephalopod and bivalve mollusks (*38*, *50*), and crustaceans [reviewed in (*26*); (*20*, *38*, *39*, *50*)]. Moreover, the uptake of $NH_4^+$ by the alga will ensure the continuous conversion of $NH_3$ into $NH_4^+$ in the symbiosome, which in turn will maintain $NH_3$ diffusion from the host cytosol. By analogy to the CCM that facilitates symbiont photosynthesis (*4*), $NH_3$ transport by ayRhp1 coupled to acid trapping of $NH_4^+$ in the symbiosome can be considered a host-controlled nitrogen concentrating mechanism (NCM). The high degree of conservation among cnidarian Rh channels (fig. S1) and the presence of an acidic symbiosome in anemones and corals from both the complex and robust clades (*4*) suggest that Rh-mediated NCMs are widespread in cnidarians. However, species- and environment-specific differences in the NCM contribution to Tamm transport may exist and must be explored.

In addition, $CO_2$-facilitated diffusion by ayRhp1 has implications for the host-controlled symbiosomal CCM (*4*). In this model, $H^+$ transport by VHA generates an acidic symbiosome that drives the DIC equilibrium toward $CO_2$ accumulation in the symbiosome space, which then diffuses into the alga where it is fixed by algal Rubisco. The presence of ayRhp1 in the symbiosome membrane may initially seem counterproductive for the CCM, as it provides a pathway for $CO_2$ to leak back into the host cell cytoplasm. Continued carbon fixation by the algae, however, ensures a more favorable gradient for $CO_2$ diffusion into the algae compared with the host cell. The $CO_2$ that backflows into the coral host cell would be hydrated by cytosolic carbonic anhydrases (CA) into $H^+$ and $HCO_3^-$ (*51*), which can then be used as substrates for VHA and $HCO_3^-$ transporters in the symbiosome membrane. Furthermore, the fluid in the coelenteron and mitochondria in the gastrodermal cells (*4*) are additional sources of $CO_2$ that can fuel symbiosome acidification (Fig. 5). This mechanism is akin to the human kidney collecting duct, where VHA, CAs, $HCO_3^-$ transporters, and Rh channels interact with each other for the purposes of $HCO_3^-$ reabsorption and Tamm excretion (*52*).

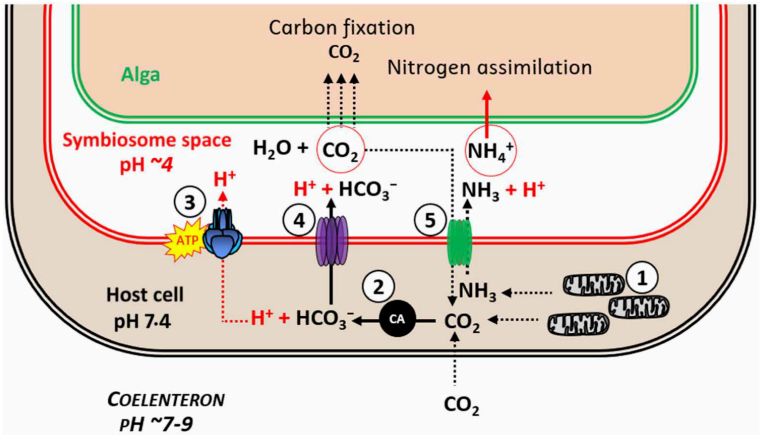


**Fig. 5. Model of the coral nitrogen concentrating mechanism in alga-containing coral host cells.** (**1**) Coral mitochondria produce $NH_3$ and $CO_2$. (**2**) Cytosolic CA catalyzes $CO_2$ hydration into $H^+$ and $HCO_3^-$. (**3**) $H^+$ and (**4**) $HCO_3^-$ are moved into the symbiosome space by VHA and an unidentified $HCO_3^-$ transporter, respectively. Inside the symbiosome, $H^+$ and $HCO_3^-$ dehydrate into $CO_2$, which diffuses into and is photosynthetically fixed by the alga. (**5**) $NH_3$ diffuses via the *A. yongei* Rhesus protein (ayRhp1) into the symbiosome space, where it is immediately protonated and trapped as $NH_4^+$. An unidentified algal transporter imports $NH_4^+$ into the alga, where it is assimilated. Some $CO_2$ also diffuses via ayRhp1 back into the host cell's cytosol, where it is rehydrated and transported back to the symbiosome space. ATP, adenosine 5′-triphosphate.

The increased proportion of cells displaying symbiosomal ayRhp1 localization during the day matches established patterns of increased Tamm delivery from host to symbiont (*53*) and symbiont nitrogen assimilation (*9*) during light conditions. The diurnal nitrogen supply is primarily used not to advance growth but to sustain a high turnover of photosystem proteins and pigments damaged by ultraviolet radiation and electron transfer, which is essential for continued and efficient photosynthesis (*9*, *54*, *55*). This situation highlights the need for unique regulatory mechanisms in photosymbiotic associations compared with symbioses with nonphotosymbiotic microbes, such as those in plant roots. Conversely, the removal of ayRhp1 from the symbiosome membrane at night would serve to restrict nitrogen supply to symbiotic algae, thus limiting the synthesis of nonphotosynthetic proteins that would be essential to sustain their growth and reproduction (*55*). This mechanism gains additional significance when we consider that the coral symbiosome is highly acidic in both light and dark conditions (*4*), and this implies a continued steep inwardly directed $pNH_3$ gradient. Moreover, alga-containing gastrodermal cells are in contact with the gastrovascular cavity or coelenteron. This compartment contains Tamm at concentrations that can be several hundred-fold higher compared with seawater (*56*) and experiences steep diel pH fluctuations that can reach pH values as high as 9 during the day and as low as 6.75 at night (*56*, *57*). The presence of ayRhp1 channels in the host plasma membrane at night would facilitate the removal of $NH_3$ from the host cell into the coelenteron, where it would be trapped as $NH_4$, further restricting nitrogen supply to the algae at night.

The regulation of nitrogen delivery via changes in ayRhp1 subcellular localization is not mutually exclusive with regulation via the GS/GDH/GOGAT pathway (*11*, *58*, *59*), and they complement each other. The involvement of this pathway is largely based on changes in gene expression or enzyme activity upon transitioning from symbiotic to aposymbiotic stages (*22*) or during long-term environmental disturbances (*60*, *61*). But despite diel mRNA expression patterns (*62*), the abundance of most metabolic enzymes in coral cells, including that of GS, does not seem to change on a diel basis (*63*). However, this does not preclude diel regulation of enzyme activity by post-translational modifications or substrate availability that could act synergistically with ayRhp1 to control nitrogen to symbiotic algae. Moreover, ayRhp1 subcellular localization was not identical in all cells at any time period, indicating finer regulation based on position on the coral colony, symbiotic stage, or some other unidentified factors.

## Perspectives and limitations

The ayRhp1- and VHA-dependent NCM identified here together with diel changes in ayRhp1 subcellular distribution provide a potential mechanism whereby coral host cells can supply nitrogen to their algal symbionts while still maintaining them in a nitrogen-limited state to control their growth under oligotrophic conditions. Alterations in nitrogen delivery to coral symbiotic algae have been linked to eutrophication and other environmental stressors that result in disruption of the symbiosis at the colony level, commonly known as coral bleaching (*64*–*69*). For example, heat stress may promote coral amino acid catabolism as a means to meet increased metabolic demand in a warmed environment, which has been suggested to trigger a feedback loop that releases symbionts from nitrogen limitation, uncouples the symbiotic relationship, and leads to bleaching (*70*). In addition, future studies must take into account that ayRhp1 is present in multiple cell types throughout coral tissues, which cannot be discerned using transcriptomics, proteomics, or metabolomics assays on bulk coral colony samples. Specifically, changes in ayRhp1 abundance could be driven by ayRhp1 in cells in the epidermis, gastrodermis, calicodermis, or combinations, and each of these conditions would reflect a unique coral response, in some cases with opposite implications for coral health. With this in mind, techniques that allow

the investigation of coral biology at the cellular and molecular levels such as nanoscale secondary ion mass spectrometry ("nano-SIMS") (*11*, *70*) and confocal microscopy (*71*–*73*) are essential complements to "-omics" techniques. In particular, confocal Airyscan microscopy will allow studying physiological processes in calcifying cells and at the symbiosome membrane in unprecedent detail. Further work is required to determine whether the observed ayRhp1 symbiosomal localization is widespread among scleractinian corals. In addition, future studies should examine wild corals to ascertain the importance of this putative Rh channel–dependent NCM in the field. Future studies could also explore the role of other environmental nitrogen sources (i.e., urea and $NO_3^-$) on host-symbiont metabolism. These are time- and materials-intensive tasks but are necessary to fully contextualize the coral NCM at the ecophysiological level.

## METHODS

### Organisms

*A. yongei* colonies were maintained in flow-through seawater at 26°C with a 10/14-hour light/dark cycle with sunrise at 0800 and sunset at 1800. These coral colonies predominantly contain *Cladocopium* species (formerly *Symbiodinium* clade C). See the Supplementary Materials and Methods for additional information on coral husbandry.

### Cloning of *ayRhp1*

Following the methods of (*15*), total RNA was collected by flash-freezing a 2-cm *A. yongei* nubbin in liquid nitrogen and crushing with a mortar and pestle into a fine powder. Powdered tissue was resuspended in TRIzol reagent (Invitrogen, Carlsbad, CA, USA), and total RNA was extracted following the manufacturer's protocol. Total RNA was cleaned and concentrated using an RNeasy Plus Mini Kit (Qiagen, Hilden, Germany). cDNA was synthesized using Super-Script III Reverse Transcriptase (Invitrogen) and Oligo(dT) primers according to the manufacturer's protocol. The resulting cDNA was used as template for all RT-PCRs. The full-length *ayRhp1* sequence was obtained and can be found on GenBank (MH025799).

Protein sequences for the phylogenetic analysis were sourced from (*74*) and GenBank via BLASTtn search. Accession numbers of all Rh sequences used in this analysis can be found in the supporting information file (Table S1).

### Plasmid preparation and cDNA synthesis for *Xenopus laevis* expression of *ayRhp1*

The open reading frame of *ayRhp1* was amplified from pCR2.1 TOPO-*ayRhp1* vector (see cloning of ayRhp1) using Q5 high-fidelity DNA polymerase (New England Biolabs, Ipswich, MA, USA) and the restriction site–containing primers (forward primer, 5′-ATAC-CCGGGATGTCTACTCGACCTCCTACG-3′; reverse primer: 5′-GGCAAGCTTTTACACTTTATCATCTCCGAC-3′), subcloned by sticky-end ligation with T4 ligase (New England Biolabs) into Xma I and Hind III restriction sites of a pGEM-HE vector containing *Xenopus* beta globin 5′- and 3′-UTR sequences flanking the cloning site. Proper insertion was verified by restriction digest using Eco R1, Bam HI, and Sph I and visualized by gel electrophoresis to confirm *ayRhp1* fragments produced were of the expected size. The pGEM-HE vector containing the *ayRhp1* insert was linearized using Sph I; the restriction enzyme was heat inactivated at 65°C and linear plasmid column purified (GeneJet PCR Purification Kit; Thermo Fisher Scientific, Waltham, MA, USA). The in vitro transcription of *ayRhp1* capped mRNA (cRNA) was performed with HiScribe T7 ARCA mRNA kit (New England Biolabs) on Sph I linearized pGEM-HE-*ayRhp1* vector followed by column purification (RNeasy MiniElute Cleanup Kit; Qiagen). The cRNA was quantified spectrophotometrically (NanoDrop, ND-1000; Thermo Fisher Scientific), and its integrity was assessed on a denaturing MOPS agarose gel.

### Oocyte microinjection

Stage VI–V oocytes were collected from mature female *X. laevis* (*75*). Briefly, the frogs were euthanized via decapitation, and the ovary was dissected and placed in $Ca^{2+}$-free oocyte ringer (OR2) solution (82.5 mM NaCl, 2.5 mM KCl, 1 mM $MgCl_2$, 1 mM $Na_2HPO_4$, 5 mM HEPES, pH 7.5) containing collagenase type VI (1 mg $ml^{-1}$; Thermo Fisher Scientific). After incubation under gentle agitation for 90 min at room temperature, collagenase activity was terminated by rinsing the oocytes three times in OR2 containing 1 mM $CaCl_2$. Oocytes were then manually sorted, rinsed, and allowed to recover in OR2 sterilized using vacuum bottle-top filters (EMD Millipore Steritop) overnight at 16°C (Fisherbrand Mini Refrigerated Incubator). Oocytes were injected with 18.4 ng of ayRhp1 cRNA (36.8 nl with 0.5 ng $nl^{-1}$) (ayRhp1) or equivalent volume of nuclease-free water (control) using a Nanoject II or III auto-nanoliter injector (Drummond Scientific, Broomall, PA, USA). Experiments were conducted 3 days postinjection; during this time, the oocytes were stored in OR2 supplemented with 2.5 mM sodium pyruvate, penicillin-streptomycin (1 mg $ml^{-1}$), and gentamicin (50 μg $ml^{-1}$). Oocytes that died during experiments were discounted from analyses. All procedures followed the Guidelines of the Canadian Council on Animal Care and were approved by the University of Manitoba Animal Research Ethics Board.

### Oocyte Tamm uptake rates

Groups of control (water-injected) or ayRhp1 (ayRhp1 cRNA-injected) oocytes (24 oocytes = 1 replicate; $n = 6$ to 8) were placed in 15-ml tubes and incubated for 1 hour at room temperature in OR2 solutions containing (a) 0 mM $NH_4Cl$, pH 7.5; (b) 1 mM $NH_4Cl$, pH 6.5; (c) 1 mM $NH_4Cl$, pH 7.5; (d) 1 mM $NH_4Cl$, pH 8.5; or (e) 10 mM $NH_4Cl$, pH 7.5. Osmolarity was maintained by substituting NaCl with $NH_4Cl$, and pH was adjusted by adding NaOH or HCl. Following incubation, oocytes were washed in ice-cold OR2 to remove excess $NH_4Cl$ and placed in groups of three oocytes in 27 μl of 6% perchloric acid to deproteinize samples (*76*). After pH neutralization with 3 M KOH, samples were diluted 1:10–1:40 with MilliQ water, and Tamm was measured using a hypochlorite-salicylate-nitroprusside–based assay (*77*). Tamm uptake rate was calculated according to the formula

$$\text{Tamm uptake rate} = \frac{[\text{Tamm}]_{t=1\text{h}} - [\text{Tamm}]_{t=0\text{h}}}{1\ \mu\text{l} \times 60\ \text{min}}$$

where $[\text{Tamm}]_{t=1\text{h}}$ is the Tamm measured in oocytes after incubation in OR2 (b) to (e) for 1 hour, $[\text{Tamm}]_{t=0\text{h}}$ is Tamm measured in oocytes in OR2 (a) before the start of the incubations, 1 μl is the average oocyte volume, and 60 min was used to calculate rates on a per minute basis. The average Tamm uptake rate of control oocytes was subtracted from that of ayRhp1 oocytes before statistical analysis (fig. S3). Tamm uptake kinetics were calculated using a nonlinear regression to fit the Michaelis-Menten equation.

### Oocyte $CO_2$ release rates

Hypercapnic OR2 was generated by aeration with 5% $CO_2$ until pH reached equilibrium. Groups of control or ayRhp1 oocytes

(25 oocytes = 1 replicate; $n = 8$) were incubated in 40 ml of hypercapnic OR2 for 1.5 hours at 16°C. Oocytes were transferred along with hypercapnic OR2 into 2-ml septum capped gas tight vials. Hypercapnic OR2 was sequentially removed from each vial, replaced with normocapnic OR2, and sealed while submerged in OR2 to prevent air bubbles. Rapid transfer from hypercapnic to normocapnic OR2 was used to generate an oocyte-to-OR2 $pCO_2$ gradient. One minute after sealing the chambers, three replicate 5-µl samples were taken with a gas tight Hamilton syringe from the vial by piercing the septum on the cap and injected into a custom-built total $CO_2$ analyzer using a Licor 850 (LI-COR Biosciences, Lincoln, NE, USA) for $CO_2$ detection as previously described (*36*). Standards of 0, 0.2, 0.3, 0.4, and 0.5 mmol $l^{-1}$ $NaHCO_3$ were used to calibrate the $CO_2$ analyzer and produced an $R^2$ of 0.99. $CO_2$ release rate was calculated according to the formula

$$CO_2 \text{ release rate} = \frac{\left(\frac{CO_2 \text{ release}_{t=1\text{min}}\ \mu\text{mol} - 0.4644}{0.1960}\right) \times 0.002\ \text{L}}{25\ \text{oocytes} \times 1\ \text{min} \times \frac{1000\ \text{nmol}}{\mu\text{mol}}}$$

where $CO_2 \text{ release}_{t\,=\,1\text{min}}$ is the $CO_2$ measured in the sample after 1 min of incubation in normocapnic OR2, 0.04644 and 0.1960 are corrections calculated from the standard curve, 0.002 L is the chamber volume, 25 oocytes are the number of oocytes per chamber, and 1 min is the $CO_2$ flux period, The integrity of oocytes in all vials was confirmed under a microscope at the end of the sampling period.

### Antibodies

Custom-made, affinity-purified anti-ayRhp1 rabbit polyclonal antibodies were developed (GenScript USA Inc., Piscataway, NJ, USA) against the peptide CHNKDAHGSHKEGSN, which is present in a putative Rhp1 protein predicted from the *Acropora digitifera* genome (XP_015769291.1) (*78*). This epitope has just one amino acid difference in ayRhp1 (CHNKDAHGS**P**KEGSN). NKA was immunolocalized with a commercially available monoclonal antibody (SC-48345, Santa Cruz Biotechnology, Dallas, TX, USA).

### ayRhp1 protein expression and antibody validation

Using methods adapted from (*4*), *A. yongei* tissue was removed from the skeleton using an airbrush loaded with homogenization buffer. Briefly, homogenate was sonicated on ice and centrifuged to pellet down debris; the supernatant was kept on ice. Sample protein concentrations were determined using a Bradford Protein Assay (Bio-Rad, Hercules, CA, USA) with a bovine serum albumin standard curve. Samples were then incubated in 4× Laemmli sample buffer (Bio-Rad) and 10% β-mercaptoethanol before heating at 90°C for 3 min and loaded onto an SDS–polyacrylamide gel electrophoresis (PAGE) gel. Following electrophoresis, proteins were transferred from the gel onto a polyvinylidene difluoride (PVDF) membrane using a Mini Tans-Blot Cell (Bio-Rad) overnight. The membrane was blocked with 5% powdered fat-free milk in TBS-T for 1 hour on a shaker at room temperature before overnight incubation on a shaker (4°C) with anti-ayRhp1 primary antibody (0.216 µg $ml^{-1}$), primary antibody with 400× excess peptide on a molar base ("preabsorption control"), or preimmune serum (0.216 µg $ml^{-1}$) diluted in blocking buffer. Membranes were washed with 4 × 15 min TBS-T washes before incubation with secondary antibody [goat anti–rabbit–horseradish peroxidase (HRP) diluted 1:10,000, Bio-Rad] for 1 hour on a shaker at room temperature. Membranes were again washed with 4 × 15 min TBS-T washes and a final 15-min TBS wash before band development with an ECL Prime Western blot Detection Kit (GE Healthcare, Chicago, IL, USA) and imaged using a Chemidoc Imaging system (Bio-Rad) (fig. S4D). See the Supplementary Materials and Methods for additional information.

### Immunofluorescence

Some *A. yongei* nubbins were fixed and decalcified, and others were brushed with a toothbrush to isolate cells prior to fixing following previously described methods (*4*, *15*, *49*, *71*, *73*) (see the Supplementary Materials and Methods for details). Tissue sections and isolated cells were incubated for 1 hour at room temperature in blocking buffer [4 ml of phosphate-buffered saline with Triton X-100 (PBS-TX), 80 µl of normal goat serum, and 0.8 µl of keyhole limpet hemocyanin solution], followed by overnight incubation (4°C) with anti-ayRhp1 antibodies (2.16 µg $ml^{-1}$), anti-ayRhp1 antibodies preabsorbed with excess peptide (8.64 µg $ml^{-1}$), or preimmune serum (2.16 µg $ml^{-1}$) alone or in combination with the anti-NKA antibody (2.00 µg $ml^{-1}$) (all in blocking buffer) (fig. S4, A to C).

Slides were washed in PBS-TX to remove unbound primary antibodies (3 × 5 min). Secondary antibodies (goat anti–rabbit–Alexa Fluor 555, goat anti–rabbit–Alexa Fluor 488, and/or goat anti–mouse–Alexa Fluor568, 4 µg/ml in blocking buffer; Invitrogen) were then added for 1 hour at room temperature followed by 4′,6-diamidino-2-phenylindole (DAPI) DNA stain (1 µg $ml^{-1}$ in blocking buffer; Invitrogen) for 5 min at room temperature and washed again in PBS-TX to remove unbound secondary antibodies and DAPI (3 × 5 min).

Epifluorescence microscopy was performed on a Zeiss AxioObserver Z1 (Carl Zeiss AG, Oberkochen, Germany) connected to a metal halide lamp. ayRhp1 and DAPI signals in tissue sections (Fig. 2 and fig. S4, A to $C_1$) were visualized using HE Cy3 [excitation (ex): 550 nm, emission (em): 570 nm] and DAPI (ex: 359 nm, em: 461 nm) filters, respectively. ayRhp1 and DAPI signals in isolated cells (fig. S5) were visualized using HE DsRed (ex: 538 to 562 nm, em: 570 to 640 nm) and FURA (ex: 335 to 345 and 375 to 385 nm, em: 505 to 530 nm) filters, respectively.

Confocal Airyscan microscopy was performed on a Zeiss AxioObserver Z1 connected to a laser scanner equipped with 405-, 488-, 561-, and 640-nm laser lines (Zeiss LSM 800 with Airyscan, Carl Zeiss AG). This device uses a 32-channel photomultiplier detector and linear deconvolution to obtain 140-nm lateral (*X*-*Y*) and 400-nm axial (*Z*) resolution. ayRhp1, NKA, and DAPI signals in tissue sections (Figs. 4, A and B, and 3) were visualized using goat anti–rabbit–Alexa Fluor 488 and goat anti–mouse–Alexa Fluor568 secondary antibodies (Invitrogen) and DAPI stain (Invitrogen), respectively (Alexa Fluor 488—ex: 517 nm, em: 497 to 574 nm; Alexa Fluor 568—ex: 577 nm, em: 560 to 643 nm; DAPI—ex: 465 nm, em: 400 to 484 nm). Three-dimensional reconstructions of *z*-stacks were generated using Imaris 9.0 (Bitplane, Zurich, Switzerland). To facilitate visualization by color-blind readers, NKA, ayRhp1, and DAPI signals are presented using the false colors violet, green, and blue, respectively, in all figures.

### Assessment of ayRhp1 subcellular localization over day-night cycles

Cell isolations were prepared from coral nubbins randomly selected from three separate tanks. Nubbins were sampled 30 min before and after sunrise and sunset (0730, 0830, 1730, and 1830 hours) as

well as halfway between lighting condition changes (1300 and 2300 hours). Samples taken during the day were continually illuminated during cell isolation and fixation, while those taken during the night were kept in the dark. At each time point, cells were immunostained for ayRhp1 and imaged as described above. Starting from the upper-right corner of the field of view, the first 50 intact alga-hosting *A. yongei* cells displaying ayRhp1 signal were counted and classified into one of two subcellular localization patterns: "symbiosomal ayRhp1 localization" (the ayRhp1 signal clearly traversed the region between the nuclei of the coral host cell and the algae) or nonsymbiosomal localization (ayRhp1 signal was absent from this region but present exterior and adjacent to the host nucleus). Cells were counted and classified in a double-blind manner: Slides were named with random identifiers by an independent person before being observed on the fluorescence microscope by another person. Classification was conducted during observation through the microscope eyepiece, as this allowed a better determination of ayRhp1 subcellular localization by rapid and repetitive adjustments to the fine focus and alternation between the Alexa Fluor 555 and DAPI channels. Cells from three separate branches were classified at each time point, resulting in a total of 150 cells per time point and 900 cells in total. Time points were matched with random slide names only once all 900 cells were classified. Raw count data are presented in data S1.

### Statistical analysis

All statistical tests were run in GraphPad Prism 7 (San Diego, CA, USA). Tamm uptake, $CO_2$ release, and ayRhp1 localization data were tested for normality and homogeneity of variance using D'Agostino and Pearson or Shapiro-Wilk normality tests and Brown-Forsythe tests. Tamm uptake data were analyzed using one-way analysis of variance (ANOVA) with Tukey's multiple comparisons. $CO_2$ release data were analyzed using a Welch's *t* test (two-tailed, unequal variance). Data from ayRhp1 localization in isolated cells were analyzed using two-way repeated-measures ANOVA followed by Dunnett's posttest using the data from 1300 hours as control. Alpha was set at 0.05 for all statistical tests.

## SUPPLEMENTARY MATERIALS

Supplementary material for this article is available at https://science.org/doi/10.1126/sciadv.abm0303

View/request a protocol for this paper from *Bio-protocol*.

## REFERENCES AND NOTES


1. M. J. H. van Oppen, M. Medina, Coral evolutionary responses to microbial symbioses. *Philos. Trans. R. Soc. Lond. B Biol. Sci.* **375**, 20190591 (2020).
2. Y. Tanaka, A. Suzuki, K. Sakai, The stoichiometry of coral-dinoflagellate symbiosis: Carbon and nitrogen cycles are balanced in the recycling and double translocation system. *ISME J.* **12**, 860–868 (2018).
3. B. L. Tang, Thoughts on a very acidic symbiosome. *Front. Microbiol.* **6**, 816 (2015).
4. K. L. Barott, A. A. Venn, S. O. Perez, S. Tambutté, M. Tresguerres, Coral host cells acidify symbiotic algal microenvironment to promote photosynthesis. *Proc. Natl. Acad. Sci. U.S.A.* **112**, 607–612 (2015).
5. O. Rahav, Z. Dubinsky, Y. Achituv, P. G. Falkowski, Ammonium metabolism in the zooxanthellate coral, *Stylophora pistillata*. *Proc. R. Soc. Lond. B.* **236**, 325–337 (1989).
6. P. A. Wright, Nitrogen excretion: Three end products, many physiological roles. *J. Exp. Biol.* **198**, 273–281 (1995).
7. A. M. Szmant, L. M. Ferrer, L. M. FitzGerald, Nitrogen excretion and O:N ratios in reef corals: Evidence for conservation of nitrogen. *Mar. Biol.* **104**, 119–127 (1990).
8. G. Cui, Y. J. Liew, Y. Li, N. Kharbatia, N. I. Zahran, A. H. Emwas, V. M. Eguiluz, M. Aranda, Host-dependent nitrogen recycling as a mechanism of symbiont control in *Aiptasia*. *PLOS Genet.* **15**, e1008189 (2019).
9. C. Kopp, M. Pernice, I. Domart-Coulon, C. Djediat, J. E. Spangenberg, D. T. L. Alexander, M. Hignette, T. Meziane, A. Meibom, Highly dynamic cellular-level response of symbiotic coral to a sudden increase in environmental nitrogen. *mBio* **4**, e00052-13 (2013).
10. C. D'Elia, S. Domotor, K. Webb, Nutrient uptake kinetics of freshly isolated zooxanthellae*. *Mar. Biol.* **167**, 157–167 (1983).
11. M. Pernice, A. Meibom, A. Van Den Heuvel, C. Kopp, I. Domart-Coulon, O. Hoegh-Guldberg, S. Dove, A single-cell view of ammonium assimilation in coral-dinoflagellate symbiosis. *ISME J.* **6**, 1314–1324 (2012).
12. T. A. V. Rees, Are symbiotic algae nutrient deficient? *Proc. R. Soc. B Biol. Sci.* **243**, 227–233 (1991).
13. T. Krueger, N. Horwitz, J. Bodin, M. E. Giovani, S. Escrig, M. Fine, A. Meibom, Intracellular competition for nitrogen controls dinoflagellate population density in corals. *Proc. Biol. Sci.* **287**, 20200049 (2020).
14. A. E. Sproles, N. L. Kirk, S. A. Kitchen, C. A. Oakley, A. R. Grossman, V. M. Weis, S. K. Davy, Phylogenetic characterization of transporter proteins in the cnidarian-dinoflagellate symbiosis. *Mol. Phylogenet. Evol.* **120**, 307–320 (2018).
15. K. L. Barott, M. E. Barron, M. Tresguerres, Identification of a molecular pH sensor in coral. *Proc. R. Soc. B* **284**, 20171769 (2017).
16. I. D. Weiner, J. W. Verlander, Ammonia transporters and their role in acid-base balance. *Physiol. Rev.* **97**, 465–494 (2017).
17. I. S. Wallace, W.-G. Choi, D. M. Roberts, The structure, function and regulation of the nodulin 26-like intrinsic protein family of plant aquaglyceroporins. *Biochim. Biophys. Acta* **1758**, 1165–1175 (2006).
18. C. M. Niemietz, S. D. Tyerman, Channel-mediated permeation of ammonia gas through the peribacteroid membrane of soybean nodules. *FEBS Lett.* **465**, 110–114 (2000).
19. R. R. Geyer, M. D. Parker, A. M. Toye, W. F. Boron, R. Musa-Aziz, Relative $CO_2/NH_3$ permeabilities of human RhAG, RhBG and RhCG. *J. Membr. Biol.* **246**, 915–926 (2013).
20. F. Gruswitz, S. Chaudhary, J. D. Ho, A. Schlessinger, B. Pezeshki, C.-M. Ho, A. Sali, C. M. Westhoff, R. M. Stroud, Function of human Rh based on structure of RhCG at 2.1 A. *Proc. Natl. Acad. Sci. U.S.A.* **107**, 9638–9643 (2010).
21. S. Baday, E. A. Orabi, S. Wang, G. Lamoureux, S. Bernèche, Mechanism of $NH_4^+$ recruitment and $NH_3$ transport in Rh proteins. *Structure* **23**, 1550–1557 (2015).
22. E. M. Lehnert, M. E. Mouchka, M. S. Burriesci, N. D. Gallo, J. A. Schwarz, J. R. Pringle, Extensive differences in gene expression between symbiotic and aposymbiotic cnidarians. *G3* **4**, 277–295 (2014).
23. Y. Ishii, S. Maruyama, H. Takahashi, Y. Aihara, T. Yamaguchi, K. Yamaguchi, S. Shigenobu, M. Kawata, N. Ueno, J. Minagawa, Global shifts in gene expression profiles accompanied with environmental changes in cnidarian-dinoflagellate endosymbiosis. *G3* **9**, 2337–2347 (2019).
24. P. Ganot, A. Moya, V. Magnone, D. Allemand, P. Furla, C. Sabourault, Adaptations to endosymbiosis in a Cnidarian-Dinoflagellate association: Differential gene expression and specific gene duplications. *PLOS Genet.* **7**, e1002187 (2011).
25. M. Hu, X. Zheng, C.-M. Fan, Y. Zheng, Lineage dynamics of the endosymbiotic cell type in the soft coral *Xenia*. *Nature* **582**, 534–538 (2020).
26. D. Weihrauch, M. O'Donnell, *Acid-Base Balance and Nitrogen Excretion in Invertebrates* (Springer International Publishing, 2017); http://link.springer.com/10.1007/978-3-319-39617-0.
27. M. Benghezal, D. Gotthardt, S. Cornillon, P. Cosson, Localization of the Rh50-like protein to the contractile vacuole in *Dictyostelium*. *Immunogenetics* **52**, 284–288 (2001).
28. K. H. Han, K. Mekala, V. Babida, H. Y. Kim, M. E. Handlogten, J. W. Verlander, I. D. Weiner, Expression of the gas-transporting proteins, Rh B glycoprotein and Rh C glycoprotein, in the murine lung. *Am. J. Physiol. Lung Cell. Mol. Physiol.* **297**, L153–L163 (2009).
29. S. F. Perry, M. H. Braun, M. Noland, J. Dawdy, P. J. Walsh, Do zebrafish Rh proteins act as dual ammonia-CO2 channels? *J. Exp. Zool. A Ecol. Genet. Physiol.* **313**, 618–621 (2010).
30. V. Endeward, J. P. Cartron, P. Ripoche, G. Gros, RhAG protein of the Rhesus complex is a CO2 channel in the human red cell membrane. *FASEB J.* **22**, 64–73 (2008).
31. C. M. Nawata, C. M. Wood, M. J. O'Donnell, Functional characterization of Rhesus glycoproteins from an ammoniotelic teleost, the rainbow trout, using oocyte expression and SIET analysis. *J. Exp. Biol.* **213**, 1049–1059 (2010).
32. X.-D. Li, D. Lupo, L. Zheng, F. Winkler, Structural and functional insights into the AmtB/Mep/Rh protein family. *Transfus. Clin. Biol.* **13**, 65–69 (2006).
33. J. Stolarski, M. V. Kitahara, D. J. Miller, S. D. Cairns, M. Mazur, A. Meibom, The ancient evolutionary origins of Scleractinia revealed by azooxanthellate corals. *BMC Evol. Biol.* **11**, 316 (2011).
34. A. M. Marini, M. Boeckstaens, F. Benjelloun, B. Chérif-Zahar, B. André, Structural involvement in substrate recognition of an essential aspartate residue conserved in Mep/Amt and Rh-type ammonium transporters. *Curr. Genet.* **49**, 364–374 (2006).
35. X. Li, S. Jayachandran, H.-H. H. T. Nguyen, M. K. Chan, Structure of the *Nitrosomonas europaea* Rh protein. *Proc. Natl. Acad. Sci. U.S.A.* **104**, 19279–19284 (2007).
36. D. J. Lee, M. Gutbrod, F. M. Ferreras, P. G. D. Matthews, Changes in hemolymph total $CO_2$ content during the water-to-air respiratory transition of amphibiotic dragonflies. *J. Exp. Biol.* **221**, jeb181438 (2018).

37. S. Sasaki, K. Ishibashi, T. Nagai, F. Marumo, Regulation mechanisms of intracellular pH of *Xenopus laevis* oocyte. *Biochim. Biophys. Acta* **1137**, 45–51 (1992).
38. J. Thomsen, N. Himmerkus, N. Holland, F. J. Sartoris, M. Bleich, M. Tresguerres, Ammonia excretion in mytilid mussels is facilitated by ciliary beating. *J. Exp. Biol.* **219**, 2300–2310 (2016).
39. P. A. Wright, C. M. Wood, A new paradigm for ammonia excretion in aquatic animals: Role of Rhesus (Rh) glycoproteins. *J. Exp. Biol.* **212**, 2303–2312 (2009).
40. D. Thiel, M. Hugenschutt, H. Meyer, A. Paululat, A. R. Quijada-Rodriguez, G. Purschke, D. Weihrauch, Ammonia excretion in the marine polychaete Eurythoe complanata (Annelida). *J. Exp. Biol.* **220**, 425–436 (2017).
41. J. G. Tidball, Fine structural aspects of anthozoan desmocyte development (Phylum Cnidaria). *Tissue Cell* **14**, 85–96 (1982).
42. L. Muscatine, E. Tambutte, D. Allemand, Morphology of coral desmocytes, cells that anchor the calicoblastic epithelium to the skeleton. *Coral Reefs* **16**, 205–213 (1997).
43. J. W. Campbell, K. V. Speeg, Ammonia and biological deposition of calcium carbonate. *Nature* **224**, 725–726 (1969).
44. R. A. Loest, Ammonia-forming enzymes and calcium-carbonate deposition in terrestrial pulmonates. *Physiol. Zool.* **52**, 470–483 (1979).
45. C. J. Crossland, D. J. Barnes, The role of metabolic nitrogen in coral calcification. *Mar. Biol.* **28**, 325–332 (1974).
46. W. J. Cai, Y. Ma, B. M. Hopkinson, A. G. Grottoli, M. E. Warner, Q. Ding, X. Hu, X. Yuan, V. Schoepf, H. Xu, C. Han, T. F. Melman, K. D. Hoadley, D. T. Pettay, Y. Matsui, J. H. Baumann, S. Levas, Y. Ying, Y. Wang, Microelectrode characterization of coral daytime interior pH and carbonate chemistry. *Nat. Commun.* **7**, 11144 (2016).
47. N. Allison, I. Cohen, A. A. Finch, J. Erez, A. W. Tudhope, Corals concentrate dissolved inorganic carbon to facilitate calcification. *Nat. Commun.* **5**, 5741 (2014).
48. J. H. Kaplan, Biochemistry of Na,K-ATPase. *Annu. Rev. Biochem.* **71**, 511–535 (2002).
49. A. A. Venn, E. Tambutté, S. Lotto, D. Zoccola, D. Allemand, S. Tambutté, Imaging intracellular pH in a reef coral and symbiotic anemone. *Proc. Natl. Acad. Sci. U.S.A.* **106**, 16574–16579 (2009).
50. M. Y. Hu, Y. J. Guh, M. Stumpp, J. R. Lee, R. D. Chen, P. H. Sung, Y. C. Chen, P. P. Hwang, Y. C. Tseng, Branchial $NH_4^+$-dependent acid-base transport mechanisms and energy metabolism of squid (*Sepioteuthis lessoniana*) affected by seawater acidification. *Front. Zool.* **11**, 55 (2014).
51. A. Bertucci, A. Moya, S. Tambutté, D. Allemand, C. T. Supuran, D. Zoccola, Carbonic anhydrases in anthozoan corals - a review. *Bioorg. Med. Chem.* **21**, 1437–1450 (2013).
52. I. D. Weiner, J. W. Verlander, Renal ammonia metabolism and transport. *Compr. Physiol.* **3**, 201–220 (2013).
53. R. Grover, J.-F. Maguer, S. Reynaud-vaganay, C. Ferrier-Pagès, Uptake of ammonium by the scleractinian coral *Stylophora pistillata*: Effect of feeding, light, and ammonium concentrations. *Limnol. Oceanogr.* **47**, 782–790 (2002).
54. E. Beraud, F. Gevaert, C. Rottier, C. Ferrier-Pages, The response of the scleractinian coral Turbinaria reniformis to thermal stress depends on the nitrogen status of the coral holobiont. *J. Exp. Biol.* **216**, 2665–2674 (2013).
55. N. Rosic, P. Kaniewska, C.-K. Chan, E. Y. Ling, D. Edwards, S. Dove, O. Hoegh-Guldberg, Early transcriptional changes in the reef-building coral Acropora aspera in response to thermal and nutrient stress. *BMC Genomics* **15**, 1052 (2014).
56. S. Agostini, Y. Suzuki, T. Higuchi, B. E. Casareto, K. Yoshinaga, Y. Nakano, H. Fujimura, Biological and chemical characteristics of the coral gastric cavity. *Coral Reefs* **31**, 147–156 (2012).
57. P. Furla, I. Galgani, I. Durand, D. Allemand, Sources and mechanisms of inorganic carbon transport for coral calcification and photosynthesis. *J. Exp. Biol.* **203**, 3445–3457 (2000).
58. D. Yellowlees, T. A. V. Rees, W. Leggat, Metabolic interactions between algal symbionts and invertebrate hosts. *Plant. Cell Environ.* **31**, 679–694 (2008).
59. C. A. Oakley, M. F. Ameismeier, L. Peng, V. M. Weis, A. R. Grossman, S. K. Davy, Symbiosis induces widespread changes in the proteome of the model cnidarian *Aiptasia*. *Cell. Microbiol.* **18**, 1009–1023 (2016).
60. D. Yellowlees, T. Rees, W. Fitt, Effect of ammonium-supplemented seawater on glutamine synthetase and glutamate dehydrogenase activities in host tissue and zooxanthellae of Pocillopora damicornis and on ammonium uptake rates of the zooxanthellae. *Pacific Sci.* **48**, 291–295 (1994).
61. J. Tang, X. Ni, J. Wen, L. Wang, J. Luo, Z. Zhou, Increased ammonium assimilation activity in the scleractinian coral *Pocillopora damicornis* but not its symbiont after acute heat stress. *Front. Mar. Sci.* **7**, 565068 (2020).
62. O. Levy, P. Kaniewska, S. Alon, E. Eisenberg, S. Karako-Lampert, L. K. Bay, R. Reef, M. Rodriguez-Lanetty, D. J. Miller, O. Hoegh-Guldberg, Complex diel cycles of gene expression in coral-algal symbiosis. *Science* **331**, 175 (2011).
63. L. B. Linsmayer, D. D. Deheyn, L. Tomanek, M. Tresguerres, Dynamic regulation of coral energy metabolism throughout the diel cycle. *Sci. Rep.* **10**, 19881 (2020).
64. N. M. Kuntz, D. I. Kline, S. A. Sandin, F. Rohwer, Pathologies and mortality rates caused by organic carbon and nutrient stressors in three Caribbean coral species. *Mar. Ecol. Prog. Ser.* **294**, 173–180 (2005).
65. C. Schlöder, L. D'Croz, Responses of massive and branching coral species to the combined effects of water temperature and nitrate enrichment. *J. Exp. Mar. Biol. Ecol.* **313**, 255–268 (2004).
66. S. A. Wooldridge, T. J. Done, C. R. Thomas, I. I. Gordon, P. A. Marshall, R. N. Jones, Safeguarding coastal coral communities on the central Great Barrier Reef (Australia) against climate change: Realizable local and global actions. *Clim. Change* **112**, 945–961 (2012).
67. P. A. Cleves, C. J. Krediet, E. M. Lehnert, M. Onishi, J. R. Pringle, Insights into coral bleaching under heat stress from analysis of gene expression in a sea anemone model system. *Proc. Natl. Acad. Sci. U.S.A.* **117**, 28906–28917 (2020).
68. L. A. Morris, C. R. Voolstra, K. M. Quigley, D. G. Bourne, L. K. Bay, Nutrient availability and metabolism affect the stability of coral–*symbiodiniaceae* symbioses. *Trends Microbiol.* **27**, 678–689 (2019).
69. J. Wiedenmann, C. D'Angelo, E. G. Smith, A. N. Hunt, F. E. Legiret, A. D. Postle, E. P. Achterberg, Nutrient enrichment can increase the susceptibility of reef corals to bleaching. *Nat. Clim. Chang.* **3**, 160–164 (2013).
70. N. Rädecker, C. Pogoreutz, H. M. Gegner, A. Cárdenas, F. Roth, J. Bougoure, P. Guagliardo, C. Wild, M. Pernice, J. B. Raina, A. Meibom, C. R. Voolstra, Heat stress destabilizes symbiotic nutrient cycling in corals. *Proc. Natl. Acad. Sci. U.S.A.* **118**, e2022653118 (2021).
71. M. E. Barron, A. B. Thies, J. A. Espinoza, K. L. Barott, A. Hamdoun, M. Tresguerres, A vesicular Na+/Ca2+ exchanger in coral calcifying cells. *PLOS ONE* **13**, e0205367 (2018).
72. P. Ganot, E. Tambutté, N. Caminiti-Segonds, G. Toullec, D. Allemand, S. Tambutté, Ubiquitous macropinocytosis in anthozoans. *eLife* **9**, e50022 (2020).
73. K. L. Barott, A. A. Venn, A. B. Thies, S. Tambutté, M. Tresguerres, Regulation of coral calcification by the acid-base sensing enzyme soluble adenylyl cyclase. *Biochem. Biophys. Res. Commun.* **525**, 576–580 (2020).
74. C.-H. Huang, J. Peng, Evolutionary conservation and diversification of Rh family genes and proteins. *Proc. Natl. Acad. Sci.* **102**, 15512–15517 (2005).
75. H. Soreq, S. Seidman, *Xenopus* oocyte microinjection: From gene to protein. *Methods Enzymol.* **207**, 225–265 (1992).
76. C. M. Veauvy, P. J. Walsh, M. D. Mcdonald, Effect of elevated ammonia on tissue nitrogen metabolites in the ureotelic gulf toadfish (*Opsanus beta*) and the ammoniotelic midshipman (*Porichthys notatus*). *Physiol. Biochem. Zool.* **82**, 345–352 (2009).
77. A. J. Kempers, C. J. Kok, Re-examination of the determination of ammonium as the indophenol blue complex using salicylate. *Anal. Chim. Acta* **221**, 147–155 (1989).
78. C. Shinzato, E. Shoguchi, T. Kawashima, M. Hamada, K. Hisata, M. Tanaka, M. Fujie, M. Fujiwara, R. Koyanagi, T. Ikuta, A. Fujiyama, D. J. Miller, N. Satoh, Using the *Acropora digitifera* genome to understand coral responses to environmental change. *Nature* **476**, 320–323 (2011).
79. R. C. Edgar, MUSCLE: A multiple sequence alignment method with reduced time and space complexity. *BMC Bioinformatics* **5**, 113 (2004).
80. A. Stamatakis, RAxML version 8: A tool for phylogenetic analysis and post-analysis of large phylogenies. *Bioinformatics* **30**, 1312–1313 (2014).
81. E. L. Sonnhammer, G. von Heijne, A. Krogh, A hidden Markov model for predicting transmembrane helices in protein sequences. *Proc. Int. Conf. Intell. Syst. Mol. Biol.* **6**, 175–182 (1998).
82. A. Krogh, B. Larsson, G. Von Heijne, E. L. L. Sonnhammer, Predicting transmembrane protein topology with a hidden Markov model: Application to complete genomes. *J. Mol. Biol.* **305**, 567–580 (2001).
83. M. E. Jørgensen, H. H. Nour-Eldin, B. A. Halkier, in *Biotechnology of Plant Secondary Metabolism: Methods and Protocols*, A. G. Fett-Neto, Ed. (Springer Science & Business Media, 2016); http://link.springer.com/10.1007/978-1-4939-3393-8, vol. 1405, pp. 99–107.
84. K. Barott, M. Tresguerres, Immunolocalization of proteins in corals: The V-type $H^+$-ATPase proton pump. *Bio-protocol* **5**, e1573 (2015).


**Acknowledgments:** We thank M. Romero (Mayo Clinic) for the gift of *Xenopus* expression vector; M. Ortega, S. Nöel, A. Serna, C. Hassabi, D. Jio, and P. Zerofski (Scripps Institution of Oceanography) for help in maintaining coral cultures; and M. Nash (University of Manitoba) for support with oocyte sorting and maintenance. **Funding:** This work was partially supported by the National Science Foundation (NSF) EF #1220641 to M.T., NSF Graduate Research (GRFP 2019271478) and SIO Doctoral Scholar Fellowships to A.B.T., Natural Sciences and Engineering Research Council of Canada (NSERC) Postgraduate Doctoral Scholarship-Doctoral to A.R.Q.-R., University of Manitoba Graduate Fellowship to H.Z., and NSERC Discovery grant (RGPIN/5013-2018) to D.W. **Author contributions:** M.T. and A.B.T. conceived the project. M.T. and D.W. directed the research. A.B.T. performed all cloning, antibody validation, and microscopy experiments. A.R.Q.-R. and H.Z. performed oocyte experiments. A.B.T., A.R.Q.-R., D.W., and M.T. analyzed the data. A.B.T. and M.T. wrote the manuscript. All authors read and edited the manuscript. **Competing interests:** The authors declare that they have no competing interests. **Data and materials availability:** All data needed to evaluate the conclusions in the paper are present in the paper and/or the Supplementary Materials.

Submitted 25 August 2021
Accepted 20 January 2022
Published 11 March 2022
10.1126/sciadv.abm0303

**Acknowledgements**

Chapter 2, in full, is a reprint of the material as it appears in Thies AB, Quijada-Rodriguez AR, Zhouyao H, Weihrauch D, Tresguerres M. 2022 A Rhesus channel in the coral symbiosome membrane suggests a novel mechanism to regulate $NH_3$ and $CO_2$ delivery to algal symbionts. Sci. Adv. 8. (doi:10.1126/sciadv.abm0303). The dissertation author was the primary investigator and author of this paper. The material is used by permission of the American Association for the Advancement of Science (AAAS).

## Appendix

Science Advances
AAAS

Supplementary Materials for

# A Rhesus channel in the coral symbiosome membrane suggests a novel mechanism to regulate $NH_3$ and $CO_2$ delivery to algal symbionts

Angus B. Thies*, Alex R. Quijada-Rodriguez, Haonan Zhouyao,
Dirk Weihrauch, Martin Tresguerres*

*Corresponding author. Email: athies@ucsd.edu (A.B.T.); mtresguerres@ucsd.edu (M.T.)

Published 11 March 2022, *Sci. Adv.* **8**, eabm0303 (2022)
DOI: 10.1126/sciadv.abm0303

**The PDF file includes:**



**Other Supplementary Material for this manuscript includes the following:**

**SI Methods**

**Organisms**

*A. yongei* nubbins were originally sourced from the Birch Aquarium at Scripps and reared in a heated flow-through seawater aquaria at Scripps Institution of Oceanography for at least 1 year prior to the experiments. These coral colonies predominantly contain *Cladocopium sp* (formerly *Symbiodinium* clade C). Average [$PO_4^{3-}$], [$NO_3^-$], [$NO_2^-$] and [$NH_4^+$] were 0.35 ± 0.02 μM, 0.29 ± 0.11 μM, 0 μM and 0.54 ± 0.1 μM, respectively (Southern California Coastal Ocean Observing System; https://sccoos.org/harmful-algal-bloom/). Temperature was kept at 26°C, light/dark cycle was 10/14h with sunrise at 08:00 and sunset at 18:00 (LED Fixture lights, Orbit Marine, model 4103-B). Light intensity in the aquaria was measured to be 120 μE (MSC15 Spectral Light Meter, Gigahertz-Optik, Amesbury, MA, USA).

**Cloning of ayRhp1**

Following the methods of (*15*), total RNA was collected by flash-freezing a 2cm *A. yongei* nubbin in liquid nitrogen and crushing with a mortar and pestle into a fine powder. Powdered tissue was resuspended in TRIzol reagent (Invitrogen, Carlsbad, CA, USA) and total RNA was extracted following the manufacturer's protocol. Total RNA was cleaned and concentrated using an RNeasy Plus Mini Kit (Qiagen, Hilden, Germany). cDNA was synthesized using SuperScript III Reverse Transcriptase (Invitrogen) and Oligo(dT) primers according to the manufacturer's protocol. The resulting cDNA was used as template for all RT-PCR reactions. The full length ayRhp1 sequence was obtained following two rounds of RT-PCR using Phusion High Fidelity taq polymerase (New England Biolabs, Ipswitch, MA, USA) and NucleoSpin gel purification (Macherey-Nagel, Duren, Germany). The first round of RT-PCR used primers designed against untranslated regions of a predicted *Acropora digitifera* Rh mRNA (XP_015769291.1) (FWD primer 5'-CCACAATTCCGTC-3', REV primer 5'-GTCCGAGACATCTTGCATACC-3'). In the second 'nested' round of RT-PCR, primers included oligonucleotide overhangs for In-Fusion Cloning (Clontech, Mountain View, CA, USA) into a pCR2.1-TOPO vector (Invitrogen) digested with EcoR 1 and EcoR V restriction enzymes. All cloned RT-PCR products were sequenced by Retrogen, Inc. (San Diego, CA, USA). The full ayRhp1 sequence can be found on Genbank (MH025799).

Protein sequences for the phylogenetic analysis were sourced from (*74*) and Genbank via BLASTtn search. Sequences were aligned using MUSCLE (*79*) and a maximum likelihood tree with 500 bootstraps was inferred by RAxML using a PROTGAMMA model of rate heterogeneity and a GTR substitution model (*80*). Accession numbers of all Rh sequences used in this analysis can be found in the supporting information file (Table S1). Prediction of transmembrane helices was performed using TMHMM 2.0 (http://www.cbs.dtu.dk/services/TMHMM-2.0/) as per (*81*, *82*).

**ayRhp1 Protein Expression and Antibody Validation in *A. yongei***

Using methods adapted from (*4*), *A. yongei* tissue was removed from the skeleton using an airbrush loaded with homogenization buffer. Homogenate was sonicated on ice for 4 x 10-sec bursts with 1 min rest in-between. The sonicated homogenate was then centrifuged (500 x g, 15 min, 4°C) to pellet down debris; the supernatant was kept on ice but not frozen. Sample

protein concentrations were determined using a Bradford Protein Assay (Bio-Rad, Hercules, CA, USA). 4x Laemmli buffer (Bio-Rad) and 10% β-mercaptoethanol were added to samples before heating at 90°C for 3 min. 22.5 µg protein and 4 µl of Precision Plus Dual Color Protein Standards (Bio-Rad) were loaded into a 10% polyacrylamide SDS-PAGE gel in a Mini-Trans Blot Cell (Bio-Rad) with running buffer (25 mM Tris, 190 mM glycine, 0.1% SDS). Electrophoresis was run for 100 min at 100 V (4°C).

Following electrophoresis, the gel was washed in distilled water for 5 min and equilibrated in Towbin buffer (25 mM Tris pH 8.3, 192 mM glycine, 20% (v/v) methanol) for 15 min. Proteins were transferred from the gel onto a PVDF membrane using a Mini Tans-Blot Cell (Bio-Rad) overnight in Towbin buffer (0.09 A, 4°C). PVDF membranes were washed in Tris-buffered Saline + 0.1% Tween detergent (TBS-T) for 15 min on a shaker at room temperature to remove excess transfer buffer prior to blocking. Membranes were then blocked with 5% powdered fat-free milk in TBS-T for 1 h on a shaker at room temperature.

Following blocking, membranes were incubated overnight on a shaker (4°C) with anti-ayRhp1 primary antibody (0.216 µg/ml), primary antibody with 400x excess peptide on a molar base ('pre-absorption control'), or pre-immune serum (0.216 µg/ml) diluted in blocking buffer. Membranes were then washed with 4 x 15-min TBS-T washes prior to incubation with secondary antibody (goat anti-rabbit-HRP diluted 1:10,000, Bio-Rad) for 1 h on a shaker at room temperature. Membranes were again washed with 4 x 15-min TBS-T washes and a final 15-min TBS wash prior to band development with an ECL Prime Western Blot Detection Kit (GE Healthcare, Chicago, IL, USA) and imaged using a Chemidoc Imaging system (Bio-Rad).

**Confirmation of ayRhp1 Protein Expression in *Xenopus* Oocytes**

Using methods adapted from (*83*), ayRhp1-expressing and control *Xenopus* oocytes were added to ice-cold homogenization buffer (250 mM sucrose, 1 mM EDTA, 30 mM TRIS in milliQ-water) spiked with protease inhibitor cocktail (MilliporeSigma, Burlington, MA, USA) at a ratio of 1 oocyte:50 µL. Oocytes were homogenized on ice by gentle pipetting and left for 20 mins at 4°C to solubilize membrane proteins. Homogenates were centrifuged (10,000 x g, 2 min, 4°C) to pellet yolk and debris; the lipid layers on top of the supernatants were removed and discarded. The supernatants were transferred to new tubes on ice and saved as crude homogenates. Sample protein concentrations were determined using a Bradford Protein Assay (Bio-Rad). 2x Laemmli buffer (Bio-Rad) and 10% β-mercaptoethanol was added to samples. Half of these homogenates were flash frozen in liquid nitrogen and returned to -80°C. The remaining crude homogenate was heated to 70°C for 15 min and 16.0 µg total protein was subjected to Western blotting as described in the Methods. The PDVF membranes were incubated overnight on a shaker (4°C) with anti-ayRhp1 antibodies (0.216 µg/ml), primary antibody with 400x excess peptide on a molar base ('pre-absorption control'), or anti-Tubulin mouse monoclonal antibody (4.7 ng/mL, 12G10 anti-alpha-tubulin, developed by J. Frankel and E.M. Nelsen, and obtained from the Developmental Studies Hybridoma Bank, created by the NICHD of the NIH and maintained at The University of Iowa, Department of Biology, Iowa City, IA 52242). PVDF membranes were processed as described in the Methods, using goat anti-rabbit-HRP or goat anti-mouse-HRP diluted 1:5,000 (Bio-Rad) as the secondary antibodies. The anti-ayRhp1 antibodies labeled a ~180 kDa band in ayRhp1-expressing oocytes which was

absent in control oocytes and in the pre-absorption control. This band corresponds to ayRhp1 trimers. (Fig. S6A).

The following day, the refrozen ayRhp1-expressing and control oocyte homogenates were thawed to promote dissociation of ayRhp1 trimers, mixed with 2x Laemmli buffer (Bio-Rad) and β-mercaptoethanol, heated to 70°C for 15 min, and subjected to Western blotting and imaging as described above. The anti-ayRhp1 antibodies labeled ~120 and ~60 kDa bands that are absent in the control oocytes and in the pre-absorption control. These bands correspond to ayRhp1 dimers and monomers, respectively. (Fig. S6B-C). In addition to confirming ayRhp1 expression in *Xenopus* oocytes, these results conform the specificity of the anti-ayRhp1 antibodies against ayRhp1.

**Immunofluorescence**

Following (*84*), *A. yongei* nubbins were fixed for immunohistochemistry by immersion in S22 buffer (450 mM NaCl, 10 mM KCl, 58 mM $MgCl_2$, 10 mM $CaCl_2$, 100 mM Hepes, pH 7.80) supplemented with 4% paraformaldehyde overnight on a rocking platform at 4°C. Nubbins were then transferred to calcium-free S22 buffer supplemented with 0.5 M EDTA to decalcify the skeleton and with 0.5% paraformaldehyde to preserve tissue fixation; this decalcification buffer was changed daily for 2 weeks. Once decalcified, nubbins were dehydrated (50% ethanol for 5 h, 70% ethanol overnight, 95% ethanol for 20 min, 100% ethanol 3 x 20 min, SafeClear for 3 x 20 min), embedded in paraffin wax (3 x 30 min) and allowed to solidify for 48 h before microtome sectioning onto glass slides. *A. yongei* tissue sections were deparaffinized and serially rehydrated in SafeClear for 3 x 10 min, 100% ethanol for 10 min, 95% ethanol for 10 min, 70% ethanol for 10 min, and PBS with 0.2% (v/v) Triton-X-100 (PBS-TX) for 10 min.

Using methods adapted from (*84*, *49*), isolated *A. yongei* cells were prepared by submerging a nubbin in 0.2 µm filtered seawater and brushed with a toothbrush for 1 min. Cells were collected via centrifugation (3,000 x g, 4 minutes, 4°C) and fixed by resuspension in S22 buffer with 4% paraformaldehyde for 15 min on ice. Fixative was removed via centrifugation (3,000 x g, 4 minutes, 4°C) and cells were resuspended in ~500µL of S22 buffer. Cells were then pipetted onto glass microscope slide and allowed to air dry at 4°C for no longer than 1 h before proceeding to immunolabeling.

Tissue sections and isolated cells were blocked for 1 h at room temperature in blocking buffer (4 ml PBS-TX, 80 µl normal goat serum, 0.8 µl keyhole limpet hemocyanin solution), followed by overnight incubation (4°C) with anti-ayRhp1 antibodies (2.16 µg/ml), anti-ayRhp1 antibodies pre-absorbed with excess peptide (8.64 µg/ml) or pre-immune serum (2.16 µg/ml) (all in blocking buffer) (Fig. S4D). Slides were washed in PBS-TX to remove unbound anti-ayRhp1 antibodies (3 x 5 min). Secondary antibodies (goat anti-rabbit-Alexa Fluor555, 4 µg/ml in blocking buffer; Invitrogen) were then added for 1 h at room temperature followed by DAPI DNA Stain (1 µg/ml; Invitrogen) for 5 min at room temperature. Slides were again washed PBS-TX to remove unbound secondary antibody (3 x 5 min) and samples were imaged using a fluorescence microscope (Zeiss AxioObserver, Carl Zeiss AG, Oberkochen, Germany).

Supplemental Figure 2.1: Maximum likelihood tree of ayRhp1 in relation to invertebrate and vertebrate Rh proteins. Rh family subgroups are denoted by color: Rh30 (yellow), Rhag (blue), Rhbg (orange), Rhcg (green), Rhp1 (light and dark purple), and Rhp2 (grey) as per (2). Cnidarian Rh proteins are highlighted within the Rhp1 subgroup (light purple). Amino acid sequences were aligned using MUSCLE and a maximum likelihood tree was generated using RAxML (500 bootstraps, PROTGAMMA model of rate heterogeneity, GTR substitution model). Sequences and the outgroup (*Nitrosoma europaea* Rh) are sourced from (2) with additional sequences identified by NCBI BLAST search. Sequence accession numbers are provided in Supplementary Table 1.

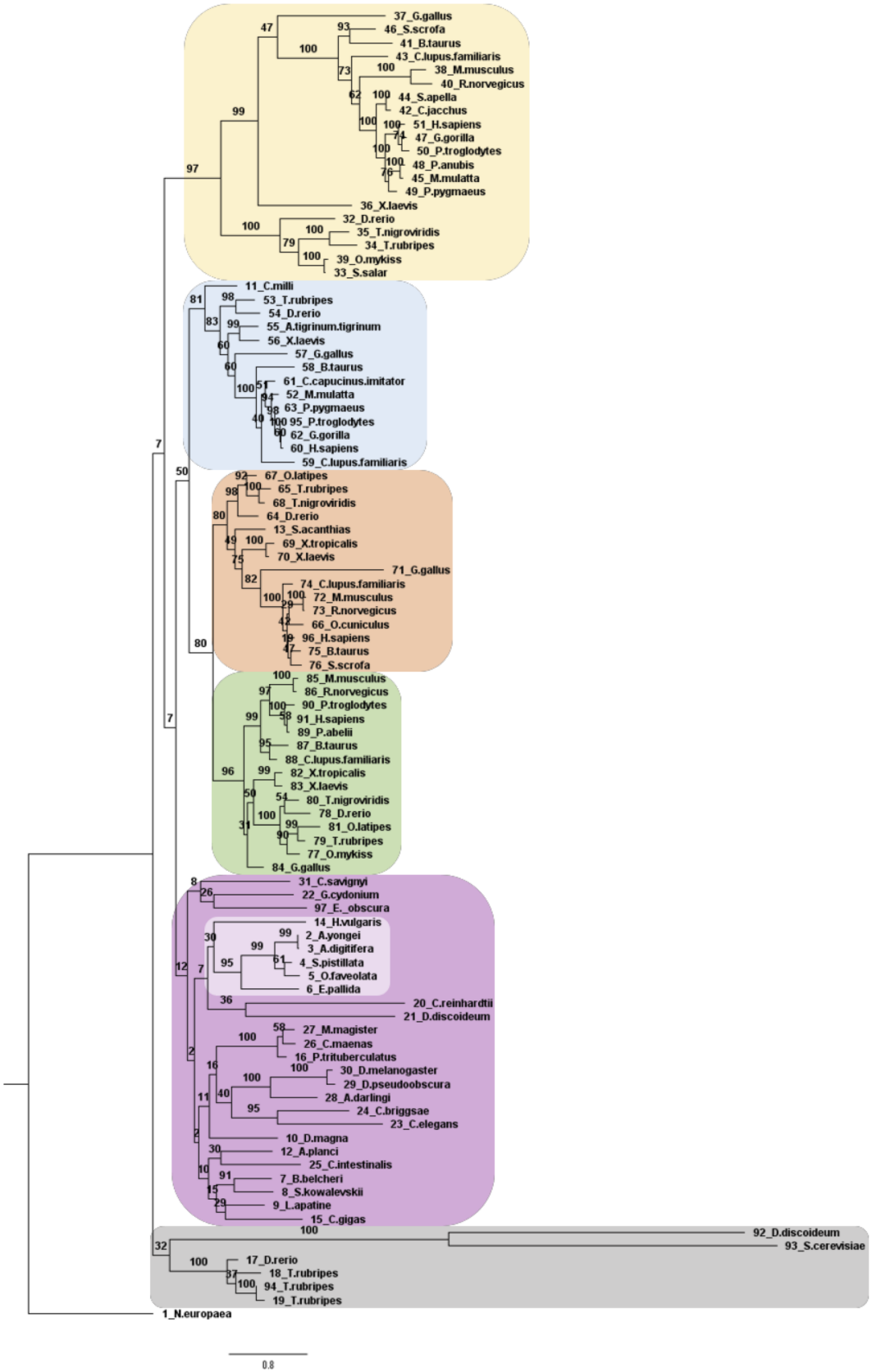
37_G.gallus
46_S.scrofa
41_B.taurus
43_C.lupus.familiaris
38_M.musculus
40_R.norvegicus
44_S.apella
42_C.jacchus
51_H.sapiens
47_G.gorilla
50_P.troglodytes
48_P.anubis
45_M.mulatta
49_P.pygmaeus
36_X.laevis
32_D.rerio
35_T.nigroviridis
34_T.rubripes
39_O.mykiss
33_S.salar
11_C.milli
53_T.rubripes
54_D.rerio
55_A.tigrinum.tigrinum
56_X.laevis
57_G.gallus
58_B.taurus
61_C.capucinus.imitator
52_M.mulatta
63_P.pygmaeus
95_P.troglodytes
62_G.gorilla
60_H.sapiens
59_C.lupus.familiaris
67_O.latipes
65_T.rubripes
68_T.nigroviridis
64_D.rerio
13_S.acanthias
69_X.tropicalis
70_X.laevis
71_G.gallus
74_C.lupus.familiaris
72_M.musculus
73_R.norvegicus
66_O.cuniculus
96_H.sapiens
75_B.taurus
76_S.scrofa
85_M.musculus
86_R.norvegicus
90_P.troglodytes
91_H.sapiens
89_P.abelii
87_B.taurus
88_C.lupus.familiaris
82_X.tropicalis
83_X.laevis
80_T.nigroviridis
78_D.rerio
81_O.latipes
79_T.rubripes
77_O.mykiss
84_G.gallus
31_C.savignyi
22_G.cydonium
97_E._obscura
14_H.vulgaris
2_A.yongei
3_A.digitifera
4_S.pistillata
5_O.faveolata
6_E.pallida
20_C.reinhardtii
21_D.discoideum
27_M.magister
26_C.maenas
16_P.trituberculatus
30_D.melanogaster
29_D.pseudoobscura
28_A.darlingi
24_C.briggsae
23_C.elegans
10_D.magna
12_A.planci
25_C.intestinalis
7_B.belcheri
8_S.kowalevskii
9_L.apatine
15_C.gigas
92_D.discoideum
93_S.cerevisiae
17_D.rerio
18_T.rubripes
94_T.rubripes
19_T.rubripes
1_N.europaea
0.8

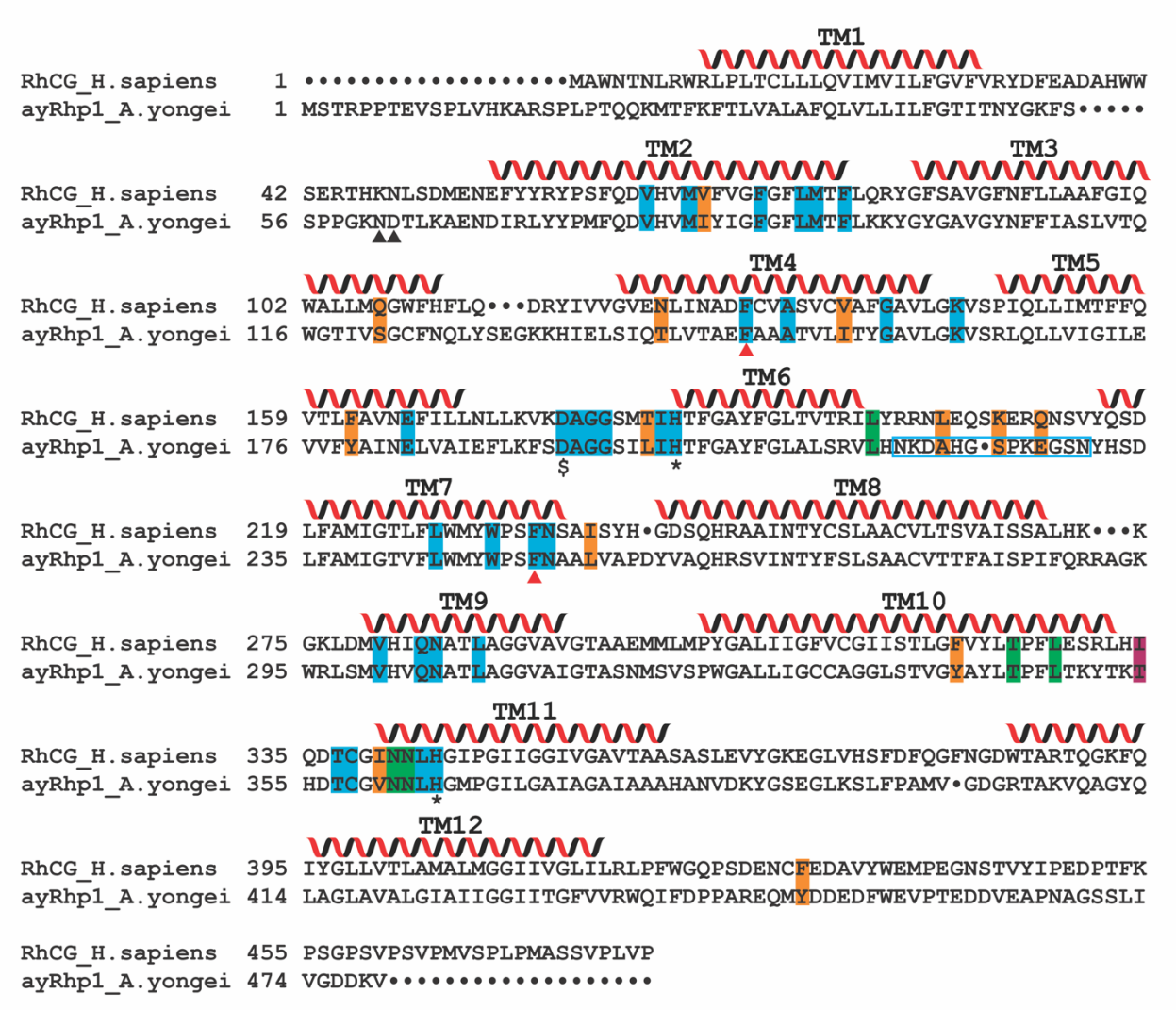


Supplemental Figure 2.2: Alignment of ayRhp1 with *Homo sapiens* RhCG (NP_001307970.1). Conserved (blue) and mismatched (orange) hydrophobic channel-lining residues, conserved (green) and mismatched (magenta) cytosolic shunt residues, N-glycan site (black filled triangles), $CO_2$ binding pocket (black outlined triangles) as discussed in (35), Phe-gate (red filled triangles), twin-Histidines (*), and the highly-conserved aspartate residues ($) as discussed in (20, 34) are marked. Gaps in sequences are denoted by black dots. The 12 transmembrane helices (TM), as predicted by TMHMM 2.0 (5, 6), for RhCG (20) and ayRhp1 are labeled with spirals.

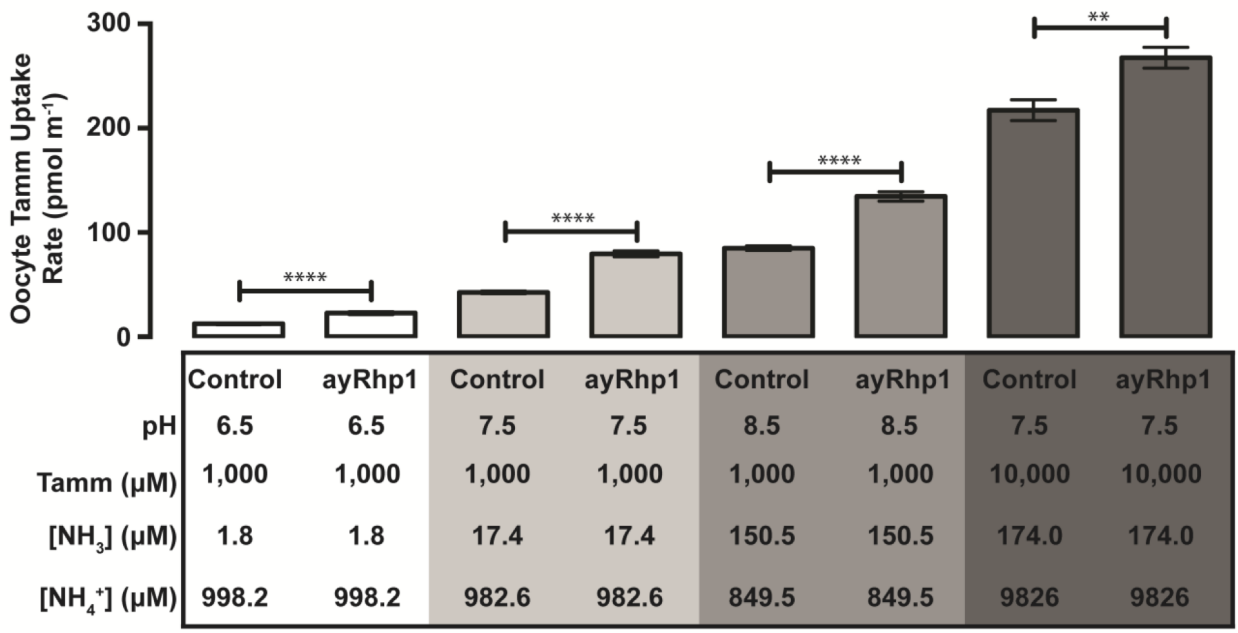


| | Control | ayRhp1 | Control | ayRhp1 | Control | ayRhp1 | Control | ayRhp1 |
|---|---|---|---|---|---|---|---|---|
| pH | 6.5 | 6.5 | 7.5 | 7.5 | 8.5 | 8.5 | 7.5 | 7.5 |
| Tamm (μM) | 1,000 | 1,000 | 1,000 | 1,000 | 1,000 | 1,000 | 10,000 | 10,000 |
| $[NH_3]$ (μM) | 1.8 | 1.8 | 17.4 | 17.4 | 150.5 | 150.5 | 174.0 | 174.0 |
| $[NH_4^+]$ (μM) | 998.2 | 998.2 | 982.6 | 982.6 | 849.5 | 849.5 | 9826 | 9826 |

Supplemental Figure 2.3: Effect of $[NH_3]$ on Tamm uptake rate in *Xenopus* oocytes expressing ayRhp1. Data shows mean ± S.E.M. of 6-14 oocytes; * denote significant differences (unpaired t-test; **$p<0.01$; ****$p<0.001$).

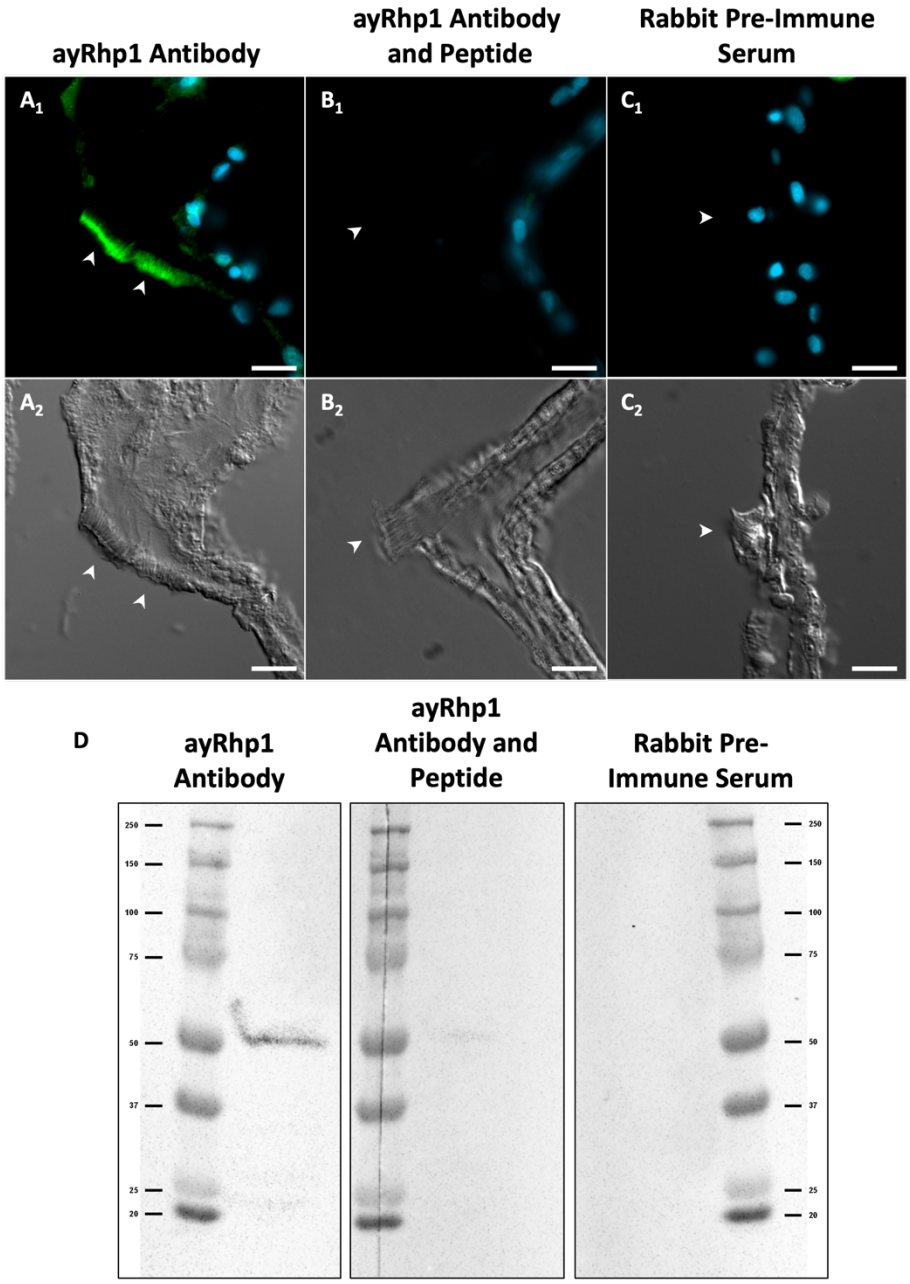


Supplemental Figure 2.4: Immunohistochemistry and Western blot validation of the custom anti-ayRhp1 antibody. Tissue sections were incubated with anti-ayRhp1 primary antibody, primary antibody with excess peptide, or pre-immune serum at an equal concentration to primary antibody alone. Anti-ayRhp1 antibody signal dissipates with peptide incubation and is absent in pre-immune serum incubations. (**$A_1$-$C_1$**) Desmocytes in tissue sections; desmocytes are the most brightly-labeled cell type in A. yongei tissues. (**$A_2$-$C_2$**) corresponding brightfield differential interference contrast images. Nuclei are shown in blue, ayRhp1 in red. White arrowheads mark corresponding locations in epifluorescence and brightfield images. Scale bars = 10 μm. (**D**) Western Blot validation of the custom ayRhp1 antibody. Membranes were labeled with anti-ayRhp1 primary antibody, primary antibody with excess peptide, or pre-immune serum at an equal concentration to primary antibody alone.

Supplemental Figure 2.5: Epifluorescence immunolocalization of ayRhp1 in isolated alga-hosting gastrodermal cells. (**$A_1$**) Algal symbiont isolated from its host cell. (**$B_1$**) A coral host cell with ayRhp1 on the symbiosome membrane. (**$C_1$**) A coral host cell containing two algal symbionts with ayRhp1 on both symbiosome membranes. (**$D_1$**) A coral host cell with ayRhp1 on the exterior and sides of the host nucleus. (**E-N**) Further representative epifluorescence images of ayRhp1 in isolated alga-hosting gastrodermal cells. (**$B_1$, $D_1$, $E_1$-$I_1$**) Cells displaying ayRhp1 in the symbiosome membrane; notice the separation of host and algal nuclei by ayRhp1. (**$D_1$, $F_1$-$N_1$**) Cells displaying non-symbiosomal ayRhp1; notice ayRhp1 signal exterior to the host nucleus and absent between the host and algal nuclei. (**$A_2$-$N_2$**) Corresponding images without brightfield differential interference contrast. Blue arrowheads mark nuclei of host cells; violet arrowheads mark ayRhp1 symbiosome localization. Nuclei are shown in blue and ayRhp1 in green. Scale bars = 5 μm.

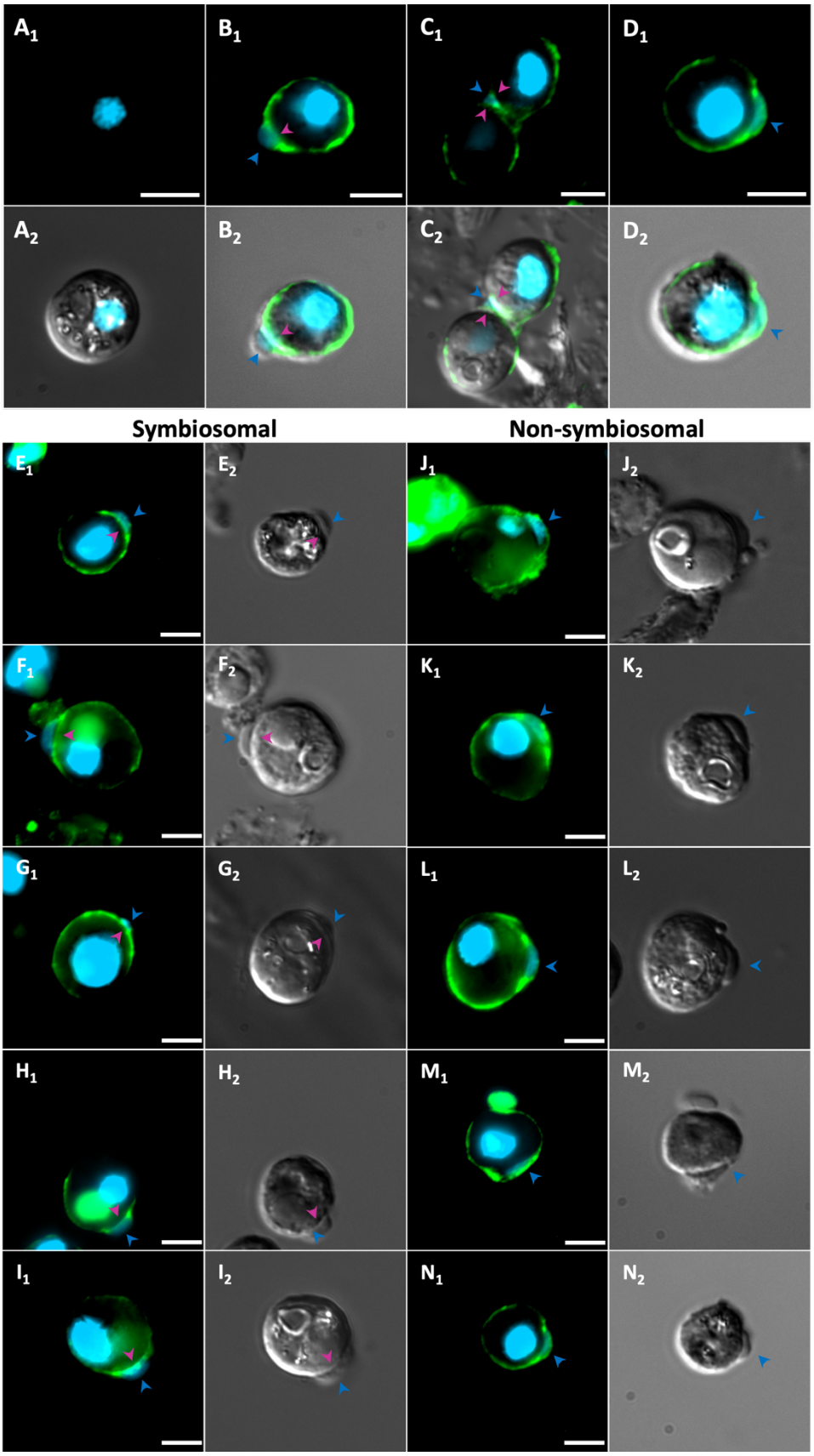
A1
B1
C1
D1
A2
B2
C2
D2
Symbiosomal
Non-symbiosomal
E1
E2
J1
J2
F1
F2
K1
K2
G1
G2
L1
L2
H1
H2
M1
M2
I1
I2
N1
N2

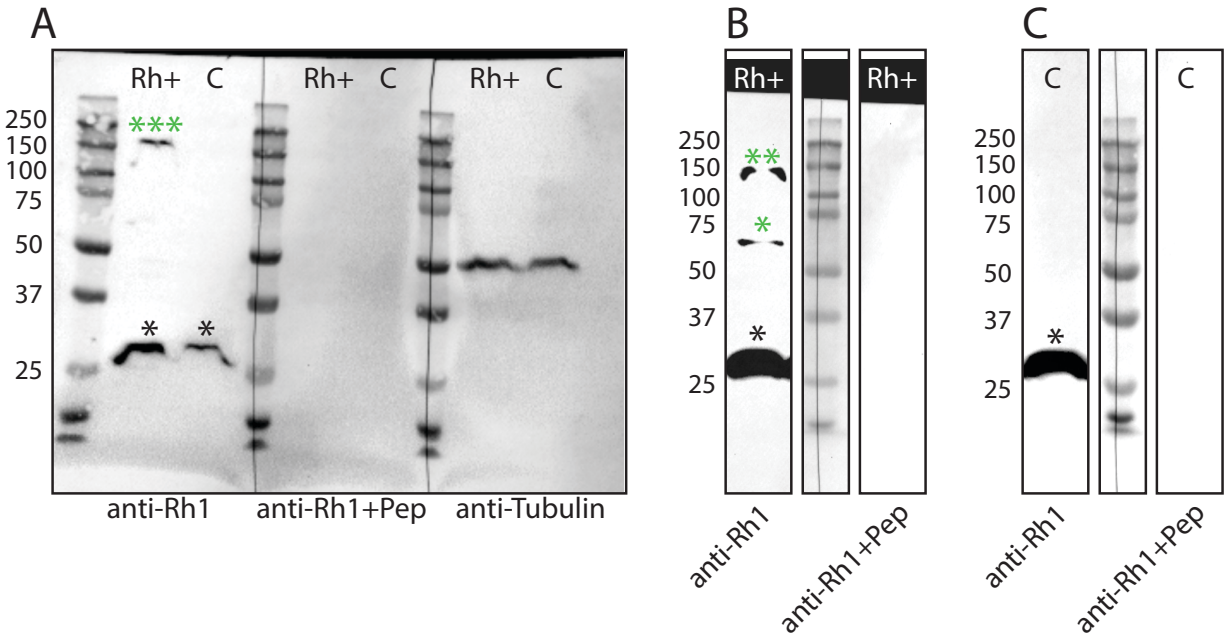


Supplemental Figure 2.6: Western blot validation of ayRhp1 expression in *Xenopus* oocytes. (**A**) Western Blot of once-thawed ayRhp1-expressing (Rh+) and control (C) oocytes, which were homogenized and heated at 70°C for 15 min before loading into the gels. PVDF membranes were incubated with anti-ayRhp1 antibodies, anti-ayRhp1 antibodies pre-incubated with excess peptide (pre-absorption control), or anti-Tubulin antibody (12G10 anti-alpha-tubulin, developed by J. Frankel and E.M. Nelsen, and obtained from the Developmental Studies Hybridoma Bank, created by the NICHD of the NIH and maintained at The University of Iowa, Department of Biology, Iowa City, IA 52242). The anti-ayRhp1 antibodies labeled a ~180 kDa band in Rh+ oocytes which was absent in C oocytes (marked with three green asterisks) and in the preabsorption control. This band corresponds to ayRhp1 trimers. The antibodies additionally labeled a ~29 kDa band in both Rh+ and C oocytes (marked with a black asterisk) which was not present in the pre-absorption control; this band represents off-target recognition of Xenopus protein(s). The anti-tubulin antibody labeled a ~50 kDa protein in both treatments demonstrating equivalent protein concentration in Rh+ and C samples. (**B, C**) Western Blots of rethawed Rh+ (B) and C (C) oocyte homogenates which were heated at 70°C for 15 min before loading into the gels. The anti-ayRhp1 antibodies labeled a ~120 kDa band (marked with two red asterisks) and a ~60 kDa band (marked with one red asterisk) that are absent in the C oocytes and in the pre-absorption control. These bands correspond to ayRhp1 dimers and monomers, respectively. The ~29 kDa band is still present in the rethawed homogenates.

Supplemental Table 2.1: NCBI accession numbers for sequences used in phylogenetic analysis (Fig. S1).

| ID | Accession Number | Organism | ID | Accession Number | Organism |
|---|---|---|---|---|---|
| 1 | AY377923.1 | Nitrosomonas europaea | 50 | Q28813.2 | Pan troglodytes |
| **2** | **MH025799** | **Acropora yongei** | 51 | P18577.2 | Homo sapiens |
| 3 | XP_015769291.1 | Acropora digitifera | 52 | NP_001027987.1 | Macaca mulatta |
| 4 | XP_022795556.1 | Stylophora pistillata | 53 | NP_001032956.1 | Takifugu rubripes |
| 5 | XP_020600999.1 | Orbicella faveolata | 54 | NP_998010.1 | Danio rerio |
| 6 | KXJ18310.1 | Exaiptasia pallida | 55 | AAV28818.1 | Ambystoma tigrinum tigrinum |
| 7 | XP_019645061.1 | Branchiostoma belcheri | 56 | XP_018121493.1 | Xenopus laevis |
| 8 | XP_006824549.1 | Saccoglossus kowalevskii | 57 | NP_989795.1 | Gallus gallus |
| 9 | XP_013381459.1 | Lingula anatine | 58 | NP_776596.1 | Bos taurus |
| 10 | KZS19566.1 | Daphnia magna | 59 | NP_001104238.1 | Canis lupus familiaris |
| 11 | AFK10779.1 | Callorhinchus milii | 60 | AHY04440.1 | Homo sapiens |
| 12 | XP_022107421.1 | Acanthaster planci | 61 | XP_017354151.1 | Cebus capucinus imitator |
| 13 | AJF44128.1 | Squalus acanthias | 62 | NP_001266499.1 | Gorilla gorilla |
| 14 | XP_002167946.3 | Hydra vulgaris | 63 | AAG00305.1 | Pongo pygmaeus |
| 15 | EKC21768.1 | Crassostrea gigas | 64 | NP_956365.2 | Danio rerio |
| 16 | AHY27545.2 | Portunus trituberculatus | 65 | NP_001027818.1 | Takifugu rubripes |
| 17 | NP_571622.1 | Danio rerio | 66 | NP_001075605.1 | Oryctolagus cuniculus |
| 18 | NP_001027816.1 | Takifugu rubripes | 67 | NP_001098561.1 | Oryzias latipes |
| 19 | NP_001027817.1 | Takifugu rubripes | 68 | Q3BBX8.1 | Tetraodon nigroviridis |
| 20 | XP_001695464.1 | Chlamydomonas reinhardtii | 69 | NP_001011175.1 | Xenopus tropicalis |
| 21 | XP_639042.1 | Dictyostelium discoideum | 70 | Q69D48.1 | Xenopus laevis |
| 22 | CAA73029.1 | Geodia cydonium | 71 | AAN34362.1 | Gallus gallus |
| 23 | AAF97864.1 | Caenorhabditis elegans | 72 | AAF19371.1 | Mus musculus |
| 24 | XP_002636925.1 | Caenorhabditis briggsae | 73 | NP_898877.1 | Rattus norvegicus |
| 25 | NP_001027959.1 | Ciona intestinalis | 74 | NP_001003017.2 | Canis lupus familiaris |
| 26 | AAK50057.2 | Carcinus maenas | 75 | NP_777148.1 | Bos taurus |
| 27 | AEA41159.1 | Metacarcinus magister | 76 | NP_999161.1 | Sus scrofa |
| 28 | ETN62951.1 | Anopheles darlingi | 77 | NP_001117995.1 | Oncorhynchus mykiss |
| 29 | AAV40852.1 | Drosophila pseudoobscura | 78 | AAM90586.1 | Danio rerio |
| 30 | NP_001261434.1 | Drosophila melanogaster | 79 | NP_001027934.1 | Takifugu rubripes |
| 31 | AAY41910.1 | Ciona savignyi | 80 | Q3BBX7.1 | Tetraodon nigroviridis |
| 32 | NP_001019990.1 | Danio rerio | 81 | NP_001116374.1 | Oryzias latipes |
| 33 | NP_001117044.1 | Salmo salar | 82 | XP_012814245.1 | Xenopus tropicalis |
| 34 | NP_001027935.1 | Takifugu rubripes | 83 | Q5U4V1.1 | Xenopus laevis |
| 35 | AAY41905.1 | Tetraodon nigroviridis | 84 | NP_001004370.1 | Gallus gallus |
| 36 | NP_001084416.1 | Xenopus laevis | 85 | AAF19373.1 | Mus musculus |
| 37 | NP_989798.1 | Gallus gallus | 86 | NP_898876.1 | Rattus norvegicus |
| 38 | AAC25123.1 | Mus musculus | 87 | NP_776597.1 | Bos taurus |
| 39 | AAP87367.1 | Oncorhynchus mykiss | 88 | NP_001041487.1 | Canis lupus familiaris |
| 40 | NP_071950.1 | Rattus norvegicus | 89 | XP_002825848.1 | Pongo abelii |
| 41 | NP_777137.1 | Bos taurus | 90 | XP_016782540.1 | Pan troglodytes |
| 42 | AAF22442.1 | Callithrix jacchus | 91 | NP_057405.1 | Homo sapiens |
| 43 | NP_001041501.1 | Canis lupus familiaris | 92 | BAB39709.1 | Dictyostelium discoideum |
| 44 | AAF22501.1 | Sapajus apella | 93 | X77608.1 | Saccharomyces cerevisiae |
| 45 | NP_001028136.3 | Macaca mulatta | 94 | AAU81656.1 | Takifugu rubripes |
| 46 | NP_999543.1 | Sus scrofa | 95 | NP_001009033.1 | Pan troglodytes |
| 47 | NP_001266526.1 | Gorilla gorilla | 96 | AF193807.1 | Homo sapiens |
| 48 | XP_003891396.1 | Papio anubis | 97 | AJO26542.1 | Erpobdella obscura |
| 49 | AAC94962.1 | Pongo pygmaeus | | | |

Supplemental Table 2.2: Cell count data used for determining diel ayRhp1 localization in coral host cells.

| Trial | Time | # cells with symbiosomal ayRhp1 signal | # cells with non-symbiosomal ayRhp1 signal |
|---|---|---|---|
| 1 | 1330 | 35 | 15 |
| 1 | 1730 | 27 | 23 |
| 1 | 1830 | 22 | 28 |
| 1 | 2300 | 12 | 38 |
| 1 | 730 | 24 | 26 |
| 1 | 830 | 31 | 19 |
| 2 | 1330 | 29 | 21 |
| 2 | 1730 | 18 | 32 |
| 2 | 1830 | 21 | 29 |
| 2 | 2300 | 15 | 35 |
| 2 | 730 | 16 | 34 |
| 2 | 830 | 25 | 25 |
| 3 | 1330 | 28 | 22 |
| 3 | 1730 | 22 | 28 |
| 3 | 1830 | 12 | 38 |
| 3 | 2300 | 12 | 38 |
| 3 | 730 | 29 | 21 |
| 3 | 830 | 28 | 22 |

# Chapter 3

## V-type $H^+$-ATPase and carbonic anhydrase support symbiont photosynthesis in *Cassiopea* amoebocytes

**Abstract**

Nutrient exchange across the symbiosome membrane is a hallmark of photosymbioses between intracellular dinoflagellate algae and their cnidarian hosts. Algae translocate photosynthetically fixed carbon and $O_2$ to the host which, in turn, supplies the symbiont with inorganic carbon to fuel continued photosynthate production. Corals and anemones employ V-type $H^+$-ATPase-driven (VHA) carbon concentrating mechanisms (CCMs) to supply symbionts with $CO_2$ thereby promoting symbiont photosynthesis. *Cassiopea xamachana*, the Upside-Down Jellyfish, is a rapidly developing model for cnidarian symbiosis. While *Cassiopea ssp.* retain the same symbionts as other cnidarians, their host cells (amoebocytes) exhibit unique developmental and architectural differences, namely being highly mobile and containing more symbionts per host cell. Given these differences, we sought to explore whether *Cassiopea* amoebocytes employ an analogous VHA-driven CCM. We additionally tested whether carbonic anhydrase (CA) contributes to the CCM. We found that *C. xamachana* amoebocytes express both VHA and CA and that VHA was expressed at the highest levels in amoebocytes. VHA localized to the symbiosome membrane surrounding symbionts while CA occasionally appeared around the periphery of the membrane. Inhibition of both VHA and CA resulted in significant reductions in $O_2$ evolution rate, a proxy for photosynthetic activity. These results suggest that host VHA and CA are functionally coupled in amoebocyte CCMs and that *C. xamachana* amoebocytes are suitable models for cnidarian host cells at large.

## Introduction

Symbiotic associations between animals and microorganisms are ubiquitous in the marine world affording both partners metabolic advantages in competitive environments. Upside-Down Jellyfish, *Cassiopea ssp.* (phylum Cnidaria, class Scyphozoa), form a characteristic endosymbiotic relationship with Symbiodiniaceae dinoflagellate algae, the same symbionts found in reef-building corals and anemones (phylum Cnidaria, class Anthozoa) and giant clams (phylum Mollusca). In Cnidarians, the symbiosis is established when free-living dinoflagellates enter the gastrovascular cavity and are endocytosed by gastrodermal cells that sequester them in an arrested phagosome known as the "symbiosome" [reviewed in (Tang 2015)]. Dinoflagellates remain photosynthetically active in symbiosis releasing photosynthates (i.e. sugars, lipids, amino acids) and $O_2$ to the animal host [reviewed in (Davy et al. 2012)] thereby satisfying the daily organic carbon demands of the animal (Verde and R. McCloskey 1998; Tanaka et al. 2018). In turn, host respiration generates ample DIC (dissolved inorganic carbon) to fuel symbiont photosynthesis, support carbon fixation, and allow continual release of photosynthates. Therefore, nutrient cycling is a hallmark of cnidarian photosymbioses with hosts evolving mechanisms to enhance nutrient transfer to their symbionts.

In the host cells of photosymbiotic cnidarians, the symbiosome is modified to support symbiont photosynthesis and nutrient cycling by concentrating $CO_2$/dissolved inorganic carbon (DIC) in the symbiont's microenvironment (Barott et al. 2015, 2022; Hambleton et al. 2019; Mashini et al. 2022; Thies et al. 2022). The need for such host cell-driven carbon concentrating mechanisms (CCM) is necessitated by algal Rubisco's low affinity for $CO_2$ which prevents carbon fixation from occurring at ambient $pCO_2$ levels, a problem exaggerated in light-limiting, low DIC environments (Leggat et al. 2002; Yee et al. 2023). In addition, $O_2$ competes with $CO_2$-binding

capacity of Rubisco in low-DIC environments thereby necessitating a continued supply of $CO_2$ to prevent the generation of reactive oxygen species and damage to symbiont photosystems (Lesser 1996; Warner et al. 1999). To concentrate DIC, the symbiosome is markedly acidic (pH <6) driven by $H^+$ pumping by animal V-type $H^+$-ATPases (VHAs) located in the symbiosome membrane (Venn et al. 2009; Barott et al. 2015). This activity establishes a steep pH gradient with the cytosol of host cells (~1000x more basic, $pH_i$ 7-8) (Venn et al. 2009; Barott et al. 2017) which can drive secondary metabolite transport across the symbiosome membrane. In corals and anemones, the symbiosomal pH gradient is employed to concentrate $CO_2$ for algal photosynthesis (Barott et al. 2015, 2022). The pH-dependent nature of DIC speciation between $CO_2$, $HCO_3^-$, and $CO_3^{2-}$ and the $pH_i$ of cnidarian host cells (pH 7-8) dictates the majority of DIC in animal cells exists as membrane-impermeable $HCO_3^-$. Given the $pK_a$ for $HCO_3^-$ to $CO_2$ conversion is 6.1, any DIC that enters the symbiosome is immediately dehydrated into $CO_2$ which can diffuse across the symbiont cell wall and accumulate at the site of carbon fixation. The identity of the transporter(s) responsible for $HCO_3^-$ movement into the symbiosome remains elusive. Notably, VHA-driven acidification across epithelia of eukaryotic cells is achieved by functional coupling with carbonic anhydrases (CA) to catalyze the interconversion of $CO_2$ and $HCO_3^-/H^+$ (Tresguerres et al. 2013, 2019). CAs have been suggested to support DIC interconversion as part of a CCM in cnidarian host cells (Weis 1993; Benazet-Tambutte et al. 1996; Al-Moghrabi et al. 1996) however, the putative contribution of CAs is not fully established: early microscopy data was hindered by limited resolution and pharmacological experiments employed CA-inhibitors at levels likely to cause off-target effects. Here, we employ *Cassiopea xamachana* host cells as a model to investigate if VHA and CA are functionally coupled in cnidarian CCMs.

Unique to *Cassiopea ssp*., newly formed symbiosomes are transported to the basal pole of the gastrodermal cell, which next detach from the endodermal cell layer and migrate into the mesoglea, the connective tissue that separates the ecto- and endodermal cell layers (Fitt and Trench 1983; Colley and Trench 1985). The mesoglea of *Cassiopea ssp.* is greatly enlarged relative to anthozoans, with two important implications: (1) it allows amoebocytes to expand without the spatial constraints imposed by the tightly packed gastrodermal cell layer. Amoebocyte cells host up to ten symbionts each, while host cells of corals and anemones typically contain only one, and very occasionally two or three (Fitt and Trench 1983; Davy et al. 2012). (2) Amebocytes roam throughout the mesoglea enabling widespread distribution of symbiont photosynthates to fuel metabolism in non-photosynthetic tissues such as muscle cells (Lyndby et al. 2020). In *C. xamachana*, photosynthate supply from symbionts can exceed host requirements by >70% and fuel a daily growth rate of 3% (Welsh et al. 2009). Notably, polyps will not develop into medusae until a specific population density of photosynthetically-active symbionts is achieved, which highlights the critical importance of the endosymbiosis on the energy budget and life cycle of *Cassiopea* (Hofmann et al. 1978; Jinkerson et al. 2022). *Cassiopea ssp.* amoebocytes therefore present a unique case study for exploring links between phagocytosis, DIC delivery, and the evolution of the symbiosome.

*C. xamachana* medusae presents an ideal model to investigate whether cnidarians employ CAs as part of the symbiosomal CCM. First, amoebocyte-bound symbionts are spatially isolated from sources of DIC including respiring non-symbiotic cells, gastric cavities, and seawater by the extensive mesoglea network. Isolation in the mesoglea presents a uniquely challenging $O_2$ and $CO_2$ microhabitat: the cnidarian mesoglea exhibits low gas permeability (Brafield and Chapman 1983) resulting in buildup of $O_2$ (Lyndby et al. 2023) and likely depletion of $CO_2$ under

illumination. In fact, *C. xamachana* (and some coral) symbionts are naturally DIC limited (Rädecker et al. 2017; Roberty et al. 2020). Given that endosymbionts are reliant on amoebocytes to supply DIC and nutrients for photosynthesis and growth, amoebocytes may therefore employ more CCMs than other cnidarians to concentrate any available DIC for photosynthesis. Accordingly, *C. xamachana* amoebocytes deliver DIC from host tissues, gastric cavities, and seawater to intracellular symbionts (Lyndby et al. 2020), yet despite their pivotal role in supporting symbiosis, the cellular mechanisms by which amoebocytes promote carbon cycling remain completely uninvestigated.

Second, amoebocytes maintain many more symbionts per host cell than any other cnidarian. Such crowding likely contributes to further DIC competition amongst symbionts suggesting that amoebocytes have adapted to maximize DIC delivery. This assertion is supported by the remarkably fast growth rate of symbionts in *C. xamachana* which is ~10-fold faster than those in stony corals (Muscatine et al. 1984; Wilkerson et al. 1988; Newkirk et al. 2018). Here, we explored the hypotheses that *C. xamachana amoebocytes* employ a VHA-driven CCM to support symbiont photosynthesis and that VHA is functionally coupled to CA. We found that (1) symbiotic amoebocytes express both VHA B subunit ($VHA_B$) and CA protein; (2) $VHA_B$ and CA localize to the symbiosome of amoebocyte host cells; (3) VHA and CA activity are required for optimal photosynthetic output. Together these results support the conclusion that *C. xamachana* amoebocytes employ a VHA-driven, CA-coupled CCM to support symbiont photosynthesis. This study additionally marks the first proteomic characterization of *Cassiopea ssp.* amoebocytes.

## Methods

*Animals*

*C. xamachana* medusae (mixed assemblage of strains T2C, JB2, JB4, and JB8) were maintained in a recirculating 100 L aquarium filled with artificial seawater with the following conditions: temperature ~25-26 °C; salinity ~36 ppt; alkalinity ~2.4 meq/L; pH ~8.1-8.2; nitrate 0 ppm; nitrite 0 ppm; total ammonia <0.5 mg/L; calcium ~400 ppm. The aquarium was illuminated on a 12 h:12 h cycle with 250 μmol photons $m^{-2}$ $s^{-1}$ (μE) of photosynthetically active radiation (Hydra 64 HD LED light, Aqua Illumination, Bethlehem, PA, USA) as determined using a MQ-510 full-spectrum quantum sensor (Apogee Instruments, Inc., Logan, UT, USA). pH and temperature were monitored using a HACH PHC101 pH Electrode (HACH, Loveland, CO, USA). Total ammonia, nitrate, and nitrite were monitored using API Water Test Kits (Mars Fishcare Inc., Chalfont, PA, USA). Calcium and alkalinity levels were measured using marine calcium and alkalinity meters (Hanna Instruments Inc., Woonsocket, RI, USA). Animals were fed daily with either freshly hatched *Artemia* (San Francisco Strain, Brine Shrimp Direct, Ogden, UT, USA) or a 50:50 mixture of PhytoFeast and OysterFeast (Reef Nutrition, Campbell, CA, USA).

*Antibodies*

Tissues were probed for VHA using a custom rabbit polyclonal antibody developed using a peptide antigen matching a conserved region of the $VHA_B$ subunit (AREEVPGRRGFPGY; GenScript Biotech Corporation, Piscataway, NJ, USA) which is 100% conserved in species ranging from corals to humans (Tresguerres et al. 2013; Barott et al. 2015, 2022; Roa and Tresguerres 2016; Armstrong et al. 2018; Damsgaard et al. 2020). Based on peptide pre-absorption controls (Figure 3.1, Supplemental Figure 3.1) these antibodies also recognize $VHA_B$ protein in *C. xamachana*. Antibodies against human CA were purchased from Rockland Inc. (Gilbertsville, PA,

USA). These antibodies detect an approximately 30 kDa protein in mammals, fishes, and osedax (Yasukawa et al. 2007; Perry et al. 2010; Tresguerres et al. 2013).

*Western Blotting*

A ~1 cm chunk of *C. xamachana* bell tissue was flash frozen in liquid nitrogen and powdered using a mortar and pestle. Powdered tissue was homogenized in S22 buffer supplemented with protease inhibitor cocktail (Sigma-Aldrich, St. Louis, MO, USA) and phosphatase inhibitors (PhosStop; Roche Applied Science, Penzberg, Germany) with a glass homogenizer on ice. Homogenate was sonicated for 3 x 30 sec bursts with 1 min rests on ice. Cell debris was pelleted with a 100 x rcf centrifugation (4 min, 4 °C). Supernatant was sonicated again for 2 x 30 sec bursts with 1 min rest on ice. Cell debris was again pelleted with a 300 x rcf centrifugation (4 min, 4 °C). Supernatant was saved and subjected to a 3000 rcf centrifugation (4 min, 4 °C) to generate epidermal (supernatant) and endodermal (pellet) fractions as described for corals (Barott et al. 2022); pellet was resuspended in 100 µL homogenization buffer. Protein concentrations in both fractions were measured using a Bradford Assay with a bovine serum albumin standard curve (BioRad, Hercules, CA, USA). Homogenates were then incubated in Laemmli Sample buffer with 5% (v/v) β-mercaptoethanol for 5 min at 95 °C ($VHA_B$) or 15 min at 70 °C (CA) and equal protein of each fraction was loaded on a sodium dodecyl sulphate–polyacrylamide gel electrophoresis gel. Proteins were separated at 60 V for 30 min followed by 200 V for 1 h in Tris-glycine running buffer (25 mM Tris-base, 192 mM glycine, 0.1% (w/v) SDS, pH 8.3). Following electrophoresis, proteins were transferred from the gel onto a polyvinylidene difluoride (PVDF) membrane using a Mini Tans-Blot Cell (Bio-Rad) filled with Towbin transfer buffer (25 mM Tris, 192 mM glycine, 20% (v/v) methanol, pH 8.3) overnight. The membrane was washed for 5 min in Tris-buffered saline with 0.1% Tween (TBS-T) on an orbital shaker at room

temperature to remove transfer buffer. The membrane was blocked for 1 h on an orbital shaker in blocking buffer (5% (w/v) fat-free milk powder in TBS-T) at room temperature and then incubated overnight at 4 °C with either 1.5 µg $ml^{-1}$ polyclonal anti-$VHA_B$ primary antibody, anti-$VHA_B$ primary antibody with 60x excess peptide on a molar basis ("preabsorption control"), or 4.4 µg $ml^{-1}$ polyclonal anti-CA primary antibody in blocking buffer. The membrane was washed with 3 x 10 min TBS-T washes before incubation with secondary antibody [goat anti–rabbit–horseradish peroxidase (HRP) diluted 1:5000, Bio-Rad] for 1 hour on a shaker at room temperature. Membranes were again washed with 3 × 10 min TBS-T washes. Bands were visualized using an ECL Prime Western blot Detection Kit (GE Healthcare, Chicago, IL, USA) and imaged using a Chemidoc Imaging system (Bio-Rad). Prediction of protein domains was performed using InterPro, signal peptides using DeepLoc 2.0, and N-glycosylation sites using NetNGlyc 1.0 (Gupta and Brunak 2001; Thumuluri et al. 2022; Paysan-Lafosse et al. 2023).

*Immunohistochemistry (IHC)*

Whole *C. xamachana* were fixed in 3% paraformaldehyde in S22 buffer (450 mM NaCl, 10 mM KCl, 58 mM $MgCl_2$, 10 mM $CaCl_2$, 100 mM Hepes, pH 7.8) overnight at 4 °C on an orbital shaker. Tissues were dehydrated, embedded in paraffin wax, and sectioned following previously described protocols for corals (Barott and Tresguerres 2015). Briefly, tissues were deparaffinized, rehydrated, permeabilized in 0.2% Triton-X (v/v) in phosphate buffered saline (PBS-TX) and incubated in blocking buffer (2% normal goat serum and 0.5% keyhole limpet hemocyanin in PBS-TX) for 1 h at room temperature. Sections were incubated overnight (4 °C) with either 0.03 µg $ml^{-1}$ polyclonal anti-$VHA_B$ primary antibody in blocking buffer, anti-$VHA_B$ primary antibody with 13x excess peptide on a molar basis ("preabsorption control") in blocking buffer, 0.03 µg $ml^{-1}$ polyclonal anti-CA primary antibody in blocking buffer or blocking buffer alone. Sections

were washed with 3 x 5 min PBS-TX washes before incubation with 4 µg $ml^{-1}$ secondary antibody (goat anti–rabbit–Alexa Fluor 488; Invitrogen, Carlsbad, CA, USA) in blocking buffer for 1 h at room temperature followed by 1 µg $ml^{-1}$ 4′,6-diamidino-2-phenylindole (DAPI) DNA stain (Invitrogen) for 5 min. Sections were washed with 3 x 5 min PBS-TX to remove unbound secondary antibodies and DAPI.

Confocal Airyscan microscopy was performed on a Zeiss AxioObserver Z1 connected to a laser scanner equipped with 405-, 488-, 561-, and 640-nm laser lines (Zeiss LSM 800 with Airyscan, Carl Zeiss AG, Oberkochen, Baden-Württemberg, Germany). This device uses a 32-channel photomultiplier detector and linear deconvolution to obtain 140-nm lateral (X-Y) and 400-nm axial (Z) resolution. $VHA_B$/CA and DNA signals in tissue sections were visualized using goat anti–rabbit–Alexa Fluor 488 and DAPI stain (Invitrogen), respectively (Alexa Fluor 488—ex: 488 nm, em: 485 to 593 nm; DAPI—ex: 405 nm, em: 400 to 480 nm). To facilitate visualization by color-blind readers, $VHA_B$/CA and DAPI signals are presented using the false colors yellow and blue, respectively, in all figures.

*Pulse Amplitude Modulated Fluorometry (PAM)*

The *in vivo* photosystem efficiency of *C. xamachana* symbionts was measured using a Diving PAM (Heinz Walz GmbH, Germany); data were recorded using the accompanying WinControl software (v3.32). Four animals were held in 100% $O_2$-saturated 0.1% (v/v) DMSO FSW (26 °C) in darkness (0 µE) for 30 min. 5 spot measurements were taken with saturating light pulses (1 s, 470 nm) to measure maximal fluorescence ($F_m$) in darkness. The same animal was then acclimated to 250 µE light for 5 min before a further 5 spot measurements were taken. This measurement procedure was repeated with 1 µM ConcanamycinA (ConcA) FSW, 20 µM Ethoxzolamide (EZ) FSW, and 100 µM 3-(3,4-dichlorophenyl)-1,1-dimethylurea (DCMU) FSW.

Baseline fluorescence in darkness ($F_0$) was monitored by a modulated measuring light (<1 μE blue LED). Maximal photochemical quantum yield in the dark ($F_v/F_m$) was calculated by: $F_v/F_m = (F_m - F_0)/F_m$. Effective photochemical quantum yield under illumination (Y(II)) was calculated as: $Y(II) = (F_m - F)/F_m$ where F is the fluorescence level determined immediately before a saturation pulse is applied. Light was provided using an ACE Light Source with a full-spectrum halogen EKE lamp (Schott AG, Mainz, Germany) and calibrated with a MQ-510 full-spectrum quantum sensor (Apogee Instruments, Inc.).

$O_2$ *Microelectrode Recordings*

Dark respiration (R) and net photosynthesis ($P_N$) for individual *C. xamachana* bell slices (~1 cm) were measured in sealed glass chambers at 26 °C using a Clark- type $O_2$ electrode (Unisense, Aarhus, Denmark) that was calibrated with anoxic (bubbling with $N_2$ gas) and 100% $O_2$-saturated 0.2 μm-filtered seawater (FSW). Experimental chambers were stirred with an internal magnetic stir bar and temperature was maintained via external water bath. Data were recorded using the accompanying SensorTrace software (v3.4.3; Unisense). R and $P_N$ were measured under darkness or 250 μE light, respectively. Light was provided using an ACE Light Source with a full-spectrum halogen EKE lamp (Schott AG) and calibrated with a MQ-510 full-spectrum quantum sensor (Apogee Instruments, Inc.). Prior to the start of all microelectrode trials, *C. xamachana* bell chunks were immobilized by trimming the outer rhopalium and nerve ring from the periphery of the bell; this halted all rhythmic pulsing of the bell and limited movement to sporadic twitching.

To test whether DMSO alone effects dark R or $P_N$ in *C. xamachana*, bell chunks were placed in 100% $O_2$-saturated FSW in darkness for 15 min before moving into sealed test chambers filled with 100% $O_2$-saturated FSW (n = 5). Dark R was measured for 15 min before illuminating the animal with 250 μE and measuring $P_N$ for 15 min. The animal was rested for 15 min in 100%

$O_2$-saturated FSW in darkness before moving into sealed test chambers filled with 100% $O_2$-saturated 0.1% (v/v) DMSO FSW. Dark R was measured for 15 min before illuminating the animal with 250 μE and measuring $P_N$ for 15 min. To ignore $O_2$ consumption spikes associated with occasional animal twitching, dark R and $P_N$ rates were determined by manually fitting trendlines to the linear portion of the $O_2$ curves before and after treatment addition (MATLAB R2022a). Trendlines were fit in a blind manner: $O_2$ curves were displayed without identifiers and a trendline fit by an independent person. Only data from the center of the curves were considered (200-800 sec).

To test whether ConcA or EZ effected dark R or $P_N$ in *C. xamachana*, bell chunks were placed in 100% $O_2$-saturated FSW in darkness for 15 min before moving into sealed test chambers filled with 100% $O_2$-saturated DMSO FSW. Dark R was measured for 15 min before illuminating the animal with 250 μE and measuring $P_N$ for 15 min. The animal was rested for 15 min in 100% $O_2$-saturated FSW in darkness before moving into sealed test chambers filled with 100% $O_2$-saturated, 1 μM ConcA (n = 6) or 20 μM EZ FSW (n = 6). Dark R was measured for 15 min before illuminating the animal with 250 μE and measuring $P_N$ for 15 min. This experiment was repeated with 100 μM DCMU FSW as a positive control (n = 4). Only bell chunks displaying a positive $P_N$ rate were included in data analysis. DMSO, ConcA, EZ, and DCMU experiments were repeated without any animal tissue (n = 3) as negative controls demonstrating that neither illumination nor drugs interacted with the microelectrode.

*Statistics*

Data were analyzed in GraphPad Prism v10.0.1 (San Diego, CA, USA). Outliers were removed using the ROUT method at 1% sensitivity and data normality and homogeneity of variance were tested using the Shapiro-Wilk normality test. PAM data were analyzed using

repeated measures one-way ANOVAs with Holm-Šidák's multiple comparisons tests. Microelectrode blank controls were analyzed with two-way repeated measure analysis of variance (ANOVA) tests. R and $P_N$ data were analyzed using Wilcoxon matched-pairs signed rank or paired T-tests.

**Results and Discussion**

*Symbiont-Hosting Amoebocytes Express $VHA_B$ and CA Protein*

Similar to coral and anemones (Barott et al. 2015, 2022), *C. xamachana* expressed $VHA_B$ by Western blotting with specific anti-$VHA_B$ and anti-CA antibodies. Anti-$VHA_B$ antibodies detected a single ~55 kDa band matching the *C. xamachana* $VHA_B$ (Ohdera et al. 2019) (Figure 3.1A). Notably, $VHA_B$ expression was highest in tissue fractions enriched for symbiont-hosting amoebocyte cells pointing to a role in maintenance of intracellular symbionts. This finding matches results from anemones where host cells expressed the highest $VHA_B$ abundance of any cell type (Barott et al. 2022). The anti-$VHA_B$ antibody's epitope is 100% conserved in *C. xamachana* and no signal was present in peptide preabsorption controls demonstrating the specificity of the anti-$VHA_B$ antibody.

Anti-CA antibodies detected two bands matching a predicted alpha-class CA present in the *C. xamachana* genome (Ohdera et al. 2019) (Figure 3.1B). This protein contains all the putative motifs of an alpha-class CA as well as two N-glycosylation sites and an extracellular signal peptide suggesting an extracellular or vesicular localization (Supplemental Figure 3.2). Amoebocytes express an ~80 kDa band while non-symbiotic cells expressed an additional ~75 kDa band matching glycosylated and un-glycosylated variants, respectively. Both CA transcripts were expressed at highest levels in non-symbiotic cells consistent with CA's myriad of physiological functions and widespread expression in marine invertebrate cells [reviewed in (Weihrauch and

O'Donnell 2017)]. The co-expression of $VHA_B$ and CA in amoebocytes suggests possible functional coupling in a CCM; we therefore employed immunohistochemical Airyscan confocal microscopy (IACM) to assess whether $VHA_B$ and CA are symbiosome-associated in amoebocytes.

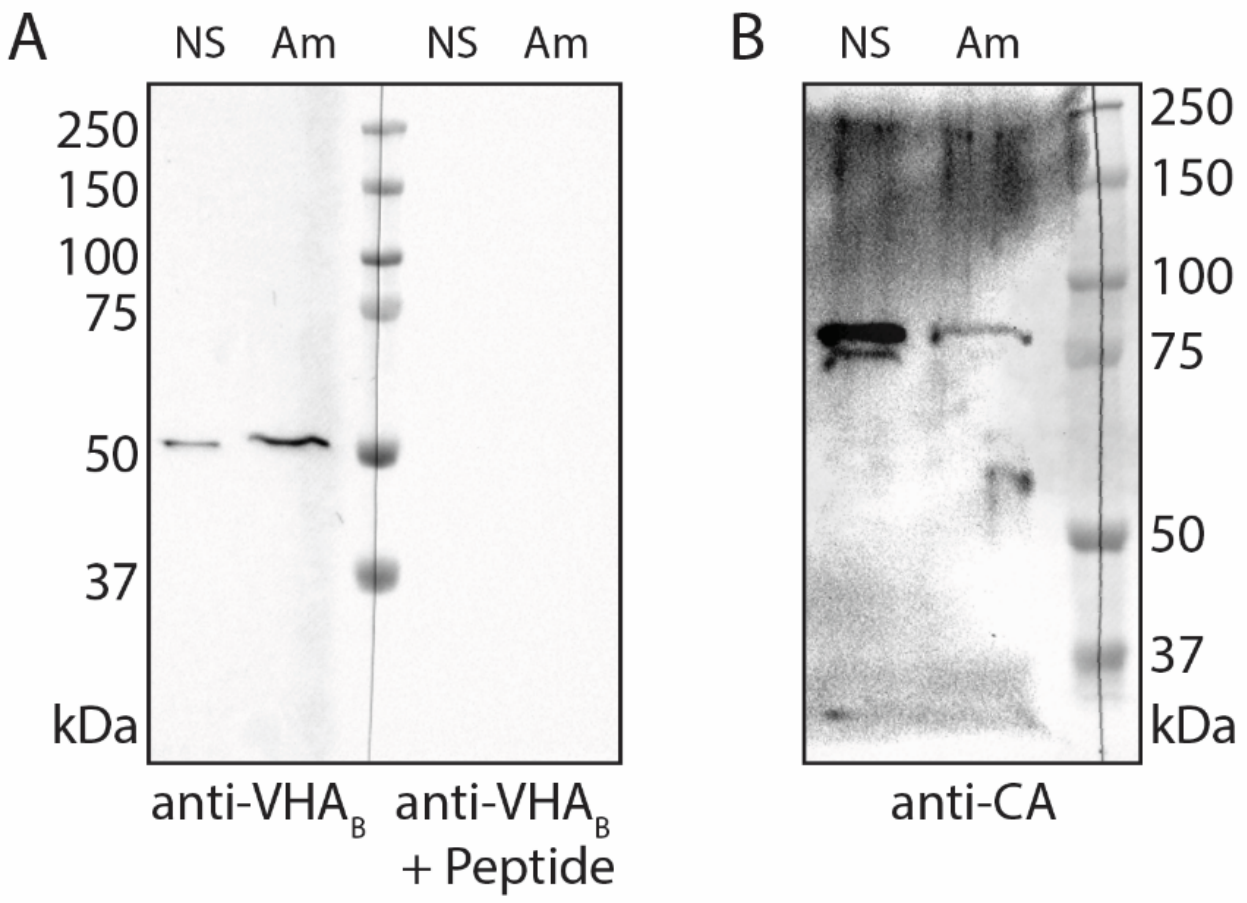


Figure 3.1: Expression of $VHA_B$ and CA in *C. xamachana*. (A) Western Blotting using a custom anti-$VHA_B$ antibody detected a single 55 kDa band present in non-symbiotic (NS) and amoebocyte (Am) cells. Blotting with antibodies preabsorbed with 60-fold excess peptide showed no signal. (B) CA expression was probed using a commercial antibody; an 80 kDa band was present in both non-symbiotic and amoebocyte cells while a 75 kDa was absent from amoebocyte cells.

*$VHA_B$ and CA are Present in the Symbiosome Suggesting a Role in Maintenance of Symbiosis*

IACM observations corroborated protein expression data: $VHA_B$ was present in epi- and endodermal cells bordering seawater and brachial cavities, respectively, as well as symbiont-hosting amoebocytes (Figure 3.2A-B). In epi- and endodermal cells, $VHA_B$ signal displayed a

punctate pattern reminiscent of intracellular vesicles. Cnidarian cells continuously pinocytose extracellular fluids (Ganot et al. 2020) and the ubiquitous involvement of $VHA_B$ in regulating vesicle trafficking, acidification, and degradation supports vesicular localization of $VHA_B$ [reviewed in (Hu et al. 2015)]. Symbiont-hosting amoebocytes displayed the strongest $VHA_B$ signal: $VHA_B$ was most abundant surrounding symbionts consistent with symbiosomal localization seen in corals and anemones (Figure 3.2C) (Barott et al. 2015, 2022). This pattern was most readily evident in the region immediately between the host and symbiont nuclei where the symbiosome membrane is easily identifiable. $VHA_B$-rich, low pH symbiosomes are common features of invertebrate-microbial associations where the pH gradient between the host cytosol and symbiosome space drives the secondary transport of metabolites (DIC, $NH_3/NH_4^+$, amino acids, etc.) between the symbiotic partners (Barott et al. 2015, 2022; Tang 2015; Thies et al. 2022). The $VHA_B$-rich symbiosomes of *C. xamachana* may retain this function as amoebocytes deliver both DIC and $NH_3/NH_4^+$ to intracellular symbionts (Lyndby et al. 2020); whether amoebocytes employ the same mechanism for $NH_3/NH_4^+$ transport present in corals (Thies et al. 2022) remains untested.

Notably, 100% of observed symbiosomes displayed $VHA_B$ signal. In contrast, corals and anemones display a heterogeneous pattern of symbiosomal $VHA_B$ expression: many symbiosomes display a punctate $VHA_B$ signal pattern rather than signal around the entire symbiosome (~86% of total cells) while others lack $VHA_B$ entirely (Barott et al. 2015, 2022). The invariable presence of $VHA_B$ in *C. xamachana* symbiosomes suggests that amoebocytes employ $VHA_B$ to drive nutrient transport more than other cnidarian host cells. This difference could be attributed to the unique low DIC/high $O_2$ characteristics of the mesoglea microenvironment or the high density of symbionts and increased competition for DIC in individual amoebocytes. The uniform expression of $VHA_B$ in amoebocyte symbiosomes additionally supports the hypothesis that while *Cassiopea*

*ssp.* amoebocytes originate from the gastroderm, they behave more akin to modified phagocytes/macrophages than sessile cnidarian host cells. As 'professional' phagocytotic immune cells, macrophages roam connective tissues phagocytosing and selectively degrading foreign material in VHA-rich, low-pH vacuoles (Lukacs et al. 1990). Phagocytotic amoebocytes of non-symbiotic jellyfish display these characteristics (Chapman 1999; LaDouceur et al. 2013) and *C. xamachana* amoebocytes selectively retain photosynthetically-competent symbionts while degrading incompatible symbionts in lysosomes (Fitt and Trench 1983). Given these similarities, future studies should focus on aspects of macrophage biology potentially coopted to support symbiont photosynthesis and distribution of photoproducts to non-symbiotic tissues.

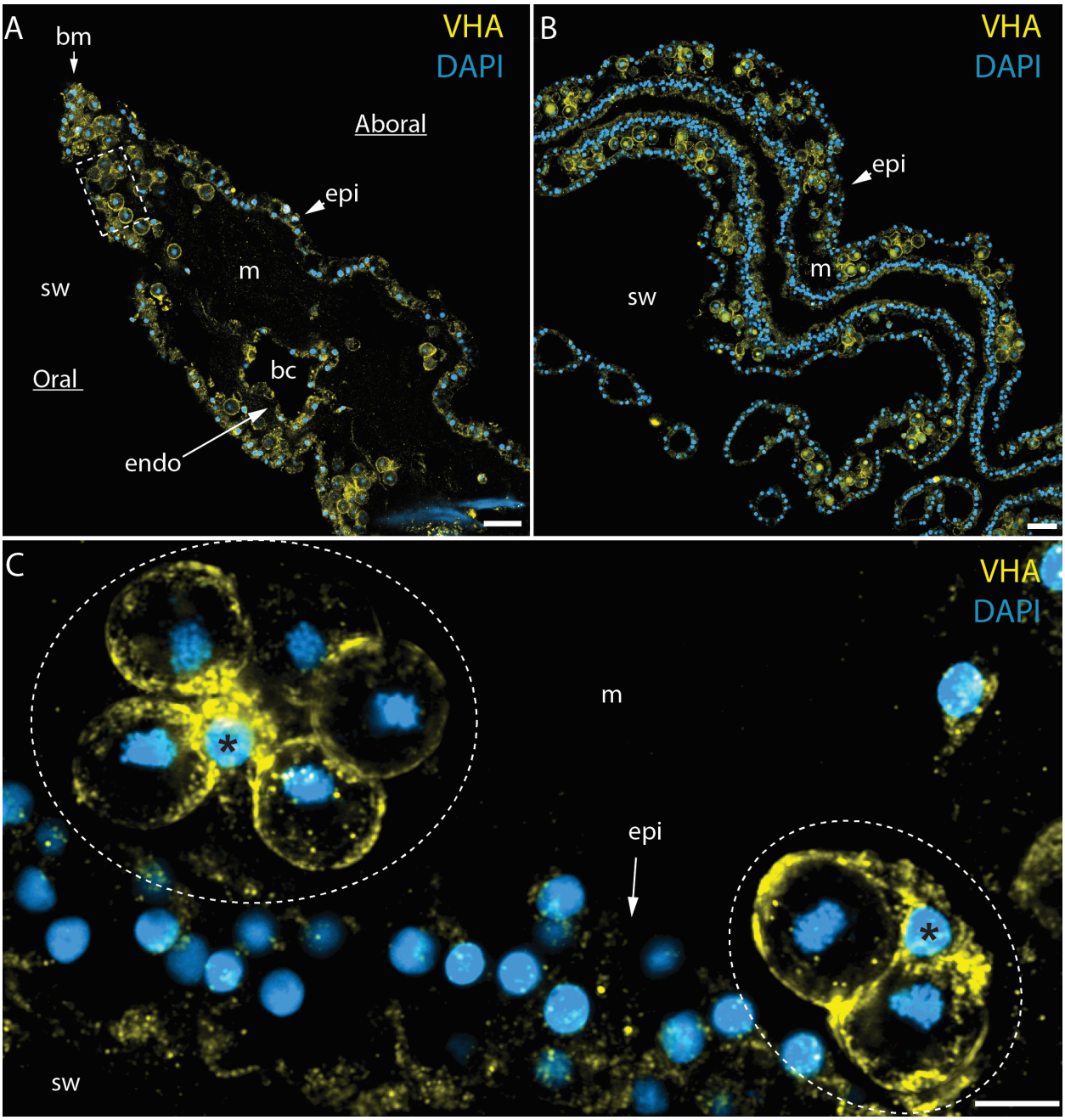


Figure 3.2: IACM localization of $VHA_B$ in *C. xamachana* tissues. (A) Cross-section of bell mantle with amoebocytes distributed throughout. Scale bar is 20 µm. (B) Cross-section of oral arms with amoebocytes distributed throughout. Scale bar is 20 µm. (C) High magnification view of the rectangular region in (A) depicting two amoebocytes containing five and two symbionts, respectively. Scale bar is 5 µm. anti-$VHA_B$ signal is shown in yellow and nuclear stain in blue. bc-brachial canal; bm-bell margin; epi-epidermis; endo-endodermis; m-mesoglea; sw-seawater; *-amoebocyte nuclei.

CA, like $VHA_B$, was most abundant in epi- and endodermal cells as well as most symbiont-bearing amoebocytes. In epi- and endodermal cells, CA displayed cytosolic localization near apical membranes bordering seawater and brachial cavities, respectively (Figure 3.3A-B). As CAs play a central role in acid-base balance, ion transport, and gas exchange, the association of CA with externally-facing membranes is not unexpected and CA likely contributes to these processes in *C. xamachana* [reviewed in (McKenna and Frost 2014; Weihrauch and O'Donnell 2017)]. In amoebocytes, CA surrounded the periphery of algal symbionts reminiscent of the symbiosomal $VHA_B$ signal pattern. We were unable however to visually distinguish if CA was present in the symbiosome lumen in addition to the amoebocyte cytosol. Given CA's extracellular signal peptide, we suggest that CA is present both in the amoebocyte cytosol and symbiosome lumen. In the cytosol ($pH_i$ 7-8), CA catalyzes the hydration of $CO_2$ into $H^+$ and $HCO_3^-$ which are shuttled into the symbiosome via VHA and a $HCO_3^-$ transporter(s). CA catalyzes the opposite reaction in the low pH symbiosome thereby concentrating $CO_2$ in the symbiont's microenvironment. While spontaneous dehydration of $HCO_3^-$ to $CO_2$ occurs in the low-pH symbiosome, the presence of CA would dramatically accelerates this process by 25,000-fold (Gilmour 2011) thereby maintaining a continual, inwards $HCO_3^-$ gradient to promote continued DIC transport and DIC saturation of Rubisco. Notably, CA association with the symbiosome membrane was heterogeneous: amoebocytes often contained both CA-rich and CA-free symbiosomes (Figure 3.3C) suggesting a transient role of CA in supporting symbiont photosynthesis. Together, the presence of $VHA_B$ and CA in the symbiosome are consistent with our hypothesis that (1) *C. xamachana* amoebocytes employ a $VHA_B$-driven CCM to promote photosynthesis and that (2) $VHA_B$ and CA may be functionally coupled in this CCM.

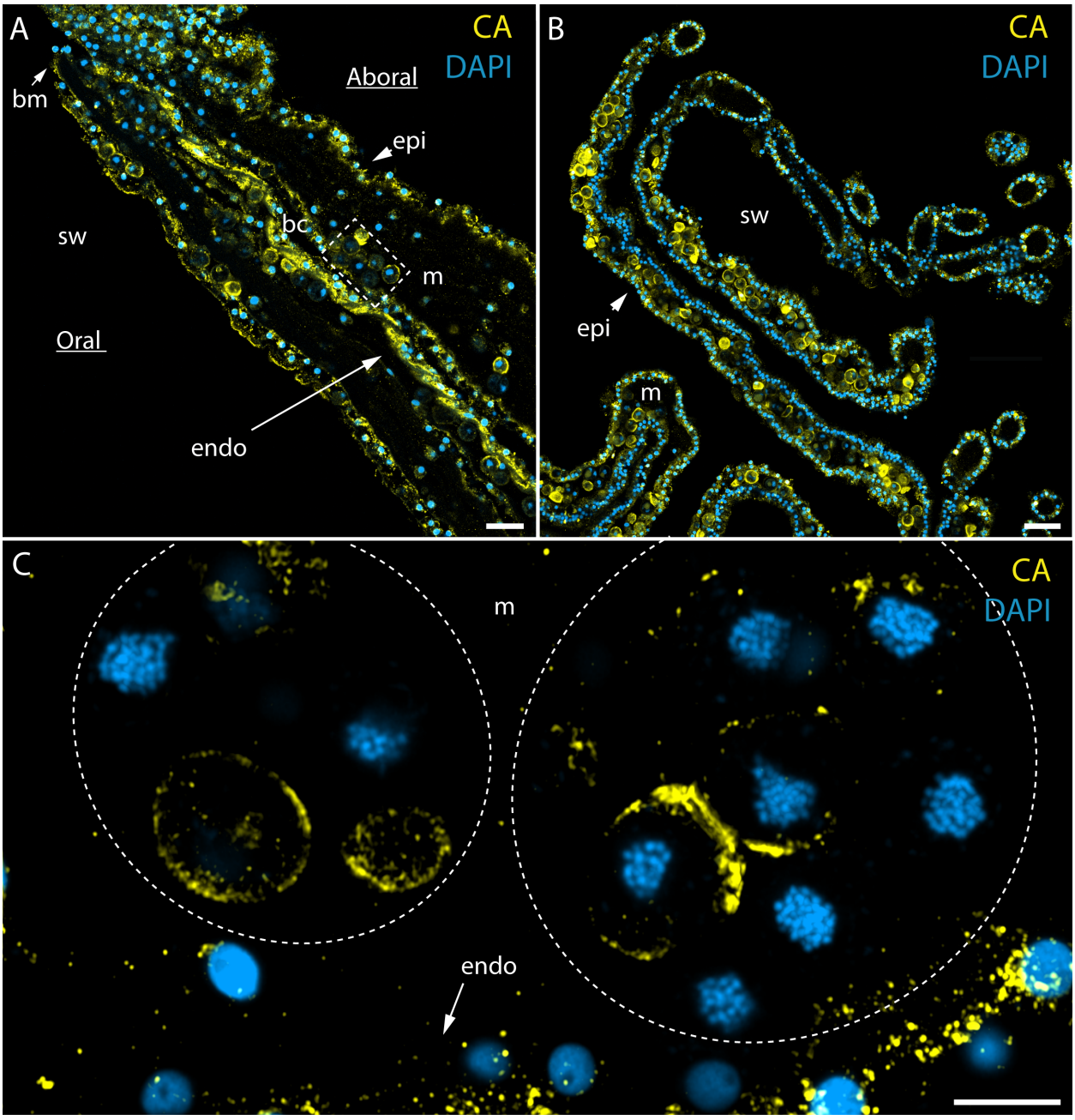


Figure 3.3: IACM localization of CA in *C. xamachana* tissues. (A) Cross-section of bell mantle with amoebocytes distributed throughout. Scale bar is 20 µm. (B) Cross-section of oral arms with amoebocytes distributed throughout. Scale bar is 20 µm. (C) High magnification view of the rectangular region in (A) depicting two amoebocytes containing five and seven symbionts, respectively. Scale bar is 5 µm. anti-CA signal is shown in yellow and nuclear stain in blue. bc-brachial canal; bm-bell margin; epi-epidermis; endo-endodermis; m-mesoglea; sw-seawater.

*C. xamachana Amoebocytes Promote Symbiont Photosynthesis*

We employed microsensor respirometry to test whether VHA and CA activities promote symbiont photosynthesis in *C. xamachana*. We measured $R_D$ and $P_N$ rates from chunks of bell tissue incubated with specific inhibitors of VHA (ConcA), CA (EZ), and photosystem II (PSII) electron transport as a positive control (DCMU). DMSO treatment alone did not alter $P_N$ and no treatment altered $R_D$ (Supplemental Figure 3.3, Supplemental Figure 3.4). PSII inhibition with DCMU ablated $O_2$ production confirming that symbionts were photosynthetically active (Figure 3.4). VHA inhibition with ConcA reduced $P_N$ by 47% (Figure 3.4) consistent with results from corals, anemones, and giant clams (Barott et al. 2015, 2022; Armstrong et al. 2018). CA inhibition with EZ similarly reduced $P_N$ by 35% (Figure 3.4).

To confirm that no treatment other than DCMU interacted with symbiont PSII to artificially decrease $P_N$, we used PAM to measure PSII efficiency: only DCMU treatment decreased PSII efficiency in both dark- and light-adapted animals (Supplemental Figure 3.5). We therefore attribute the decreased $P_N$ of ConcA- and EZ-treated animals to altered activity of VHA and CA. These results demonstrate that VHA and CA activities promote symbiont photosynthesis in *C. xamachana*.

Our interpretation is backed by previous results demonstrating that VHA inhibition does not lower $P_N$ in symbionts freshly isolated from corals (Barott et al. 2015) and that ConcA does not impair symbiont light harvesting machinery (Yee et al. 2023). While free-living algal symbionts employ CA-enhanced CCMs, we believe that the observed decreases in $P_N$ during EZ exposure are specifically attributable to *C. xamachana* CA: first, Symbiodiniaceae symbionts downregulate CCM-associated CAs *in hospite* due to increased DIC access afforded by host CCMs (Mashini et al. 2023). Second, algal cell walls are less permeable to small molecules in low pH

environments such as the symbiosome (Lavoie et al. 2012). Given that the coral symbiosome is acidified to pH ~4 by VHA $H^+$-pumping and that *C. xamachana* symbiosomes contain more VHA than corals, *C. xamachana* symbionts likely exist in a similarly acidic microenvironment and are less amenable to drug delivery *in hospite*. Finally, the low concentration of EZ used, the short trial times, and immediate responses to drug addition suggest that the observed effect is attributable to altered function of host CA.

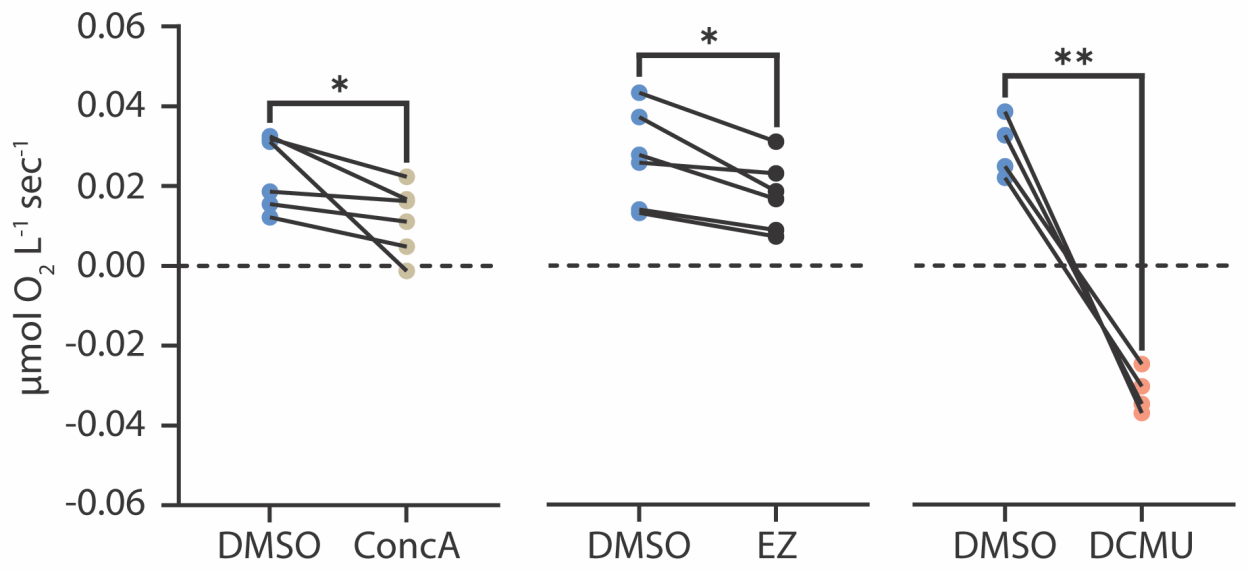


Figure 3.4: Effect of VHA, CA, and PSII inhibition on $P_N$ in *C. xamachana*. Chunks of bell tissue were incubated with DMSO then either ConcA (1 µM), EZ (20 µM), or DCMU (100 µM) under 250 µE light. All treatments lowered $P_N$ more than DMSO alone (Paired T-tests; p = 0.0445, p = 0.0115, and p = 0.0022 respectively). N = 5 for all treatments.

*VHA and CA Are Functionally Coupled in Amoebocyte CCMs*

The results presented here indicate that *C. xamachana* amoebocytes employ a VHA-driven, CA-coupled CCM to support symbiont photosynthesis. In this model (1) CA generates cytosolic pools of $H^+$ and $HCO_3^-$; (2) VHA and $HCO_3^-$ transporters concentrate $H^+$ and $HCO_3^-$ in the symbiosome; (3) symbiosomal CA catalyzes the instantaneous formation of $CO_2$ in the symbiont's microenvironment; (4) $CO_2$ freely diffuses along the inwards partial pressure gradient established by symbiont carbon fixation to fuel continued photosynthesis (Figure 3.5). The symbiosomal

VHA-driven CCM was originally documented in reef-building corals and later in anemones (Barott et al. 2015, 2022) but this study presents the first putative evidence for VHA-CA coupling. We propose that host VHA-CA coupling may be a feature common to all cnidarian-Symbiodiniaceae photosymbioses given (1) the presence of functional VHA-dependent, host-controlled CCMs across multiple classes representing significant evolutionary, morphological, and physiological differences; (2) the exclusive retention of Symbiodiniaceae symbionts in intracellular digestive compartments, and (3) the ubiquitous coupling of VHA and CAs in digestive mechanisms. An analogous VHA-driven CCM exists in giant clams (phylum Mollusca) which host Symbiodiniaceae symbionts (Armstrong et al. 2018); here, however, symbionts are retained extracellularly in the gastric lumen and VHA pumps $H^+$ across the apical membrane of epithelial cells. We posit that host CAs play a homologous role in this association, however, further investigation is required.

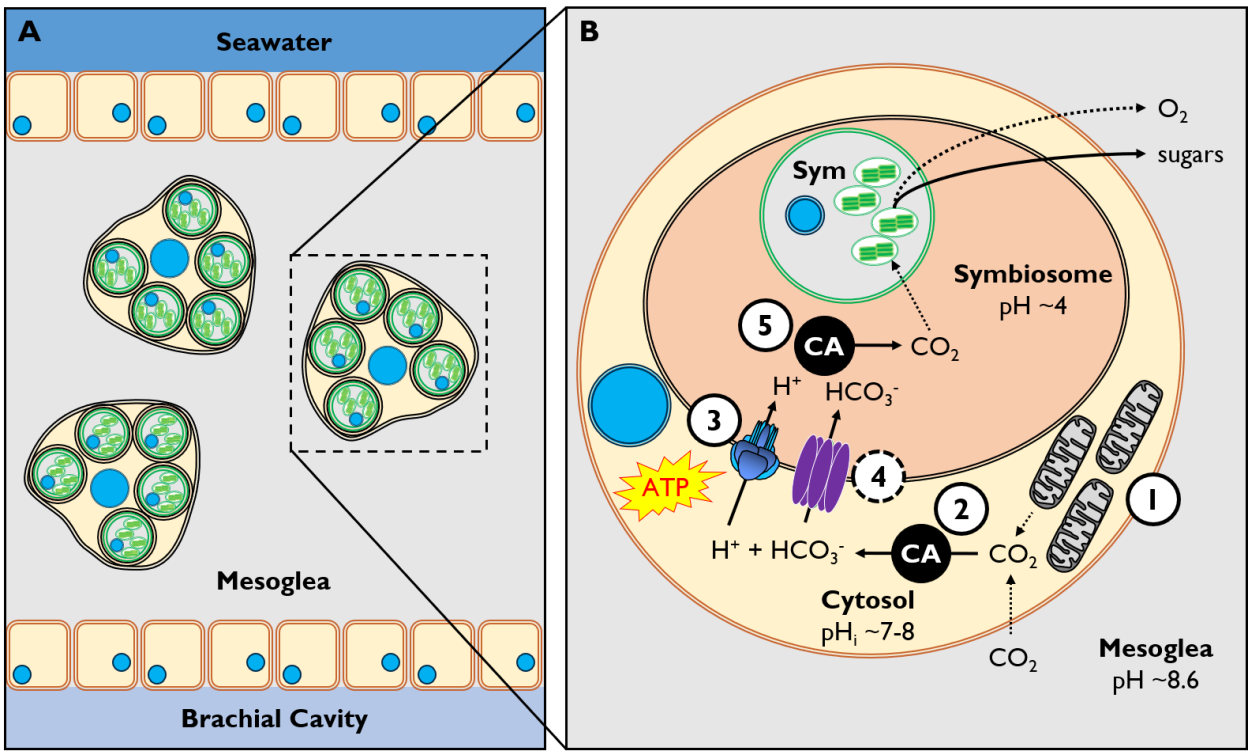


Figure 3.5: Model of host-driven CCM in *C. xamachana* amoebocytes. (A) Amoebocytes bearing many symbionts transit the mesoglea. (B) For clarity, while amoebocytes contain many symbiosome-bound symbionts, only a single symbiosome is pictured with a greatly reduced symbiont. (1) $CO_2$ enters the amoebocyte cytosol via diffusion from the mesoglea or production in mitochondria. (2) CA hydrates $CO_2$ into $H^+$ and $HCO_3^-$. (3) $H^+$ is transported into the symbiosome by host VHA while (4) $HCO_3^-$ enters via an unidentified transporter(s). (5) In the symbiosome, CA catalyzes the dehydration of $H^+$ and $HCO_3^-$ into $CO_2$ which diffuses into the symbiont (Sym) and the site of carbon fixation. Photosynthesis evolves $O_2$ which diffuses back into the animal host while fixed sugars are translocated via unknown mechanisms.

**Acknowledgements**

We thank Dr. Monica Medina and Dr. Victoria Sharp (Pennsylvania State University) and Dr. Phil Cleves (Carnegie Institution for Science) for providing *C. xamachana* animals for this project. We thank Charles Trautner, Elisa Prohroff, Victoria Vasquez, Bryan Delgado, Ryan Myers, and Maitri Paul for their help maintaining *C. xamachana* cultures. This work was partially supported by National Science Foundation Graduate Research (GRFP 2019271478), Scripps Institution of Oceanography Doctoral, and Achievement Rewards for College Scientists Fellowships to A.B.T.

Chapter 3 is currently being prepared for submission for publication of the material. Thies AB, Wangpraseurt D, Tresguerres M (*in prep*). V-type $H^+$-ATPase and Carbonic Anhydrase Support Symbiont Photosynthesis in *Cassiopea* Amoebocytes. The dissertation author was the primary investigator and author of this material.

**Appendix**

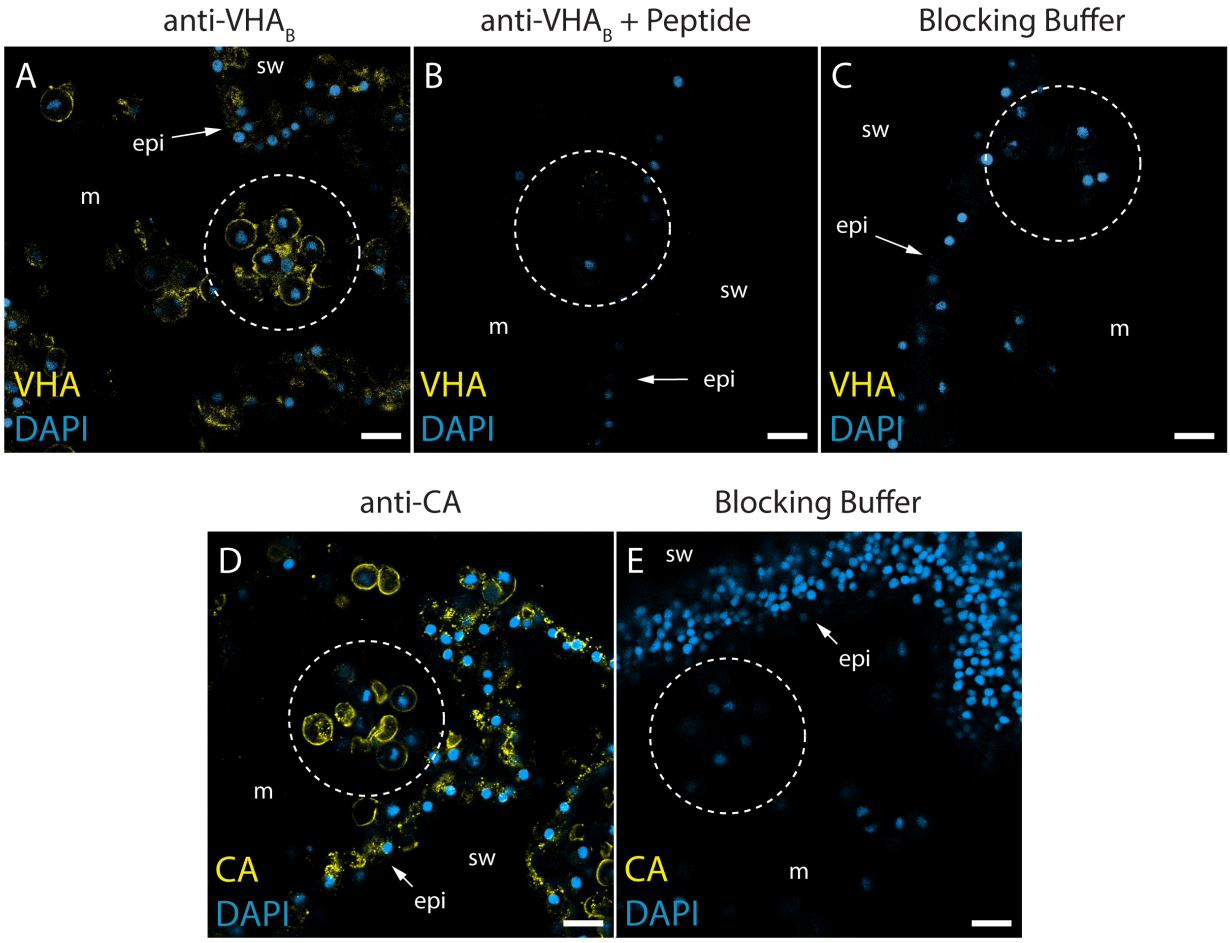


Supplemental Figure 3.1: IHC validation of antibodies in *C. xamachana* amoebocytes. (A) anti-VHA$_B$ antibodies. (B) anti-VHA$_B$ antibodies incubated with 13-fold excess peptide. (C) Blocking buffer only. (D) anti-CA antibodies. (E) Blocking buffer only. Antibody signal is shown in yellow and nuclear stain in blue. Amoebocytes are marked in dashed circles. All scale bars are 10 µm. epi-epidermis; m-mesoglea; sw-seawater.

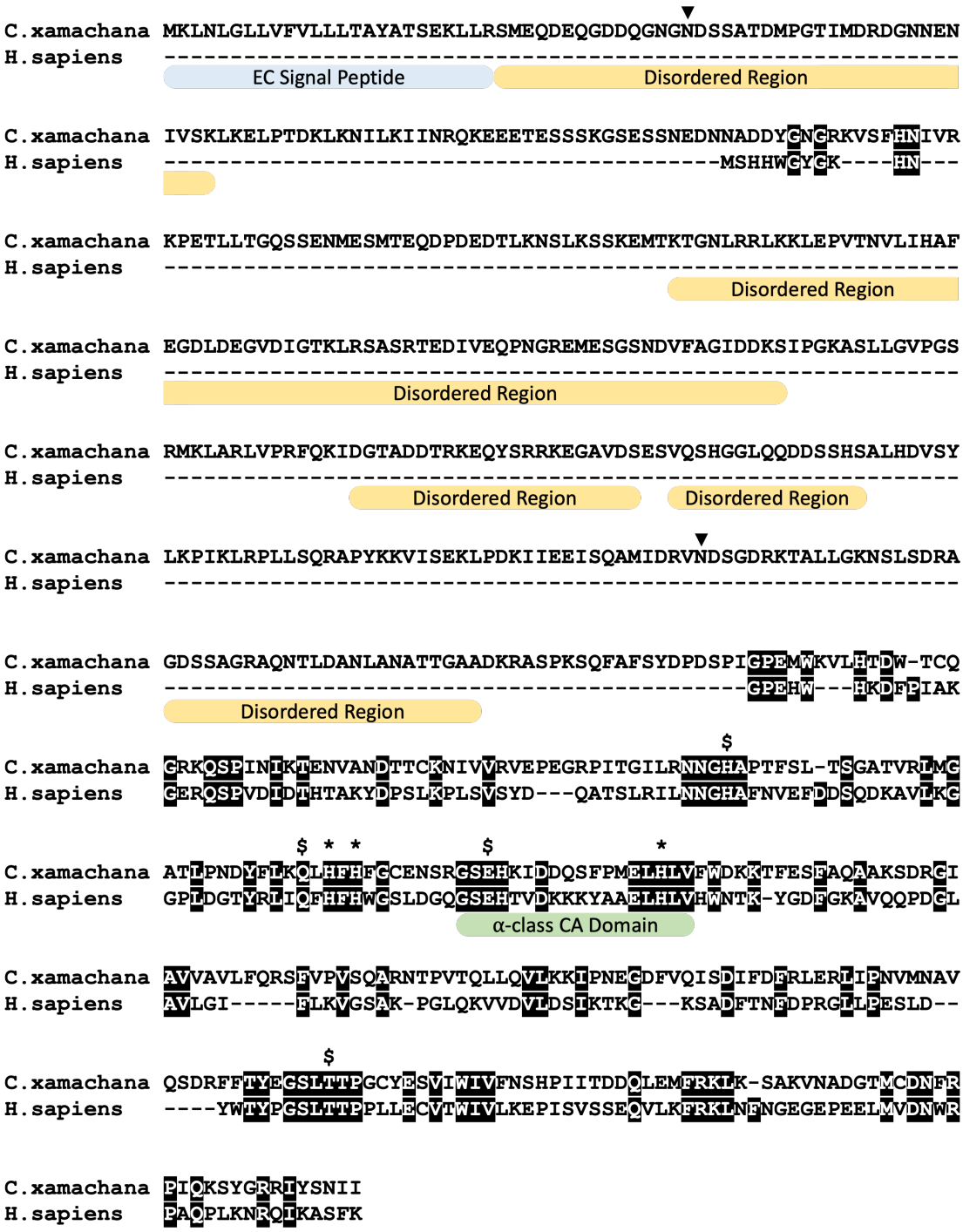


Supplemental Figure 3.2: Alignment of *C. xamachana* CA (Protein ID 1670; (Ohdera et al. 2019)) with *H. sapiens* CAII (NP_000058.1). Conserved residues are highlighted in black (BoxShade). Extracellular signal peptide (EC Signal Peptide) as predicted by DeepLoc v2.0 (Thumuluri et al. 2022), disordered regions and α-class carbonic anhydrase domain as predicted by InterPro v98.0 (Paysan-Lafosse et al. 2023), N-linked glycosylation sites (black triangles) as predicted by NetNGlyc v1.0 (Gupta and Brunak 2001) and conserved active sites ($) and zinc-binding domains (*) as discussed in (Supuran 2008) are marked.

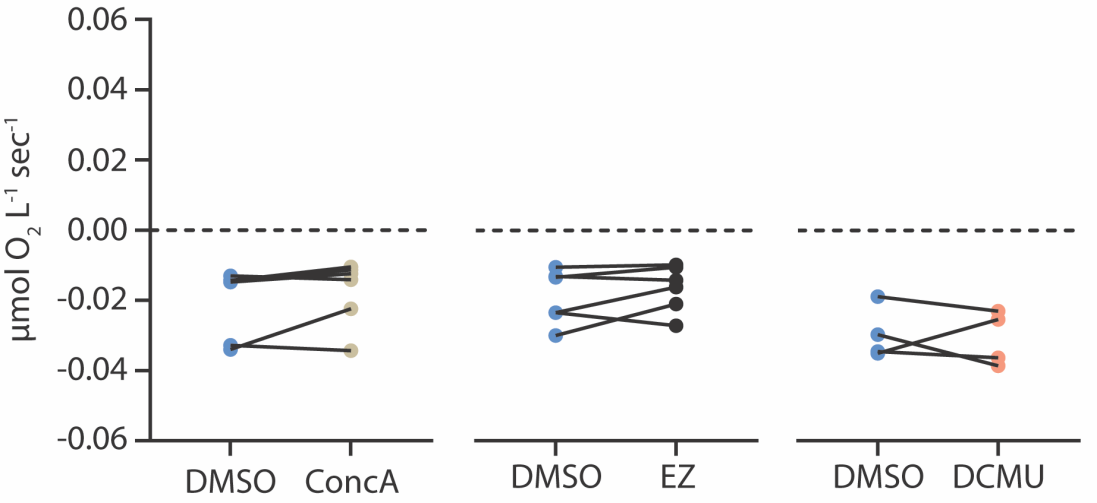


Supplemental Figure 3.3: Effect of VHA, CA, and PSII inhibition on $R_D$ in *C. xamachana*. Chunks of bell tissue were incubated with DMSO then either ConcA (1 µM), EZ (20 µM), or DCMU (100 µM) in darkness. No treatment altered $R_D$. N = 5 for all treatments.

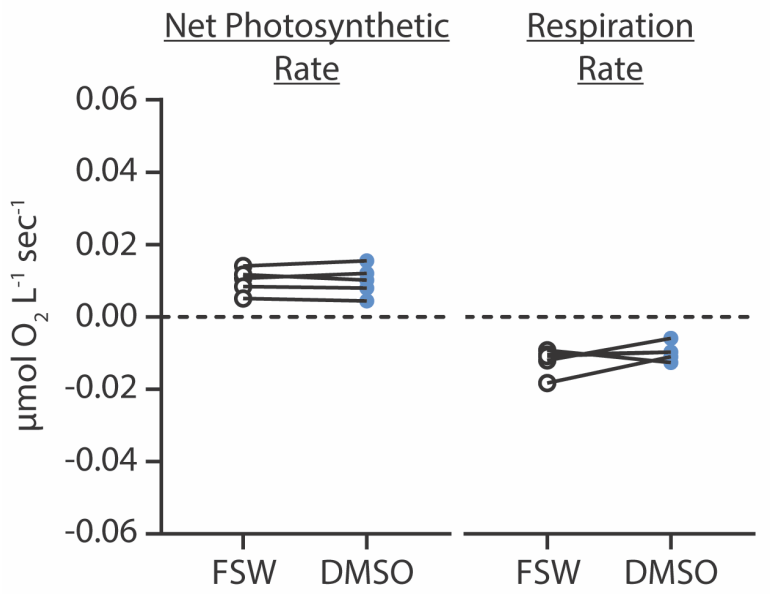


Supplemental Figure 3.4: Effect of DMSO on $P_N$ and $R_D$ in *C. xamachana*. Chunks of bell tissue were incubated with FSW then DMSO under 250 µE light or in darkness. DMSO treatment did not alter $P_N$ nor $R_D$. N = 5 for all treatments.

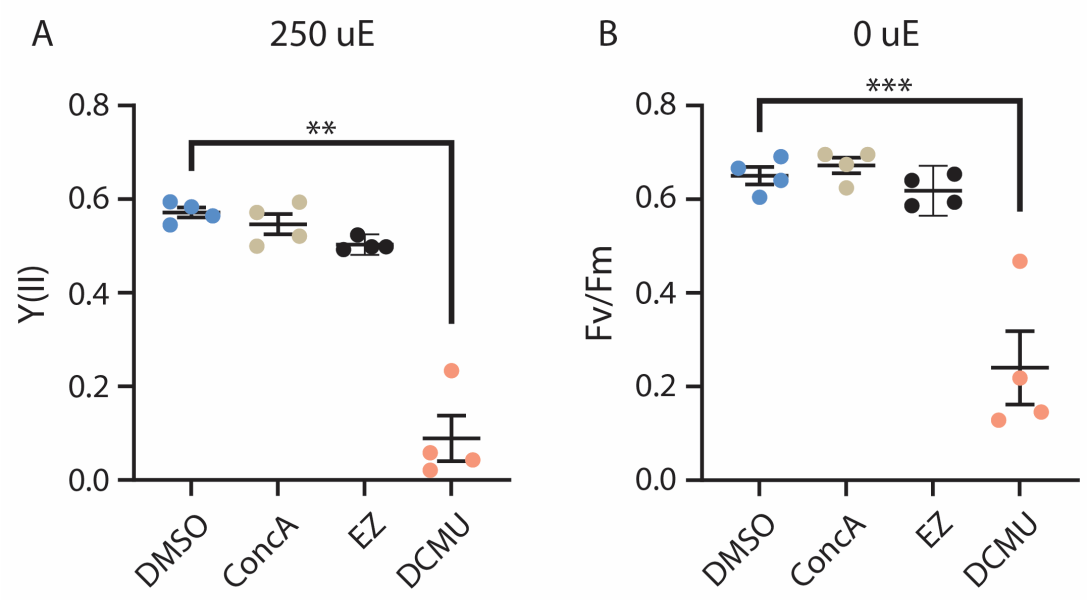


Supplemental Figure 3.5: PAM confirms that only DCMU lowers PSII efficiency in *C. xamachana* symbionts. (A) Effective photochemical quantum yield under illumination (Y(II)). (B) Maximal photochemical quantum yield in the dark (Fv/Fm). Whole animals were incubated with DMSO in darkness for 30 min before 5 spot measurements were taken. The same animal was then acclimated to 250 µE light for 5 min before a further 5 spot measurements were taken. This measurement procedure was repeated with 1 µM ConcA, 20 µM EZ, and 100 µM DCMU in FSW. No treatment altered Y(II) or Fv/Fm other than DCMU (Repeated Measures One-Way ANOVA; $p < 0.0001$ and $p = 0.0005$ respectively). N = 4 for all treatments.

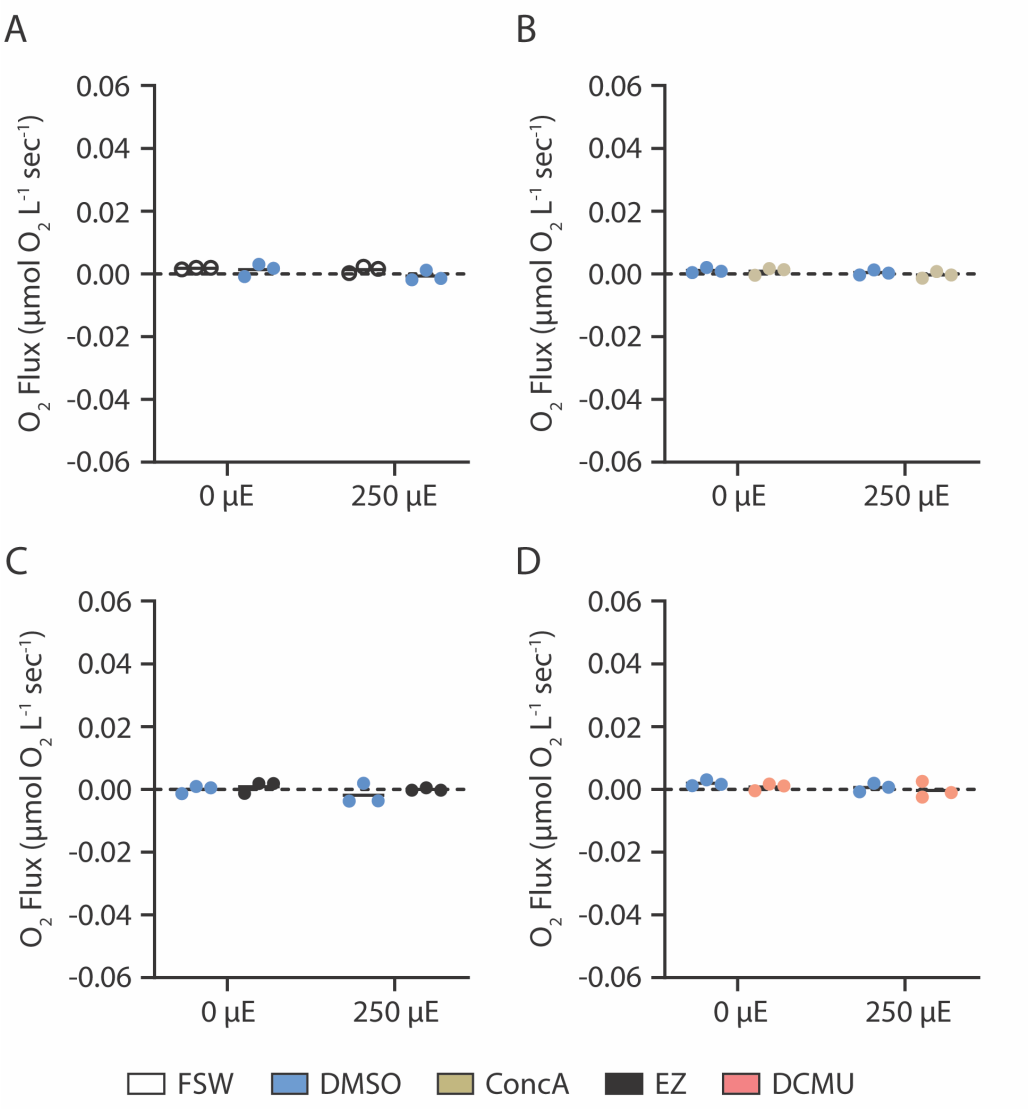


Supplemental Figure 3.6: Respirometry microsensor is not affected by light exposure nor drug treatment. Addition of (A) DMSO, (B) ConcA, (C) EZ, nor (D) DCMU significantly changed microelectrode readings in empty respirometry chambers.

## References


Al-Moghrabi S, Goiran C, Allemand D, et al (1996) Inorganic carbon uptake for photosynthesis by the symbiotic coral-dinoflagellate association II. Mechanisms for bicarbonate uptake. Journal of Experimental Marine Biology and Ecology 199:227–248. https://doi.org/10.1016/0022-0981(95)00202-2

Armstrong EJ, Roa JN, Stillman JH, Tresguerres M (2018) Symbiont photosynthesis in giant clams is promoted by V-type H + -ATPase from host cells. Journal of Experimental Biology. https://doi.org/10.1242/jeb.177220

Barott K, Tresguerres M (2015) Immunolocalization of proteins in corals: the V-type H+-ATPase proton pump. bio-protocol 5:1–10

Barott KL, Barron ME, Tresguerres M (2017) Identification of a molecular pH sensor in coral. Proceedings of the Royal Society B 284:20171769. https://doi.org/10.1098/rspb.2017.1769

Barott KL, Thies AB, Tresguerres M (2022) V-type H + -ATPase in the symbiosome membrane is a conserved mechanism for host control of photosynthesis in anthozoan photosymbioses. Royal Society Open Science 9:. https://doi.org/10.1098/rsos.211449

Barott KL, Venn AA, Perez SO, et al (2015) Coral host cells acidify symbiotic algal microenvironment to promote photosynthesis. Proceedings of the National Academy of Sciences of the United States of America 112:607–612. https://doi.org/10.1073/pnas.1413483112

Benazet-Tambutte S, Allemand D, Jaubert J (1996) Inorganic Carbon Supply to Symbiont Photosynthesis of the Sea Anemone, Anemonia viridis: Role of the Oral Epithelial Layers. Symbiosis 20:199–217

Brafield AE, Chapman G (1983) Diffusion of Oxygen Through the Mesogloea of the Sea Anemone Calliactis Parasitica. Journal of Experimental Biology 107:181–187. https://doi.org/10.1242/jeb.107.1.181

Chapman DM (1999) Microanatomy of the bell rim of Aurelia aurita (Cnidaria: Scyphozoa) . Canadian Journal of Zoology 77:34–46. https://doi.org/10.1139/z98-193

Colley NJ, Trench RK (1985) Cellular events in the reestablishment of a symbiosis between a marine dinoflagellate and a coelenterate. Cell and Tissue Research 239:93–103. https://doi.org/10.1007/BF00214908

Damsgaard C, Lauridsen H, Harter TS, et al (2020) A novel acidification mechanism for greatly enhanced oxygen supply to the fish retina. eLife 9:1–20. https://doi.org/10.7554/eLife.58995

Davy SK, Allemand D, Weis VM (2012) Cell biology of cnidarian-dinoflagellate symbiosis. Microbiology and Molecular Biology Reviews 76:229–261. https://doi.org/10.1128/MMBR.05014-11

Fitt WK, Trench RK (1983) Endocytosis of the symbiotic dinoflagellate *Symbiodinium microadriaticum freudenthal* by endodermal cells of the scyphistomae of *Cassiopeia xamachana* and resistance of the algae to host digestion. Journal of Cell Science 64:195–212. https://doi.org/10.1242/jcs.64.1.195

Ganot P, Tambutté E, Caminiti-Segonds N, et al (2020) Ubiquitous macropinocytosis in anthozoans. eLife 9:1–25. https://doi.org/10.7554/elife.50022

Gilmour KM (2011) Carbonic Anhydrase in Gas Transport and Exchange. In: Encyclopedia of Fish Physiology. Elsevier, pp 899–908

Gupta R, Brunak S (2001) Prediction of glycosylation across the human proteome and the correlation to protein function. In: Biocomputing 2002. WORLD SCIENTIFIC, pp 310–322

Hambleton EA, Jones VAS, Maegele I, et al (2019) Sterol transfer by atypical cholesterol-binding NPC2 proteins in coral-algal symbiosis. eLife 8:1–26. https://doi.org/10.7554/eLife.43923

Hofmann DK, Neumann R, Henne K (1978) Strobilation, budding and initiation of scyphistoma morphogenesis in the rhizostome Cassiopea andromeda (Cnidaria: Scyphozoa). Marine Biology 47:161–176. https://doi.org/10.1007/BF00395637

Hu Y-B, Dammer EB, Ren R-J, Wang G (2015) The endosomal-lysosomal system: from acidification and cargo sorting to neurodegeneration. Translational Neurodegeneration 4:18. https://doi.org/10.1186/s40035-015-0041-1

Jinkerson RE, Russo JA, Newkirk CR, et al (2022) Cnidarian-Symbiodiniaceae symbiosis establishment is independent of photosynthesis. Current Biology 32:2402-2415.e4. https://doi.org/10.1016/j.cub.2022.04.021

LaDouceur EEB, Garner MM, Wynne J, et al (2013) Ulcerative Umbrellar Lesions in Captive Moon Jelly ( Aurelia aurita ) Medusae. Veterinary Pathology 50:434–442. https://doi.org/10.1177/0300985812461363

Lavoie M, Le Faucheur S, Boullemant A, et al (2012) The Influence of pH On Algal Cell Membrane Permeability and Its Implications for The Uptake of Lipophilic Metal Complexes. Journal of Phycology 48:293–302. https://doi.org/10.1111/j.1529-8817.2012.01126.x

Leggat W, Marendy EM, Baillie B, et al (2002) Dinoflagellate symbioses: strategies and adaptations for the acquisition and fixation of inorganic carbon. Functional Plant Biology 29:309. https://doi.org/10.1071/pp01202

Lesser MP (1996) Elevated temperatures and ultraviolet radiation cause oxidative stress and inhibit photosynthesis in ymbiotic dinoflagellates. Limnology and Oceanography 41:271–283. https://doi.org/10.4319/lo.1996.41.2.0271

Lukacs GL, Rotstein OD, Grinstein S (1990) Phagosomal acidification is mediated by a vacuolar-type H(+)-ATPase in murine macrophages. Journal of Biological Chemistry 265:21099–21107. https://doi.org/10.1016/S0021-9258(17)45332-4

Lyndby NH, Murray MC, Trampe E, et al (2023) The mesoglea buffers the physico-chemical microenvironment of photosymbionts in the upside-down jellyfish Cassiopea sp. Frontiers in Ecology and Evolution 11:1–12. https://doi.org/10.3389/fevo.2023.1112742

Lyndby NH, Rädecker N, Bessette S, et al (2020) Amoebocytes facilitate efficient carbon and nitrogen assimilation in the Cassiopea-Symbiodiniaceae symbiosis: Nutrient transport in Cassiopea. Proceedings of the Royal Society B: Biological Sciences 287:. https://doi.org/10.1098/rspb.2020.2393rspb20202393

Mashini AG, Oakley CA, Beepat SS, et al (2023) The Influence of Symbiosis on the Proteome of the Exaiptasia Endosymbiont Breviolum minutum. Microorganisms 11:292. https://doi.org/10.3390/microorganisms11020292

Mashini AG, Oakley CA, Grossman AR, et al (2022) Immunolocalization of Metabolite Transporter Proteins in a Model Cnidarian-Dinoflagellate Symbiosis. Applied and Environmental Microbiology. https://doi.org/10.1128/aem.00412-22

McKenna R, Frost SC (2014) Overview of the Carbonic Anhydrase Family. In: Sub-Cellular Biochemistry. pp 3–5

Muscatine L, Falkowski PG, Porter JW, Dubinsky Z (1984) Fate of photosynthetic fixed carbon in light- and shade-adapted colonies of the symbiotic coral Stylophora pistillata. Proceedings of the Royal Society of London Series B Biological Sciences 222:181–202. https://doi.org/10.1098/rspb.1984.0058

Newkirk CR, Frazer TK, Martindale MQ (2018) Acquisition and proliferation of algal symbionts in bleached polyps of the upside-down jellyfish, Cassiopea xamachana. Journal of Experimental Marine Biology and Ecology 508:44–51. https://doi.org/10.1016/j.jembe.2018.08.010

Ohdera A, Ames CL, Dikow RB, et al (2019) Box, stalked, and upside-down? Draft genomes from diverse jellyfish (Cnidaria, Acraspeda) lineages: Alatina alata (Cubozoa), Calvadosia cruxmelitensis (Staurozoa), and Cassiopea xamachana (Scyphozoa). GigaScience 8:1–15. https://doi.org/10.1093/gigascience/giz069

Paysan-Lafosse T, Blum M, Chuguransky S, et al (2023) InterPro in 2022. Nucleic Acids Research 51:D418–D427. https://doi.org/10.1093/nar/gkac993

Perry SF, Braun MH, Genz J, et al (2010) Acid-base regulation in the plainfin midshipman (Porichthys notatus): An aglomerular marine teleost. Journal of Comparative Physiology

B: Biochemical, Systemic, and Environmental Physiology 180:1213–1225. https://doi.org/10.1007/s00360-010-0492-8

Rädecker N, Pogoreutz C, Wild C, Voolstra CR (2017) Stimulated Respiration and Net Photosynthesis in Cassiopeia sp. during Glucose Enrichment Suggests in hospite CO2 Limitation of Algal Endosymbionts. Frontiers in Marine Science 4:2–5. https://doi.org/10.3389/fmars.2017.00267

Roa JN, Tresguerres M (2016) Soluble adenylyl cyclase is an acid-base sensor in epithelial base-secreting cells. American Journal of Physiology - Cell Physiology 311:C340–C349. https://doi.org/10.1152/ajpcell.00089.2016

Roberty S, Béraud E, Grover R, Ferrier-Pagès C (2020) Coral productivity is co-limited by bicarbonate and ammonium availability. Microorganisms 8:. https://doi.org/10.3390/microorganisms8050640

Supuran CT (2008) Carbonic Anhydrases - An Overview. Current Pharmaceutical Design 14:. https://dx.doi.org/10.2174/138161208783877884

Tanaka Y, Suzuki A, Sakai K (2018) The stoichiometry of coral-dinoflagellate symbiosis: carbon and nitrogen cycles are balanced in the recycling and double translocation system. ISME Journal 12:860–868. https://doi.org/10.1038/s41396-017-0019-3

Tang BL (2015) Thoughts on a very acidic symbiosome. Frontiers in Microbiology 6:4–7. https://doi.org/10.3389/fmicb.2015.00816

Thies AB, Quijada-Rodriguez AR, Zhouyao H, et al (2022) A Rhesus channel in the coral symbiosome membrane suggests a novel mechanism to regulate NH 3 and CO 2 delivery to algal symbionts. Science Advances 8:. https://doi.org/10.1126/sciadv.abm0303

Thumuluri V, Almagro Armenteros JJ, Johansen AR, et al (2022) DeepLoc 2.0: multi-label subcellular localization prediction using protein language models. Nucleic Acids Research 50:W228–W234. https://doi.org/10.1093/nar/gkac278

Tresguerres M, Katz S, Rouse GW (2013) How to get into bones: proton pump and carbonic anhydrase in Osedax boneworms. Proceedings of the Royal Society B 280:20130625. https://doi.org/10.1098/rspb.2013.0625

Tresguerres M, Milsom WK, Perry SF (2019) CO2 and acid-base sensing. In: Fish Physiology, 1st edn. Elsevier Inc., pp 33–68

Venn AA, Tambutté E, Lotto S, et al (2009) Imaging intracellular pH in a reef coral and symbiotic anemone. Proceedings of the National Academy of Sciences of the United States of America 106:16574–9. https://doi.org/10.1073/pnas.0902894106

Verde E, R. McCloskey L (1998) Production, respiration, and photophysiology of the mangrove jellyfish Cassiopea xamachana symbiotic with zooxanthellae: effect of jellyfish size and season. Marine Ecology Progress Series 168:147–162

Warner ME, Fitt WK, Schmidt GW (1999) Damage to photosystem II in symbiotic dinoflagellates: A determinant of coral bleaching. Proceedings of the National Academy of Sciences 96:8007–8012. https://doi.org/10.1073/pnas.96.14.8007

Weihrauch D, O'Donnell M (2017) Acid-Base Balance and Nitrogen Excretion in Invertebrates. Springer International Publishing, Cham

Weis VM (1993) Effect of dissolved inorganic carbon concentration on the photosynthesis of the symbiotic sea anemone Aiptasia pulchella Carlgren: Role of carbonic anhydrase. Journal of Experimental Marine Biology and Ecology 174:209–225. https://doi.org/10.1016/0022-0981(93)90018-J

Welsh DT, Dunn RJK, Meziane T (2009) Oxygen and nutrient dynamics of the upside down jellyfish (cassiopea sp.) and its influence on benthic nutrient exchanges and primary production. Hydrobiologia 635:351–362. https://doi.org/10.1007/s10750-009-9928-0

Wilkerson FP, Kobayashi D, Muscatine L (1988) Mitotic index and size of symbiotic algae in Caribbean Reef corals. Coral Reefs 7:29–36. https://doi.org/10.1007/BF00301979

Yasukawa Z, Sato C, Kitajima K (2007) Identification of an inflammation-inducible serum protein recognized by anti-disialic acid antibodies as carbonic anhydrase II. Journal of Biochemistry 141:429–441. https://doi.org/10.1093/jb/mvm047

Yee DP, Samo TJ, Abbriano RM, et al (2023) The V-type ATPase enhances photosynthesis in marine phytoplankton and further links phagocytosis to symbiogenesis. Current Biology 33:2541-2547.e5. https://doi.org/10.1016/j.cub.2023.05.020

# Chapter 4

## Effects of light intensity on the expression, localization, and function of V-type $H^+$-ATPase in the reef-building coral *Stylophora pistillata*

**Abstract**

Tropical coral reefs are built by coral animals (phylum Cnidaria) that form a photosymbiotic relationship with dinoflagellate algae (Family Symbiodiniaceae). Symbiont photosynthate production during the day (fixed carbon, $O_2$) can satisfy most of the host's energy demands and is linked to light enhanced calcification (LEC). In return, the host provides symbionts with $CO_2$, to promote photosynthesis through carbon concentrating mechanisms (CCMs). As increased light levels stimulate symbiont photosynthetic rates, we hypothesized that corals acclimated to high light conditions would employ more V-type $H^+$-ATPase-driven (VHA) CCMs in host cells. To test this hypothesis, we established a recirculating aquarium system (RAS) with water chemistry modeled on Pacific coral reefs containing *Stylophora pistillata* under either 100, 500, or 1400 μE light. Coral VHA protein abundance increased with increasing light levels. In addition, abundance of soluble adenyl cyclase (sAC), a putative molecular pH sensor, was higher in the 500 and 1400 μE light treatments. $Na^+/K^+$-ATPase (NKA) abundance did not change across light treatments. Both VHA and sAC were widely distributed throughout coral tissues, including the symbiont containing cells. However, $O_2$ microsensor respirometry revealed that VHA inhibition did not affect $O_2$ evolution rate (a proxy for photosynthetic activity) in corals raised at 100 and 500 μE light and it increased it in corals raised at 1400 μE. Thus, our results indicate that the VHA-driven CCM was not functional under our experimental conditions and that VHA participates in a net $O_2$-consuming process in high light conditions. We speculate that this process may involve VHA-dependent LEC-related pHi and pH regulation of calcifying cells and the extracellular calcifying fluid (ECF), respectively.

## Introduction

The success of coral reef ecosystems in oligotrophic tropical waters is owed to the intracellular photosymbiosis between Symbiodiniaceae dinoflagellate algae and reef-building scleractinian corals. Algal symbionts remain photosynthetically active *in hospite* capturing light energy to fix $CO_2$ into sugars and evolve $O_2$. Any fixed carbon produced in excess of the algae's needs is released to the coral host as substrate for growth and metabolism. Release of fixed carbon and $O_2$ provides corals with ample substrate to fuel aerobic respiration and sustain high ATP regeneration rates during the day. Given sufficient symbiont density and light input, the released fixed carbon can meet over 100% of a coral's daily energy requirements (Tanaka et al. 2018). In turn, aerobic respiration throughout the coral colony produces $CO_2$ which regenerates substrate for symbiont photosynthesis creating a semi-closed carbon cycling loop. Furthermore, $O_2$ consumption by the coral holobiont amplifies the outwards $O_2$ diffusion gradient from algae ameliorating $O_2$ buildup that could slow photosynthesis via product accumulation. However, some fixed carbon is incorporated as new cellular material by algal symbionts, the microbial community, and the host mandating the transport of additional dissolved inorganic carbon (DIC) from seawater to the symbionts for continual photosynthesis (Muscatine et al. 1984; Tanaka et al. 2018).

DIC demands of symbionts are intrinsically linked to the light regime a coral colony experiences with those in higher light undergoing higher photosynthetic rates and fixing more DIC. Light attenuation occurs exponentially with depth and water turbidity due to suspended particulate matter also affects light penetration in a linear matter. *S. pistillata* for example can be found in light environments ranging from <50 μE at 65m depth to ~1500 μE at 5m of photosynthetically active radiation (PAR) (Mass et al. 2007). Symbionts in low light environments increase their photosynthetic pigments and photosynthetic efficiency to capture and utilize all available light

energy but still produce fewer photosynthates than symbionts in higher light environments (Mass et al. 2007). As a result of receiving fewer photosynthates, corals exhibit lower respiration, calcification, and growth rates (Anthony and Hoegh-Guldberg 2003a, b) and some coral species increase heterotrophic feeding to increase their energy budget (Lesser et al. 2010). Coral colonies acclimated to high light conditions tend to present the opposite phenotypes: symbionts show decreased photosynthetic pigments content and photosynthetic efficiency while corals exhibit increased respiration, calcification, and growth rates. Despite their lower pigment content and photosynthetic efficiency, symbionts exhibit higher rates of gross photosynthesis in high light conditions due to overall greater solar input. Chronic exposure to high light conditions (>1500 μE) can be harmful however as the rate of photodamage to symbiont photosystems can outpace repair mechanisms (Langdon and Atkinson 2005; reviewed in Tyystjärvi 2013).

Like light attenuation with depth, diel (day-night) and seasonal cycles have predictable effects on light availability; however, other light regimes are dynamic over timescales ranging from milliseconds to weeks: shifting surface waves act as lenses focusing light intensity up to ~9000 μE and >350 times per minute (Stramski and Dera 1988), clouds and storms can decrease irradiance by 40-fold and last minutes to weeks (Falkowski and Chen 2003), and tides alter the depth of corals which changes light quantity and spectral quality. Dynamic solar input dictates that symbiont photosynthetic rates are always changing and DIC supply may not always match demand. In these cases, DIC-limitation compounded by damaged photosystems (Langdon and Atkinson 2005) can result in the generation of reactive oxygen species (ROS) (Wooldridge 2009): DIC-limitation of the Calvin-Benson cycle slows regeneration of NADPH to $NADP^+$, the terminal electron acceptor in the electron transport chain (ETC), without which, the ETC becomes blocked (reviewed in Murata et al. 2007). As the ETC becomes over-reduced by continued excitation

energy, readily-available $O_2$ becomes the energetically favorable terminal electron acceptor thereby producing ROS (Lesser 1996a). ROS are harmful to both symbionts and coral host (Lesser 2006). In fact, many believe that ROS production is the unifying mechanism explaining coral bleaching (reviewed in Lesser 2011). It is unsurprising then that photosymbiotic hosts have evolved mechanisms to saturate symbionts with DIC to promote continued photosynthesis and avoid ROS production.

As discussed in Chapters 2 and 3, corals, anemones, and jellyfish employ V-type $H^+$-ATPase (VHA) to concentrate $CO_2$ in the symbiont's microenvironment. *In hospite*, corals' algal symbionts are retained in modified phagosomes ("symbiosomes") of gastrodermal host cells ("symbiocytes"). The symbiosome supports symbiont photosynthesis by concentrating $CO_2$ in the symbiont's microenvironment (Barott et al. 2015b, 2022). The need for such symbiocyte-driven carbon concentrating mechanisms (CCMs) is necessitated by algal Rubisco's low affinity for $CO_2$ which prevents carbon fixation from occurring at ambient $pCO_2$ levels, a problem exaggerated in light- or DIC-limiting environments (Leggat et al. 2002; Yee et al. 2023). In addition, $O_2$ competes with $CO_2$-binding capacity of Rubisco in low-$CO_2$ environments thereby necessitating a continued supply of $CO_2$ to prevent the generation of ROS and damage to symbiont photosystems (Lesser 1996b; Warner et al. 1999). The pH-dependent nature of DIC speciation between $CO_2$, $HCO_3^-$, and $CO_3^{2-}$ and the $pH_i$ of cnidarian host cells dictates the majority of DIC in animal cells exists as membrane-impermeable $HCO_3^-$. The symbiosome is markedly acidic however (pH <6) driven by $H^+$ pumping by coral VHA located in the symbiosome membrane (Venn et al. 2009; Barott et al. 2015b). Given the $pK_a$ for $HCO_3^-$ to $CO_2$ conversion is 6.1, any $HCO_3^-$ that enters the symbiosome is dehydrated into $CO_2$ which can freely diffuse across the symbiont cell wall. While metabolic $CO_2$ generated by the host is the major source of DIC for symbiont photosynthesis, the identity of

the transporter(s) responsible for $HCO_3^-$ movement into the symbiosome remains elusive. Photosynthetic $CO_2$ consumption exerts a strong alkalinizing force on the cytosol of symbiocytes and the coelenteron during the day, while nighttime respiration acidifies these compartments: pHi of *S. pistillata* symbiocytes shifts from ~7.4 in the day to ~7 at night (Laurent et al. 2013) and coelomic pH ranges from ~9 in the day to ~6.75 at night (Furla et al. 2000; Agostini et al. 2012).

A second significant sink for DIC is coral calcification, the process of depositing a $CaCO_3$ skeleton beneath the animal. This process is orchestrated by calcifying cells which initiate the intracellular formation and extracellular deposition of amorphous $CaCO_3$ (ACC) and skeletal organic matrix (SOM) proteins and elevate the pH of the extracellular calcifying fluid (ECF) to promote precipitation and prevent dissolution of $CaCO_3$ aragonite crystals (reviewed in Tambutté et al. 2011; Mass et al. 2017). Intracellular ACC formation is better understood in calcifying cells of sea urchin larvae where high pH vesicles are enriched for DIC to form amorphous mineral before exocytosing their cargo into the high pH calcifying space (Beniash et al. 1997). Corals are believed to employ a similar mechanism (Mass et al. 2017) and maintain high ECF pH. ECF pH displays a cyclical pattern shifting from 8.1-8.4 in the dark to 8.7-9.3 in the light (Al-Horani et al. 2003; Venn et al. 2011). Exact pH values differ between studies but the pattern of high ECF pH under illumination is universal. At these values, the aragonite saturation state is 3-11-fold hypersaturated in the dark and 20-30-fold in the light enabling calcification during the night and day. Conspicuously, reef-building corals demonstrate higher rates of calcification in the light, a phenomenon dubbed light-enhanced calcification (LEC); the magnitude of LEC also increases with increasing light irradiance (Goreau and Goreau 1959; Vandermeulen 1975). The stimulatory effect of light on calcification is linked to photosynthesis and not just to light itself (Colombo-Pallotta et al. 2010). While several theories have been proposed to explain this link, none are

mutually exclusive and many are complimentary: (1) photosynthesis titrates $H^+$ produced during calcification allowing for continued export of acid from the ECF (2) symbionts remove $PO_4^{3-}$, an ion that interferes with aragonite formation, generated by animal metabolism, (3) photosynthates are used as precursors to produce SOM proteins, (4) $O_2$ and fixed carbon produced by symbionts fuels aerobic metabolism generating DIC and ATP in calcifying cells thereby accelerating the calcification process by providing substrate and energy for pHi/ECF pH regulation (reviewed in Allemand et al. 2011). To maintain the ECF's high pH, calcifying cells must export $H^+$ produced during mineral formation from (1) the ECF into the cytosol and (2) the cytosol into the mesoglea and aboral endoderm. Despite this burden, pHi of calcifying cells remains constant at ~7.4 in both light and dark conditions (Venn et al. 2011) suggesting they employ robust pH-sensory and regulatory mechanisms.

Recent work established that calcification rates and ECF pH are regulated by soluble adenyl cyclase (sAC) (Barott et al. 2020). sAC is directly stimulated by $HCO_3^-$ to produce cyclic adenosine monophosphate (cAMP), the ubiquitous secondary messenger molecule. In conjunction with carbonic anhydrases (CAs), sAC acts as a molecular pH sensor that can coordinate downstream cellular ion transport via protein kinase A (PKA) (Alzamora et al. 2010) activity in acid-base regulatory epithelia and calcifying cells of many marine organisms including sea urchins and marine fishes (Toyofuku et al. 2017; Kwan et al. 2020; Chang et al. 2023). In fish gill cells, sAC regulates VHA activity to export $H^+$ in response to acid-base disturbances of extra- and intracellular origin. In foraminifera, outwards $H^+$ pumping by VHA raises pHi and maintains a pool of $CO_3^{2-}$ for calcification (Toyofuku et al. 2017). Given its established role in coordinating biomineralization and ECF pH, sAC may likewise regulate calcifying cell pHi through modulating VHA activity, if VHA is present. Corals produce cAMP at the highest rate of any animal

suggesting that sAC is particularly important for regulating responses to acid-base disturbances (Barott et al. 2013). Notably, cAMP production fluctuates over diurnal cycles, periods when corals experience profound acid-base disturbances associated with photosynthesis and calcification. sAC may therefore participate in regulating symbiocyte pHi and coelomic pH in addition.

In this chapter, we investigate the role of environmental light levels in regulating VHA-driven CCMs and VHA's potential role in pHi regulation of calcifying cells during LEC in *S. pistillata*. We established a recirculating aquarium system (RAS) with water chemistry modeled on Pacific coral reefs and raised corals under either 100, 500, or 1400 µE light. We evaluated the abundance and localization of VHA and sAC proteins using Western blotting and immunohistochemistry, respectively. VHA's contribution to CCMs was tested using pharmacology and $O_2$ microsensor respirometry.

**Methods**

*Animals*

*S. pistillata* colonies were maintained in two recirculating 100 L aquaria (RAS) filled with artificial seawater: salinity (S1: 34.9 ± 1.0 ppt, S2: 34.6 ± 0.9 ppt), temperature (S1: 26.3 ± 0.8 °C, S2: 25.9 ± 0.8 °C), pH (S1: 8.0 ± 0.1, S2: 8.1 ± 0.1), alkalinity (S1: 1.67 ± 0.41 meq $L^{-1}$, S2: 1.70 ± 0.26 meq $L^{-1}$), calcium (S1: 379.0 ± 21.2 ppm, S2: 380.7 ± 20.9 ppm), nitrite (S1: 0.0 ± 0.0 ppm, S2: 0.0 ± 0.0 ppm), nitrate (S1: 0.0 ± 0.0 ppm, S2: 0.0 ± 0.0 ppm), and total ammonia (S1: 0.02 ± 0.08 mg $L^{-1}$, S2: 0.02 ± 0.09 mg $L^{-1}$) (Supplemental Figure 4.1). Dissolved $CO_2$ ($dCO_2$) was measured after the experimental period: 12.76 ± 2.20 µmol $L^{-1}$. The aquaria were illuminated on a 12 h:12 h cycle with 100 ± 28 µmol photons $m^{-2}$ $s^{-1}$ (µE), 500 ± 14 µE, or 1400 ± 141 µE of photosynthetically active radiation covering the full visible spectrum (Hydra 64 HD LED light, Aqua Illumination, Bethlehem, PA, USA) as determined using a MQ-510 full-spectrum quantum

sensor (Apogee Instruments, Inc., Logan, UT, USA). pH and temperature were monitored using a HACH PHC101 pH Electrode (HACH, Loveland, CO, USA). Total ammonia, nitrate, and nitrite were monitored using API Water Test Kits (Mars Fishcare Inc., Chalfont, PA, USA). Calcium and alkalinity levels were measured using marine calcium and alkalinity meters (Hanna Instruments Inc., Woonsocket, RI, USA). $dCO_2$ was measured using a Qubit Systems S157 $CO_2$ Analyzer connected to a S400 Rapid $dCO_2$ Sampling System calibrated with $N_2$ and 1000 ppm $CO_2$ gasses (Kingston, Ontario, Canada). Animals were fed daily with either freshly-hatched Artemia (San Francisco Strain, Brine Shrimp Direct, Ogden, UT, USA) or a 50:50 mixture of PhytoFeast and OysterFeast (Reef Nutrition, Campbell, CA, USA).

*Antibodies*

Tissues were probed for $VHA_B$ using custom rabbit polyclonal antibodies developed against a peptide antigen matching a region of the $VHA_B$ subunit (AREEVPGRRGFPGY; GenScript Biotech Corporation, Piscataway, NJ, USA) which is 100% conserved in species ranging from corals to humans (Tresguerres et al. 2013; Barott et al. 2015b; Roa and Tresguerres 2016; Armstrong et al. 2018; Damsgaard et al. 2020; Barott et al. 2022). These antibodies were previously validated for IHC and Western blotting in *S. pistillata* (Barott et al. 2015b). Tissues were probed for sAC using custom rabbit polyclonal antibodies developed against a peptide antigen (LPGDKHEDDPARAL, GenScript) spanning the second catalytic domain of *Acropora digitifera* sAC (Barott et al. 2017). These antibodies were validated for sAC from *S. pistillata* by IHC and Western blotting (Barott et al. 2020). Tissues were probed for NKA using a commercially available mouse monoclonal antibody (SC-48345, Santa Cruz Biotechnology, Dallas, TX, USA) derived from a polyclonal line previously validated in *S. pistillata* (Barott et al. 2015a).

*Western Blotting*

Using methods adapted from (Barott et al. 2015b), *S. pistillata* tissues were removed from their skeletons using an airbrush loaded with homogenization buffer [(S22 buffer supplemented with protease inhibitor cocktail (P2714; Sigma-Aldrich, St. Louis, MO, USA) and phosphatase inhibitors (PhosStop; Roche Applied Science, Penzberg, Germany)]. The homogenate was sonicated on ice for 3 x 15 sec bursts with 1 min rest in-between. The sonicated homogenate was then centrifuged (500 x g, 15 min, 4 °C) to pellet down debris and symbiotic algae. The supernatant was then centrifuged (21,000 x g, 30 min, 4 °C) and the membrane-enriched pellet was resuspended in 150 µL homogenization buffer and frozen at -80 °C overnight. Protein concentrations in membrane-enriched fractions were determined using a Bradford Protein Assay (Bio-Rad, Hercules, CA, USA). Membrane-enriched fractions were mixed with 2x Laemmli buffer (Bio-Rad) containing 10% β-mercaptoethanol. Aliquots for $VHA_B$ and sAC blotting were denatured at 90 °C for 5 min while those for NKA were incubated at room temperature (21 °C) for 15 min. 25 µg protein and 4 µl of Precision Plus Dual Color Protein Standards (Bio-Rad) were loaded into a 10% polyacrylamide SDS-PAGE gel in a Mini-Trans Blot Cell (Bio-Rad) with running buffer (25 mM Tris, 190 mM glycine, 0.1% SDS). Electrophoresis was run for 2 h at 100 V (4 °C). Following electrophoresis, the gel was rinsed with distilled water and equilibrated in Towbin buffer (25 mM Tris pH 8.3, 192 mM glycine, 20% (v/v) methanol) for 15 min. Proteins were transferred from the gel onto a PVDF membrane using a Mini Tans-Blot Cell (Bio-Rad) overnight in Towbin buffer (0.09 A, 4°C). PVDF membranes were washed in Tris-Buffered Saline + 0.1% Tween detergent (TBS-T) for 15 min on a shaker at room temperature to remove excess transfer buffer prior to blocking. PDVF membranes were then blocked with 10% powdered fat-free milk in TBS-T for 1 h on a shaker at room temperature. Following blocking, membranes were

incubated overnight on a shaker (4 °C) with anti-$VHA_B$ (0.329 µg/ml), anti-sAC (0.55 µg/ml), or anti-NKA (0.2 µg/ml) primary antibodies in blocking buffer. Membranes were washed with 3 x 10 min TBS-T washes prior to incubation with secondary antibody (goat anti-rabbit-HRP diluted 1:10,000, Bio-Rad) for 1 h on a shaker at room temperature. Membranes were again washed with 3 x 10 min TBS-T washes prior to band development with an ECL Prime Western Blot Detection Kit (GE Healthcare, Chicago, IL, USA) and imaged using a Chemidoc Imaging system (Bio-Rad) (Supplemental Figure 4.2).

*Immunohistochemistry (IHC)*

*S. pistillata* colonies were fixed and decalcified following previously described methods (Barott and Tresguerres 2015; Barott et al. 2015b, 2017, 2020; Thies et al. 2022). Briefly, tissues were fixed in 3% paraformaldehyde in S22 buffer overnight at 4 °C on an orbital shaker. To decalcify the tissues, samples were incubated in Ca-free S22 buffer supplemented with 0.5 M EDTA and 0.5% paraformaldehyde changed daily for two weeks. Tissues were dehydrated, embedded in paraffin wax, and sectioned following previously described protocols for corals (Barott and Tresguerres 2015). Tissues were deparaffinized, rehydrated, permeabilized in 0.2% Triton-X (v/v) in phosphate buffered saline (PBS-TX) and incubated in blocking buffer (2% normal goat serum and 0.5% keyhole limpet hemocyanin in PBS-TX) for 1 h at room temperature. Sections were incubated overnight (4 °C) with either anti-$VHA_B$ (0.98 µg/ml), anti-sAC (1.10 µg/ml), or anti-NKA (0.80 µg/ml) primary antibodies in blocking buffer or blocking buffer alone (negative control). Sections were washed with 3 x 5 min PBS-TX washes before incubation with 4 µg $ml^{-1}$ secondary antibody (goat anti–rabbit–Alexa Fluor 555 or goat anti–mouse–Alexa Fluor 568; Invitrogen, Carlsbad, CA, USA) in blocking buffer for 1 h at room temperature followed by 1 µg $ml^{-1}$ 4′,6-diamidino-2-phenylindole (DAPI) DNA stain (Invitrogen) for 5 min. Sections were

washed with 3 x 5 min PBS-TX to remove unbound secondary antibodies and DAPI. Samples were mounted in ProLong Gold Antifade Mountant (P36930; Invitrogen). Native Symbiodiniaceae chlorophyll A (ChlA) signal is retained during this protocol. Negative control images are presented in (Supplemental Figure 4.4).

Confocal Airyscan microscopy was performed on a Zeiss AxioObserver Z1 connected to a laser scanner equipped with 405-, 488-, 561-, and 640-nm laser lines (Zeiss LSM 800 with Airyscan, Carl Zeiss AG, Oberkochen, Baden-Württemberg, Germany). This device uses a 32-channel photomultiplier detector and linear deconvolution to obtain 140-nm lateral (X-Y) and 400-nm axial (Z) resolution.

$O_2$ *Microelectrode Recordings*

Dark respiration ($R_D$) and net photosynthesis ($P_N$) was measured for individual *S. pistillata* colonies. 1 cm length clippings were placed in sealed glass respirometry chambers and dissolved $O_2$ was measured using a Clark-type $O_2$ electrode (Unisense, Aarhus, Denmark) that was calibrated with anoxic (bubbling with $N_2$ gas) and 100% $O_2$-saturated 0.2 μm-filtered seawater (FSW, 25 °C, 35 ppt salinity). Experimental chambers were stirred with an internal magnetic stir bar and temperature was maintained via external water bath. Data were recorded using the accompanying SensorTrace software (v3.4.3; Unisense). Light was provided using an ACE Light Source with a full-spectrum halogen EKE lamp (Schott AG, Mainz, Germany) and calibrated with a MQ-510 full-spectrum quantum sensor (Apogee Instruments, Inc.). Coral clippings were preincubated in darkness for 15 min prior to experimental recordings to allow $R_D$ to stabilize. Clippings were then moved to respirometry chambers filled with FSW and $R_D$ was measured for 15 min. The chamber was then illuminated with 100, 500, or 1400 μE light, depending on experimental treatment and $P_N$ was measured for 15 min. Following FSW recordings, the animal was moved into fresh FSW

and incubated in darkness for 15 min. Clippings were then moved into fresh respirometry chambers filled with solutions of 0.667 µL/mL DMSO or 0.667 µL/mL ConcanamycinA (ConcA; 1µM final concentration) dissolved in FSW. $R_D$ was measured for 15 min prior to illumination at the treatment light level and $P_N$ recording for 15 min. Linear trendlines were fit to the full 15 min recordings. N = 6 for all experimental treatments.

*Statistics*

Data were analyzed in GraphPad Prism v10.0.1 (San Diego, CA, USA). Outliers were removed using the ROUT method at 1% sensitivity and data normality and homogeneity of variance were tested using the Shapiro-Wilk normality test. Western blot data were analyzed with Brown-Forsythe and Welch ANOVAs or Kruskal-Wallis tests. Respirometry data were analyzed using 2-Way RM ANOVAs with the Geisser-Greenhouse correction and Dunett's multiple comparisons tests.

**Results and Discussion**

*Changes in Visual Appearance and Polyp Behavior Associated with Light Level*

Corals grew in the RAS under all light conditions however, their appearance differed between treatments. *S. pistillata* grown at 100 µE appeared brown (Supplemental Figure 4.5) consistent with an abundance of algal symbionts in their tissues and high chlorophyll content per symbiont. In contrast, *S. pistillata* grown at 1400 µE shifted to a light pink-white coloration indicative of a shift in pigment content in both the coral and symbionts. Commonly referred to as the "pink pigmentation response," this phenotype results from production of nonfluorescent chromoproteins and fluorescent proteins in coral cells and altered chlorophyll per symbiont (Suzuki et al. 2024). Corals grown at 500 µE displayed an intermediate color phenotype. Additionally, polyps of corals at 100 µE were fully-extended during the day while those at 1400

μE remained retracted (Supplemental Figure 4.5A,C,D,F). Polyp extension/retraction is a behavior used to modulate light availability to symbionts and allows animals to self-shade in high-light environments (Wangpraseurt et al. 2014). We interpret this behavior as evidence that corals at 1400 μE are actively limiting light delivery to symbionts, possibly as a photoprotective mechanism.

*Protein Expression of VHA, sAC, and NKA*

Similar to *S. pistillata* grown in flowthrough aquaria (Barott et al. 2015a, b, 2020), *S. pistillata* corals raised in the RAS expressed $VHA_B$, sAC, and NKA protein by Western blotting of whole tissue homogenate (Supplemental Figure 4.2). Anti-$VHA_B$, -sAC, and -NKA antibodies detected single ~50, ~90, or ~130 kDa bands, respectively, matching *S. pistillata* proteins and consistent with previous findings. Notably, corals raised at 500 or 1400 μE expressed 1.7- or 2.7-fold more $VHA_B$ than those raised at 100 μE (Figure 4.1A; ANOVA: $F_{2, 12.9} = 21.21$, $p = 0.0009$). Increased light availability enables faster rates of symbiont photosynthesis and consequently, requires faster rates of DIC delivery into symbiosomes. Increased abundance of $VHA_B$ in corals grown at higher light conditions suggests that hosts upregulate the VHA-powered CCMs to meet symbionts' DIC demands, prevent carbon-limitation, overcome $O_2$ competition for rubisco, and thus maximize their photosynthetic output. Symbiosomal VHA could titrate $H^+$ generated by daytime calcification and direct it into the CCM. Alternatively, $VHA_B$ could be expressed in cells other than symbiocytes such as epidermal cells bordering seawater, non-symbiotic gastrodermal cells, or potentially even calcifying cells. Calcification rates increase with light irradiance and generates $H^+$ which must be exported from sites of calcification to the coelenteron or seawater; VHA in the basolateral membrane of calcifying cells or apical membrane of aboral endodermal cells could perform this function.

sAC expression increased 2.1-fold from 100 to 500 μE (Figure 4.1B; ANOVA: $F_{2, 6.776} = 2.099$, $p = 0.0009$) but it did not increase further at 1400 μE. The increased sAC abundance at 500 and 1400 μE suggests that *S. pistillata* experience more frequent and/or larger magnitude pH disturbances at higher light levels possibly associated with higher rates of photosynthesis and calcification.

Finally, NKA expression did not vary among light treatments (Figure 4.1C; Kruskal-Wallis: $p = 0.2003$); this is surprising given that (1) NKA is present in the basolateral membrane of calcifying cells and potentially energizes secondary active transport to support calcification (Barott et al. 2015a; Thies et al. 2022) and (2) calcification rates increase with light irradiance. However, as Western blotting used homogenates of whole tissues, this result could be explained by coincident downregulation of NKA in other tissues.

Western blotting on bulk tissues cannot determine the localization of proteins in specific cell subtypes or subcellular compartments which complicates interpreting the physiological significance of the observed protein abundance patterns in response to light. Thus, we employed immunofluorescence confocal microscopy (ICM) to establish the cellular and subcellular localizations of $VHA_B$ and sAC. Given the time required to obtain and analyze high quality images via ICM, we were limited to observing only samples from 100 and 1400 μE conditions.

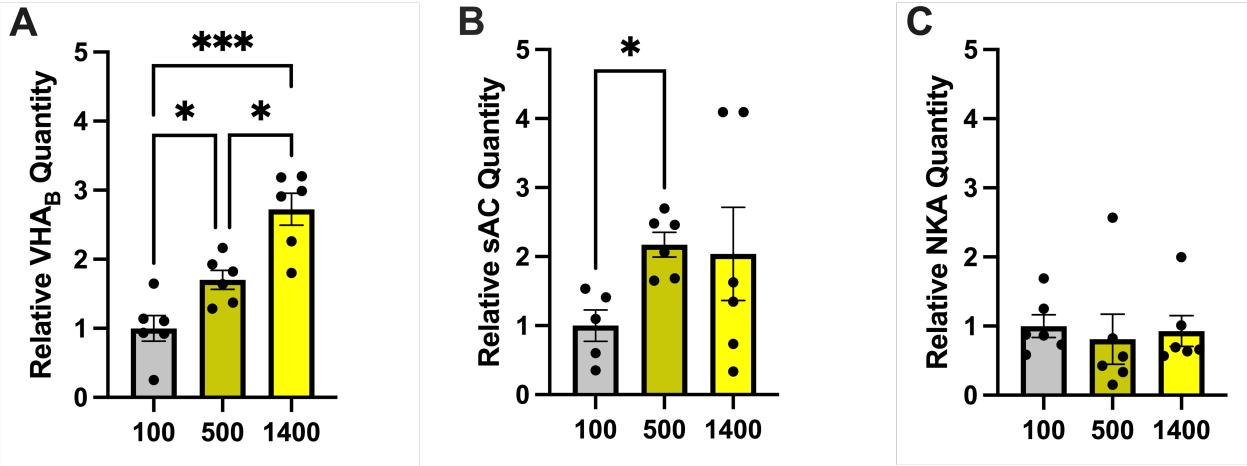


Figure 4.1: Relative VHA$_B$, sAC, and NKA protein abundance in *S. pistillata* raised at 100, 500, and 1400 µE. Protein abundance was measured by Western blot (Supplemental Figure 4.2). n = 5-6 for all treatments, error bars = ± SEM. Data were tested using Brown-Forsythe and Welch 1-Way ANOVAs or Kruskal-Wallis tests; * ($p < 0.05$), *** ($p < 0.001$).

*VHA$_B$ Is Present in Epidermal Cells, Symbiocytes, and Calcifying Cells*

In epidermal cells from corals grown at 100 µE, VHA$_B$ immunofluorescence displayed a faint and punctate pattern (Figure 4.2, Supplemental Figure 4.6). This localization may be related to the ubiquitous involvement of VHA$_B$ in regulating vesicle dynamics (reviewed in Hu et al. 2015) and to the continuous pinocytosis of extracellular fluids by Cnidarian cells (Ganot et al. 2020). In addition to stronger vesicular-like staining, epidermal VHA$_B$ in corals grown at 1400 µE displayed strong apical membrane localization including in microvilli projecting into mucus and seawater (Figure 4.2). This pattern suggests that *S. pistillata* grown at 1400 µE employ VHA to excrete excess $H^+$ into their environment or energize the absorption or excretion of other molecules.

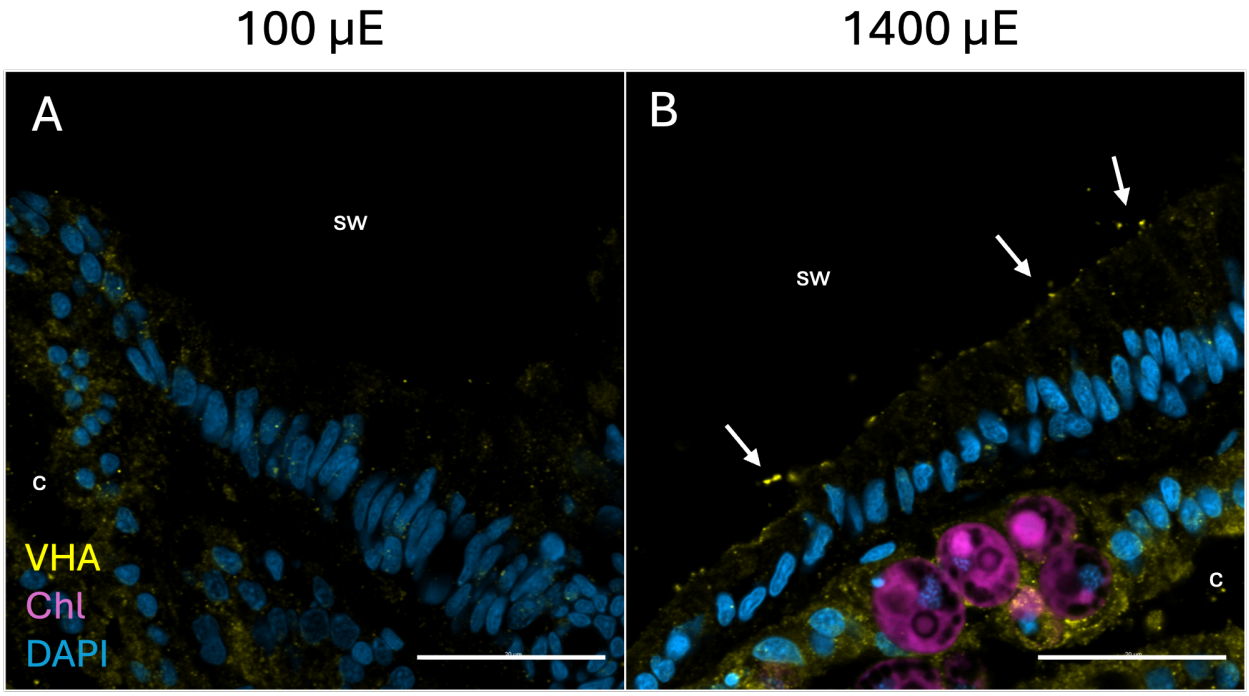


Figure 4.2: $VHA_B$ localization in epidermal cells of *S. pistillata* raised at 100 and 1400 µE. Scale bar is 20 µm. sw – seawater, c – coelenteron.

Symbiocytes in the tentacle and coenosarc gastric cavity (Figure 4.3Figure 4.4) displayed robust $VHA_B$ signal in corals from both light levels. At 100 µE, $VHA_B$ localized to vesicles associated with the apical membrane where exchange with the coelenteron occurs. Akin to epidermal cells, this pattern supports a role for VHA in symbiocyte pinocytosis of coelomic fluids and phagocytosis of suspended particles (reviwed in Hu et al. 2015; Ganot et al. 2020). In contrast, symbiocytes from corals raised at 1400 µE showed increased $VHA_B$ signal encircling symbionts consistent with $VHA_B$ in the symbiosome membrane. This observation supports our hypothesis that *S. pistillata* grown in high light employ more VHA-driven CCMs than those in low light to meet the DIC demands of symbionts; functional respirometry experiments were employed to test this hypothesis (see below). Notably, RAS-raised *S. pistillata* displayed occasional symbiosomal VHA localization, markedly less common than reported in (Barott et al. 2015b). This discrepancy

could be explained by putative differences in water chemistry (alkalinity, $dCO_2$, dissolved nutrients) between studies.

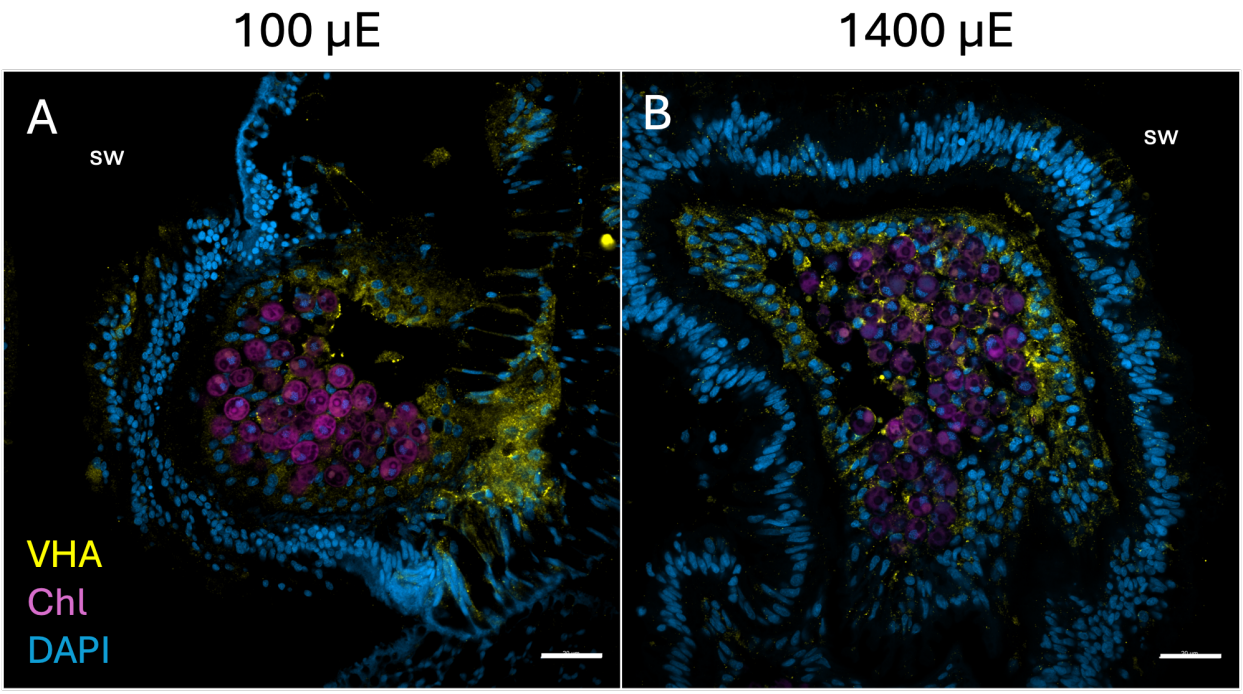


Figure 4.3: $VHA_B$ localization in the tentacle of *S. pistillata* raised at 100 and 1400 µE. Scale bar is 20 µm. sw – seawater.

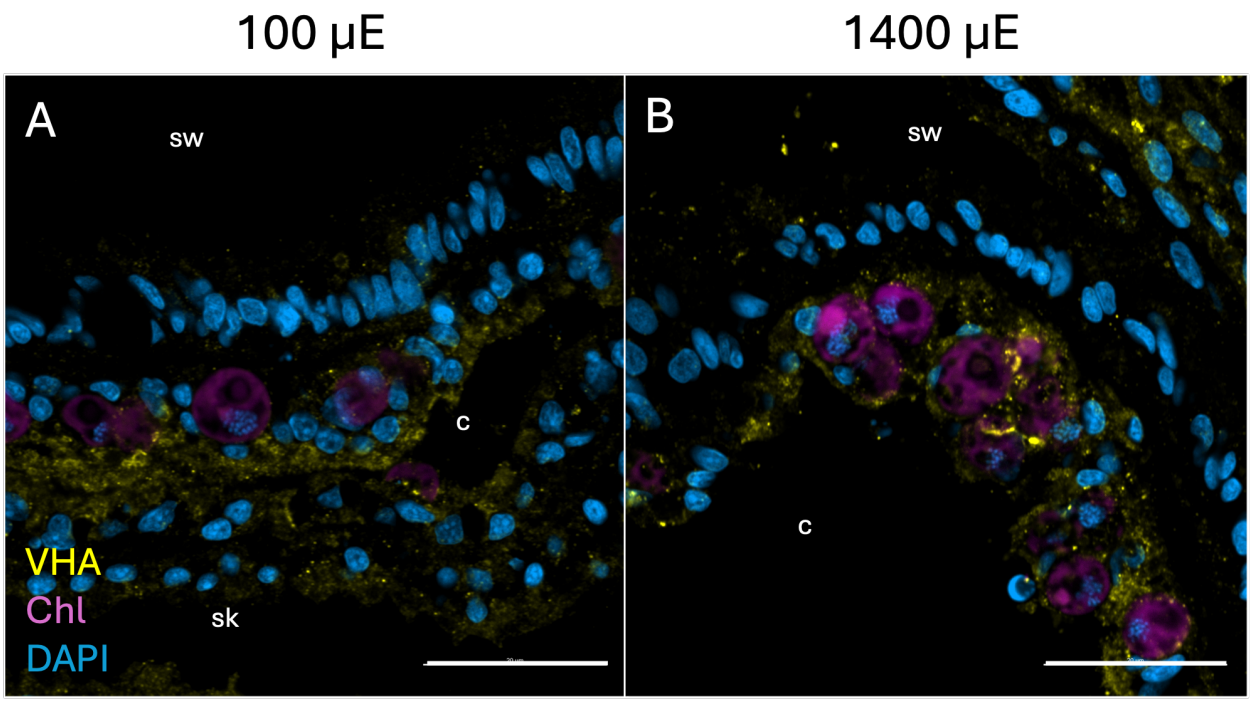


Figure 4.4: $VHA_B$ localization in symbiocytes of *S. pistillata* raised at 100 and 1400 µE. Scale bar is 20 µm. sw – seawater, sk – skeleton, c – coelenteron.

Notably, calcifying cells from *S. pistillata* grown at both 100 and 1400 µE displayed strong $VHA_B$ signal, a localization which has never been reported (Supplemental Figure 4.6). Discerning $VHA_B$'s subcellular localization in the calcifying cells was complicated however by the morphology of this cell type: they are extremely thin (<300 nm) and form an interdigitating intercellular meshwork that makes identifying apical and basolateral membranes very challenging (Barott et al. 2015a; Barron et al. 2018). To overcome this limitation, we employed Airyscan confocal microscopy (140 nm xy-resolution) on samples co-labeled with NKA, which is present in the basolateral membrane of coral calcifying cells (Barott et al. 2015a; Thies et al. 2022). Airyscan observations revealed that $VHA_B$ localized to cytosolic vesicles, basolateral membranes, and apical membranes facing the ECF and skeleton (Figure 4.5C-D). Calcifying cells from corals grown at 1400 µE tended to show higher $VHA_B$ signal suggesting that VHA is involved in a light-

sensitive process. The role of VHA in calcifying cells is discussed in detail in the following sections.

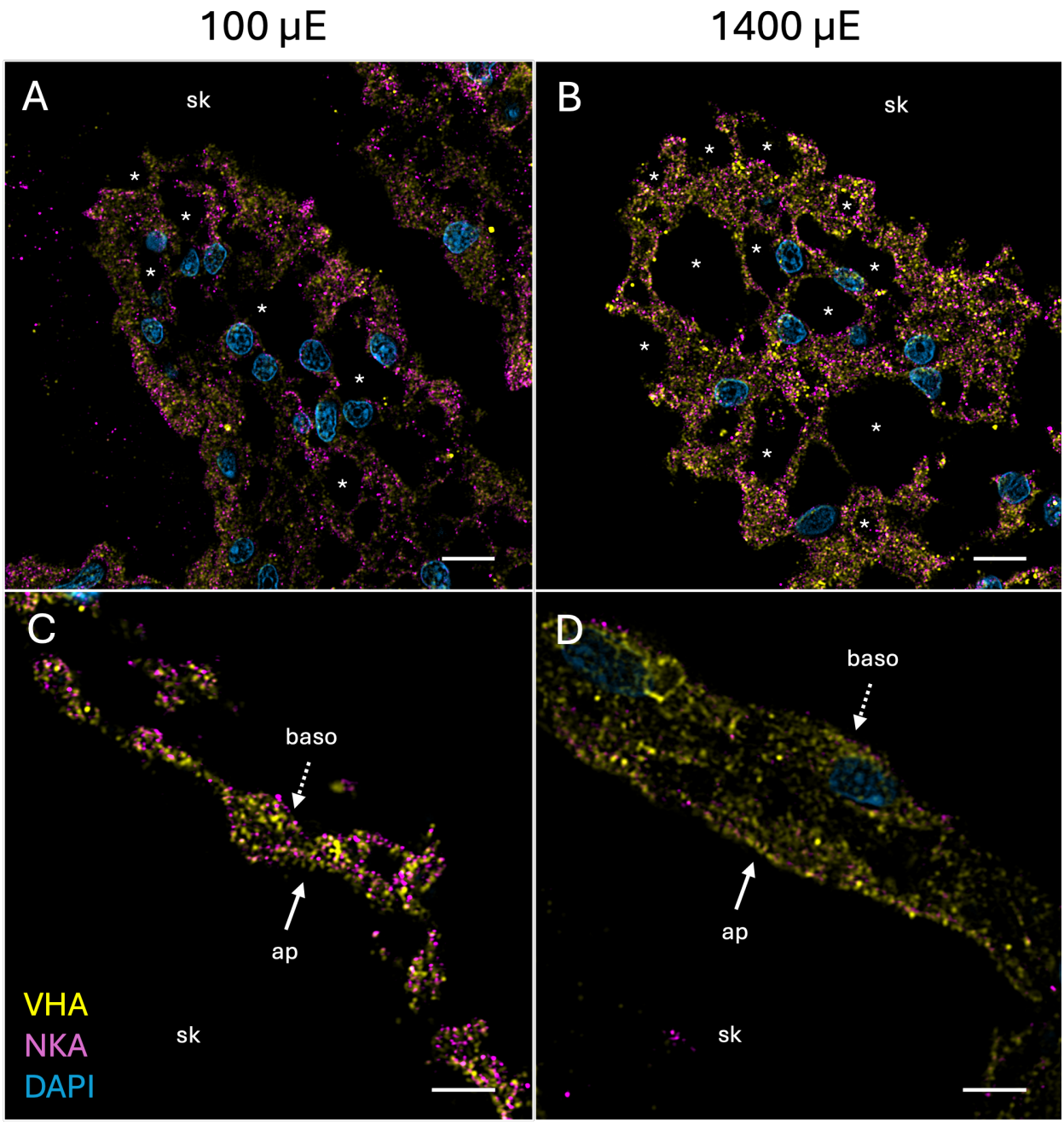


Figure 4.5: $VHA_B$ localization in two morphologies of calcifying cells of *S. pistillata* raised at 100 and 1400 µE. (A-B) Extensions of calcifying cells with apical pits. (C-D) Single layers of calcifying cells. Scale bar is 5 µm (A-B) and 3 µm (C-D). sk – skeleton, * – apical pits, ap – apical membrane, baso – basolateral membrane.

*sAC Is Widely Expressed in S. pistillata Tissues*

Coral sAC was widely expressed in all cell types consistent with it's central physiological role as a pH sensor (Barott et al. 2013, 2017; reviewed in Tresguerres et al. 2017). sAC displayed diffuse cytosolic localization in epidermal cells from corals grown at both 100 and 1400 µE (Figure 4.6, Supplemental Figure 4.7). Here, sAC may play a role in regulating metabolism, pHi, or pH of the mucus layer produced by epidermal cells. As the mucus layer hosts an extensive microbiome which contributes to both pathogen defense (Rohwer et al. 2002; Shnit-Orland and Kushmaro 2009) and nutrient cycling (Siboni et al. 2008), sAC may play an important role in regulating coral-microbe interactions along the mucus-epidermal boundary and deserves future attention.

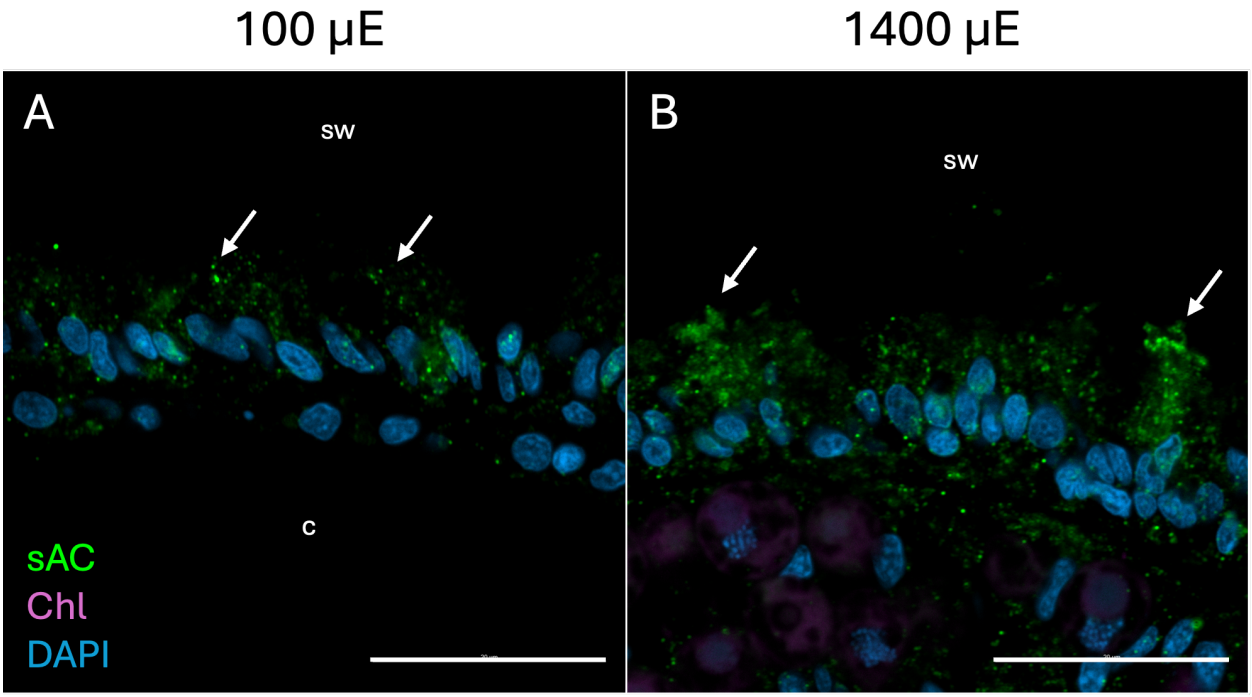


Figure 4.6: sAC localization in epidermal cells of *S. pistillata* raised at 100 and 1400 µE. Scale bar is 20 µm. sw – seawater, c – coelenteron.

Symbiocytes in the tentacle displayed diffuse sAC signal both around the symbionts and in proximity to the cell membrane in contact with the coelenteron (Figure 4.7). These patterns were similar between *S. pistillata* raised at 100 and 1400 µE. sAC displayed similar localization patterns

in symbiocytes lining the gastrovascular cavity and channels in the coenosarc (Figure 4.8); however, sAC in corals raised at 1400 µE associated more closely with the apical membrane facing the coelenteron than those raised at 100 µE. This shift suggests that gastrodermal cells experience stronger or more prolonged acid-base disturbances at high light conditions. Notably, calcification acidifies the coelenteron by producing waste $H^+$ as a byproduct of $CaCO_3$ formation. Photosynthesis exerts an opposite alkalizing effect on symbiocytes, and subsequently the coelenteron, that is proportional to both symbiont density and environmental light levels (Crovetto et al. 2024). While calcification increases with light irradiance, the alkalinizing force of photosynthesis counteracts acidification by consuming $CO_2$ and $H^+$. sAC is poised to play an essential role in sensing and regulating symbiocyte pHi under these dynamic pH stresses associated with the diel cycle.

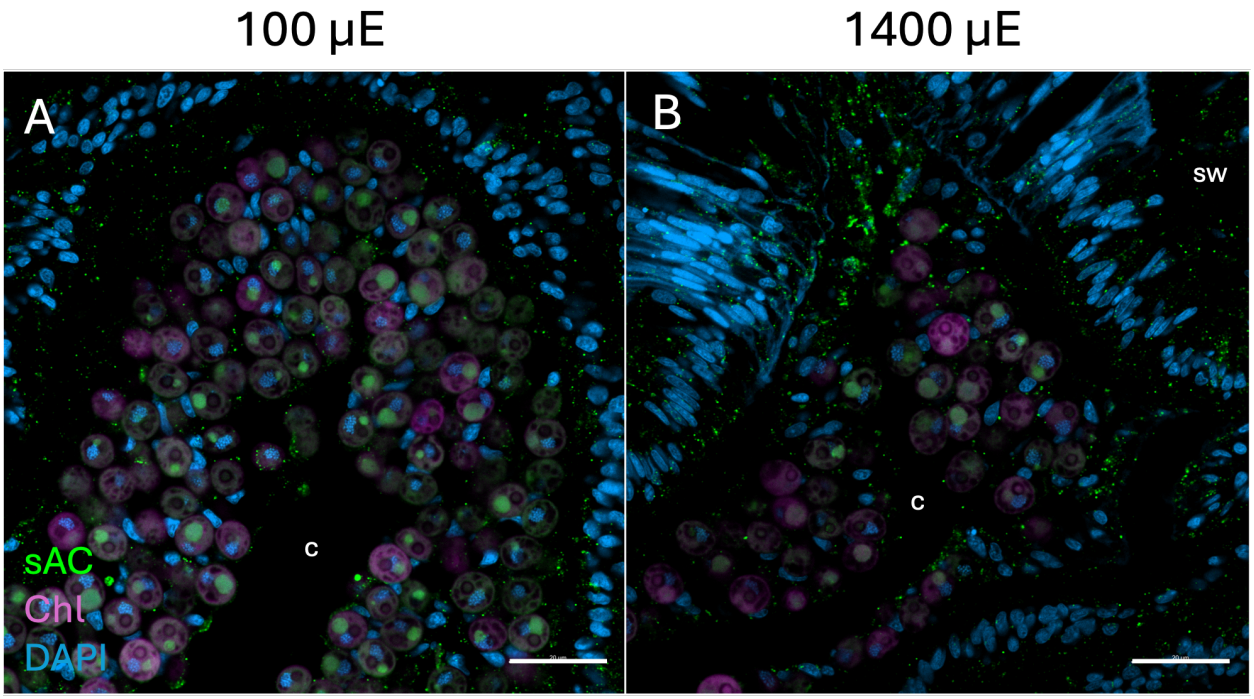


Figure 4.7: sAC localization in the tentacle of *S. pistillata* raised at 100 and 1400 µE. Scale bar is 20 µm. sw – seawater, c – coelenteron.

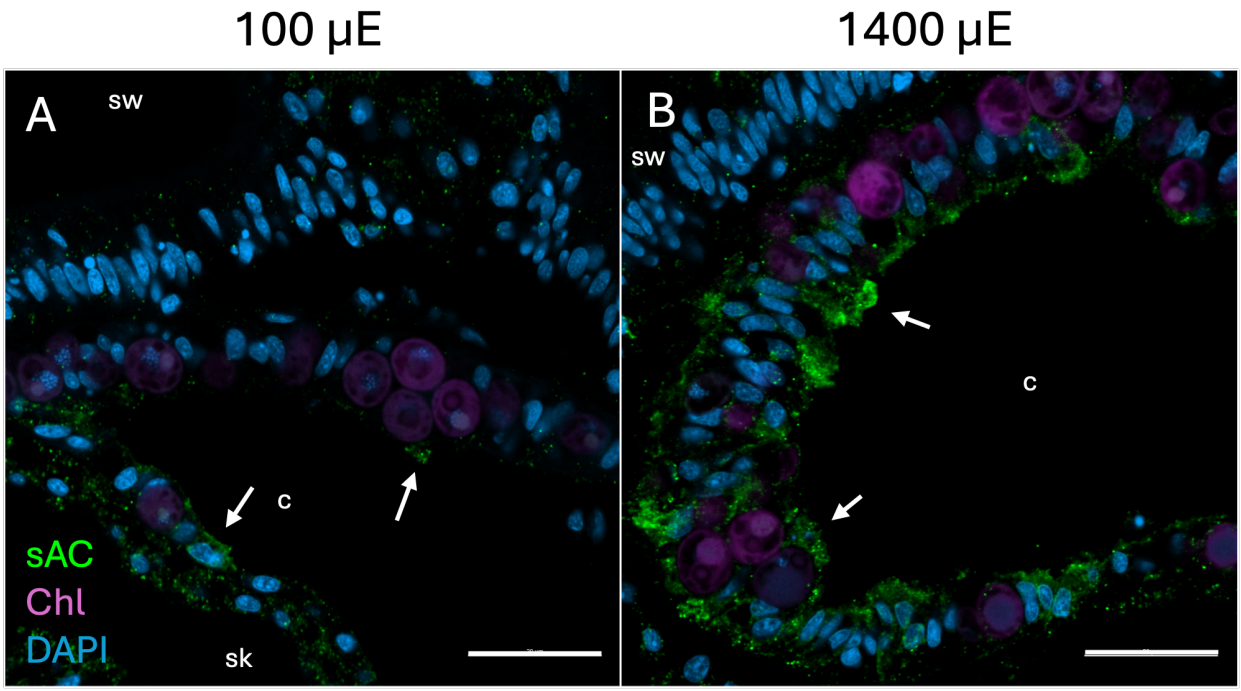


Figure 4.8: sAC localization in symbiocytes of *S. pistillata* raised at 100 and 1400 µE. Scale bar is 20 µm. sw – seawater, sk – skeleton, c – coelenteron. Arrows indicate sAC localization near the apical membrane facing the coelenteron.

Calcifying cells from *S. pistillata* grown at both 100 and 1400 µE displayed strong sAC signal (Figure 4.9) as previously described for *S. pistillata* grown at 170 µE (Barott et al. 2020). Airyscan observation revealed that sAC was present in the cytosol forming microdomains near basolateral membranes and apical membranes/apical pits facing the ECF and skeleton (Figure 4.9C-D). These patterns support sAC's role in mediating the alkalinization of the ECF to promote calcification (Barott et al. 2020). Unlike $VHA_B$, sAC signal was unchanged between the 100 and 1400 µE treatments, possibly explained by sAC's role as a biosensor which does not act directly on cellular biochemistry, but rather effects downstream mechanisms via cAMP production. Given this method of action, sAC expression at 100 µE may already be sufficient to respond to pH disturbances generated by calcification.

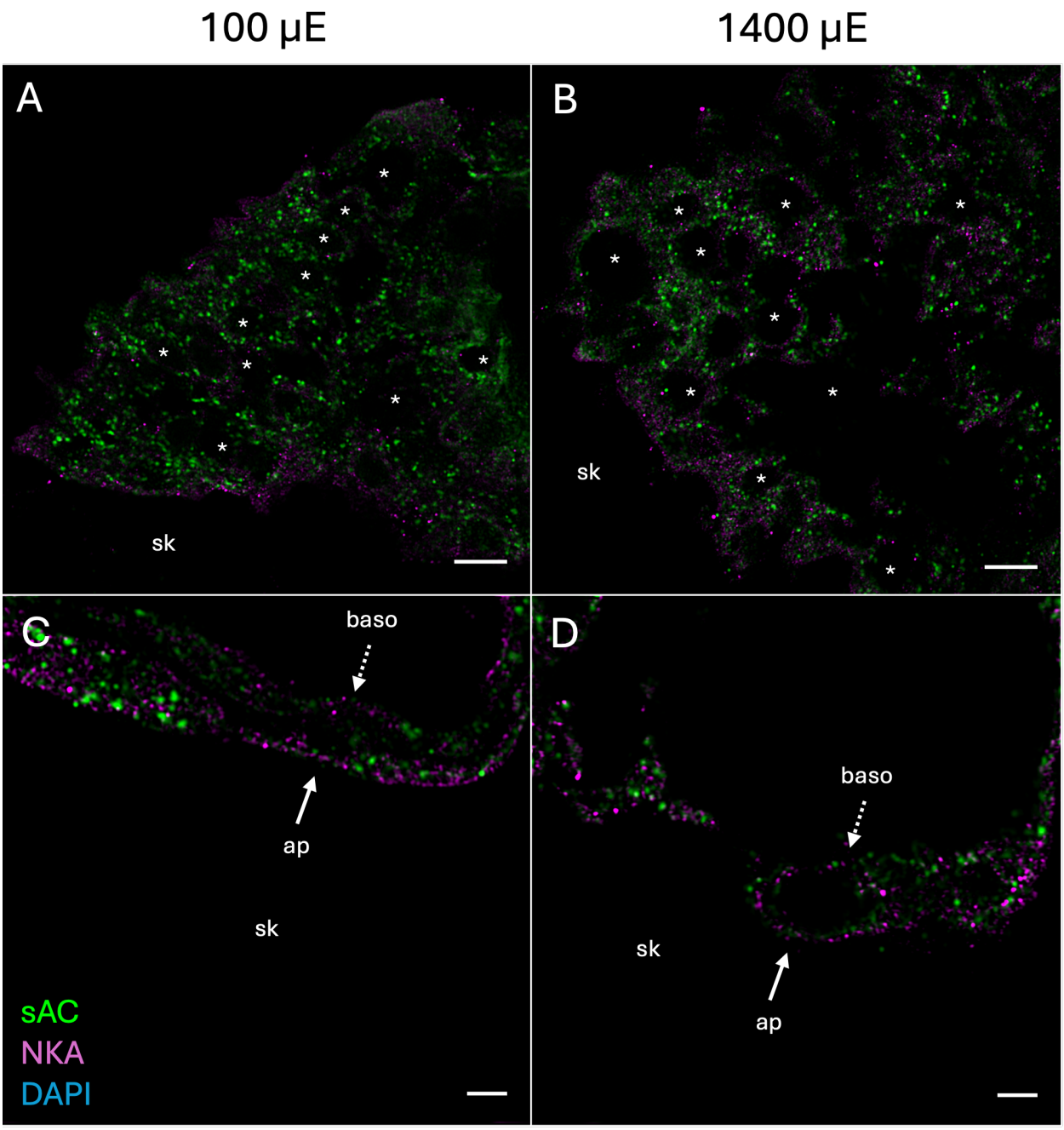


Figure 4.9: sAC localization in two morphologies of calcifying cells of *S. pistillata* raised at 100 and 1400 µE. (A-B) Extensions of calcifying cells with apical pits. (C-D) Single layers of calcifying cells. Scale bar is 5 µm (A-B) and 2 µm (C-D). sk – skeleton, * – apical pits, ap – apical membrane, baso – basolateral membrane.

*VHA Inhibition Stimulates* $P_N$ *in High Light Conditions*

We employed $O_2$ microsensor respirometry to test whether (1) VHA activity promoted symbiont photosynthesis in RAS-raised *S. pistillata* and (2) whether environmental light levels altered VHA's contribution to coral CCMs. We measured $R_D$ and $P_N$ rates from 1 cm branch clippings incubated with either DMSO or DMSO and ConcA, a specific inhibitor of VHA (Figure 4.10). Neither drug nor light treatment altered $R_D$ indicating that metabolic rate was unaffected during the experiment (2-Way ANOVA: Light Level-$R_D$: $F_{1.960, 9.799} = 3.87$, $p = 0.0581$; Drug-$R_D$: $F_{1.000, 5.000} = 0.40$, $p = 0.5520$; Light Level x Drug-$R_D$: $F_{1.824, 9.121} = 1.09$, $p = 0.3686$). Surprisingly, neither drug nor light treatment altered $O_2$ evolution (Light Level-$P_N$: $F_{1.154, 5.768} = 5.259$, $p = 0.0607$; Drug-$P_N$: $F_{1.000, 5.000} = 3.845$, $p = 0.1072$; Light Level x Drug-$P_N$: $F_{1.573, 7.687} = 2.254$, $p = 0.1727$). Subsequent comparisons revealed that rather than decreasing $O_2$ evolution, ConcA treatment in fact stimulated $P_N$ in 1400 μE-acclimated corals by ~1.6-fold ($p = 0.0466$). Corals grown at 100 μE treated with ConcA tended to display the same stimulation (~2.1-fold) but fell short of significance ($p = 0.1132$).

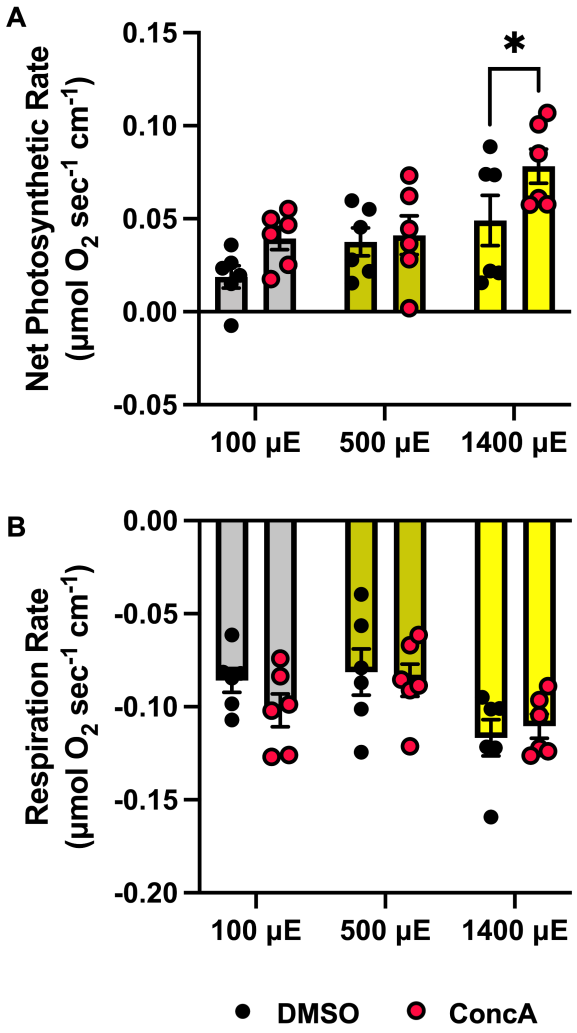


Figure 4.10: Effect of VHA inhibition on $P_N$ and $R_D$ rates of *S. pistillata*. Clippings were incubated in darkness and 100, 500, or 1400 µE light with FSW then either DMSO or ConcA (1 µM). Neither light level nor ConcA treatment altered $R_D$ rates of corals. VHA inhibition increased $P_N$ rate in *S. pistillata* raised at 1400 µE ($p = 0.0466$). n = 6 for all treatments. Data were tested using 2-Way RM ANOVA with the Geisser-Greenhouse correction and Dunnett's multiple comparisons tests.

In conjunction with the relatively low abundance of symbiosomal $VHA_B$ in all observed samples, our respirometry results support the conclusion that RAS-raised *S. pistillata* do not employ VHA-driven CCMs. This result contrasts with previous work showing that VHA inhibition decreased $P_N$ by 30% in *S. pistillata* grown at 170 µE and by ~80% in Acropora yongei grown at150 µE (Barott et al. 2015b). This discrepancy could be explained by potential differences in $pCO_2$, alkalinity, dissolved nutrients and other water chemistry parameters between studies.

Differences in $pCO_2$ are a particularly interesting explanation: elevated environmental $pCO_2$ is hypothesized to fertilize photosynthesis in carbon-limited systems (reviewed in Albright 2018) potentially decreasing the need for CCMs employed by both hosts and free-living symbionts. *S. pistillata's* symbionts are naturally carbon-limited (Roberty et al. 2020) therefore increased $pCO_2$ could have this effect. RAS $pCO_2$ was determined to be 436 ± 75 ppm (Figure 4.11A). This measurement was taken over a weekend (Friday evening-Monday morning) when few people were in Hubbs Hall and is likely lower than weekday averages when human respiration increases building air $pCO_2$ to 700-900 ppm (personal observations); for example, $pCO_2$ on Friday evening reached 548 ppm after the lab was occupied. Unfortunately, comparable data is not available from Barott et al.'s flowthrough aquaria but seasonal $pCO_2$ recordings are available from reef flats in Fall (344 ± 96 ppm), Winter (326 ± 126 ppm), and Spring (374 ± 163 ppm) (Kline et al. 2015). RAS $pCO_2$ is higher than the reef flat in all three seasons and suggests potential relief, or at least lessened carbon-limitation for animals in this study (Figure 4.11B). A caveat to this comparison is that VHA-driven CCMs have not yet been documented in corals on natural reefs.

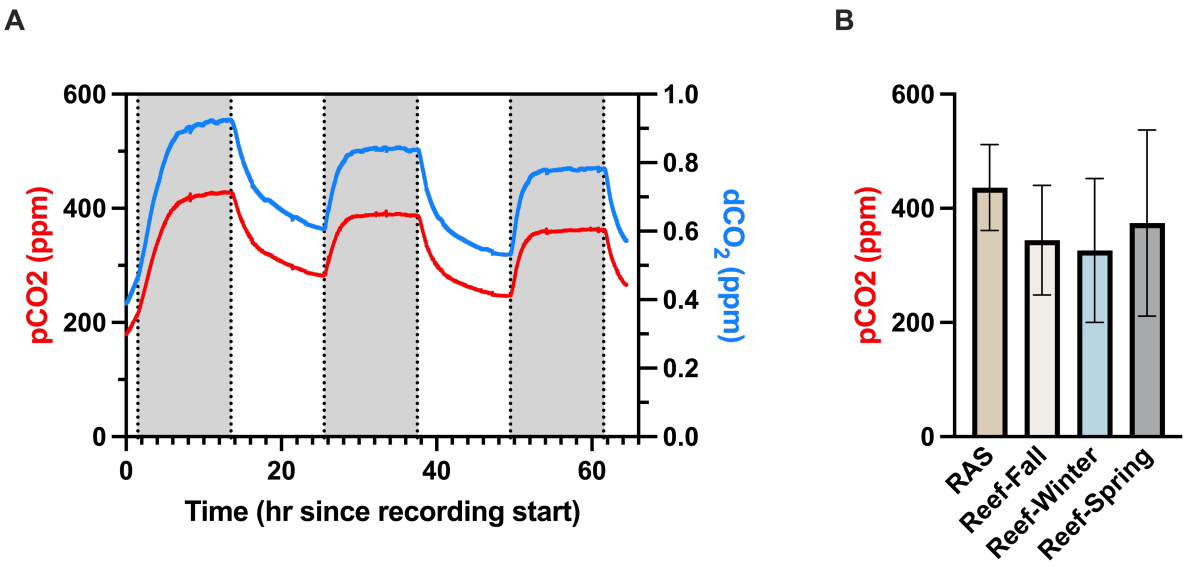


Figure 4.11: RAS $CO_2$ levels. (A) Partial pressure of $CO_2$ ($pCO_2$) and dissolved $CO_2$ ($dCO_2$) over a 65 hour period (5:30 pm May 31 to 10:30 am June 3, 2024). Sampling resolution was at one minute intervals. $pCO_2$ was measured using a Qubit Systems S157 $CO_2$ Analyzer connected to a S400 Rapid $dCO_2$ Sampling System. $dCO_2$ was calculated according to Henry's Law. (B) Comparison of RAS $pCO_2$ levels to conditions on a reef flat in three seasons (Kline et al. 2015).

*VHA May Support Calcification*

Our findings indicate that RAS-grown *S. pistillata* employ VHA in net-$O_2$ consuming processes under illumination. Several lines of evidence suggest that this mechanism is related to supporting pH regulation in the calcifying cells and the ECF, in particular under high light irradiance. First, $VHA_B$ was present in calcifying cells at all light treatments and it appeared to increase in the high light treatment. Interestingly, $VHA_B$ expression increased with light treatment in a non-linear manner (log curve) mirroring the behavior of LEC rates in multiple coral species (Mallon et al. 2022). Second, while coral calcification occurs in both light and darkness, VHA inhibition only decreased $P_N$ under high light illumination and had no impact on dark $O_2$ consumption ($R_D$) pointing to involvement in a light-related process. This activation in high light conditions could be triggered by sAC/cAMP signaling and PKA-dependent phosphorylation in response to changes in pHi/intracellular bicarbonate levels (Alzamora et al. 2010). Third, VHA has been hypothesized to play a role in calcifying cell pHi regulation: basolateral VHA could

export $H^+$ generated during biomineralization into the mesoglea and aboral gastroderm (Zoccola et al. unpublished results, as in Allemand et al. 2004). Finally, VHA regulates foraminifera pHi to support calcification in this manner (Toyofuku et al. 2017) and recent work demonstrated that VHA contributes to pHi regulation in sea urchin calcifying cells via $H^+$ sequestration in vesicles (Hu et al. 2020). Thus, VHA may play similar roles in coral calcifying cells.

$VHA_B$ localized to three distinct subcellular compartments in calcifying cells suggesting unique mechanistic roles: (1) intracellular vesicles, (2) the basolateral membrane, and (3) the apical membrane facing the ECF and the skeleton. In vesicles, VHA likely maintains pHi by concentrating $H^+$ generated by biomineralization to favor continued mineral precipitation, a homologous role to that of sea urchins (Hu et al. 2020) (Figure 4.12). Acidic vesicles would be trafficked to the basolateral membrane where membrane fusion leads to exocytosis of their cargo. Vesicle fusion could explain VHA's presence on the basolateral membrane; alternatively, a permanent population of basolateral VHA could exist to maintain pHi in the manner proposed by (Allemand et al. 2004). Initially, VHA's presence on the apical membrane of calcifying cells appears paradoxical: how does acidifying the ECF, a compartment that must be alkaline (pH 8-9; Venn et al. 2011) promote biomineralization? Coccolithophores present a similarly confusing situation where VHA localizes to high pH calcifying vesicles (Corstjens et al. 2001). The explanation may lie with the larvae of lepidopteran insects which employ VHA in goblet cells to alkalinize their midgut to pH 10-12 (reviewed in Onken and Moffett 2017). Briefly, VHA pumping in apical pits charges the membrane to above +200 mV energizing $K^+/2H^+$ antiport and resulting in net alkalinization. Concurrent excretion of $HCO_3^-$ results in $CO_3^{2-}$ production and formation of $K_2CO_3$ mineral. A conserved role may be present in coral calcifying cells to maintain high ECF pH. Notably, coral biomineralization is believed to occur intracellularly with gradual production

of amorphous calcium carbonate in calcifying vesicles; vesicles later fuse with the apical membrane and deposit their cargo into the ECF (Hayes and Goreau 1977; Mass et al. 2017). With this model in mind, VHA's vesicular localization could be interpreted as driving alkalinization of calcifying vesicles rather than, or in addition to, pHi regulation of calcifying cells. Future experiments are required to elucidate VHA's contributions to these mechanisms: first, determination of calcifying cell cytosol, vesicles, and ECF pH under VHA inhibition. This can be accomplished by SNARF-1 imaging of living *S. pistillata* microcolonies grown on glass coverslips. Second, measurement of calcification rates under VHA inhibition. Live-imaging of intracellular ACC formation and skeletal deposition under microcolonies incubated with calcein could achieve this goal.

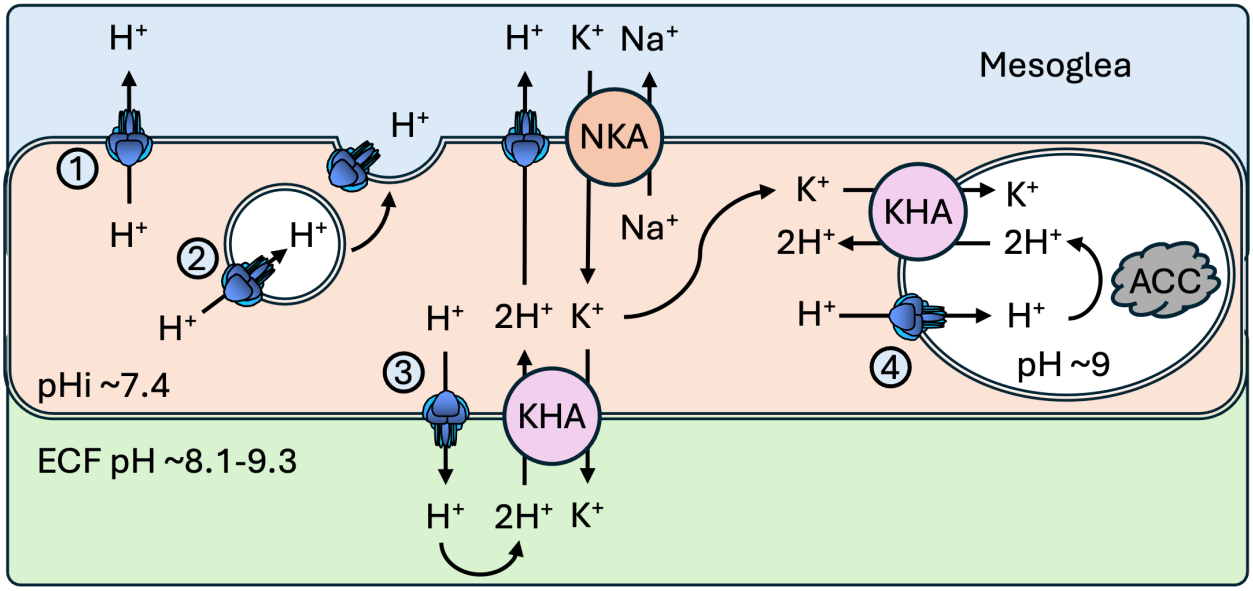


Figure 4.12: Proposed model for VHA-driven pHi and ECF pH regulation in calcifying cells. (1) Basolateral VHA pumps $H^+$ into the mesoglea as proposed by Zoccola et al. unpublished results, as in Allemand et al. 2004. (2) VHA concentrates cytosolic $H^+$ in vesicles for transport to and fusion with the basolateral membrane. (3) Apical VHA energizes $K^+/2H^+$ antiport resulting in net alkalinization of the ECF (as in the midgut of lepidopteran insects). (4) Vesicular VHA energizes $K^+/2H^+$ antiport resulting in net alkalinization of ACC-forming vesicles. Blue icons, VHA. KHA, unidentified $K^+/2H^+$ antiporter. NKA, $Na^+/K^+$-ATPase.

**Acknowledgements**

We thank Ryan Myers, Charles Trautner, Elisa Prohroff, Victoria Vasquez, Bryan Delgado, and Maitri Paul for their help maintaining *S. pistillata* aquaria. This work was partially supported by National Science Foundation Graduate Research (GRFP 2019271478) and Achievement Rewards for College Scientists Fellowships to A.B.T.

Chapter IV is currently being prepared for submission for publication of the material. Thies AB and Tresguerres M (*in prep*). Effects of light on the expression, localization, and function of V-type $H^+$-ATPase in *Stylophora pistillata*. The dissertation author was the primary investigator and author of this material.

## Appendix

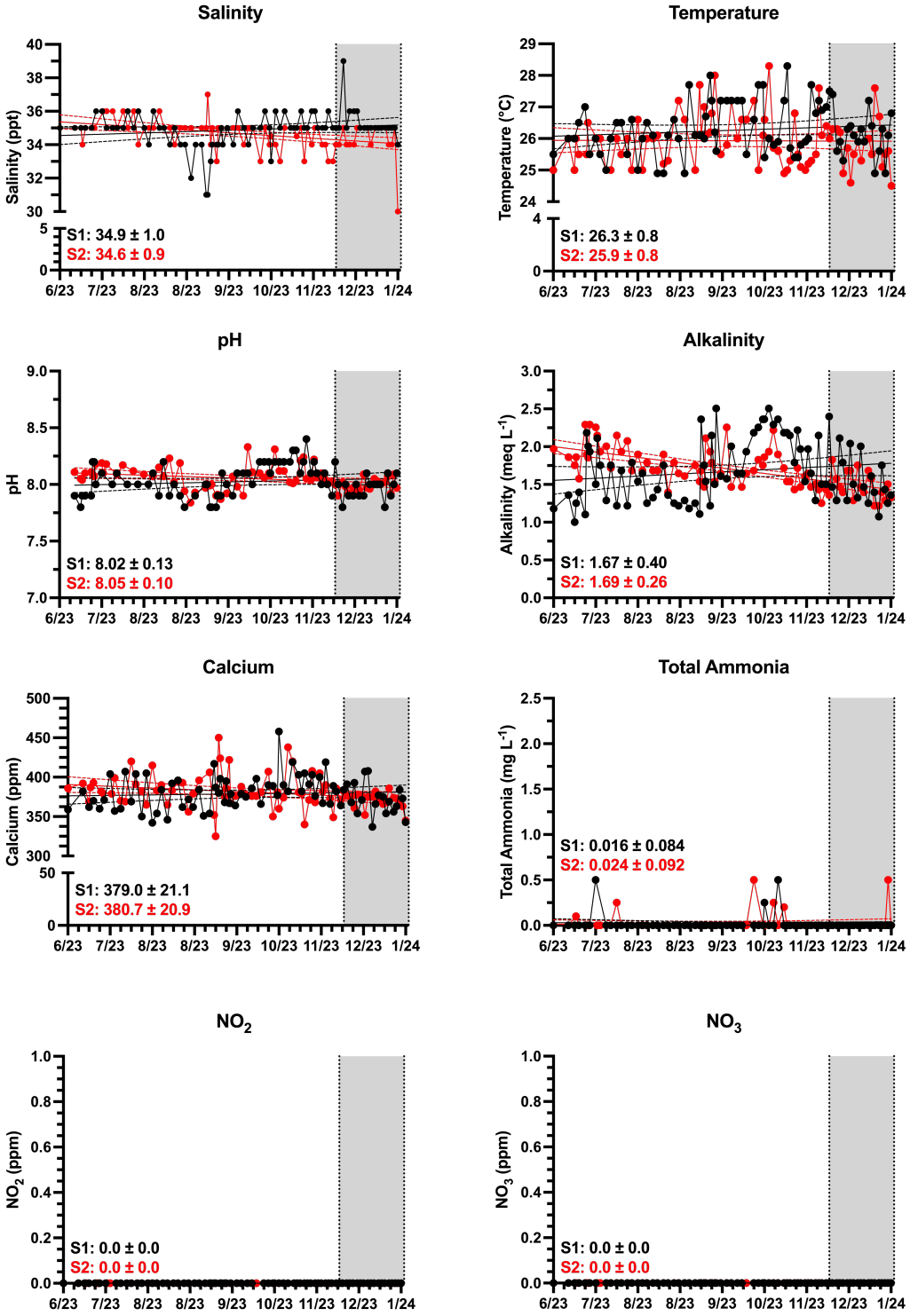


Supplemental Figure 4.1:RAS chemistry during acclimation and experimental period. *S. pistillata* were acclimated to light regimes for six months prior to experimentation. Samples for ICM and WB were collected on 12/6/2023 and respirometry experiments were conducted during the following four weeks (shaded dates, 12/6/2023-1/18/2024).

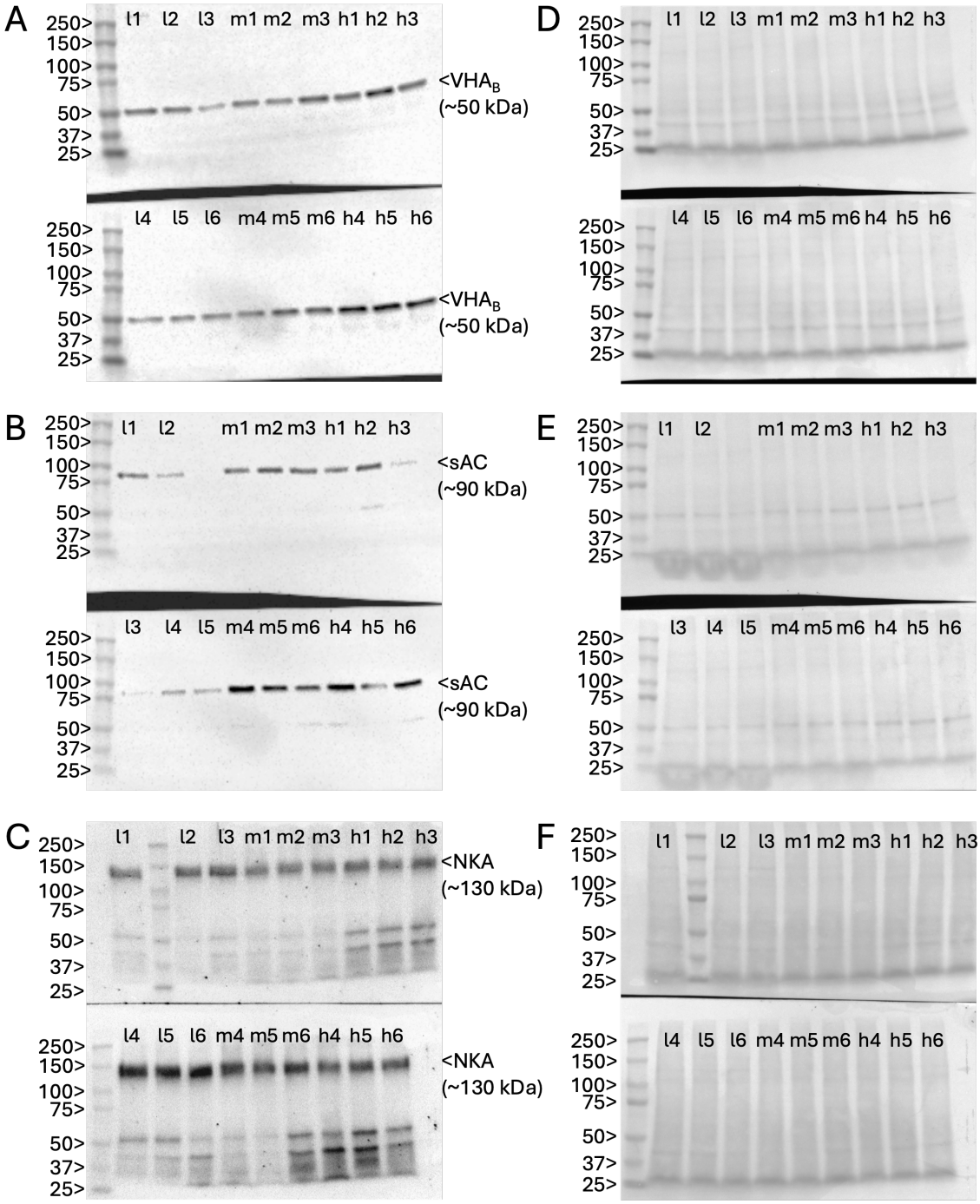


Supplemental Figure 4.2: $VHA_B$, sAC, and NKA protein abundance in *S. pistillata* raised at 100 (lanes l1-6), 500 (lanes m1-6), and 1400 µE (lanes h1-6). (a-c) Protein abundance was quantified by Western blotting with custom polyclonal anti-$VHA_B$ and anti-sAC antibodies and commercial monoclonal NKA antibody. (A-C) Western blots of replicate colonies probed for $VHA_B$, sAC, and NKA respectively. (D-F) Ponceau stained blots were used to standardize protein expression data by total protein loaded per lane for each corresponding blot. Blots labeled for $VHA_B$ were gently stripped and reprobed for sAC; faint bands at ~50 kDa remain from previous labeling however no 90 kDa band is present on the $VHA_B$-labeled blots confirming antibody specificity.

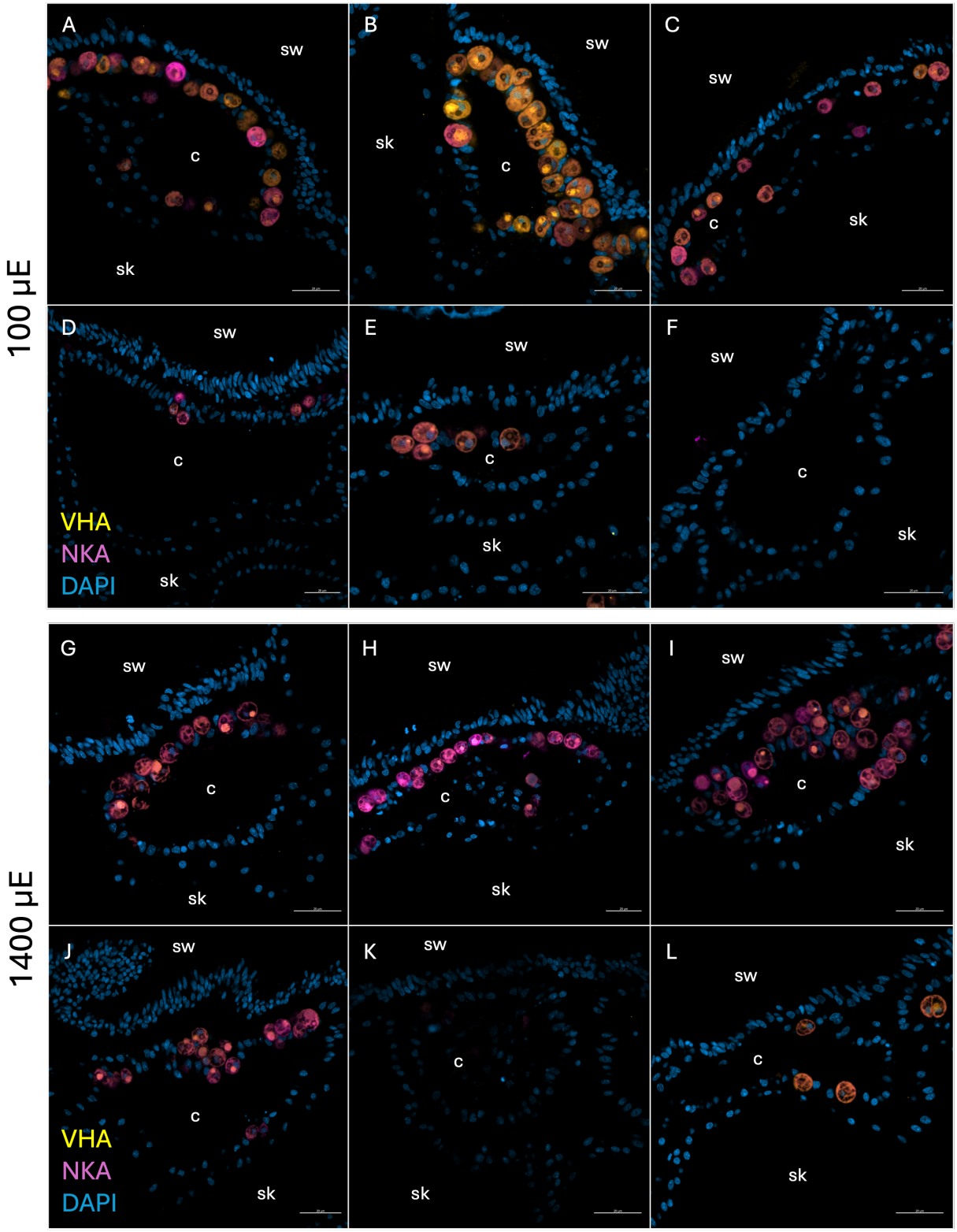


Supplemental Figure 4.3: Secondary antibody negative controls for ICM localization of both $VHA_B$ and NKA in *S. pistillata* tissue sections. Colonies were grown at 100 (A-F) and 1400 µE (G-L) for three months. Scale bar is 20 µm. sw – seawater, sk – skeleton, c – coelenteron.

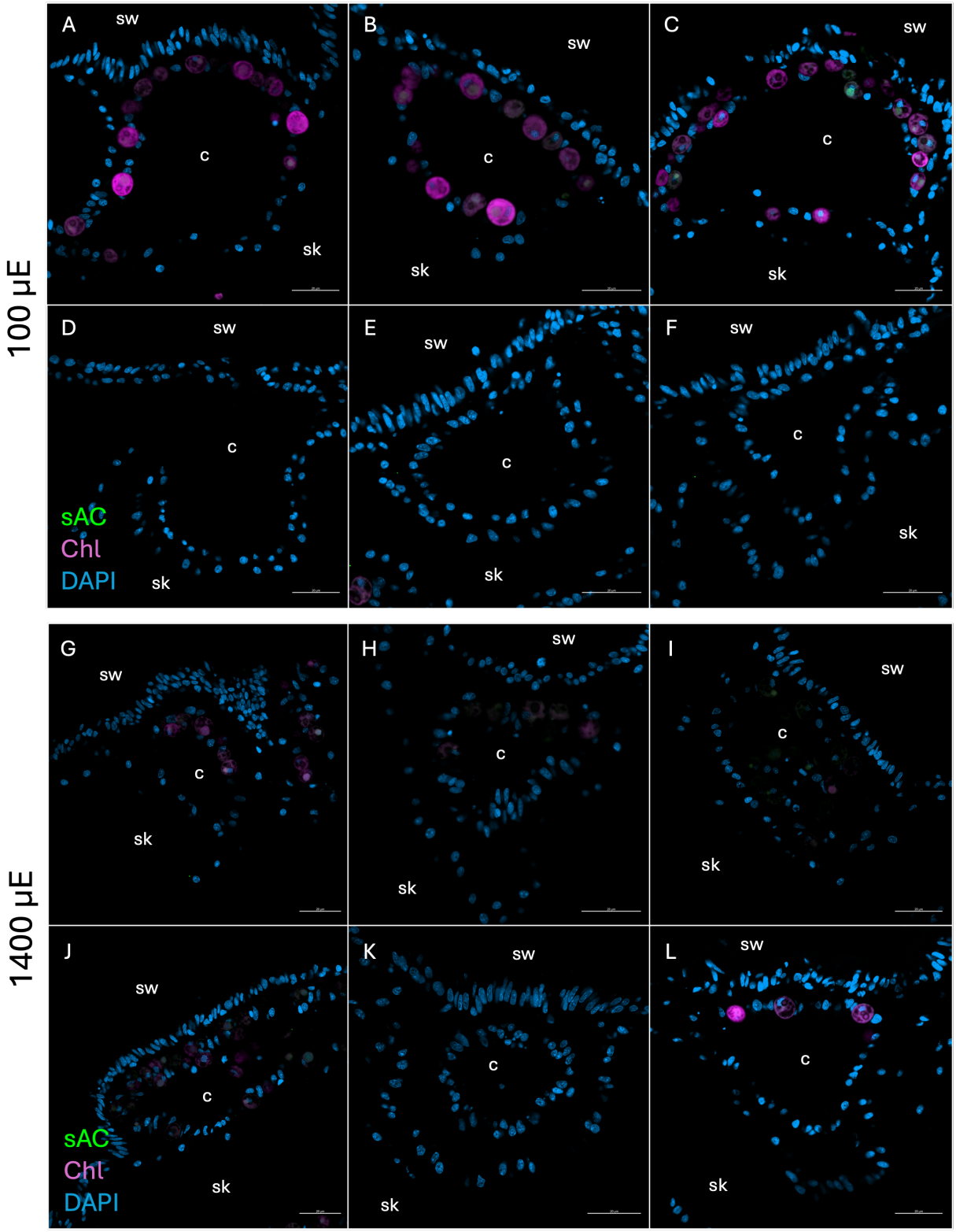


Supplemental Figure 4.4: Secondary antibody negative controls for ICM localization of sAC in *S. pistillata* tissue sections. Colonies were grown at 100 (A-F) and 1400 µE (G-L) for three months. Scale bar is 20 µm. sw – seawater, sk – skeleton, c – coelenteron.

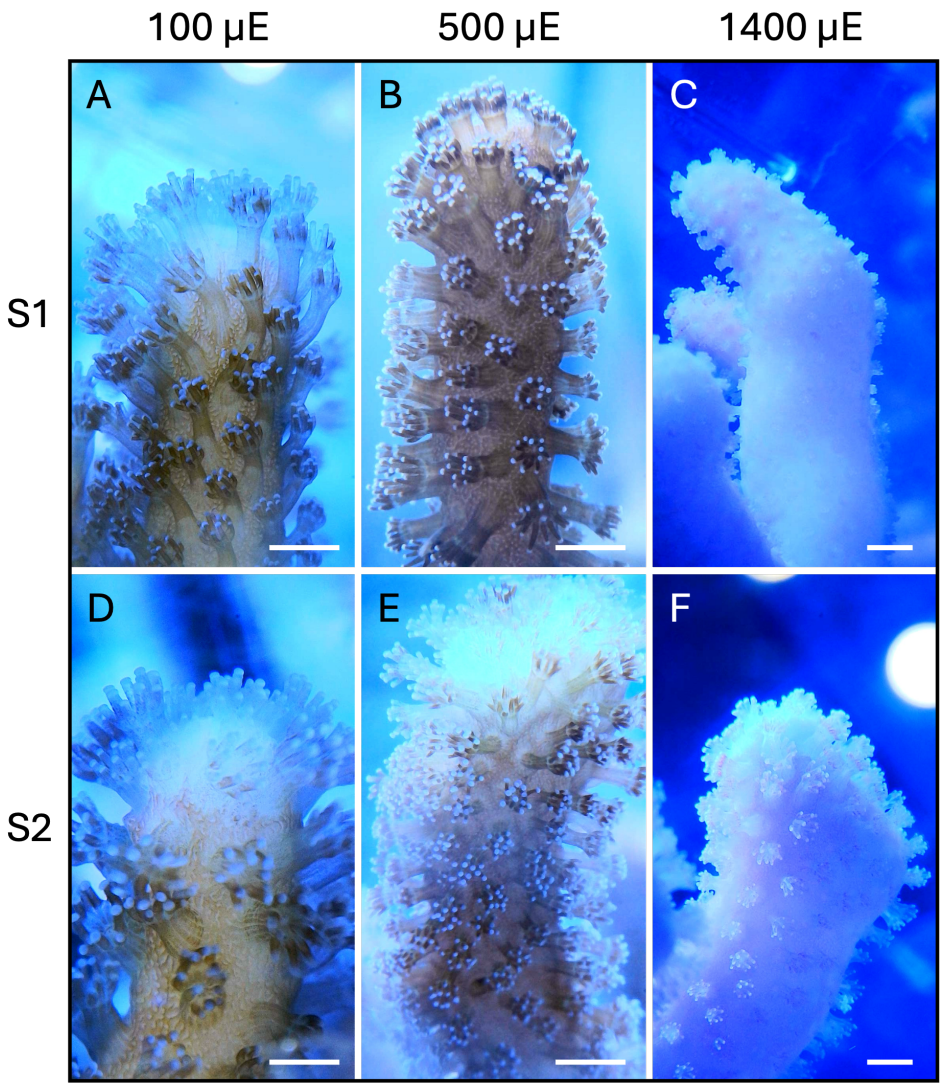


Supplemental Figure 4.5: RAS-raised *S. pistillata* from 100, 500, and 1400 µE treatments. Sump 1 (S1), sump 2 (S2). Scale bar is 5 mm.

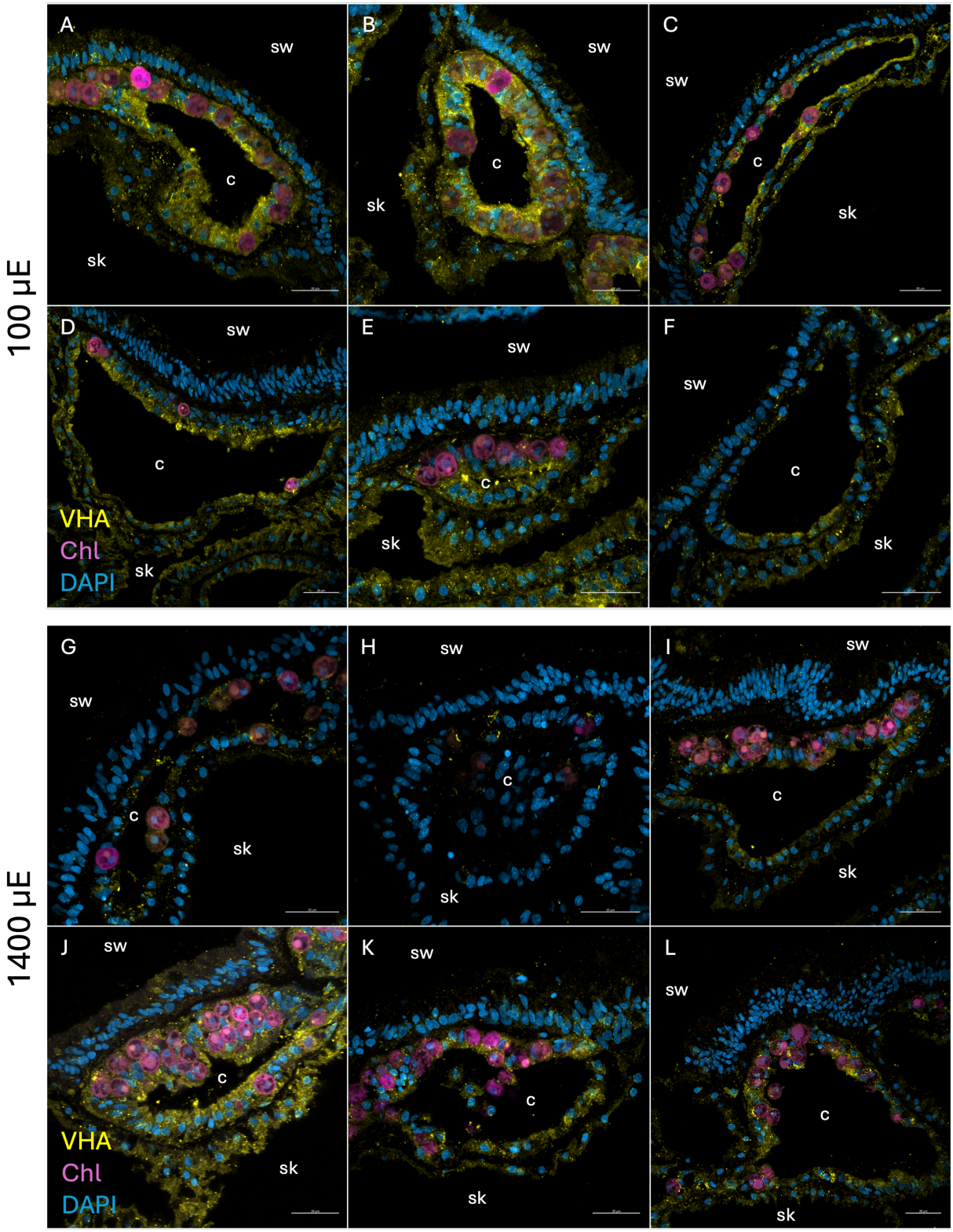


Supplemental Figure 4.6: ICM localization of $VHA_B$ in *S. pistillata* tissue sections. Colonies were grown at 100 (A-F) and 1400 µE (G-L) for three months. Scale bar is 20 µm. sw – seawater, sk – skeleton, c – coelenteron.

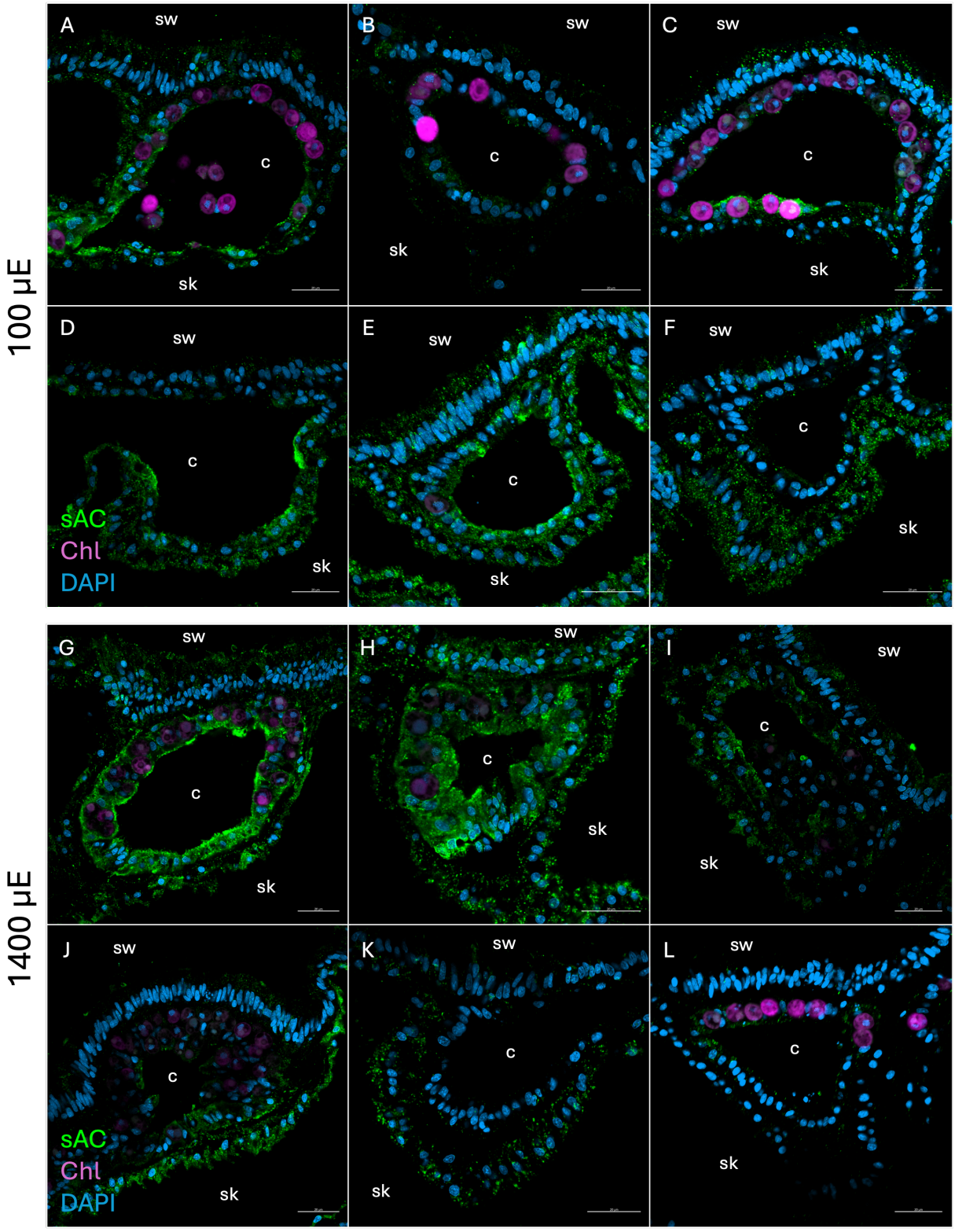


Supplemental Figure 4.7: ICM localization of sAC in *S. pistillata* tissue sections. Colonies were grown at 100 (A-F) and 1400 µE (G-L) for three months. Scale bar is 20 µm. sw – seawater, sk – skeleton, c – coelenteron.

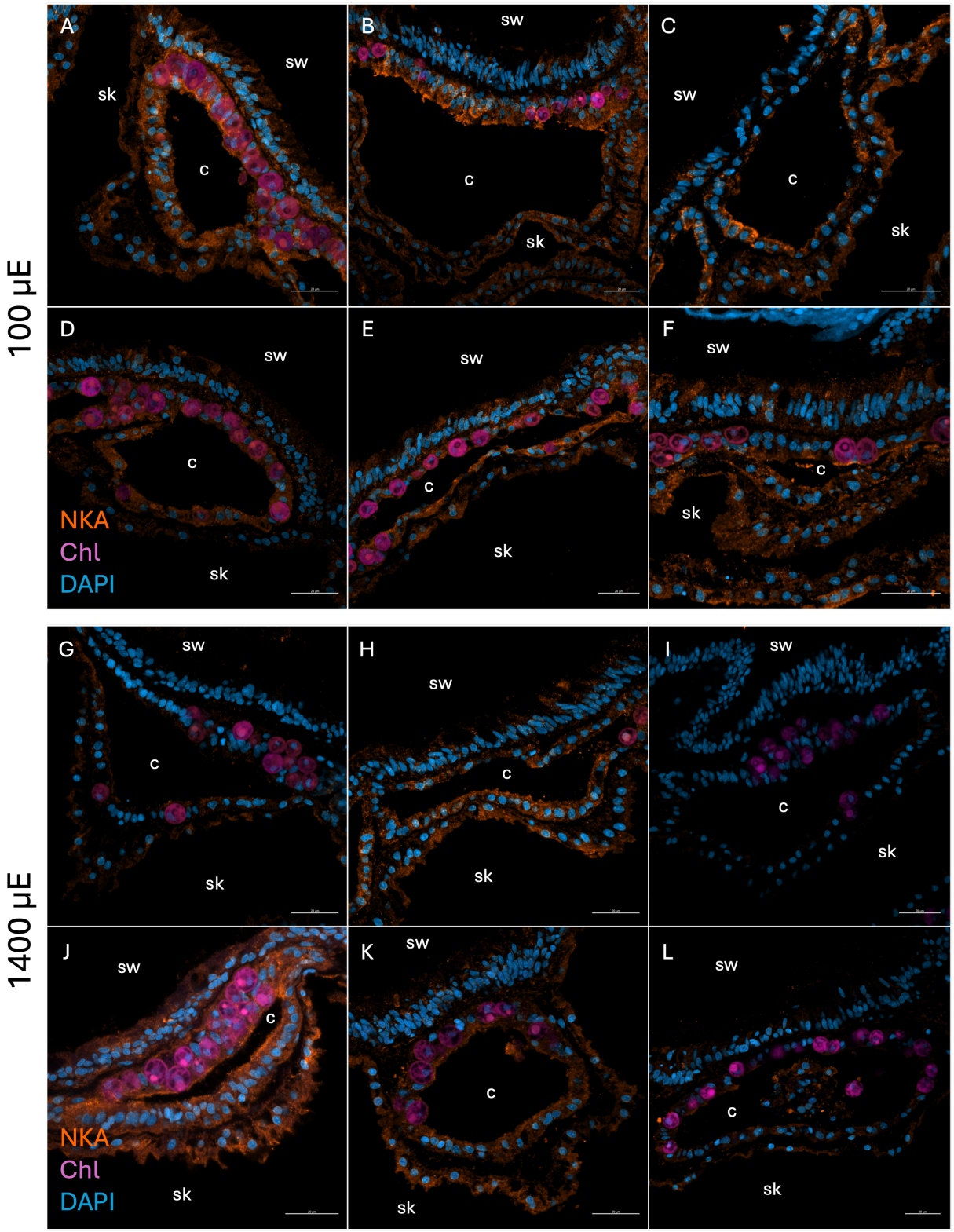


Supplemental Figure 4.8: ICM localization of NKA in *S. pistillata* tissue sections. Colonies were grown at 100 (A-F) and 1400 µE (G-L) for three months. Scale bar is 20 µm. sw – seawater, sk – skeleton, c – coelenteron.

**References**

Agostini S, Suzuki Y, Higuchi T, et al (2012) Biological and chemical characteristics of the coral gastric cavity. Coral Reefs 31:147–156. https://doi.org/10.1007/s00338-011-0831-6

Albright R (2018) Ocean Acidification and Coral Bleaching. In: Coral Bleaching: Patterns, Processes, Causes and Consequences. Springer International Publishing, pp 295–323

Al-Horani FA, Al-Moghrabi SM, de Beer D (2003) The mechanism of calcification and its relation to photosynthesis and respiration in the scleractinian coral Galaxea fascicularis. Marine Biology 142:419–426. https://doi.org/10.1007/s00227-002-0981-8

Allemand D, Ferrier-Pagès C, Furla P, et al (2004) Biomineralisation in reef-building corals: From molecular mechanisms to environmental control. Comptes Rendus - Palevol 3:453–467. https://doi.org/10.1016/j.crpv.2004.07.011

Allemand D, Tambutté É, Zoccola D, Tambutté S (2011) Coral Calcification, Cells to Reefs. In: Dubinsky Z, Stambler N (eds) Coral Reefs: An Ecosystem in Transition. Springer Netherlands, Dordrecht, pp 119–150

Alzamora R, Thali RF, Gong F, et al (2010) PKA regulates vacuolar H+-ATPase localization and activity via direct phosphorylation of the A subunit in kidney cells. Journal of Biological Chemistry 285:24676–24685. https://doi.org/10.1074/jbc.M110.106278

Anthony KRN, Hoegh-Guldberg O (2003a) Kinetics of photoacclimation in corals. Oecologia 134:23–31. https://doi.org/10.1007/s00442-002-1095-1

Anthony KRN, Hoegh-Guldberg O (2003b) Variation in coral photosynthesis, respiration and growth characteristics in contrasting light microhabitats: an analogue to plants in forest gaps and understoreys? Functional Ecology 17:246–259. https://doi.org/10.1046/j.1365-2435.2003.00731.x

Armstrong EJ, Roa JN, Stillman JH, Tresguerres M (2018) Symbiont photosynthesis in giant clams is promoted by V-type H + -ATPase from host cells. Journal of Experimental Biology. https://doi.org/10.1242/jeb.177220

Barott K, Tresguerres M (2015) Immunolocalization of proteins in corals: the V-type H+-ATPase proton pump. bio-protocol 5:1–10

Barott KL, Barron ME, Tresguerres M (2017) Identification of a molecular pH sensor in coral. Proceedings of the Royal Society B 284:20171769. https://doi.org/10.1098/rspb.2017.1769

Barott KL, Helman Y, Haramaty L, et al (2013) High adenylyl cyclase activity and in vivo cAMP fluctuations in corals suggest central physiological role. Scientific Reports 3:. https://doi.org/10.1038/srep01379

Barott KL, Perez SO, Linsmayer LB, Tresguerres M (2015a) Differential localization of ion transporters suggest distinct cellular mechanisms for calcification and photosynthesis

between two coral species. Am J Physiol Regul Integr Comp Physiol 13:170–184. https://doi.org/10.1121/1.4929899

Barott KL, Thies AB, Tresguerres M (2022) V-type H + -ATPase in the symbiosome membrane is a conserved mechanism for host control of photosynthesis in anthozoan photosymbioses. Royal Society Open Science 9:. https://doi.org/10.1098/rsos.211449

Barott KL, Venn AA, Perez SO, et al (2015b) Coral host cells acidify symbiotic algal microenvironment to promote photosynthesis. Proceedings of the National Academy of Sciences of the United States of America 112:607–612. https://doi.org/10.1073/pnas.1413483112

Barott KL, Venn AA, Thies AB, et al (2020) Regulation of coral calcification by the acid-base sensing enzyme soluble adenylyl cyclase. Biochemical and Biophysical Research Communications 525:576–580. https://doi.org/10.1016/j.bbrc.2020.02.115

Barron ME, Thies AB, Espinoza JA, et al (2018) A vesicular Na+/Ca2+ exchanger in coral calcifying cells. Plos One 13:e0205367. https://doi.org/10.1371/journal.pone.0205367

Beniash E, Aizenberg J, Addadi L, Weiner S (1997) Amorphous calcium carbonate transforms into calcite during sea urchin larval spicule growth. Proc R Soc Lond B 264:461–465. https://doi.org/10.1098/rspb.1997.0066

Chang WW, Thies AB, Tresguerres M, Hu MY-A (2023) Soluble adenylyl cyclase coordinates intracellular pH homeostasis and biomineralization in calcifying cells of a marine animal. American Journal of Physiology-Cell Physiology 324:C777–C786. https://doi.org/10.1152/ajpcell.00524.2022

Colombo-Pallotta MF, Rodríguez-Román A, Iglesias-Prieto R (2010) Calcification in bleached and unbleached Montastraea faveolata: evaluating the role of oxygen and glycerol. Coral Reefs 29:899–907. https://doi.org/10.1007/s00338-010-0638-x

Corstjens PLAM, Araki Y, González EL (2001) A coccolithophorid calcifying vesicle with a vacuolar-type ATPase proton pump: cloning and immunolocalization of the $V_0$ subunit *c*. Journal of Phycology 37:71–78. https://doi.org/10.1046/j.1529-8817.1999.014012071.x

Crovetto L, Venn AA, Sevilgen DS, et al (2024) Spatial variability of and effect of light on the coelenteron pH of a reef coral. Communications Biology 7:. https://doi.org/10.1038/s42003-024-05938-8

Damsgaard C, Lauridsen H, Harter TS, et al (2020) A novel acidification mechanism for greatly enhanced oxygen supply to the fish retina. eLife 9:1–20. https://doi.org/10.7554/eLife.58995

Falkowski PG, Chen Y-B (2003) Photoacclimation of Light Harvesting Systems in Eukaryotic Algae. In: Green BR, Parson WW (eds) Light-Harvesting Antennas in Photosynthesis. Springer Netherlands, Dordrecht, pp 423–447

Furla P, Galgani I, Durand I, Allemand D (2000) Sources and mechanisms of inorganic carbon transport for coral calcification and photosynthesis. The Journal of experimental biology 203:3445–3457

Ganot P, Tambutté E, Caminiti-Segonds N, et al (2020) Ubiquitous macropinocytosis in anthozoans. eLife 9:1–25. https://doi.org/10.7554/elife.50022

Goreau TF, Goreau NI (1959) The physiology of skeleton formation in corals. II. Calcium deposition by hermatypic corals under various conditions in the reef. The Biological Bulletin 117:239–250. https://doi.org/10.2307/1538903

Hayes RL, Goreau NI (1977) Intracellular crystal-bearing vesicles in the epidermis of scleractinian corals, *Astrangia danae* (Agassiz) and *Porites porites* (Pallas). The Biological Bulletin 152:26–40. https://doi.org/10.2307/1540724

Hu MY, Petersen I, Chang WW, et al (2020) Cellular bicarbonate accumulation and vesicular proton transport promote calcification in the sea urchin larva. Proc R Soc B

Hu Y-B, Dammer EB, Ren R-J, Wang G (2015) The endosomal-lysosomal system: from acidification and cargo sorting to neurodegeneration. Translational Neurodegeneration 4:18. https://doi.org/10.1186/s40035-015-0041-1

Kline DI, Teneva L, Hauri C, et al (2015) Six month in situ high-resolution carbonate chemistry and temperature study on a coral reef flat reveals asynchronous pH and temperature anomalies. PLoS ONE 10:1–26. https://doi.org/10.1371/journal.pone.0127648

Kwan GT, Smith TR, Tresguerres M (2020) Immunological characterization of two types of ionocytes in the inner ear epithelium of Pacific Chub Mackerel (Scomber japonicus). Journal of Comparative Physiology B - Biochemical Systemic and Environmental Physiology. https://doi.org/10.1007/s00360-020-01276-3

Langdon C, Atkinson MJ (2005) Effect of elevated pCO $_2$ on photosynthesis and calcification of corals and interactions with seasonal change in temperature/irradiance and nutrient enrichment. J Geophys Res 110:2004JC002576. https://doi.org/10.1029/2004JC002576

Laurent J, Tambutte S, Tambutte E, et al (2013) The influence of photosynthesis on host intracellular pH in scleractinian corals. Journal of Experimental Biology 216:1398–1404. https://doi.org/10.1242/jeb.082081

Leggat W, Marendy EM, Baillie B, et al (2002) Dinoflagellate symbioses: strategies and adaptations for the acquisition and fixation of inorganic carbon. Functional Plant Biology 29:309. https://doi.org/10.1071/pp01202

Lesser MP (1996a) Elevated temperatures and ultraviolet radiation cause oxidative stress and inhibit photosynthesis in ymbiotic dinoflagellates. Limnology and Oceanography 41:271–283. https://doi.org/10.4319/lo.1996.41.2.0271

Lesser MP (2006) Oxidative stress in marine environments: Biochemistry and physiological ecology. Annual Review of Physiology 68:253–278. https://doi.org/10.1146/annurev.physiol.68.040104.110001

Lesser MP (2011) Coral Bleaching: Causes and Mechanisms. In: Dubinsky Z, Stambler N (eds) Coral Reefs: An Ecosystem in Transition. Springer Netherlands, Dordrecht, pp 405–419

Lesser MP (1996b) Elevated temperatures and ultraviolet radiation cause oxidative stress and inhibit photosynthesis in ymbiotic dinoflagellates. Limnology and Oceanography 41:271–283. https://doi.org/10.4319/lo.1996.41.2.0271

Lesser MP, Slattery M, Stat M, et al (2010) Photoacclimatization by the coral Montastraea cavernosa in the mesophotic zone: light, food, and genetics. Ecology 91:990–1003. https://doi.org/10.1890/09-0313.1

Mallon J, Cyronak T, Hall ER, et al (2022) Light-driven dynamics between calcification and production in functionally diverse coral reef calcifiers. Limnology & Oceanography 67:434–449. https://doi.org/10.1002/lno.12002

Mass T, Einbinder S, Brokovich E, et al (2007) Photoacclimation of Stylophora pistillata to light extremes: metabolism and calcification. Mar Ecol Prog Ser 334:93–102. https://doi.org/10.3354/meps334093

Mass T, Giuffre AJ, Sun C-Y, et al (2017) Amorphous calcium carbonate particles form coral skeletons. Proceedings of the National Academy of Sciences 114:201707890. https://doi.org/10.1073/pnas.1707890114

Murata N, Takahashi S, Nishiyama Y, Allakhverdiev SI (2007) Photoinhibition of photosystem II under environmental stress. Biochimica et Biophysica Acta (BBA) - Bioenergetics 1767:414–421. https://doi.org/10.1016/j.bbabio.2006.11.019

Muscatine L, Falkowski PG, Porter JW, Dubinsky Z (1984) Fate of photosynthetic fixed carbon in light- and shade-adapted colonies of the symbiotic coral Stylophora pistillata. Proceedings of the Royal Society of London Series B Biological Sciences 222:181–202. https://doi.org/10.1098/rspb.1984.0058

Onken H, Moffett DF (2017) Acid–Base Loops in Insect Larvae with Extremely Alkaline Midgut Regions. In: Weihrauch D, O'Donnell M (eds) Acid-Base Balance and Nitrogen Excretion in Invertebrates: Mechanisms and Strategies in Various Invertebrate Groups with Considerations of Challenges Caused by Ocean Acidification. Springer International Publishing, Cham, pp 239–260

Roa JN, Tresguerres M (2016) Soluble adenylyl cyclase is an acid-base sensor in epithelial base-secreting cells. American Journal of Physiology - Cell Physiology 311:C340–C349. https://doi.org/10.1152/ajpcell.00089.2016

Roberty S, Béraud E, Grover R, Ferrier-Pagès C (2020) Coral productivity is co-limited by bicarbonate and ammonium availability. Microorganisms 8:. https://doi.org/10.3390/microorganisms8050640

Rohwer F, Seguritan V, Azam F, Knowlton N (2002) Diversity and distribution of coral-associated bacteria. Marine Ecology Progress Series 243:1–10. https://doi.org/10.3354/meps243001

Shnit-Orland M, Kushmaro A (2009) Coral mucus-associated bacteria: a possible first line of defense: Coral mucus-associated bacteria. FEMS Microbiology Ecology 67:371–380. https://doi.org/10.1111/j.1574-6941.2008.00644.x

Siboni N, Ben-Dov E, Sivan A, Kushmaro A (2008) Global distribution and diversity of coral-associated Archaea and their possible role in the coral holobiont nitrogen cycle. Environmental Microbiology 10:2979–2990. https://doi.org/10.1111/j.1462-2920.2008.01718.x

Stramski D, Dera J (1988) On the mechanism for producing flashing light under a wind-disturbed water surface. Oceanologica 25:

Suzuki T, Casareto BE, Yucharoen M, et al (2024) Coexistence of nonfluorescent chromoproteins and fluorescent proteins in massive Porites spp. corals manifesting a pink pigmentation response. Frontiers in Physiology. https://doi.org/10.3389/fphys.2024.1339907

Tambutté S, Holcomb M, Ferrier-Pagès C, et al (2011) Coral biomineralization: From the gene to the environment. Journal of Experimental Marine Biology and Ecology 408:58–78. https://doi.org/10.1016/j.jembe.2011.07.026

Tanaka Y, Suzuki A, Sakai K (2018) The stoichiometry of coral-dinoflagellate symbiosis: carbon and nitrogen cycles are balanced in the recycling and double translocation system. ISME Journal 12:860–868. https://doi.org/10.1038/s41396-017-0019-3

Thies AB, Quijada-Rodriguez AR, Zhouyao H, et al (2022) A Rhesus channel in the coral symbiosome membrane suggests a novel mechanism to regulate NH3 and CO2 delivery to algal symbionts. Science Advances 8:. https://doi.org/10.1126/sciadv.abm0303

Toyofuku T, Matsuo MY, De Nooijer LJ, et al (2017) Proton pumping accompanies calcification in foraminifera. Nat Commun 8:14145. https://doi.org/10.1038/ncomms14145

Tresguerres M, Barott KL, Barron ME, et al (2017) Cell Biology of Reef-Building Corals: Ion Transport, Acid/ Base Regulation, and Energy Metabolism. In: Acid-Base Balance and Nitrogen Excretion in Invertebrates: Mechanisms and Strategies in Various Invertebrate Groups with Considerations of Challenges Caused by Ocean Acidification. pp 193–218

Tresguerres M, Katz S, Rouse GW (2013) How to get into bones: proton pump and carbonic anhydrase in Osedax boneworms. Proceedings of the Royal Society B 280:20130625. https://doi.org/10.1098/rspb.2013.0625

Tyystjärvi E (2013) Photoinhibition of Photosystem II*. In: International Review of Cell and Molecular Biology

Vandermeulen JH (1975) Studies on reef corals. III. Fine structural changes of calicoblast cells in Pocillopora damicornis during settling and calcification. Mar Biol 31:69–77. https://doi.org/10.1007/BF00390649

Venn A, Tambutté E, Holcomb M, et al (2011) Live tissue imaging shows reef corals elevate pH under their calcifying tissue relative to seawater. PLoS ONE 6:. https://doi.org/10.1371/journal.pone.0020013

Venn AA, Tambutté E, Lotto S, et al (2009) Imaging intracellular pH in a reef coral and symbiotic anemone. Proceedings of the National Academy of Sciences of the United States of America 106:16574–9. https://doi.org/10.1073/pnas.0902894106

Wangpraseurt D, Larkum AWD, Franklin J, et al (2014) Lateral light transfer ensures efficient resource distribution in symbiont-bearing corals. Journal of Experimental Biology 217:489–498. https://doi.org/10.1242/jeb.091116

Warner ME, Fitt WK, Schmidt GW (1999) Damage to photosystem II in symbiotic dinoflagellates: A determinant of coral bleaching. Proceedings of the National Academy of Sciences 96:8007–8012. https://doi.org/10.1073/pnas.96.14.8007

Wooldridge SA (2009) A new conceptual model for the warm-water breakdown of the coralalgae endosymbiosis. Marine and Freshwater Research 60:483–496. https://doi.org/10.1071/MF08251

Yee DP, Samo TJ, Abbriano RM, et al (2023) The V-type ATPase enhances photosynthesis in marine phytoplankton and further links phagocytosis to symbiogenesis. Current Biology 33:2541-2547.e5. https://doi.org/10.1016/j.cub.2023.05.020

# Chapter 5

## Co-Authored Publications

**Abstract**

Acid/base disturbances have significant effects on nearly all physiological processes so sensing and regulating levels of $CO_2$, $H^+$, and $HCO_3^-$ in cells to maintain acid/base homeostasis is a prerequisite for all uni- and multicellular life. $CO_2$ is both the main end product of aerobic respiration and the substrate for photosynthetic carbon fixation. In fluids, $CO_2$ dissolves into carbonic acid which dissociates into $H^+$ and $HCO_3^-$ (pKa 6.37), a reaction catalyzed by carbonic anhydrase (CA). $HCO_3^-$ can further deprotonate into $H^+$ and $CO_3^{2-}$ (pKa 10.3); $HCO_3^-$ and $CO_3^{2-}$ collectively form the dissolved inorganic carbon (DIC) pool. Intracellular levels of $HCO_3^-$, and by extension $CO_2$, are sensed by transmembrane and soluble adenylyl cyclases (tmACs and sACs) which produce the ubiquitous secondary messenger molecule cyclic adenosine monophosphate (cAMP). $HCO_3^-$-stimulated cAMP production can modulate nearly every aspect of cell biology through protein kinase A (PKA)-dependent phosphorylation, exchange protein activated by cAMP (EPAC), and cyclic nucleotide gated channels. Downstream transport of $H^+$ and $HCO_3^-$ to counteract pH disturbances are achieved by the V-type $H^+$-ATPase (VHA) and $HCO_3^-$ transporters (BTs) amongst others. In this chapter, we present several co-authored studies that review pH microenvironments in corals, explore the role of sAC in coral and sea urchin calcification, identify sAC's role in pHi regulation and hemoglobin- $O_2$ binding in trout red blood cells, demonstrate VHA's involvement in promoting anemone photosynthesis, examine the role of VHA in sacoglossan kleptoplasty, and establish VHA's contribution to promoting symbiont selectivity in the bobtail squid. Sections and figures produced by the author of this dissertation are included as well as the abstracts of the studies.

*Extreme pH microenvironment in coral cells*

The acid–base relevant molecules $CO_2$, $H^+$, and $HCO_3^-$ are substrates and end products of some of the most essential physiological functions including aerobic and anaerobic respiration, ATP hydrolysis, photosynthesis, and calcification. The structure and function of many enzymes and other macromolecules are highly sensitive to changes in pH, and thus maintaining acid/base homeostasis in the face of metabolic and environmental disturbances is essential for proper cellular function. On the other hand, $CO_2$, $H^+$, and $HCO_3^-$ have regulatory effects on various proteins and processes, both directly through allosteric modulation and indirectly through signal transduction pathways. Life in aquatic environments presents organisms with distinct acid/base challenges that are not found in terrestrial environments. These include a relatively high $CO_2$ relative to $O_2$ solubility that prevents internal $CO_2/HCO_3^-$ accumulation to buffer pH, a lower $O_2$ content that may favor anaerobic metabolism, and variable environmental $CO_2$, pH and $O_2$ levels that require dynamic adjustments in acid–base homeostatic mechanisms. Additionally, some aquatic animals purposely create acidic or alkaline microenvironments that drive specialized physiological functions. For example, acidifying mechanisms can enhance $O_2$ delivery by red blood cells, lead to ammonia trapping for excretion or buoyancy purposes, or lead to $CO_2$ accumulation to promote photosynthesis by endosymbiotic algae. On the other hand, alkalinizing mechanisms can serve to promote calcium carbonate skeletal formation. This nonexhaustive review summarizes some of the distinct acid–base homeostatic mechanisms that have evolved in aquatic organisms to meet the particular challenges of this environment.

## 8 | EXTREME pH MICROENVIRONMENT IN CORAL CELLS

Reef-building corals that host photosymbiotic algae experience some of the most extreme acid–base disturbances found among animals. While a carbon concentrating mechanism (CCM) promotes photosynthesis by acidifying the algal microenvironment to pH values as low as 4, skeleton calcification is promoted by creating an alkaline microenvironment where pH values can be greater than 9 (reviewed in Tresguerres et al., 2017). Remarkably, this 100,000-fold difference in $[H^+]$ exists over just a few hundred microns that separate the cells that host symbiotic algae from those that build the skeleton (Figure 7a). Since corals lack specialized organs, acid–base homeostasis relies on regulatory mechanisms within each individual cell.

The enzyme ribulose-1,5-bisphosphate carboxylase/oxygenase (rubisco) catalyzes the first major step in photosynthetic $CO_2$ fixation (Cooper, Filmer, Wishnick, & Lane, 1969). However, rubisco's relatively low affinity for $CO_2$ compared to contemporary environmental $PCO_2$ levels and to its significant affinity for $O_2$ may lead to photorespiration and diminished carbon fixation efficiency (Tamiya & Huzisige, 1948). In response, many phytoplankton species have developed CCMs that elevate $PCO_2$ at the site of rubisco (Reinfelder, 2011). Likewise, a CCM is essential for sustaining the photosynthetic activity of coral's symbiotic algae (Yellowlees, Rees, & Leggat, 2008). However, these algae reside inside an intracellular compartment of coral gastrodermal cells called the symbiosome (Figure 7), which can be modulated by the coral host cell. Recently, a novel host-controlled CCM has been identified whereby VHA that is abundantly expressed in the symbiosome membrane acidifies the lumen down to pH~4 (Barott, Venn, Perez, Tambutté, & Tresguerres, 2015; Figure 7b,c). Together with $HCO_3^-$ transport through yet unidentified mechanisms, this VHA-dependent acidification is

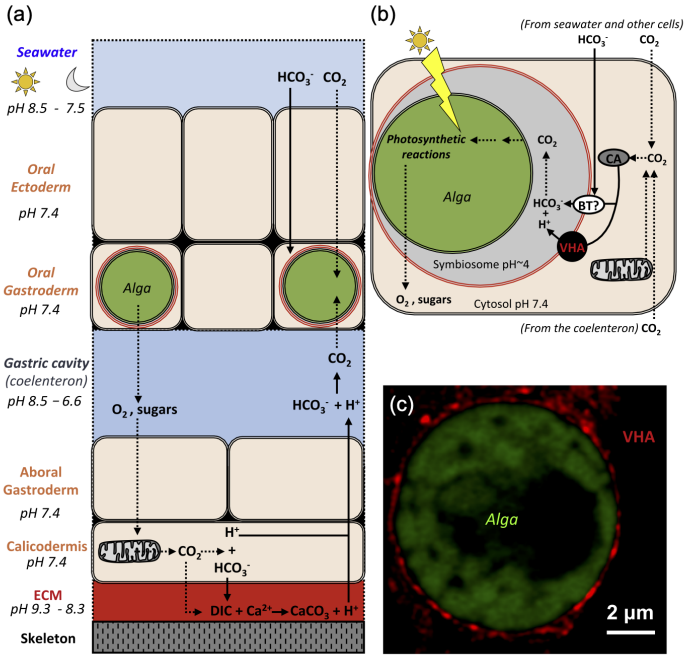


**FIGURE 7** Extreme pH microenvironments in corals. (a) Simplified coral histology diagram showing the movements of acid–base relevant molecules between seawater, host cells with algal symbionts, and the site of calcification (ECM: extracellular calcifying medium). Together with $Ca^{2+}$ transport into the ECM and vesicular transport of amorphous $CaCO_3$ (not shown), the alkaline pH in the SCM promotes coral skeleton formation. DIC: dissolved inorganic carbon ($CO_2$+$HCO_3^-$+$CO_3^{2-}$). The pH of extracellular and intracellular compartments is noted to the left (sun and moon indicating day- and nighttime pH for seawater respectively). Photosynthesis and calcification are linked by translocation of photosynthetic products to the site of calcification (i.e., oxygen and sugars) and calcification byproducts ($H^+$) to host cells. (b) Schematic of a coral host cell containing an algal symbiont to illustrate the CCM. The alga is not drawn to scale to allow for clarity but usually occupies >90% of a host cell's volume. BT: $HCO_3^-$ transporter; CA: carbonic anhydrase; VHA: V-Type $H^+$-ATPase. (c) VHA immunostaining (red signal) of a symbiont-containing coral gastrodermal cell showing abundant VHA presence in the symbiosome membrane. The other proteins involved in transport of ions and other molecules are omitted for simplicity, and in many cases their identities are unknown [Color figure can be viewed at wileyonlinelibrary.com]

thought to drive $CO_2$ flux into the symbiosome lumen and thereby enhance the delivery of $CO_2$ to the site of fixation. VHA activity in the coral symbiosome membrane has been proposed to additionally slow down symbiotic alga cell division, as well as to drive the transport of phosphates, amino acids, sugars, and ammonia by acid-trapping (Tang, 2015; Tresguerres et al., 2017; Figure 7). The presence of an analogous VHA-driven CCM in giant clams that host symbiotic algae in their gut (Armstrong, Roa, Stillman, & Tresguerres, 2018) suggests that this mechanism has evolved convergently in different species.

While coral photosynthesis requires an acidified microenvironment, it alkalinizes the rest of the coral because it consumes $CO_2$ and $H^+$ and it generates $OH^-$ (Allemand, Furla, & Bénazet-Tambutté, 1998). At the onset of photosynthesis, the pHi of the coral host cells immediately increases from approximately 7.0 to 7.4 (Barott et al., 2017; Laurent, Tambutte, Tambutte, Allemand, & Venn, 2013). The rate of photosynthesis increases linearly with light irradiance, and so does the initial alkalinization of the host cell cytoplasm. However, pHi plateaus after approximately 20 min despite the continuous photosynthetic activity, indicating the activation of pHi regulatory mechanisms (Laurent et al., 2013). At this time, cytosolic $H^+$ is being replenished at the same rate as they are being consumed by photosynthesis and a new steady state is reached. The molecular mechanisms involved in this response are unknown. Although certain AEs is a common mechanism used to counteract an intracellular alkalosis (Figure 2), they extrude $HCO_3^-$ from the cell and this would conflict with the need for dissolved inorganic carbon transport for photosynthesis. Alternatively, transport of $HCO_3^-$ into the symbiosome as proposed in Figure 4b would fulfill the need for both pHi regulation and CCM. Intracellular buffering is also important to help cope with the immediate alkalinizing effect of algal photosynthesis, and this is reflected in symbiont-containing cells having approximately 25% higher buffering capacity compared to symbiont-free cells (Laurent et al., 2014). Indeed, their buffering capacity is higher than that of mussel retractor muscle (Zange, Grieshaber, & Jans, 1990) and squid mantle (Pörtner, Boutilier, Tang, & Toews, 1990), which may imply that the magnitude of the alkaline challenge induced by symbiont photosynthesis is greater than the acidic challenge resulting from muscle contraction.

On the other hand, coral calcification takes place in an actively alkalinized environment and represents a source of acidic stress for the rest of the coral. The cells responsible for coral skeleton formation are called calicoblastic cells and form an epithelium that is situated directly above the extracellular calcifying fluid (ECF) that separates it from the skeleton. The calicoblastic cells express an abundance of SLC4 transporters that presumably help deliver $HCO_3^-$ to the ECF (Barott, Perez, Linsmayer, & Tresguerres, 2015; Tresguerres et al., 2017; Zoccola et al., 2015). These cells also express $Na^+/Ca^{2+}$ exchangers (Barron et al., 2018) and plasma membrane $Ca^{2+}$-ATPases that help deliver the required $Ca^{2+}$ (Barott, Perez et al., 2015; Zoccola et al., 2004); the latter might additionally mediate $H^+$ removal from the ECF. The combined activities of these transporters generate an elevated aragonite saturation state in the ECF that promotes skeleton calcification and counteracts its dissolution. Some of these transporters are likely under regulatory control by sAC, which is expressed in calicoblastic cells and mediates the alkalinization of the ECF and the growth of skeletal $CaCO_3$ crystals (Barott, Venn, Thies, Tambutté, & Tresguerres, 2020). A similar role of sAC in regulating $CaCO_3$ precipitation has been demonstrated or proposed in the intestine of marine teleosts (Tresguerres, Levin, Buck, & Grosell, 2010) and in the teleost inner ear (Kwan, Smith, & Tresguerres, 2020). Thus, an evolutionary pattern is emerging whereby sAC-regulated transepithelial acid–base relevant ion-transport generates alkaline conditions that promote calcification in extracellular space.

Other components of the coral calcification mechanism include acidic proteins that promote $Ca^{2+}$ precipitation (Mass et al., 2013), and abundant vesicles in the calicoblastic cells that are formed by macropinocytosis from the ECF (Ganot et al., 2020) and potentially also by transcytosis from the oral tissues (Mass et al., 2017). Interestingly, calcifying foraminifera produces their chambered shells by endocytosis of seawater into vesicles, which they subsequently alkalinize to a pH > 9.0 thus promoting $CaCO_3$ precipitation (Bentov, Brownlee, & Erez, 2009; de Nooijer, Toyofuku, & Kitazato, 2009). Incubation with the VHA inhibitor bafilomycin A1 significantly decreased $H^+$ efflux from the newly forming chambers and resulted in weakly calcified chamber walls, indicating the involvement of VHA in calcification (Toyofuku et al., 2017). A similar role for VHA in calcification was proposed in the calcifying vesicle of coccolitophorids, which are another eukaryotic phytoplankton with an external $CaCO_3$ shell (Corstjens, Araki, & González, 2001; Mackinder et al., 2011). It is worth investigating whether VHA is also present in the vesicles within coral calicoblastic cells and whether it plays a role in coral skeleton formation.

The $H^+$ that is removed from the ECF during calcification eventually reaches the coral gut cavity, where they combine with $HCO_3^-$ to form $CO_2$ that may be used by photosynthesis within the symbiotic algae (Figure 7b). Thus, coral calcification and photosynthesis are linked to each other through the complementary and synergistic production and consumption of $CO_2$, $H^+$, and $HCO_3^-$. This is one of the mechanisms by which the photosynthetic activity of the symbiotic algae stimulates coral skeletal growth, a phenomenon known as "light enhanced calcification" (Kawaguti & Sakumoto, 1948).

## 9 | SUMMARY

As substrates and products of many biochemical reactions $CO_2$, $H^+$, and $HCO_3^-$ molecules are intrinsically linked to aerobic and anaerobic metabolism, $O_2$ transport, ammonia homeostasis, metabolic communication between symbiotic partners, and calcification. Future comparative studies at all levels of the organization will undoubtedly continue to reveal novel aspects about the evolutionary links between intra- and extracellular acid–base regulation and their effects on multiple aspects of organismal physiology. From a practical perspective, understanding the effects of metabolic and environmental

*Regulation of coral calcification by the acid-base sensing enzyme sAC*

Coral calcification is intricately linked to the chemical composition of the fluid in the extracellular calcifying medium (ECM), which is situated between the calcifying cells and the skeleton. Here we demonstrate that the acid-base sensing enzyme sAC is expressed in calcifying cells of the coral *Stylophora pistillata*. Furthermore, pharmacological inhibition of sAC in coral microcolonies resulted in acidification of the ECM as estimated by the pH-sensitive ratiometric indicator SNARF, and decreased calcification rates, as estimated by calcein labeling of crystal growth. These results indicate that sAC activity modulates some of the molecular machinery involved in producing the coral skeleton, which could include ion-transporting proteins and vesicular transport. To our knowledge this is the first study to directly demonstrate biological regulation of the alkaline pH of the coral ECM and its correlation with calcification.

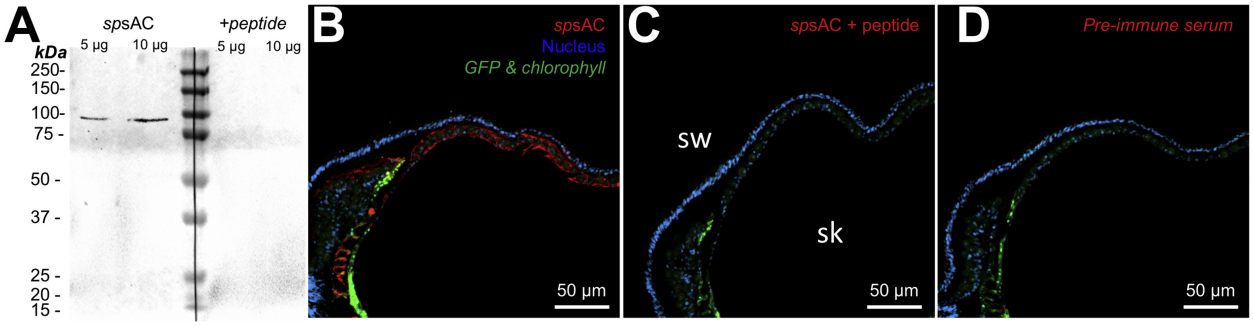


Figure 5.2: Presence of sAC in the coral *S. pistillata*. (A) Western blot in coral tissue homogenates showing a specific band of ~90 kDa. Left: anti-spsAC antibodies; Right: peptide preabsorption control. The total amount of protein loaded in the gel is shown above each lane. (B-D) Immunohistochemistry in coral tissue sections. sw: seawater; sk: skeleton. spsAC (red), endogenous GFP and chlorophyll (green), DAPI (blue).

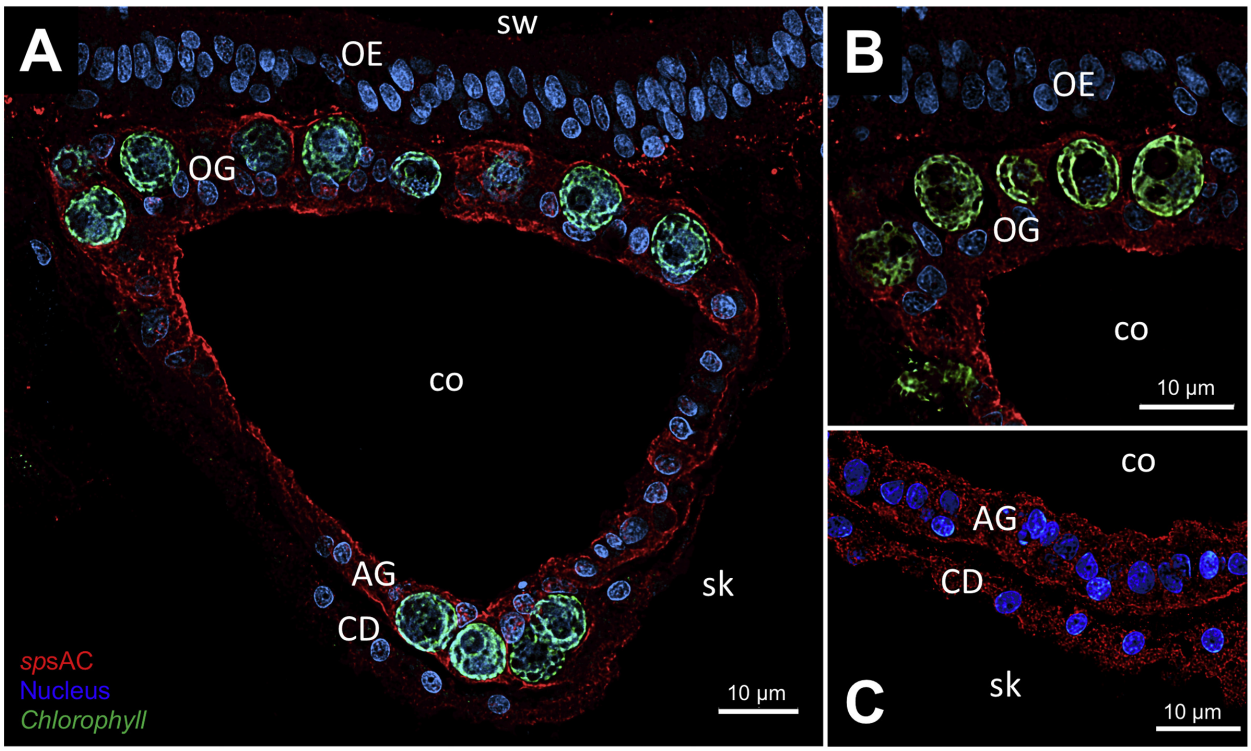


Figure 5.3: Cellular localization of sAC in *S. pistillata*. (A) Representative coenosarc section demonstrating widespread spsAC localization throughout the coral tissues. (B) Detail of oral tissues showing abundant spsAC expression in cells of the oral gastroderm (OG) and limited expression throughout the oral ectoderm (OE). (C) Detail of aboral tissues showing abundant spsAC expression in cells of the aboral gastrodermal (AG) and calicodermis (CD). co, coelenteron; sk, skeleton; sw, seawater.

*sAC coordinates pHi homeostasis and biomineralization in calcifying cells of sea urchins*

Biomineralizing cells concentrate DIC and remove protons from the site of mineral precipitation. However, the molecular regulatory mechanisms that orchestrate pH homeostasis and biomineralization of calcifying cells are poorly understood. Here, we report that the acid-base sensing enzyme sAC coordinates pHi regulation in the calcifying primary mesenchyme cells (PMCs) of sea urchin larvae. Single-cell transcriptomics, in situ hybridization, and immunocytochemistry elucidated the spatiotemporal expression of sAC during skeletogenesis. Live pHi imaging of PMCs revealed that the downregulation of sAC activity with two structurally unrelated small molecules inhibited pHi regulation of PMCs, an effect that was rescued by the addition of cell-permeable cAMP. Pharmacological sAC inhibition also significantly reduced

normal spicule growth and spicule regeneration, establishing a link between PMC pHi regulation and biomineralization. Finally, increased expression of sAC mRNA was detected during skeleton remineralization and exposure to $CO_2$-induced acidification. These findings suggest that transcriptional regulation of sAC is required to promote remineralization and to compensate for acidic stress. This work highlights the central role of sAC in coordinating acid-base regulation and biomineralization in calcifying cells of a marine animal.

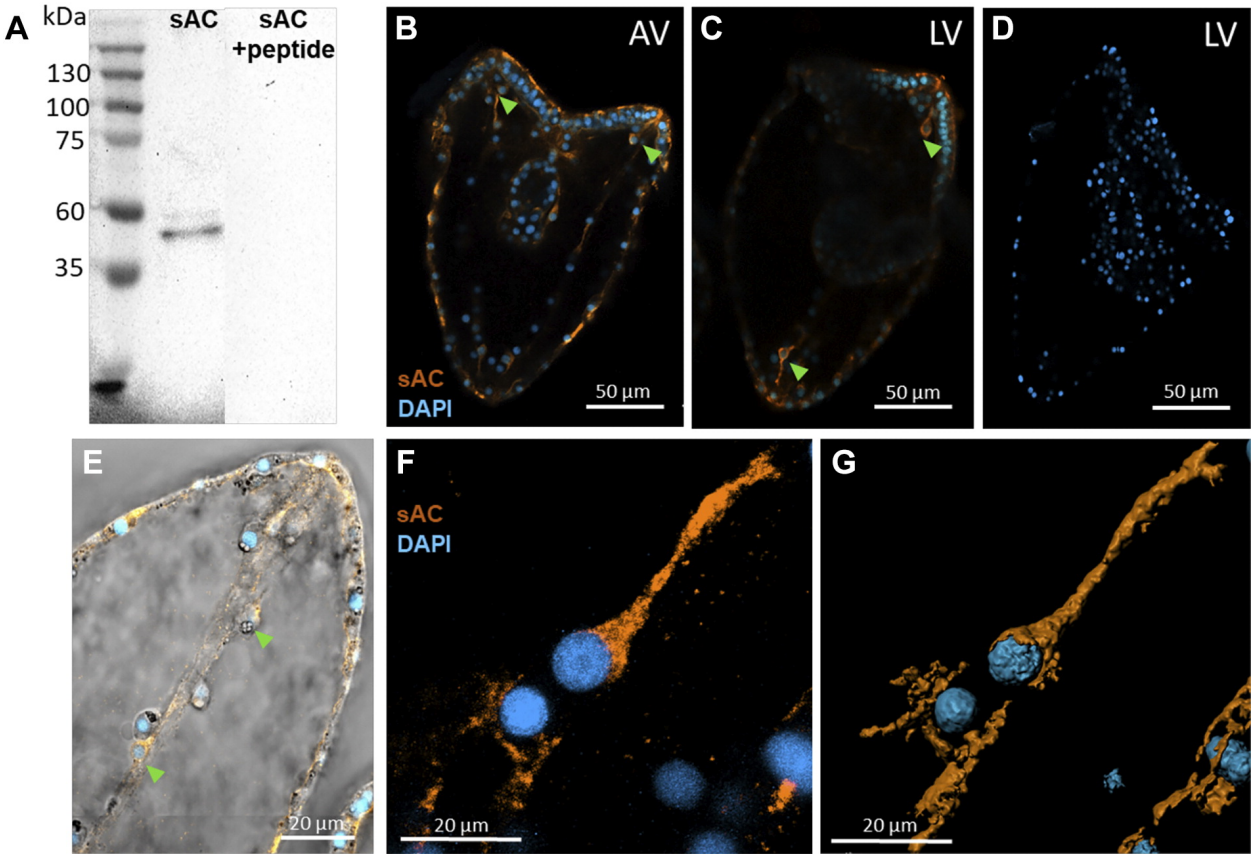


Figure 5.4: Immunocytological analyses of sAC in the sea urchin larva. A: Western blot analysis using the anti-coral sAC antibody against crude protein extracts of sea urchin larvae. The right lane shows the peptide preabsorption control. B, C: immunolocalization of sAC in 3 dpf sea urchin larva. sAC-positive PMCs were indicated by arrowhead. D: negative control without addition of the primary antibody. E: merged image of sAC immunostaining and bright field. sAC-positive PMCs attaching to spicule were indicated by arrowhead. F: reconstituted 3-D image of sAC staining. The sAC signal followed the shape of PMC syncytial cables and is highlighted in G. AV, anal view; dpf, day post fertilization; LV, lateral view; sAC, soluble adenylyl cyclase; PMC, primary mesenchyme cell; 3-D, three-dimensional. sAC protein (orange), nuclei (blue).

*sAC is an acid-base sensor in rainbow trout red blood cells that regulates pHi and hemoglobin-$O_2$ binding*

Our aim was to identify the physiological role of the acid-base sensing enzyme, sAC, in red blood cells (RBC) of the model teleost fish, rainbow trout. We used: i) super-resolution microscopy to determine the subcellular location of sAC protein; ii) live-cell imaging of RBC $pH_i$ with specific sAC inhibition (KH7 or LRE1) to determine its role in cellular acid-base regulation; iii) spectrophotometric measurements of hemoglobin- $O_2$ (Hb-$O_2$) binding in steady-state conditions; and iv) during simulated arterial-venous transit, to determine the role of sAC in systemic $O_2$ transport. Distinct pools of sAC protein were detected in the RBC cytoplasm, at the plasma membrane and within the nucleus. Inhibition of sAC decreased the setpoint for RBC $pH_i$ regulation by ~0.25 pH units compared to controls and slowed the rates of RBC $pH_i$ recovery after an acid-base disturbance. RBC $pH_i$ recovery was entirely through the anion exchanger (AE) that was in part regulated by $HCO_3^-$-dependent sAC signaling. Inhibition of sAC decreased Hb-$O_2$ affinity during a respiratory acidosis compared to controls and reduced the cooperativity of $O_2$ binding. During *in vitro* simulations of arterial-venous transit, sAC inhibition decreased the amount of $O_2$ that is unloaded by ~11%. sAC represents a novel acid-base sensor in the RBCs of rainbow trout, where it participates in the modulation of RBC $pH_i$ and blood $O_2$ transport though the regulation of AE activity. If substantiated in other species, these findings may have broad implications for our understanding of cardiovascular physiology in vertebrates.

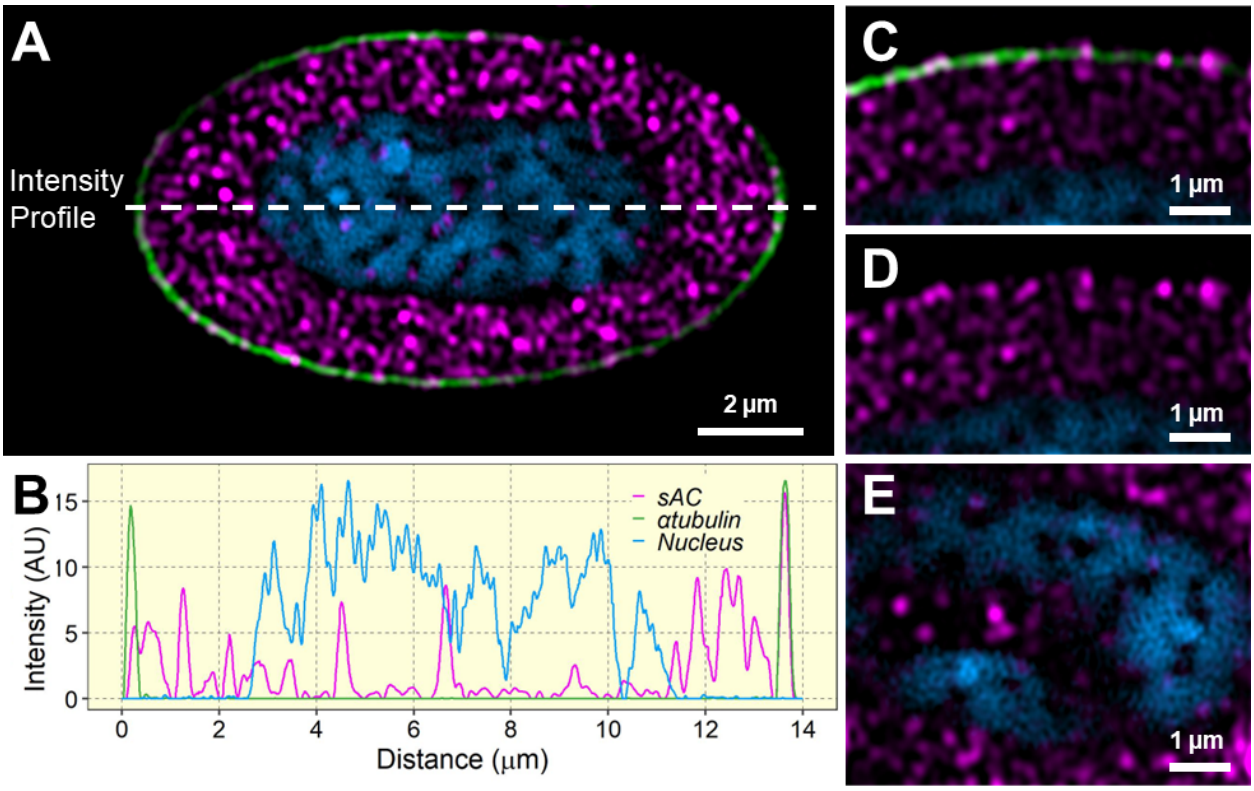


Figure 5.5: (A) Immunocytochemical localization of sAC in rainbow trout RBC. Blood was incubated in tonometers for one hour and fixed cells were immuno-stained with an anti-sAC antibody (magenta) raised against the C1 subunit of the rainbow trout protein, with an anti-α-tubulin antibody to visualize the marginal band (green) and with DAPI to visualize the cell nucleus (blue). (B) Signal intensity profiles for sAC, α-tubulin and DAPI, along a transect through the RBC (see panel A for orientation). Distinct pools of sAC protein were detected (C) in association with the plasma membrane; (D) in the RBC cytoplasm; and (E) within the nucleus. Results are representative of $N = 6$ fish.

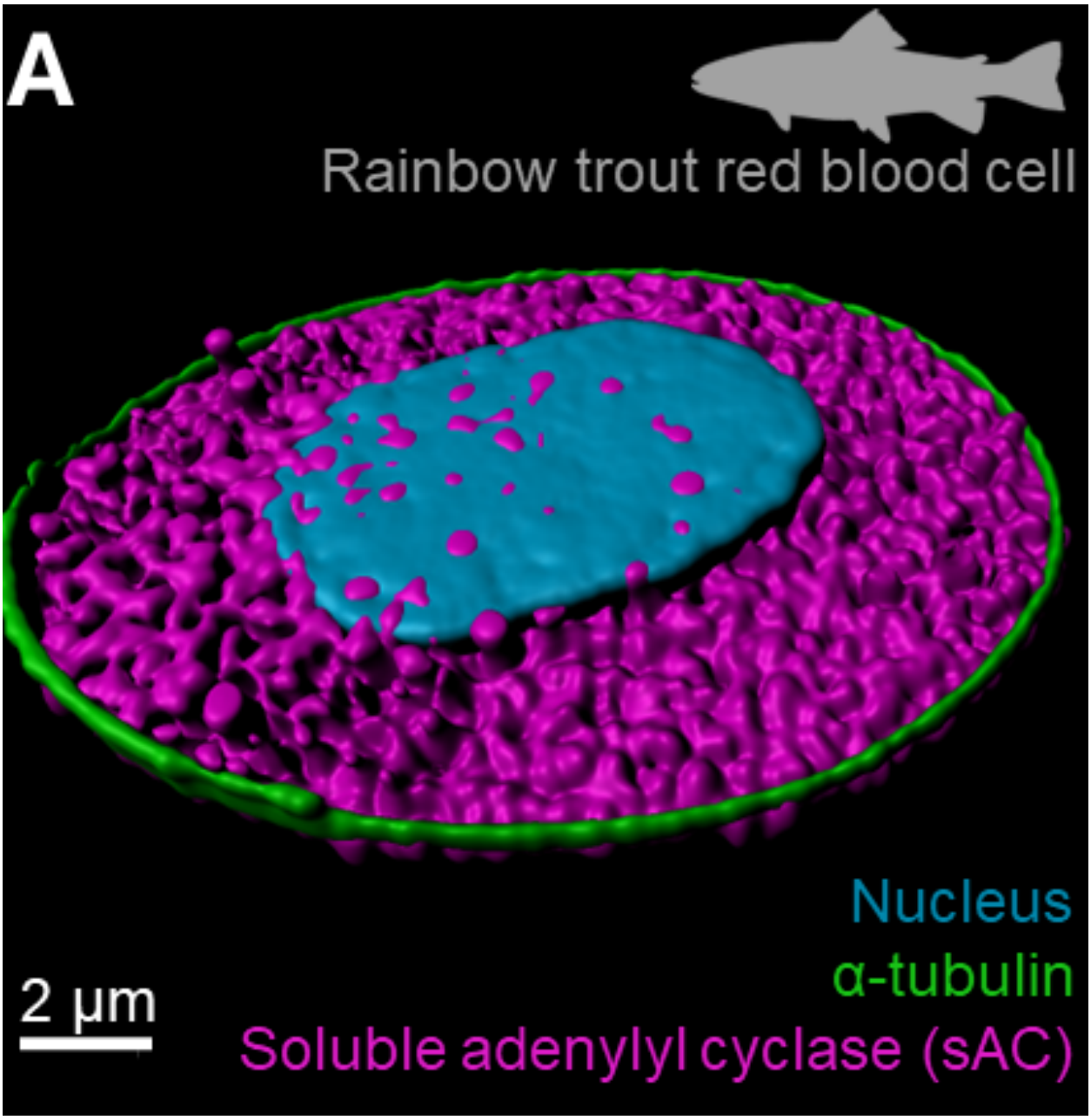


Figure 5.6: 3D render of a rainbow trout RBC immunocytochemically labeled for sAC (magenta), α-tubulin to visualize the marginal band (green), and with DAPI to visualize the cell nucleus (blue). Redner was created using Imaris 10.0.

*VHA in the symbiosome membrane is a conserved mechanism for host control of photosynthesis in anthozoan photosymbioses*

In reef-building corals (order Scleractinia) and giant clams (phylum Molluca), VHA in host cells is part of a CCM that regulates photosynthetic rates of their symbiotic algae. Here, we show that VHA plays a similar role in the sea anemone *Anemonia majano*, a member of the order Actinaria and sister group to the Scleractinia, which in contrast to their colonial calcifying coral relatives is a solitary, soft-bodied taxa. Western blotting and immunofluorescence revealed that VHA was abundantly present in the host-derived symbiosome membrane surrounding the photosymbionts. Pharmacological inhibition of VHA activity in individual anemones resulted in an approximately 80% decrease of photosynthetic $O_2$ production. These results extend the presence of a host-controlled VHA-dependent CCM to non-calcifying cnidarians of the order Actiniaria, suggesting it is widespread among photosymbiosis between aquatic invertebrates and Symbiodiniaceae algae.

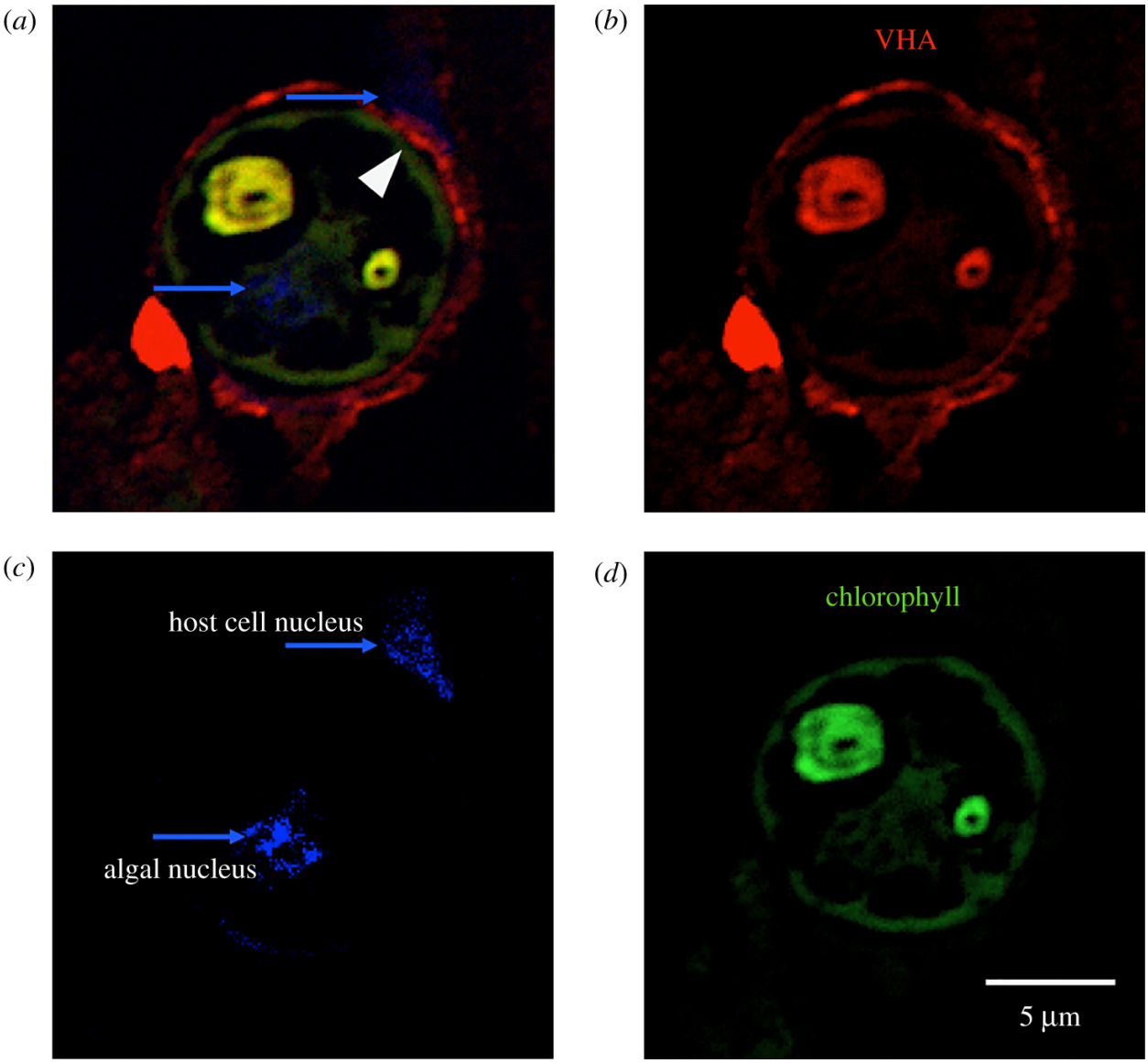


Figure 5.7: VHA is present in the symbiosome membrane of *A. majano* algal containing gastrodermal cells. (a) Composite image showing VHA immunofluorescence signal (red), DAPI nuclear staining (blue) and chlorophyll autofluorescence (green). (b) VHA, (c) DAPI and (d) chlorophyll individual channels. Notice that VHA is present in the thin region between the host cell nucleus (blue arrow in c) and the algae, indicative of symbiosomal localization (white arrowhead in a).

*VHA Does Not Drive a CCM in the Kleptoplastic Sacoglossan Elysia crispata*

A subset of sacoglossan sea slugs (Phylum Gastropoda, Class Sacoglossa) can steal functional chloroplasts from algal prey, a behavior known as "kleptoplasty" which enables the slug to survive months of starvation using photosynthates derived solely from the plastid. During digestion, plastids are phagocytosed by gland tubule cells and are retained intracellularly in modified lysosomes, "slugosomes," reminiscent of symbiosomes in corals and anemones. In cnidarian symbiosomes, hosts promote photosynthesis in their dinoflagellate symbionts by employing a VHA-powered CCM. It remains unclear however if sacoglossan slugs support ongoing photosynthesis by providing inorganic carbon to intracellular plastids. We exploded if sacoglossan slugs employ a homologous VHA-driven CCM in slugosomes to promote plastid photosynthesis using immunofluorescence Airyscan confocal microscopy, respirometry, and pulse amplitude fluorometry in the model *E. crispata*. We additionally tested if P2X4 purinergic receptors contribute to pH regulation in the slugosome as activation of P2X4 can trigger lysosomal acidification in vertebrates. We found that while slugosomes are VHA-rich, functional respirometry experiments did not support a role of VHA in a CCM. Notably, P2X4 inhibition did lower $O_2$ evolution in *E. crispata*, suggesting its involvement in regulating slugosome function through an unidentified mechanism. No drugs used in this study effected plastid photosynthetic machinery supporting out conclusions.

Figure 5.8: Immunocytochemical localization of $VHA_B$ in digestive gland tubule cells of the kleptoplastic sacoglossan *E. crispata*. (A) Cross section of a digestive tubule. (B) Tubule cell at the terminus of a tubule extension. $VHA_B$ signal is shown in yellow, chlorophyll in violet, and nuclei in blue. Scale bar is 5 μm. gl – gut lumen.

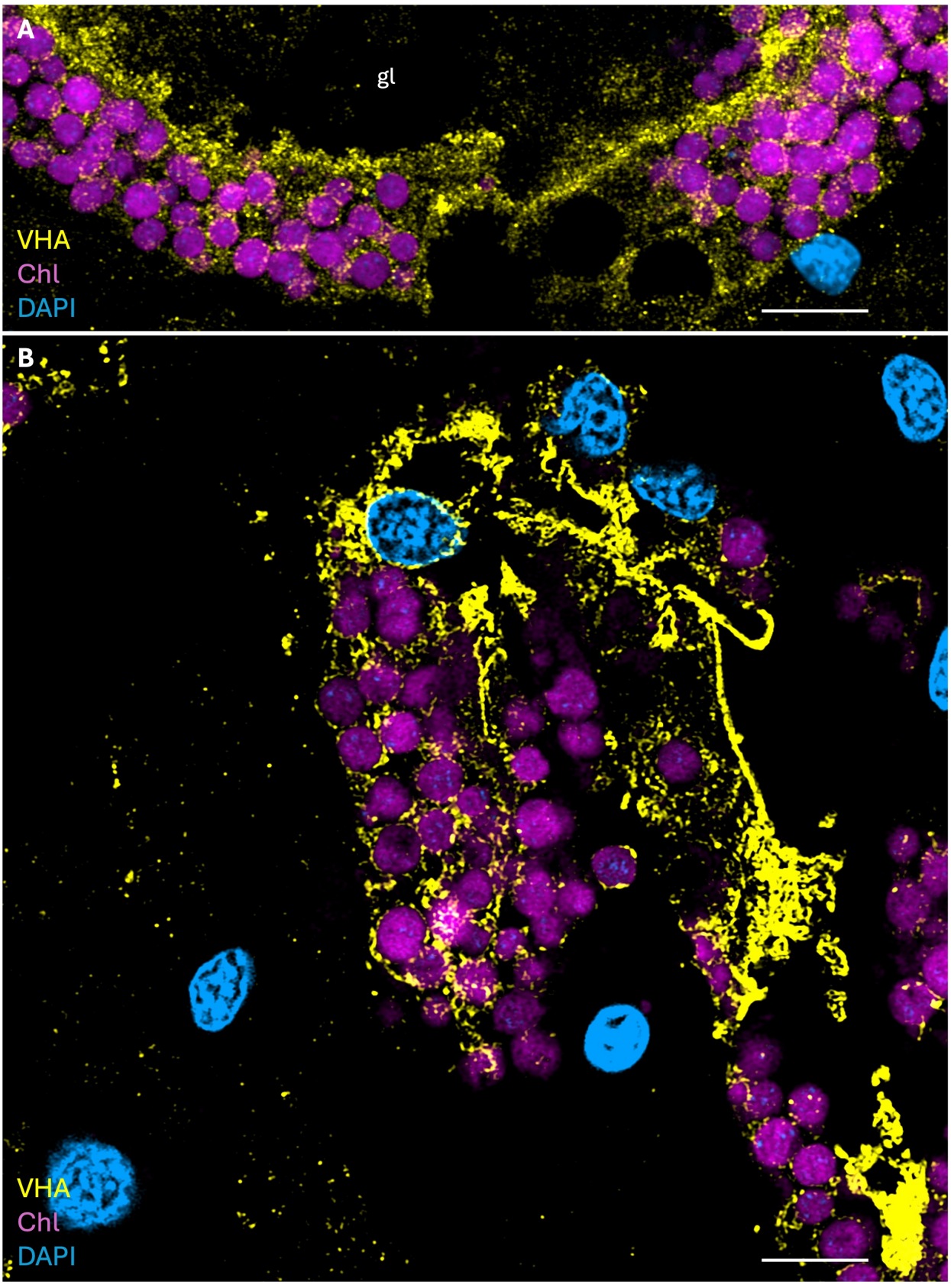
A
gl
VHA
Chl
DAPI
B
VHA
Chl
DAPI

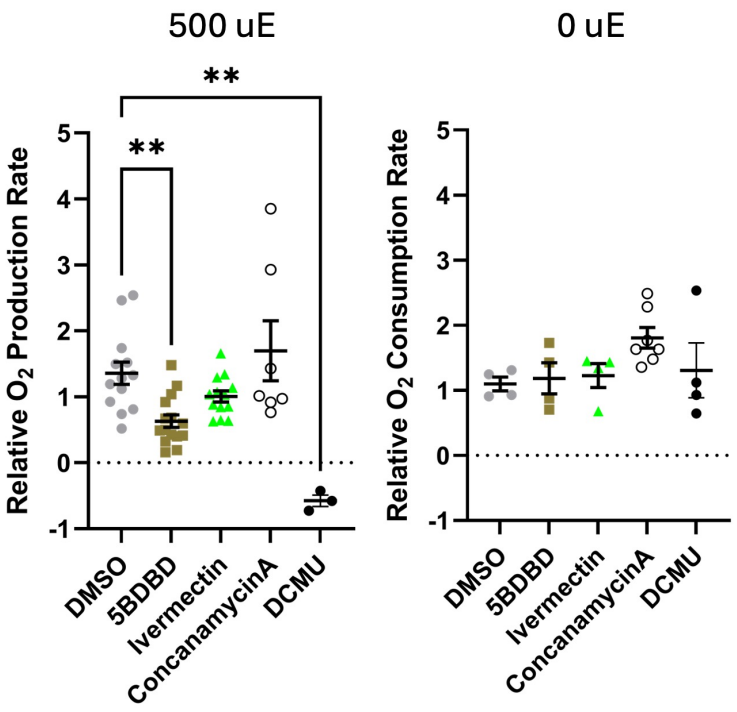


Figure 5.9: Effect of P2X4 and VHA on $P_N$ $R_D$ of *E. crispata*. *E. crispata* tissue chunks were treated with DMSO, inhibitors of P2X4, VHA, or photosystem II (5BDBD, ConcanamycinA, DCMU), or a P2X4 agonist (Ivermectin). $O_2$ evolution or consumption rates were measured in the light or dark, respectively. Data were tested using a 1-Way ANOVA with Dunnett's multiple comparisons tests. ** denotes $p < 0.01$. n = 3-12 per treatment.

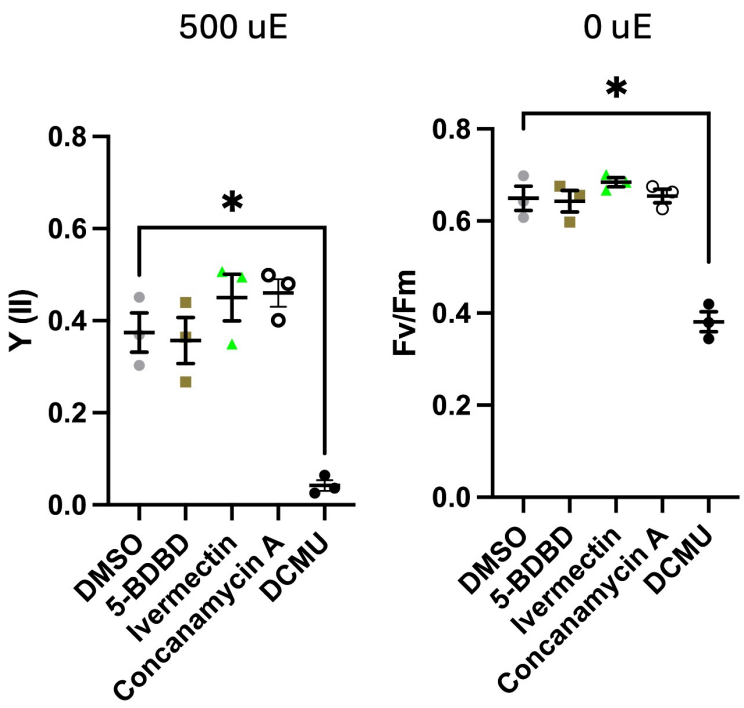


Figure 5.10: PAM confirms that only DCMU lowers photosystem II efficiency in *E. crispata*. Effective photochemical quantum yield under illumination (Y(II)) or maximal photochemical quantum yield in the dark (Fv/Fm) are presented. Whole animals were exposed to either DMSO, 5BDBD, Ivermectin, ConcanamycinA, or DCMU in darkness for 30 min before 5 spot measurements were taken. The same animal was then acclimated to 500 µE light for 5 min before a further 5 spot measurements were taken. No treatment altered Y(II) or Fv/Fm other than the positive control DCMU. Data were tested using a Repeated Measures 1-Way ANOVA. ** denotes $p < 0.05$. $n = 4$ per treatment.

*The acidic microenvironment produced by VHA promotes specificity during symbiont recruitment in the squid-vibrio association.*

Animals often acquire their microbial symbionts from the environment, but the mechanisms underlying how specificity of the association is achieved are poorly understood. We demonstrate that the proton pump, VHA, plays a key role in the establishment of the model light-organ symbiosis between the squid *Euprymna scolopes* and its bacterial partner *Vibrio fischeri*. Recruitment of *V. fischeri* from the surrounding seawater is mediated by juvenile-specific ciliated fields on the organ's surface. These epithelia export acidic mucus containing antimicrobials with low-pH optima, creating a chemical environment that fosters recruitment of *V. fischeri* specifically. We provide evidence that this critical acidic landscape is created by activity of VHA, which is abundant in apical regions of the epithelia. VHA inhibition abolished epithelial-cell acidity, resulting in increased mucus pH and inefficient symbiont colonization. Thus, VHA provides a mechanistic link between host modulation of microenvironmental acidity, immune function, and selection of microbial symbionts, a strategy for specificity that may govern many symbiotic systems.

Figure 5.11: Immunocytochemical localization of the $VHA_B$ protein within the ciliated fields of the juvenile light organ's superficial epithelium. (A) Illustration indicating the position of the light organ in the mantle cavity, and the appendage tissue (dashed yellow line) showing the region of cells displayed in the rest of this figure. (B, B') Confocal microscopy image of areas of $VHA_B$-antibody ($aVHA_B$) labeling. (B) Strong labeling occurred in the apical surfaces of the epithelia (white box), enlarged below and in (B'). Inset: immunocytochemical control staining showed undetectable labeling. (B') Imaris 3D rendering highlighting the close association of the antibody with the epithelial nuclei. (C,C') Labeling of host cilia was detectable at higher sensitivity. (C) *Left,* confocal image of antibody labeling (white arrows); *right*, Imaris rendering. (C') Increased magnification and Imaris rendering. (D) *Upper*, low and high magnification images of Lysosensor-stained acidic regions associated with epithelial nuclei; *lower*, Imaris rendering at even higher magnification, providing evidence that the nuclear regions wrap around (white arrows) the acidic regions. (E) Immuno-electron micrograph of the distal edges of ciliated epithelial cells. *Left*, an image defining the ciliated region; *right*, enlargement of the area in the black box, including points of $VHA_B$ labeling (red arrows). LIS, lateral intracellular space; MV, microvilli; TW, terminal web.

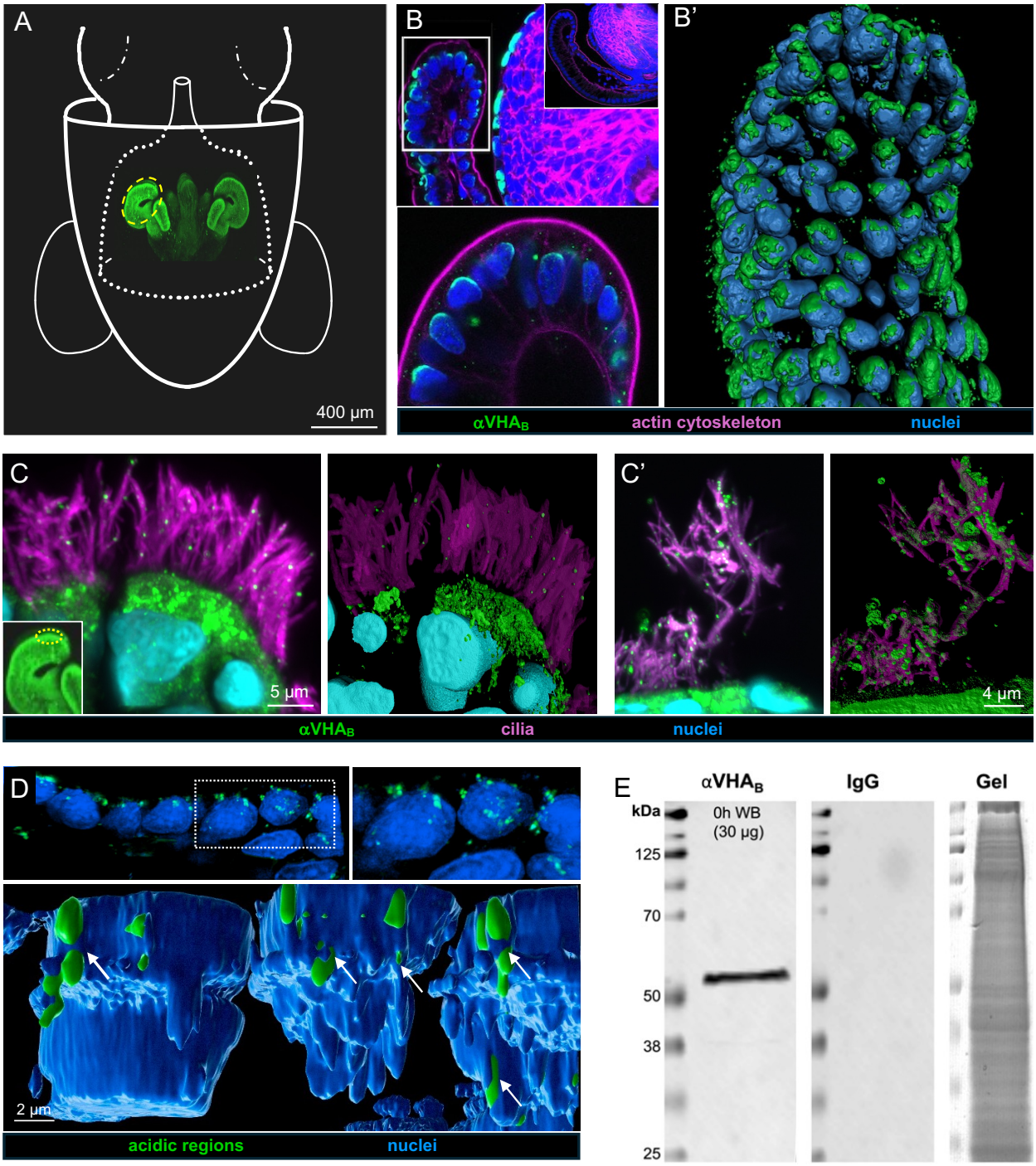
A
400 µm
B
B'
αVHA$_B$
actin cytoskeleton
nuclei
C
5 µm
C'
4 µm
αVHA$_B$
cilia
nuclei
D
2 µm
acidic regions
nuclei
E
αVHA$_B$
IgG
Gel
kDa
0h WB
(30 µg)
125
70
50
38
25

**Acknowledgements**

This work was partially supported by National Science Foundation Graduate Research (GRFP 2019271478), Scripps Institution of Oceanography Doctoral, and Achievement Rewards for College Scientists Fellowships to A.B.T.

Chapter 5, in part, is a reprint of the material as it appears in Tresguerres M, Clifford AM, Harter TS, Roa JN, Thies AB, Yee DJ, and Brauner CJ. 2020. Evolutionary links between intra- and extracellular acid-base regulation in fish and other aquatic animals. Journal of Experimental Zoology Part A: Ecological and Integrative Physiology 1, 17 (10.1002/jez.2367). The dissertation author was a co-author of this paper. The material is used by permission of John Wiley & Sons, Inc.

Chapter 5, in part, is a reprint of the material as it appears in Barott KL, Venn AA, Thies AB, Tambutté S, Tresguerres M. 2020. Regulation of coral calcification by the acid-base sensing enzyme soluble adenylyl cyclase. Biochemical and Biophysical Research Communications 525, 3 (10.1016/j.bbrc.2020.02.115). The dissertation author was a co-author of this paper. The material is used by permission of Elsevier.

Chapter 5, in part, is a reprint of the material as it appears in Chang WW, Thies AB, Tresguerres M, Hu MY. 2023. Soluble adenylyl cyclase coordinates intracellular pH homeostasis and biomineralization in calcifying cells of a marine animal. American Journal of Physiology-Cell Physiology 324, 3 (10.1152/ajpcell.00524.2022). The dissertation author was a co-author of this paper. The material is used by permission of The American Physiological Society.

Chapter 5, in part, is a reprint of the material as it appears in Harter TS, Smith EA, Salmerón C, Thies AB, Delgado B, Wilson RW, Tresguerres M. 2024. Soluble adenylyl cyclase is an acid-base sensor in rainbow trout red blood cells that regulates intracellular pH and haemoglobin- $O_2$

binding. Acta Physiologica. The dissertation author was a co-author of this paper. The material is used by permission of Acta Physiologica (10.1111/apha.14205).

Chapter 5, in part, is a reprint of the material as it appears in Barott KL, Thies AB, Tresguerres M. 2022. V-type $H^+$-ATPase in the symbiosome membrane is a conserved mechanism for host control of photosynthesis in anthozoan photosymbioses. Royal Society Open Science 9, 1 (10.1098/rsos.211449). The dissertation author was a co-author of this paper. The material is used by permission of The Royal Society.

Chapter 5, in part, contains material currently being prepared for submission for publication. Allard C, Thies AB, Leatz E, Tresguerres M, Bellono N. (in prep) VHA Does Not Drive a CCM in the Kleptoplastic Sacoglossan *Elysia crispata*. The dissertation author was a co-author of this paper.

Chapter 5, in part, is a reprint of the material as it appears in McFall-Ngai M, Viliunas J, Hargadon A, Koehler S, Chen G, Ladinsky M, Kuwabara J, Thies AB, Tresguerres M, Ruby E. (in prep) The acidic microenvironment produced by a V-type ATPase promotes specificity during symbiont recruitment in the squid-vibrio association. The dissertation author was a co-author of this paper.

# Chapter 6

# Synopsis

**Synopsis**

Cnidarian-Symbiodiniaceae photosymbioses enable the success of coral reefs, biodiverse ecosystems that protect coastlines from storm activity, feed millions worldwide, produce natural products of biomedical interest, and generate millions of dollars through tourism for local communities (Smith 1978; reviewed in Carté 1996 and Knowlton et al. 2010). In symbiosis, animal hosts are afforded access to an abundance of fixed carbon and $O_2$ released by intracellular algal symbionts which fuels ATP production, growth, and calcification. In return, hosts respire and concentrate $CO_2$ in the alga's microenvironment to sustain continued photosynthesis. Algae additionally gain access to the nitrogenous waste products of the host, which, in otherwise oligotrophic tropical waters, enables optimal photosynthesis through repair and synthesis of photosynthetic apparatuses. The host mechanisms and environmental factors that regulate these nutrient exchange pathways remain poorly studied precluding a deeper understanding of coral reef health and the evolution of photosymbioses. In this dissertation, I examined mechanisms of inorganic carbon and nitrogen exchange in cnidarian-algal photosymbioses to bridge this knowledge gap. Specifically, this work focused on the roles of V-type $H^+$-ATPase (VHA) and the VHA-associated Rhesus protein and carbonic anhydrase (CA) enzymes in the corals *Acropora yongei* and *Stylophora pistillata* as well the jellyfish *Cassiopea xamachana*. Additionally, I presented my contributions to seven co-authored publications that concern pH microenvironments in corals, explore the role of soluble adenyl cyclase (sAC) in coral and sea urchin calcification, identify sAC's role in pHi regulation and hemoglobin- $O_2$ binding in trout red blood cells, demonstrate VHA's involvement in promoting anemone photosynthesis, examine the role of VHA in sacoglossan kleptoplasty, and establish VHA's contribution to promoting symbiont selectivity in the bobtail squid.

In Chapter 2, I described a VHA-powered, Rhesus protein-dependent nitrogen concentrating mechanism (NCM) regulated over diel cycles that supplies $NH_3/NH_4^+$ (Total ammonia, Tamm) to coral symbionts *in hospite* (Thies et al. 2022). Our task was complicated by Rh proteins' disputed roles as $NH_3$ gas channels, $NH_4^+$ channels, or dual $NH_3/NH_4^+$ channels. We overcame this obstacle by developing a novel assay to directly measure Tamm movement through the *A. yongei* Rhesus protein (ayRhp1) heterologous expressed in *Xenopus* oocytes. We additionally conceived a method for measuring $CO_2$ movement through heterologously expressed proteins. These advances ultimately allowed us to conclude that ayRhp1 is a duel $NH_3/CO_2$ gas channel that is insensitive to $NH_4^+$ gradients. The use of super-resolution Airyscan confocal microscopy and custom-made polyclonal anti-ayRhp1 antibodies were essential to determining that ayRhp1 was present on the symbiosome membrane surrounding algal symbionts. In coordination with VHA which establishes a pH gradient across the symbiosome membrane, symbiosomal ayRhp1 enables directed movement of Tamm into the symbiont's microenvironment. ayRhp1's presence on the symbiosome membrane was dynamic with ayRhp1 being preferentially present during hours of peak photosynthesis. This is the first report of diel changes in proteomic makeup of the cnidarian symbiosome membrane and furthers the notion that this interface can be dynamically modified by the host cell to control the physiology of the alga over short timescales. As additional members of the symbiosomal proteome are identified, care should be taken to document their abundance over diel timescales and in healthy vs. stressed host health states.

In Chapter 3, we demonstrated that amoebocyte host cells of the photosymbiotic jellyfish *C. xamachana* employ a VHA-driven, CA-coupled carbon concentrating mechanism (CCM) that promotes symbiont photosynthesis. Using custom antibodies, we found that amoebocyte host cells

express both VHA and CA around the periphery of algal symbionts and that VHA was expressed at the highest levels in amoebocytes. Pharmacological inhibition of both VHA and CA resulted in significant reductions in the $O_2$ evolution rate, a proxy for photosynthetic activity. We additionally validated our pharmacological experiments using pulse amplitude modulated fluorometry (PAM) demonstrating that neither our VHA nor CA inhibitor interacted with symbiont photosynthetic machinery. These results suggest that host VHA and CA are functionally coupled in amoebocyte CCMs and that *C. xamachana* amoebocytes are suitable models for cnidarian host cells at large. Photosymbiosis in *Cassiopea ssp*. evolved independently from that of corals and anemones with symbionts being hosted in highly motile amoebocytes rather than sessile host cells of corals or anemones. Additionally, amoebocytes exhibit unique developmental and architectural differences from those of other cnidarians, namely performing immune functions, containing more symbionts per host cell, and originating from gastrodermal tissues before differentiating and migrating into the connective mesoglea. Together these factors link immune response, food digestion and convergent evolution of photosymbiosis across cnidarian taxa.

In Chapter 4, we explored how the coral *S. pistillata* regulates VHA-driven CCMs when acclimated to differing environmental light regimes. Our initial hypothesis was that corals grown under high light conditions would employ more CCMs to match DIC delivery to increased symbiont photosynthetic rates. We found that VHA expression increased with increasing light levels (2.7-fold, 100 vs. 1400 μE) suggesting corals employed more CCMs. Notably, confocal immunohistochemistry revealed that very few coral host cells contained VHA-rich symbiosomes indicating that CCMs were not widely present. We instead observed consistent labeling of calcifying cells in corals from all light conditions suggesting that VHA was not participating in CCMs, but rather supporting pHi/pHe regulation to support continued calcification. $O_2$

microsensor respirometry further demonstrated that rather than decreasing $O_2$ evolution as expected in a CCM, VHA-inhibition increased $O_2$ production in high-light animals. These results indicate that VHA participates in a net $O_2$-consuming process, likely LEC-related pHi and pHe regulation of calcifying cells and the subcalicoblastic medium (SCM), respectively. The altogether lack of VHA-driven CCMs in this population of corals is surprising given that CCMs are well-documented in multiple coral species (Barott et al. 2015); further work should explore the environmental variables controlling CCM regulation. Additional experiments to elucidate VHA's contribution to SCM pHe regulation and calcification could also be performed.

In Chapter 5, I presented seven studies on topics related to acid-base regulation which I co-authored during my PhD. These studies review pH microenvironments in corals, explore the role of sAC in coral and sea urchin calcification, identify sAC's role in pHi regulation and hemoglobin-$O_2$ binding in trout red blood cells, demonstrate VHA's involvement in promoting anemone photosynthesis, examine the role of VHA in sacoglossan kleptoplasty, and establish VHA's contribution to promoting symbiont selectivity in the bobtail squid. This collection of work epitomizes the comparative nature of research in the Tresguerres Lab and was largely accomplished during 2021-2022 when most of my dissertation work was paused due to Covid limitations.

**Final Thoughts**

Applying molecular biology techniques to study the cell biology of cnidarian-algal photosymbioses has long-presented an expensive challenge to our field resulting in a dominance of "-omics" studies. These studies have generated numerous hypotheses about the role of microbes in coral health and coral colony responses to environmental stress but often do not identify mechanisms responsible for their proposed models. Thankfully, rapid progress is unlocking the

potential of cnidarians as flexible model systems to test and refine these hypotheses: numerous *annotated* cnidarian genomes are published on NCBI and ReefGenomics, CRISPR protocols are now available for use in coral and hydroid models (Cleves et al. 2018; Sanders et al. 2018), and cheap and rapid tissue clearing methods now exist (Hsu et al. 2022), and combined with advancements in microscope technology, allow for super resolution imaging of whole tissues to determine the subcellular localization of proteins. The emergence of laboratory-amenable models like *Cassiopea ssp*. further strengthens our hand and leaves this author excited and hopeful for the future of photosymbiosis research.

## References


Barott KL, Venn AA, Perez SO, et al (2015) Coral host cells acidify symbiotic algal microenvironment to promote photosynthesis. Proceedings of the National Academy of Sciences of the United States of America 112:607–612. https://doi.org/10.1073/pnas.1413483112

Carté BK (1996) Potential of Marine Biomedical Natural Products research and medical applications. Oxford Journals 46:271–286

Cleves PA, Strader ME, Bay LK, et al (2018) CRISPR/Cas9-mediated genome editing in a reef-building coral. Proceedings of the National Academy of Sciences 115:5235–5240. https://doi.org/10.1073/pnas.1722151115

Hsu CW, Cerda J, Kirk JM, et al (2022) EZ Clear for simple, rapid, and robust mouse whole organ clearing. eLife 11:1–25. https://doi.org/10.7554/eLife.77419

Knowlton N, Brainard RE, Fisher R, et al (2010) Coral Reef Biodiversity. In: Life in the World's Oceans: Diversity, Distribution, and Abundance. Wiley-Blackwell, pp 65–78

Sanders SM, Ma Z, Hughes JM, et al (2018) CRISPR/Cas9-mediated gene knockin in the hydroid *Hydractinia symbiolongicarpus*. BMC Genomics 19:342592. https://doi.org/10.1186/s12864-018-5032-z

Smith SV (1978) Coral-reef area and the contributions of reefs to processes and resources of the world's oceans Production of methane and carbon dioxide from methane thiol and dimethyl sulphide by anaerobic lake sediments. Nature 273:225–226

Thies AB, Quijada-Rodriguez AR, Zhouyao H, et al (2022) A Rhesus channel in the coral symbiosome membrane suggests a novel mechanism to regulate NH3 and CO2 delivery to algal symbionts. Science Advances 8:. https://doi.org/10.1126/sciadv.abm0303